Studies of Bromodomain and Extra-Terminal Domain Proteins in Pancreatic Neuroendocrine Tumours

Omair A. Shariq

St. Hilda's College

University of Oxford

A thesis submitted for the degree of

Doctor of Philosophy

Trinity 2024

Acknowledgements

I am profoundly grateful to Professor Rajesh Thakker for the opportunity to pursue my DPhil studies within his group. Raj's mentorship has been instrumental in shaping my personal and professional growth over the years. His unwavering support for my scientific endeavours and career aspirations, combined with his enthusiasm and wisdom, has been invaluable. I consider myself exceptionally fortunate to have learned from such a distinguished mentor. My heartfelt appreciation also extends to Professor Duncan Richards, my co-supervisor. His approachability and invaluable advice on various aspects of my thesis were crucial in navigating and troubleshooting experiments, significantly contributing to the success of this project. I owe a great debt of gratitude to Dr Kate Lines, my daily mentor in the laboratory, whose passion for scientific enquiry and ability to make complex concepts accessible have been continually inspiring. I would like to thank all members of the Thakker group for their collaborative spirit and for creating a welcoming and enjoyable work environment. Special thanks go to Dr Katherine English, my lab partner within 'Team NETs', for the countless enriching discussions and shared experience of navigating basic science research as a clinician.

I am grateful for the financial support provided by the Clarendon Scholarship and the Climax Clinical Research Training Fellowship, which were instrumental in supporting my research and time at Oxford.

I extend my thanks to our collaborators, who played pivotal roles in this work. Particular thanks go to Dr Andreas Selberherr for providing the PNET tissue blocks essential for the immunohistochemistry findings, Dr Helen Ferry for her expertise with flow cytometry, and Dr Matthew Baxter for his guidance on bioinformatics analyses. It was a pleasure to collaborate with Dr Rab Prinjha and Dr Inma Rioja at GSK, both of whom are pioneers in their field. At the Mayo Clinic, I am grateful to Dr John Stulak, Dr David Farley and Dr William F. Young, who were early supporters of my desire to take time out of surgical training to pursue a DPhil. I am particularly grateful to the late Professor Gloria Petersen, whose encouragement and kindness have had a lasting impact on me. Her generous provision of RNA samples was instrumental in my studies and is remembered with deep appreciation.

Last, but certainly not least, I am forever thankful for the constant support and understanding from my friends and family; especially my wife, Jessi, whose steadfast love and support have been my pillars of strength.

Statement of Originality

All results presented in this thesis were generated by myself, except where explicitly stated.

Clinical data collection from collaborating sites in the study of children and adolescents with multiple endocrine neoplasia type 1 (MEN1) was undertaken by Dr Philippa Prentice (University of Cambridge, UK) and Dr Andreas Selberherr (Medical University of Vienna, Austria). I managed data collection at the University of Oxford, UK, and Mayo Clinic, USA, and was also responsible for the secure and anonymous storage of all data, as well as performing subsequent analyses.

Flow cytometry studies were conducted in collaboration with Dr Helen Ferry (University of Oxford), who physically ran samples on the flow cytometer while I prepared all the samples and conducted the data analysis. The *ex vivo* neoplastic islet compound treatments were performed by Dr Kate Lines and Dr Katherine English. I carried out the animal husbandry and mouse genotyping, as well as data analysis.

For the *in vitro* next-generation sequencing studies, library preparation and sequencing was performed by staff within the Wellcome Trust Centre for Human Genetics (University of Oxford) after I had performed all the compound treatments, RNA-extractions and chromatin immunoprecipitations. For the frozen tissue RNA sequencing study, RNA extraction was performed by the Biospecimen Accessioning and Processing Core Facility (Mayo Clinic) while library preparation and sequencing were performed by the Genome Analysis Core Facility (Mayo Clinic). I was responsible for all subsequent bioinformatics analyses.

Abstract

Pancreatic neuroendocrine tumours (PNETs) occur sporadically or within familial syndromes, such as multiple endocrine neoplasia type 1 (MEN1), in which they are the leading cause of mortality. Up to 60% of PNETs present with metastases, for which current therapies are largely non-curative, and I have therefore explored the effectiveness of epigenetic modifiers, focusing on inhibitors of the bromodomain and extra-terminal domain (BET) family of epigenetic 'readers' (BRD2, BRD3, BRD4 and BRDT). BET proteins contain two bromodomains (BDs), BD1 and BD2, that bind to acetylated lysine residues, upregulating the transcription of cancer-promoting genes. The BET inhibitor JQ1 (which targets BD1 and BD2 non-selectively) is reported to be efficacious in preclinical PNET models, but is limited by poor bioavailability and a short half-life. Moreover, the clinical relevance of BET proteins in human PNETs and differences between BD1 and BD2 remain underexplored. The aims of my thesis were to: 1) explore the occurrence and outcomes of MEN1-associated tumours in children and adolescents; 2) characterise BET expression in PNETs; and 3) assess the efficacy and mechanisms of non-selective (I-BET151) and selective BD1 and BD2 inhibitors (BD1i and BD2i, respectively) in preclinical PNET models.

My studies revealed that PNETs develop in one-third of children and adolescents with MEN1, ~15% with metastases. Immunohistochemistry indicated BET protein overexpression in human PNETs relative to adjacent islets. BD2i minimally affected viability, apoptosis, and cell cycle progression *in vitro*, whereas BD1i had moderate effects. However, combining BD1i and BD2i synergistically reduced viability, achieving effects comparable to I-BET151. Similar viability effects were observed in *ex vivo* neoplastic islets from pancreatic β-cell specific *Men1* knockout mice. Combined BD1i and BD2i also led to broader changes in gene expression and histone acetylation than single-domain targeting, albeit to a lesser extent than with I-BET151. The cell cycle-related genes for the transcription factor *E2F2* and Cytoskeleton-Associated Protein 2-Like (*CKAP2L*) were identified as direct BET inhibitor targets, both of which were downregulated by combined BD1i and BD2i, and whose expression correlated with progression-free survival.

In summary, this thesis highlights the clinical relevance of BET proteins in PNETs, and demonstrates that combined use of BD1i and BD2i surpasses single-domain targeting in efficacy. Finally, *E2F2* and *CKAP2L* emerge as key BET inhibitor targets with prognostic value, suggesting their importance in PNET pathogenesis and as predictors of treatment response.

Contents

List of Figures **xii**

List of Tables **xvi**

List of Abbreviations **xvii**

Chapter 1: Introduction **1**

1.1 Pancreatic neuroendocrine tumours 1

1.1.1 Clinical classification and nomenclature of PNETs 4

1.1.1.1 Tumour functionality 4

1.1.1.2 Tumour grading 6

1.1.1.3 Tumour staging 7

1.1.2 Overview of the clinical management of PNETs 9

1.1.2.1 Surgical resection versus watchful waiting 9

1.1.2.2 Cytoreductive surgery and hepatic-directed therapies 10

1.1.2.3 Systemic therapies 11

1.1.3 Multiple endocrine neoplasia type 1 (MEN1) 13

1.1.4 Genomic landscape of PNETs 16

1.1.4.1 Insights gained from familial PNET syndromes . 16

1.1.4.2 Molecular profiling of sporadic PNETs 17

1.2 Epigenetics 20

1.2.1 Histone modifications 21

1.2.2 DNA methylation 23

1.2.3 Epigenetic dysregulation in PNETs 23

1.2.4 Bromodomain and extra-terminal domain proteins 25

1.2.4.1 BET protein inhibition as a treatment for PNETs 28

1.3 Thesis objectives 30

Chapter 2: Methods **31**

2.1 Multiple endocrine neoplasia type 1 (MEN1) paediatric patient cohort study 32

2.1.1 Ethics approval . . . 32
2.1.2 Study population . . . 32
2.1.3 Surveillance screening . . . 33
2.1.4 Data collection . . . 35
2.2 Histology and immunohistochemistry . . . 36
2.2.1 Medical University of Vienna PNET samples . . . 36
2.2.2 Sectioning and mounting . . . 36
2.2.3 Deparaffinization and rehydration . . . 36
2.2.4 Antigen retrieval and endogenous peroxidase blocking . . . 37
2.2.5 Antibody staining . . . 37
2.2.6 Dehydration . . . 38
2.2.7 Haematoxylin and eosin (H&E) staining . . . 38
2.2.8 Image acquisition and Qupath software analysis . . . 39
2.3 *In vitro* experiments . . . 40
2.3.1 Cell lines . . . 40
2.3.2 Cell counting . . . 41
2.3.3 Epigenetic inhibitors . . . 42
2.3.4 Epigenetic inhibitor screen . . . 42
2.3.5 Proliferation time-course studies . . . 43
2.3.6 Dose-response curves . . . 44
2.3.7 Drug synergy studies . . . 45
2.3.8 Drug washout studies . . . 46
2.3.9 Apoptosis assays . . . 47
2.3.10 Crystal violet assays . . . 48
2.3.11 Propidium iodide (PI) cell cycle analysis . . . 49
2.3.12 Quantitative real-time PCR (qPCR) . . . 51
2.3.12.1 RNA extraction . . . 51
2.3.12.2 Complementary DNA (cDNA) synthesis . . . 51
2.3.12.3 qPCR analysis . . . 51
2.3.13 Western blotting . . . 52
2.3.13.1 Preparation of protein lysates . . . 52
2.3.13.2 Immunodetection of proteins . . . 53
2.4 Next-generation sequencing and bioinformatics . . . 54
2.4.1 RNA sequencing (RNA-seq) of BON1 PNET cells . . . 54
2.4.1.1 Preparation of samples and RNA extraction . . . 55
2.4.1.2 Library preparation and sequencing . . . 55
2.4.1.3 *In vitro* RNA-seq bioinformatics analysis . . . 56
2.4.2 RNA-seq of human PNET samples . . . 58

2.4.2.1 Mayo Clinic PNET samples 58
2.4.2.2 Sample preparation and RNA extraction from frozen tissue 58
2.4.2.3 Library preparation and sequencing 59
2.4.2.4 Human PNET samples RNA-seq bioinformatics analysis 60
2.4.3 Thiol(SH)-linked alkylation for the metabolic sequencing of RNA (SLAM-seq) 60
2.4.3.1 Principles of assay 60
2.4.3.2 Optimisation of metabolic labelling 62
2.4.3.3 Preparation of samples, RNA extraction and alkylation 64
2.4.3.4 Library preparation and sequencing 64
2.4.3.5 SLAM-seq bioinformatics analysis 65
2.4.4 Chromatin immunoprecipitation with next-generation sequencing (ChIP-Seq) 66
2.4.4.1 Principles of assay 66
2.4.4.2 Preparation of chromatin samples and cross-linking 67
2.4.4.3 Optimisation of sonication conditions 68
2.4.4.4 Chromatin sonication and immunoprecipitation . 69
2.4.4.5 DNA purification 70
2.4.4.6 Library preparation and sequencing 71
2.4.4.7 ChIP-seq bioinformatics analysis 72
2.5 Mouse studies 74
2.5.1 Ethics approval 74
2.5.2 Housing and animal husbandry 74
2.5.3 Mouse strains 74
2.5.4 Mouse genotyping 75
2.5.5 Histology and immunofluorescence 77
2.5.5.1 Tissue preparation and sectioning 77
2.5.5.2 Antigen retrieval and blocking 77
2.5.5.3 Antibody staining 78
2.5.5.4 Image acquisition 78
2.5.6 *Ex vivo* neoplastic mouse islet drug studies 78
2.5.6.1 Pancreas digestion and islet purification 78
2.5.6.2 Islet plating and compound treatments 79
2.6 Data visualisation 80
2.7 Statistical analysis 80

Chapter 3: Multiple endocrine neoplasia type 1 in children and adolescents: clinical features and treatment outcomes **81**
3.1 Aims . . . 81
3.2 Results . . . 84
3.2.1 Clinical features of cohort and tumour development . . . 84
3.2.2 Primary hyperparathyroidism (PHPT) . . . 87
3.2.3 Pancreatic and duodenal neuroendocrine tumours (PD-NETs) 89
3.2.4 Pituitary tumours . . . 93
3.2.5 Adrenal tumours . . . 95
3.2.6 *MEN1* genetic analysis and genotype-phenotype correlations 95
3.3 Discussion . . . 97

Chapter 4: Characterisation of BET expression in PNETs **102**
4.1 Aims . . . 103
4.2 Results . . . 104
4.2.1 BET proteins are overexpressed in human PNETs compared to normal pancreatic islets . . . 104
4.2.2 BET expression remains consistent across PNET subtype, stage and grade . . . 108
4.2.3 *BRD2* is the highest expressed BET gene in PNET cell lines and in human tumours . . . 112
4.2.4 RNA-seq and pathway analysis reveals dysregulation of E2F signalling in metastatic PNETs . . . 114
4.2.5 Cell cycle master regulators are activated in metastatic PNETs 118
4.2.6 The transcriptome of metastatic PNETs is enriched with BET inhibitor target genes . . . 121
4.2.7 Mapping of the BET protein cistrome in PNET cells reveals enrichment of cancer-related and neuronal lineage pathways 122
4.2.8 E2F transcription factor binding motifs are enriched within BRD2 and BRD4 peak regions . . . 127
4.2.9 BET proteins bind to the promoter regions of key cell cycle regulators . . . 128
4.3 Discussion . . . 129
4.3.1 BET proteins are overexpressed in human PNETs . . . 130
4.3.2 *BRD2* is the most abundant BET gene in PNETs . . . 131
4.3.3 BET mRNA and protein expression does not vary by PNET stage or grade . . . 132
4.3.4 Dysregulation of cell cycle-related pathways may link BET protein activity to aggressive PNET behaviour . . . 133

4.3.5 Genes associated with oxidative phosphorylation are upregulated in metastatic PNETs . . . 135
4.3.6 CTLA4 is an inhibited upstream regulator in metastatic PNETs . . . 136

Chapter 5: Phenotypic effects of current and next-generation BET inhibitors in PNET cell lines 138
5.1 Aims . . . 139
5.2 Results . . . 140
5.2.1 I-BET151 shows comparable efficacy to JQ1 in reducing viability in PNET cell lines . . . 140
5.2.2 BD1- and BD2-selective BET inhibitors have differing effects on PNET cell viability . . . 141
5.2.3 Simultaneous BD1 and BD2 inhibition synergistically reduces PNET cell viability . . . 144
5.2.4 Simultaneous BD1 and BD2 inhibition increases apoptosis in PNET cell lines . . . 150
5.2.5 Simultaneous BD1 and BD2 inhibition alters PNET cellular morphology and decreases viability in a time-dependent manner . . . 151
5.2.6 The effects of simultaneous BD1 and BD2 inhibition on cell viability persist after compound washout . . . 154
5.2.7 Simultaneous BD1 and BD2 inhibition causes cell cycle arrest in human PNET cell lines . . . 155
5.2.8 Effects of BET inhibitors on neoplastic pancreatic islets *ex vivo* . . . 157
5.3 Discussion . . . 157
5.3.1 First-generation BET inhibitors are effective in PNET cell lines . . . 158
5.3.2 MIN6 cells are relatively resistant to the effects of BET inhibition . . . 159
5.3.3 BD1- and BD2-selective BET inhibitors have differential effects in PNET cell lines . . . 160

Chapter 6: Characterisation of transcriptomic and epigenomic responses to BET inhibition *in vitro* 163
6.1 Aims . . . 164
6.2 Results . . . 165

6.2.1 Simultaneous BD1 and BD2 inhibition induces more extensive gene expression changes than targeting either domain individually 165
6.2.2 Simultaneous BD1 and BD2 inhibition downregulates a broad range of Hallmark pathways, including those implicated in metastatic PNETs 168
6.2.3 Simultaneous BD1 and BD2 inhibition disrupts RNA and protein synthesis machinery while BD1-selective inhibition predominantly affects cell cycle pathways 170
6.2.4 The upstream regulator CKAP2L is inhibited by BD1-selective and combined BD1/BD2 inhibition 172
6.2.5 I-BET151 has a broader impact on modulating downstream gene expression than combined treatment with GSK789 and GSK620. 175
6.2.6 SLAM-seq identifies direct transcriptional targets of BD-selective and non-selective inhibition 177
6.2.7 I-BET151 and GSK789/GSK620 have distinct and overlapping effects on the nascent transcriptome 182
6.2.8 Integrated analysis of SLAM-seq and RNA-seq identifies *E2F2* and *CKAP2L* as early and late targets, respectively, of dual BD inhibition 184
6.2.9 ChIP-seq reveals alterations in genome-wide H3K27ac enrichment after BET inhibition 187
6.2.10 Regions of H3K27ac loss following BET inhibition coincide with genome-wide BET protein binding sites 193
6.2.11 BET inhibitors regulate the expression of PNET-relevant genes by reducing H3K27ac occupancy at super-enhancers 193
6.2.12 Integrated ChIP-seq and transcriptomic analyses identify BET inhibitor candidates with clinical relevance in PNETs 201
6.3 Discussion 206
6.3.1 The rationale for domain-selective BET inhibitors 207
6.3.2 BD1-selective, BD2-selective and dual BD inhibition are each associated with distinct transcriptional changes in BON1 cells 208
6.3.3 Differences in transcriptomic response between I-BET151 and combination GSK789/GSK620 treatment 210
6.3.4 *CKAP2L* and *E2F2* are clinically-relevant BET inhibitor targets in patients with PNETs 212

Chapter 7: Conclusions **215**

7.1 Study context 215
7.2 Summary of major findings 216
7.3 Limitations 219

Chapter 8: Future studies **222**
8.0.1 Validation of bioinformatics/*in silico* data 222
8.0.2 Plans for *in vivo* studies including current and next-generation BET inhibitors 224
8.0.3 Combining BET inhibitors with other targeted therapies . 226

References **229**

List of Figures

Figure 1.1 The human pancreas contains both endocrine and exocrine compartments . . . 2
Figure 1.2 Overview of MEN1-related manifestations . . . 14
Figure 1.3 Overview of selected altered molecular pathways in PNETs 19
Figure 1.4 Overview of epigenetic modifications . . . 22
Figure 1.5 Phylogenetic tree of the human bromodomain family . . 26
Figure 1.6 Domain organisation of human BET family members . . 27

Figure 2.1 Overview of Qupath analysis . . . 40
Figure 2.2 Dose-response matrix for GSK789 and GSK620 synergy studies . . . 46
Figure 2.3 Flow cytometry cell cycle analysis gating strategy . . . 50
Figure 2.4 Overview of SLAM-seq experiment . . . 62
Figure 2.5 Viability of BON1 cells upon treatment with 4sU . . . 63
Figure 2.6 Overview of ChIP-seq workflow . . . 66
Figure 2.7 Optimisation of ChIP-seq sonication regimen . . . 69
Figure 2.8 Mouse genotyping . . . 76

Figure 3.1 Flow chart of the study population . . . 84
Figure 3.2 Age-related penetrance of MEN1-related manifestations . 86
Figure 3.3 Postoperative outcomes after parathyroidectomy . . . 88
Figure 3.4 Tumour growth trajectories in patients with NF-PNETs 91
Figure 3.5 Schematic representation of the genomic organisation of the *MEN1* gene . . . 96

Figure 4.1 BET protein expression in human PNETs . . . 106
Figure 4.2 BET proteins are over-expressed in human PNETs compared to normal pancreatic islets . . . 107
Figure 4.3 BET protein expression does not vary by PNET subtype 108
Figure 4.4 BET protein expression does not vary by PNET subtype 109
Figure 4.5 BET gene expression by PNET subtype, stage and grade 111
Figure 4.6 mRNA expression of BET genes in PNET cell lines and human tumours . . . 113

Figure 4.7 Western blot analysis of BET protein expression in PNET cell lines 114
Figure 4.8 RNA-seq in human PNETs reveals upregulation of BET-protein relevant transcriptional programs 116
Figure 4.9 Gene set enrichment analyses of metastatic vs localised PNETs 118
Figure 4.10 Ingenuity Pathway Analysis in metastatic PNETs 120
Figure 4.11 BET-inhibitor target gene expression is enriched in metastatic PNETs 122
Figure 4.12 ChIP-seq maps the BET protein cistrome in BON1 PNET cells 124
Figure 4.13 Pathway analysis reveals enrichment of cancer-related and neuronal lineage pathways in BET protein peaks 126
Figure 4.14 E2F transcription factor binding motifs are enriched within BRD2 and BRD4 peak regions 127
Figure 4.15 BET proteins bind to the promoters of cell cycle regulators 129

Figure 5.1 I-BET151 is as effective as JQ1 in reducing PNET cell viability 140
Figure 5.2 Affinity and selectivity profiles of BET inhibitors 141
Figure 5.3 BD1- and BD2-selective BET inhibitors have differing effects on PNET cell viability 142
Figure 5.4 Crystal violet staining of PNET cell lines treated with BET inhibitors 144
Figure 5.5 Combined BD1 and BD2 inhibition enhances suppression of PNET cell viability 145
Figure 5.6 PNET cell viability is unaffected by negative enantiomer BET inhibitor compounds 146
Figure 5.7 The addition of a negative enantiomer BD1 inhibitor (GSK791) to GSK620 does not affect PNET cell viability 147
Figure 5.8 Combined BD1 and BD2 inhibition demonstrates consistent efficacy across different inhibitors in PNET cell lines 148
Figure 5.9 GSK789 and GSK620 synergistically reduce PNET cell line viability 149
Figure 5.10 Dual BD inhibition induces apoptosis in PNET cell lines 151
Figure 5.11 Time-dependent morphological and viability changes in PNET cell lines after BET inhibitor treatment 153
Figure 5.12 The effects of simultaneous BD1 and BD2 inhibition on cell viability persist after compound washout 154

Figure 5.13 Dual BD inhibition induces cell cycle arrest in human PNET cell lines 156
Figure 5.14 Immunofluorescence staining of islets from *Men1*$^{L/L}$*/RIP2-Cre* and wild-type mice and results of *ex vivo* drug studies 158

Figure 6.1 Simultaneous BD1 and BD2 inhibition induces more extensive gene expression changes than targeting either domain individually 167
Figure 6.2 Simultaneous BD1 and BD2 inhibition downregulates Hallmark pathways implicated in metastatic PNETs . . 169
Figure 6.3 Dual bromodomain inhibition disrupts RNA and protein synthesis machinery while BD1-selective inhibition downregulates cell cycle pathways 171
Figure 6.4 Differential effects of BD1-selective and dual BD inhibition on neuronal development pathways and cell architecture 172
Figure 6.5 CKAP2L is a key upstream regulator that is inhibited by BD1-specific and combined BD1/BD2 inhibition 174
Figure 6.6 I-BET151 has a more pronounced effect on downregulating gene expression compared to combined treatment with GSK789 and GSK620 176
Figure 6.7 I-BET151 has a more pronounced effect on upregulating gene expression compared to combined treatment with GSK789 and GSK620 177
Figure 6.8 Metabolic RNA labelling with SLAM-seq reveals distinct effects of BD-selective and non-selective BET inhibition on nascent transcription 178
Figure 6.9 SLAM-seq identifies direct transcriptional targets of BD-selective and dual-BD inhibition 179
Figure 6.10 Maximal inhibition of direct BET protein targets requires simultaneous targeting of both BD1 and BD2 180
Figure 6.11 BD1-selective inhibition upregulates chromatin remodelling genes while combined BD1 and BD2 inhibition triggers cellular stress response pathways . . . 181
Figure 6.12 Combined treatment with GSK789/GSK620 decreases nascent transcription to a greater extent than I-BET151. 183
Figure 6.13 Both GSK789/GSK620 and I-BET151 upregulate nascent transcription of genes involved in chromatin remodelling 184
Figure 6.14 Integration of SLAM-seq and RNA-seq reveals temporal changes in gene expression following BET inhibition . . . 185

Figure 6.15 BET inhibition alters genome-wide H3K27ac enrichment in BON1 cells 188
Figure 6.16 BET inhibition leads to decreased H3K27ac enrichment predominantly at promoter regions 190
Figure 6.17 Simultaneous BD1 and BD2 inhibition decreases H3K27ac enrichment at promoters of genes involved in RNA processing and translation 191
Figure 6.18 Simultaneous BD1 and BD2 inhibition increases H3K27ac enrichment at distal regulatory elements of genes involved in pancreas development and differentiation 192
Figure 6.19 Regions of H3K27ac loss following BET inhibition coincide with genome-wide BET protein occupancy 194
Figure 6.20 Characterisation of the SE landscape in BON1 cells . . . 196
Figure 6.21 SE-driven genes in BON1 cells are implicated in endocrine lineage 197
Figure 6.22 *NKX2-2* and *RFLNA* are BET inhibitor-responsive, SE-driven genes in BON1 cells and human PNETs . . . 198
Figure 6.23 *RASD1* and *SLC39A14* are BET inhibitor-responsive, SE-driven genes in BON1 cells and human PNETs . . . 200
Figure 6.24 Integrated ChIP-seq and SLAM-seq analysis identifies direct targets of simultaneous BD1 and BD2 inhibition . 202
Figure 6.25 Integrated ChIP-seq and RNA-seq analysis identifies downstream transcriptional changes following loss of H3K27ac enrichment 203
Figure 6.26 Simultaneous BD1 and BD2 inhibition leads to greater loss of H3K27ac occupancy at promoters of key BET inhibitor target genes 204
Figure 6.27 *E2F2* and *CKAP2L* mRNA expression levels correlate with Ki-67 index in human PNETs 205
Figure 6.28 High *E2F2* and *CKAP2L* mRNA expression levels are associated with worse survival outcomes in human PNETs 206

List of Tables

Table 1.1 Clinical features and incidence rates of functioning PNETs 5
Table 1.2 Overview of the 2022 WHO classification system for pancreatic neuroendocrine neoplasms 6
Table 1.3 Comparison of the AJCC 7th edition with the ENETS and AJCC 8th edition staging systems for PNETs 8
Table 1.4 Selected key randomised trials of systemic treatments in NETs 12

Table 2.1 Screening protocol and definitions of MEN1 manifestations 34
Table 2.2 List of primary antibodies used for immunohistochemistry 38
Table 2.3 Overview of PNET cell lines used in this thesis. 41
Table 2.4 BET inhibitor compounds used in this thesis 42
Table 2.5 List of human and mouse QuantiTect primers used for qPCR 52
Table 2.6 List of primary antibodies used for Western blotting . . . 54
Table 2.7 List of antibodies used for ChIP-seq 70

Table 3.1 Studies in the literature that describe paediatric and adolescent MEN1 cohorts 83
Table 3.2 Details of 56 MEN1 patients with manifestations detected at $\leq$ 18 years of age 85
Table 3.3 Characteristics and treatment outcomes of 8 patients with insulinomas at $\leq$ 18 years of age 90
Table 3.4 Characteristics and treatment outcomes of 15 patients diagnosed with NF-PNETs at $\leq$ 18 years old 92
Table 3.5 Characteristics of 18 patients diagnosed with pituitary adenomas at $\leq$ 18 years of age 94
Table 3.6 Frequency of MEN1 manifestations at 18 years of age according to genotype 98

Table 4.1 Overview of human PNET FFPE blocks from the University of Vienna cohort (n = 53) 105
Table 4.2 Overview of human PNET frozen samples from the Mayo Clinic cohort (n = 46) 110

List of Abbreviations

AA	Adrenal adenoma
ACTH	Adrenocorticotropic hormone
AJCC	American Joint Committee on Cancer
AKT	Protein kinase B
ALT	Alternative lengthening of telomeres
AMY2B	Amylase, alpha 2B
ANOVA	Analysis of variance
ARID2	AT-rich interaction domain 2
ARX	Aristaless related homeobox
AT-rich	Adenine thymine-rich
ATAD2	ATPase family, AAA domain containing 2
ATF4	Activating transcription factor 4
ATM	Ataxia telangiectasia mutated
ATPase	Adenosine triphosphatase
ATRX	Alpha thalassemia/mental retardation syndrome X-linked
AURKA	Aurora kinase A
BAF	BRG1/BRM-associated factor
BAZ1A/B	Bromodomain adjacent to zinc finger domain 1A/B
BCA	Bicinchoninic acid
BD	Bromodomain
BD1	Bromodomain 1
BD2	Bromodomain 2
BEND2	BEN domain containing 2
BET	Bromodomain and extra-terminal domain
BETi	BET inhibitor
BRCA1	Breast cancer gene 1
BRCA2	Breast cancer gene 2
BRD2	Bromodomain containing 2
BRD3	Bromodomain containing 3
BRD4	Bromodomain containing 4
BRD4(L)	Bromodomain containing 4 long isoform
BRD4(S)	Bromodomain containing 4 short isoform
BRD7	Bromodomain containing 7
BRDT	Bromodomain testis-specific

BrdU	Bromodeoxyuridine
BRG1	Brahma-related gene 1
BRIP1	BRCA1 interacting protein C-terminal helicase 1
BRPF	Bromodomain and PHD finger containing
BRWD	Bromodomain and WD repeat domain containing
BSA	Bovine serum albumin
BWA	Burrows-Wheeler aligner
BZIP	Basic leucine zipper
C2CD4A	C2 calcium-dependent domain containing 4A
CCND1	Cyclin D1
CDK	Cyclin-dependent kinase
CDKN	Cyclin-dependent kinase inhibitor
CHD4	Chromodomain helicase DNA binding protein 4
CHEK2	Checkpoint kinase 2
CHGA	Chromogranin A
ChIP-qPCR	Chromatin immunoprecipitation qPCR
ChIP-seq	Chromatin immunoprecipitation with next-generation sequencing
CK2	Casein kinase 2
CKAP2L	Cytoskeleton-associated protein 2 like
CP	Completion pancreatectomy
CpG-binding	Cytosine-phosphate-Guanine-binding
CpG	Cytosine-phosphate-Guanine
CREBBP	CREB binding protein
CT	Computed tomography
CTD	C-terminal domain
dH_2O	Distilled water
DAB	3,3'-Diaminobenzidine
DAPI	4',6-Diamidino-2-phenylindole
DAXX	Death-domain associated protein
DEPDC5	DEP domain containing 5
DHRS2	Dehydrogenase/reductase 2
DMSO	Dimethyl sulfoxide
DNMT	DNA methyltransferase
DOTATATE	DOTA(0)-Tyr(3)-octreotate
DP	Distal pancreatectomy
DTT	Dithiothreitol
E1A	Adenovirus early region 1A
E2F	Early region 2 binding factor
EDTA	Ethylenediaminetetraacetic acid
EEF1A2	Eukaryotic translation elongation factor 1 alpha 2

EGTA	Ethylene glycol-bis(β-aminoethyl ether)-N,N,N',N'-tetraacetic acid
EMA	European Medicines Agency
ENCODE	Encyclopedia of DNA elements
ENETS	European Neuroendocrine Tumour Society
EP300	E1A binding protein p300
ERK	Extracellular signal-regulated kinases
ET	Extra-terminal
EUS	Endoscopic ultrasound
EWSR1	Ewing sarcoma breakpoint region 1
FBS	Fetal bovine serum
FC	Fold change
FCS	Flow cytometry standard
FDA	Food and Drug Administration
FDR	False discovery rate
FFPE	Formalin-fixed paraffin-embedded
FLI1	Friend leukemia virus integration 1
FLT3	Fms-like tyrosine kinase 3
FOXJ1	Forkhead box J1
FOXM1	Forkhead box M1
FOXO1	Forkhead box O1
FRAP	Fluorescence recovery after photobleaching
GAPDH	Glyceraldehyde-3-phosphate dehydrogenase
GCN5L2	General control of amino acid synthesis protein 5-like 2
GLI1	Glioma-associated oncogene homolog 1
GLP1R	Glucagon-like peptide-1 receptor
GO:BP	Gene ontology:biological process
GRCh38	Genome reference consortium human build 38
GREAT	Genomic regions enrichment of annotations tool
GSEA	Gene set enrichment analysis
GSK	GlaxoSmithKline
GTF3C6	General transcription factor IIIC subunit 6
H32K27ac	Histone H3 lysine 27 acetylation
H3K14	Histone H3 lysine 14
H3K4me3	Histone H3 lysine 4 trimethylation
H3K9	Histone H3 lysine 9
H3K9me2/3	Histone H3 lysine 9 di-/trimethylation
HAT	Histone acetyltransferase
HBSS	Hanks' balanced salt solution
HCl	Hydrochloric acid
HDAC	Histone deacetylase
HDM	Histone demethylase

HEPES	4-(2-Hydroxyethyl)piperazine-1-ethanesulfonic acid
HGVS	Human genome variation society
HIC1	Hypermethylated in cancer 1
HIFs	Hypoxia-inducible factors
HMT	Histone methyltransferase
HOMER	Hypergeometric optimisation of motif enrichment
HPF	High power field
IAA	Iodoacetamide
IGF-1	Insulin-like growth factor 1
IGF1R	Insulin-like growth factor 1 receptor
IGFR	Insulin-like growth factor receptor
IGV	Integrative genomics viewer
IL-2	Interleukin 2
IMMT	Inner membrane mitochondrial protein
INHBE	Inhibin beta E
INS	Insulin
INSM1	Insulinoma-associated protein 1
IP	Immunoprecipitation
IPA	Ingenuity pathway analysis
IRB	Institutional Review Board
IRF2	Interferon regulatory factor 2
IRX2	Iroquois homeobox 2
IV	Intravenous
JHDM6	JmjC domain-containing histone demethylation protein 6
JNK	c-Jun N-terminal kinase
JunD	Jun D proto-oncogene
KDM	Lysine-specific demethylase
KEGG	Kyoto encyclopedia of genes and genomes
KMT	Lysine methyltransferase
KRAS	Kirsten rat sarcoma viral oncogene homolog
TAg	Large tumour antigen
LAR	Long-acting release
LiCl	Lithium chloride
LINCS	Library of integrated network-based cellular signatures
MACS2	Model-based analysis of ChIP-seq 2
MAFA	MAFA transcription factor
MAPK	Mitogen-activated protein kinase
MAX	Myc-associated factor X
MBD	Methyl-CpG-binding domain
MCM	Minichromosome maintenance protein
MED1	Mediator complex subunit 1
MEK	Mitogen-activated protein kinase kinase

MEN1	Multiple endocrine neoplasia type 1
MEN4	Multiple endocrine neoplasia type 4
MGMT	O-6-methylguanine-DNA methyltransferase
MLL	Mixed lineage leukemia
MLP	Metastasis-like primary
MRI	Magnetic resonance imaging
MSH	MutS homolog
MSigDB	Molecular signatures database
MTA	Material transfer agreement
mTOR	Mechanistic target of rapamycin
MTORC1	Mechanistic target of rapamycin complex 1
MutS	MutS homolog
MutY	MutY DNA glycosylase
MXD4	MAX dimerisation protein 4
NaCl	Sodium chloride
$NaHCO_3$	Sodium bicarbonate
NEC	Neuroendocrine carcinoma
NES	Normalised enrichment score
NET	Neuroendocrine tumour
NeuroD1	Neuronal differentiation 1
NF-PNET	Non-functional pancreatic neuroendocrine tumour
NF1	Neurofibromatosis type 1
NFAT	Nuclear factor of activated T-cells
NFIC	Nuclear factor I/C
NGS	Next generation sequencing
NHS	National Health Service
NKX2-2	NK2 homeobox 2
NLRC5	NLR family CARD domain containing 5
NMC	NUT midline carcinoma
NR	Not reported
NSD3	Nuclear receptor binding SET domain protein 3
NUT	Nuclear protein in testis
OGTT	Oral glucose tolerance test
OR	Odds ratio
ORR	Objective response rate
OS	Overall survival
P-TEFb	Positive transcription elongation factor b
PA	Pituitary adenoma
PALB2	Partner and localiser of BRCA2
PARP	Poly(ADP-ribose) polymerase
PAX5	Paired box protein 5
PB1	Protein polybromo-1

PBS	Phosphate buffered saline
PC	Principal component
PCA	Principal component analysis
PCAF	P300/CBP-associated factor
PCR	Polymerase chain reaction
PD-NETs	Pancreatic or duodenal neuroendocrine tumours
PD	Pancreaticoduodenectomy
PDAC	Pancreatic ductal adenocarcinoma
PDLIM2	PDZ and LIM domain protein 2
PDX1	Pancreatic and duodenal homeobox 1
PFA	Paraformaldehyde
PFS	Progression-free survival
PHD	Plant homeodomain
PHIP	Pleckstrin homology domain interacting protein
PHPT	Primary hyperparathyroidism
PI	Propidium iodide
PI3K	Phosphoinositide 3-kinase
PID	Pathway interaction database
PK	Pharmacokinetic
PMS2	Postmeiotic segregation increased 2
PO	Per os
POLR2A	RNA polymerase II subunit A
PR/SET	PR domain containing protein 9
PRDM16	PR domain containing 16
PRKCDBP1	Protein kinase C delta binding protein 1
PRRT	Peptide receptor radionuclide therapy
PTEN	Phosphatase and tensin homolog
PTH	Parathyroid hormone
PTHrp	Parathyroid hormone-related protein
PVDF	Polyvinylidene difluoride
qPCR	quantitative polymerase chain reaction
RAS	Rat sarcoma virus
RASD1	Ras homolog family member D1
RB	Retinoblastoma
RFLNA	Ret finger protein-like family member A
RIN	RNA integrity number
RNA-seq	RNA sequencing
RNF216	Ring finger protein 216
ROSE	Rank ordering of super-enhancers
RPKM	Reads per kilobase per million mapped reads
RPM	Revolutions per minute

RPMI	Roswell Park Memorial Institute
RTK	Receptor tyrosine kinase
S100	S100 calcium-binding protein
SC	Subcutaneous
SDS-PAGE	Sodium dodecyl sulfate polyacrylamide gel electrophoresis
SE	Super-enhancer
SEM	Standard error of the mean
SEMA6C	Semaphorin-6C
SETD2	SET domain containing 2
SIX	Sine oculis homeobox homolog
scRNA-seq	Single-cell RNA sequencing
SLAM-seq	Thiol(SH)-linked alkylation for the metabolic sequencing of RNA
SLC39A14	Solute carrier family 39 member 14
SMAD3	SMAD family member 3
SMARCA	Switch/sucrose non-fermentable related, matrix associated, actin dependent regulator of chromatin, subfamily A
SNAI2	Snail family transcriptional repressor 2
SNP	Single nucleotide polymorphism
SSA	Somatostatin analogue
SSTR	Somatostatin receptor
STRING	Search Tool for the Retrieval of Interacting Genes/Proteins
SV40	Simian virus 40
SWI/SNF	SWItch/Sucrose non-fermentable
TACE	Transarterial chemoembolisation
TAE	Transarterial embolisation
TAF1	TATA-box binding protein associated factor 1
TARE	Transarterial radioembolisation
TATA-box	TATA box
TBS-T	Tris buffered saline with Tween
TCGA	The Cancer Genome Atlas
TET	Ten-eleven translocation
TGF	Transforming growth factor
TIAM1	T-lymphoma invasion and metastasis-inducing protein 1
TMEM233	Transmembrane protein 233
TNF	Tumour necrosis factor
TNM	Tumour node metastasis
TP53	Tumour protein P53
TP53I13	Tumour protein p53-inducible protein 13
TP53INP1	Tumour protein P53 inducible nuclear protein 1
TPM4	Tropomyosin 4
TPM	Transcripts per million
TPRS1	Tumour protein p53-regulated apoptosis-inducing protein 1

TRIM	Tripartite motif containing
Tris-HCl	Tris(hydroxymethyl)aminomethane hydrochloride
TSC	Tuberous sclerosis complex
TSS	Transcription start site
TTS	Transcription termination site
U/mL	Units per millilitre
US	Ultrasound
USA	United States of America
USP22	Ubiquitin-specific peptidase 22
UTR	Untranslated region
VEGF	Vascular endothelial growth factor
VEGFR	Vascular endothelial growth factor receptor
VHL	Von Hippel-Lindau disease
VIP	Vasoactive intestinal peptide
VIPoma	Vasoactive intestinal peptide-oma
WDR9	WD repeat domain 9
WES	Whole exome sequencing
WGS	Whole genome sequencing
WHO	World Health Organisation
wt	Wild-type
YY1	Yin Yang 1
ZMYND11	Zinc finger, MYND-type containing 11
ZNF217	Zinc finger protein 217

1 Introduction

Chapter-specific table of contents

1.1 Pancreatic neuroendocrine tumours 1
1.1.1 Clinical classification and nomenclature of PNETs . . 4
1.1.2 Overview of the clinical management of PNETs . . . 9
1.1.3 Multiple endocrine neoplasia type 1 (MEN1) 13
1.1.4 Genomic landscape of PNETs 16
1.2 Epigenetics 20
1.2.1 Histone modifications 21
1.2.2 DNA methylation 23
1.2.3 Epigenetic dysregulation in PNETs 23
1.2.4 Bromodomain and extra-terminal domain proteins . 25
1.3 Thesis objectives 30

1.1 Pancreatic neuroendocrine tumours

The human pancreas is an elongated glandular organ that is located behind the stomach and lies transversely in the retroperitoneum. Anatomically, it can be arbitrarily divided into four parts: the head, neck, body and tail. The pancreas serves both exocrine and endocrine functions, with the majority (~95%) of its mass consisting of acinar (exocrine) cells that secrete digestive enzymes such as

amylase, pancreatic lipase and trypsinogen into the pancreatic ducts.[1] In contrast, its endocrine function includes the release of hormones directly into the bloodstream from clusters of cells known as the islets of Langerhans **(Figure 1.1)**. These islets, comprising <5% of the overall pancreatic mass, consist of different cell types: α-cells that produce glucagon; β-cells that produce insulin, amylin and C-peptide; γ-cells or PP-cells that produce pancreatic polypeptide; δ-cells that produce somatostatin and ε-cells that produce ghrelin, each playing a distinct role in the systemic regulation of glucose homeostasis and paracrine control of pancreatic secretions.[2] Glucagon and insulin raise and lower, respectively, blood glucose levels, while somatostatin inhibits the release of both hormones. Pancreatic polypeptide acts to self-modulate exocrine and endocrine secretions in response to food intake and ghrelin plays a key role in appetite regulation.[2]

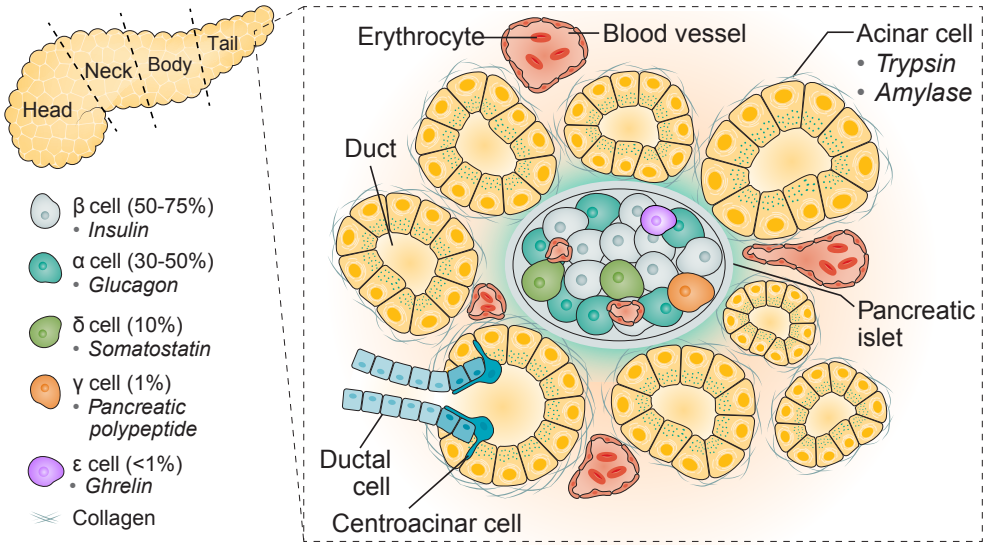

Figure 1.1. The human pancreas contains both endocrine and exocrine compartments. Anatomically, the pancreas is divided into a head, neck, body and tail. The endocrine pancreas consists of five distinct cell types, which include (in order of frequency) insulin-secreting β-cells, glucagon-secreting α-cells, somatostatin-secreting δ-cells, pancreatic polypeptide-secreting γ- or PP-cells, and ghrelin-secreting ε-cells. Cell types in figure are labelled with their approximate frequency in parentheses and associated hormones in italics. The exocrine pancreas makes up approximately 95% of the pancreatic tissue and comprises acinar cells that produce digestive enzymes, such as trypsin and amylase, and a network of ductal cells that transport these enzymes to the intestine. Centroacinar cells are terminal end-duct cells that interface with acini. Figure adapted from Ellis et al.[3]

Studies of pancreatic development have highlighted a significant degree of evolutionary conservation across a diverse array of species, emphasising the pancreas's essential roles in metabolic regulation and digestive processes.[4] Mammals, birds, reptiles, and amphibians all share a structurally unified pancreas with similar histology and modes of development. In certain fish species, a variation in this pattern exists where islet cells are segregated into Brockmann bodies, which are distinct from the exocrine pancreas.[4] Whilst invertebrates lack a pancreas entirely, the presence of functionally analogous endocrine cells within their digestive systems and brains suggests an evolutionary path in which endocrine regulatory mechanisms may have 'migrated' from dispersed sites in the gut or nervous system to become centralised within the pancreas in vertebrates.[4,5]

Across various species, pancreatic endocrine cells and neuronal cells share a remarkable number of phenotypic and genetic similarities. Both cell types function as secretory units, releasing hormones or neurotransmitters when triggered by external stimuli. This process involves a conserved mechanism in which cell depolarisation leads to an influx of calcium ions, prompting the fusion of storage vesicles with the plasma membrane. Additionally, the developmental biology of both cell types involves several shared transcription factors, such as Islet-1 (Isl1), Neurogenic differentiation 1 (NeuroD1), Paired box gene 4 and 6 (Pax4 and Pax6, respectively) and NK2 homeobox 2 (Nkx2.2), all of which are instrumental for both pancreatic endocrine and neuronal differentiation.[6] Despite these well established parallels, however, lineage and chimera studies indicate that pancreatic islets derive from the endoderm and not the neural crest.[7–9] Nonetheless, more recent work suggests that the murine pancreas may contain a small population of neural crest-derived multipotent precursor cells.[10,11] Moreover, human neural progenitors have been successfully differentiated into insulin-producing cells that express pancreas islet markers.[12] These observations suggest that common ancient developmental pathways may regulate the differentiation of both islet cells and neurons, despite their distinct cellular origins.

Tumours that arise from islet cells are known as pancreatic neuroendocrine tumours (PNETs). PNETs account for 3-5% of all pancreatic malignancies and have an incidence of 1–3 cases per 100,000 individuals per year.[13,14] However, incidence rates are steadily increasing, secondary to improved detection with cross-sectional imaging and endoscopy.[14] Furthermore, PNETs have been reported in 1-10% of individuals in autopsy series, suggesting that many tumours remain undiagnosed.[15,16] These tumours are referred to as 'neuroendocrine' as they exhibit morphological features shared by neurons, as described above, such as the presence of synaptic-like vesicles and the expression of neuronal proteins such as synaptophysin, neuron-specific enolase and chromogranin A, whilst also containing secretory granules typically seen in endocrine cells.[17]

1.1.1 Clinical classification and nomenclature of PNETs

1.1.1.1 Tumour functionality

PNETs are broadly classified into functioning or non-functioning tumours (NF-PNETs), based on their clinical presentation and hormone secretion patterns. Functioning tumours, which account for ~30% of PNETs, present with distinct clinical syndromes caused by the uncontrolled secretion of specific hormones and are named after the hormone that predominates their symptoms (e.g., insulinoma, gastrinoma, somatostatinoma or vasoactive intestinal peptide [VIP]-oma) **(Table 1.1)**. In contrast, the majority (~60-80%) of PNETs are non-functioning and do not lead to clinical symptoms related to hormone overproduction, although they may still secrete various peptides, such as chromogranins, neuron-specific enolase and pancreatic polypeptide, which can be detected as serum tumour markers.[18,19]

Table 1.1. Clinical features and incidence rates of functioning PNETs

Tumour	Hormone	Incidence (per million per year)	Signs and symptoms
Insulinoma	Insulin	1-3	Neuroglycopenic symptoms: confusion, visual changes, irritability, weakness, tiredness Sympathoadrenal symptoms: palpitations, sweating
Gastrinoma	Gastrin	0.5-2	Abdominal pain, gastro-oesophageal reflux, diarrhea, peptic ulcer disease
Glucagonoma	Glucagon	0.01 - 0.1	Diarrhoea, depression, deep venous thrombosis, necrolytic migratory erythema, glucose intolerance
VIPoma	Vasoactive-intestinal peptide	0.05 - 0.2	Watery diarrhoea, hypokalaemia, dehydration, achlorydia
Somatostatinoma	Somatostatin	Rare	Diabetes mellitus, cholelithiasis, diarrhoea
ACTH-oma	ACTH	Rare	Cushing's syndrome
PTHrp-oma	PTHrp	Rare	Hypercalcaemia-related: bony pain, osteoporosis, nephrolithiasis, neurocognitive symptoms

ACTH, adrenocorticotropic hormone; PTHrp, parathyroid hormone-related protein

Functioning PNETs generally have a more favourable prognosis than their non-functioning counterparts, as they tend to be diagnosed at an earlier stage due to the severity of symptoms caused by hormone oversecretion. Nonetheless, they may still present with life-threatening manifestations, such as hypoglycaemic seizures in patients with insulinomas, or bleeding peptic ulcers secondary to gastrinoma (known as the Zollinger-Ellison syndrome).[20] Hormone secretion syndromes can also have a deleterious impact on patients' health-related quality of life due to symptoms such as diarrhoea, fatigue and loss of appetite.[21] NF-PNETs are often detected at a later stage, with ~60% of patients presenting with advanced disease at diagnosis, usually in the form of liver metastases. The presence of distant metastases portends a poor prognosis, with a median survival of only 24 months (compared to 136 months for patients with disease localised to the pancreas).[22] Thus, while PNETs are, in general, less aggressive than pancreatic ductal adenocarcinoma (PDAC), they are not invariably indolent and do have the potential to metastasise.

1.1.1.2 Tumour grading

Grade is an important determinant of prognosis in PNETs, based on tumour morphology (differentiation) and immunohistochemical markers of proliferation (Ki-67 index or mitotic count per mm^2), per the World Health Organisation (WHO) classification system. Since its first introduction in 1980,[23] the WHO classification system for PNETs has undergone several revisions, with the most recent being published in 2022 **(Table 1.2)**.[24]

Table 1.2. Overview of the 2022 WHO classification system for pancreatic neuroendocrine neoplasms

Neoplasm	Classification	Diagnostic criteria
Well-differentiated NET	NET, Grade 1	<2 mitoses/2 mm^2 and/or Ki-67 <3%
	NET, Grade 2	2–20 mitoses/2 mm^2 and/or Ki-67 3–20%
	NET, Grade 3	>20 mitoses/2 mm^2 and/or Ki-67 >20%
Poorly differentiated NEC	Small cell NEC	>20 mitoses/2 mm^2 and/or Ki-67 >20% (often >70%), and small cell cytomorphology
	Large cell NEC	>20 mitoses/2 mm^2 and/or Ki-67 >20% (often >70%), and large cell cytomorphology

NEC, neuroendocrine carcinoma

Prior to 2017, well-differentiated PNETs were classified into two grades based on proliferation rates: low-grade (G1; Ki-67 index <3% or mitoses/mm^2 <2%) and intermediate-grade (G2; Ki-67 index 3-20% or mitoses/mm^2 2-20%). Tumours with high proliferation rates (G3; Ki-67 index >20 % or mitoses/mm^2 >20%) were uniformly classified as poorly differentiated high-grade neuroendocrine carcinomas (NECs).[25] However, it has since been recognised that not all G3 tumours are morphologically poorly differentiated. A subset—typically with Ki-67 indices in the 20-55% range—exhibits well-differentiated histological features, limited responsiveness to platinum-based chemotherapy and a prognosis that is comparatively better than that of poorly differentiated carcinomas.[26–28] This recognition led to the introduction of a separate G3 PNET category in subsequent versions of the WHO classification system, distinguishing tumours with high proliferation rates but well-differentiated morphology from poorly differentiated

NECs.[29] This revised prognostic stratification is supported by studies showing distinct survival outcomes amongst the four groups, with median overall survival (OS) rates of ~85 months for G1, ~67 months for G2 and ~51-54 months for G3 well-differentiated PNETs. Meanwhile, NECs exhibit the worst prognosis, with a median OS of ~11-36 months.[26,27,30] Thus, despite NECs retaining and/or expressing neuroendocrine features, they are biologically and clinically distinct from their PNET counterparts. In 2017, the term 'neuroendocrine neoplasm' was introduced by the WHO as an umbrella term encompassing all tumour grades.[29] For the purposes of this thesis, however, the term 'PNET' will specifically refer to well-differentiated G1-G3 tumours, as my studies did not include NECs.

1.1.1.3 Tumour staging

In addition to tumour grade, disease stage is another important prognostic factor that guides the management of patients with PNETs. The European Neuroendocrine Tumour Society (ENETS) initially proposed a Tumour-Node-Metastasis (TNM) staging system for PNETs in 2006.[31] Subsequently, the American Joint Committee on Cancer (AJCC) developed their own TNM staging system for PNETs in the 2010 AJCC Cancer Staging Manual (7th edition) **(Table 1.3)**.[32] This system was extrapolated from the staging system used for exocrine PDAC.[33] However, concerns regarding the validity of both systems were raised, particularly due to the ENETS classification's inability to discriminate effectively between early disease stages, and the AJCC 7th edition's low proportion of patients classified as stage III (indicating invasion of the coeliac or mesenteric vessels).[33–35] These issues reflect the distinct biological and growth characteristics of PNETs compared to PDACs. In response, the AJCC introduced a revised staging system specifically for PNETs in its 2017 Cancer Staging Manual (8th edition) **(Table 1.3)**.[36] This update aligns more closely with the ENETS definitions for T stage, while simplifying the classification by consolidating ENETS stages IIA and IIB into a unified stage II, and stages IIIA and IIIB into a single stage III. Validation studies across multiple centres have demonstrated that the AJCC 8th edition staging system offers improved discrimination of survival

outcomes compared to both the 7th edition and the original ENETS system.[37,38] Importantly, this staging system does not apply to high-grade, poorly differentiated NECs, which are staged according to the criteria set for exocrine PDAC.[39]

Table 1.3. Comparison of the AJCC 7th edition with the ENETS and AJCC 8th edition staging systems for PNETs

	AJCC 7th edition[32]	**ENETS[31] and AJCC 8th edition[36]**
T1	Limited to the pancreas, ≤ 2 cm in greatest dimension	Tumour limited to the pancreas, ≤ 2 cm
T2	Limited to the pancreas, > 2 cm in greatest dimension	Tumour limited to the pancreas, 2–4 cm
T3	Beyond the pancreas but without involvement of the superior mesenteric artery	Tumour limited to the pancreas, > 4 cm, or invading the duodenum or common bile duct
T4	Involvement of the celiac axis or superior mesenteric artery (unresectable tumour)	Tumour invades adjacent organs (stomach, spleen, colon, adrenal gland) or the wall of large vessels (coeliac axis or superior mesenteric artery)
N0	No regional lymph node metastasis	
N1	Regional lymph node metastasis	
M0	No distant metastasis	
M1	Distant metastasis* (M1a: metastasis confined to liver; M1b: metastasis in at least one extrahepatic site; M1c: both hepatic and extrahepatic metastases)	

AJCC 7th edition				**ENETS and AJCC 8th edition**			
Stage	**T**	**N**	**M**	**Stage**	**T**	**N**	**M**
IA	T1	N0	M0	**I**	T1	N0	M0
IB	T2	N0	M0	**II(A)****	T2	N0	M0
IIA	T3	N0	M0	**II(B)****	T3	N0	M0
IIB	T1-3	N1	M0	**III(A)****	T4	N0	M0
III	T4	Any N	M0	**III(B)****	Any T	N1	M0
IV	Any T	Any N	M1	**IV**	Any T	Any N	M1

*M1a, M1b and M1c are only used in the AJCC 8th edition.
**Stage II(A/B) and III(A/B) are only used in the ENETS system.

Although current treatment paradigms for PNETs are based on both the grade and stage of the disease, there are significant variations in clinical outcomes even amongst patients categorised within the same grade or stage. This variability complicates the development of personalised treatment strategies. Consequently,

there is an unmet need for enhanced prognostic and predictive biomarkers that can refine prognosis assessments and facilitate more tailored treatment decisions for individual patients.

1.1.2 Overview of the clinical management of PNETs

1.1.2.1 Surgical resection versus watchful waiting

Surgery remains the definitive curative approach for PNETs, with localised functional tumours requiring resection to manage hormonal symptoms and prevent metastasis, regardless of size. The decision to resect or monitor NF-PNETs is more nuanced and depends on their potential malignancy. This is based on the observation that many small low-grade PNETs exhibit indolent behaviour; thus, active surveillance may avoid the morbidity associated with pancreatic resection. Identifying reliable predictors of aggressive behaviour, however, remains challenging. The literature suggests that tumours >2 cm are associated with a increased risk of lymph node metastasis (ranging from 22% to 50%) and generally warrant surgical removal.[40]

Recent preliminary results from the Asymptomatic Small Pancreatic Endocrine Neoplasms (ASPEN) study—a prospective cohort study comparing active surveillance to surgery in 500 patients with asymptomatic NF-PNET measuring ≤2 cm—revealed that only 2% of the 406 patients undergoing surveillance experienced tumour progression.[41] An interim analysis from a smaller prospective study of 76 patients by the Dutch Pancreatic Cancer Group showed that tumour progression occurred in 11% of patients with NF-PNETs who opted for upfront surveillance rather than surgery.[42] Both studies suggest that a watch-and-wait strategy may be preferable for G1 and G2 NF-PNETs ≤2 cm, although the follow-up period in these analyses was limited. Nonetheless, a subset of patients with tumours below this size threshold may still harbour aggressive features, including metastases.[43] The challenge of reliably predicting indolent behaviour based on size alone continues to fuel debate over the optimal size cut-off for surgery.[44] In general, however, the

prevailing consensus from most expert society guidelines is that asymptomatic NF-PNETS >2 cm should undergo resection, while tumours 1–2 cm in size represent a grey area where resection can be considered depending on patient preference, comorbidities, tumour grade and access to follow up care.[45–47]

1.1.2.2 Cytoreductive surgery and hepatic-directed therapies

Patients who succumb to PNETs typically often do so due to liver failure caused by widespread hepatic metastases, which may be found in 40-60% of patients with NF-PNETs at the time of diagnosis.[13,48] Unlike other intra-abdominal malignancies, PNETs generally exhibit a slower growth pattern, allowing surgical metastatectomy to alleviate the morbidity associated with hormone oversecretion and potentially offer a survival benefit in selected cases.[49] Operative strategies typically include hepatic wedge resections and ultrasound-guided radiofrequency ablation for deeper tumours, while extensive hepatic lobectomies are avoided due to their high morbidity. Previously, it was suggested that the benefits of hepatic cytoreduction justified the risks only if at least a 90% reduction in tumour burden could be achieved.[50,51] However, more recent data suggests that a threshold of 70% may be sufficient, as these patients showed survival outcomes and biochemical response rates comparable to those who underwent more aggressive resections.[52,53] For patients in whom the extent of disease burden precludes achieving 70% cytoreduction, resection of the primary tumour may still confer a survival benefit. Nonetheless, data in support of this are derived from retrospective series that may be subject to selection bias.[18,54–56]

For patients who are not suitable candidates for surgery due to comorbidities or advanced disease extent, several hepatic-directed therapies are available to decrease metastatic burden and provide palliative symptom relief. These modalities leverage the fact that PNET liver metastases primarily draw their blood supply from the hepatic arteries, in contrast to healthy liver tissue, which is predominantly supplied by the portal system. Available transarterial therapies include transarterial

embolisation (TAE), transarterial chemoembolisation (TACE) and transarterial radioembolisation (TARE).[57]

TAE involves the administration of gel foam powder into the hepatic artery using an angiography catheter, a technique known as bland embolisation. TACE combines the delivery of chemotherapy directly to the tumour with the embolisation process, known as chemoembolisation. TARE entails the administration of radioactive isotopes, such as yttrium-90, that are tagged to glass or resin microspheres, which are then selectively targeted to the tumour. The response rates associated with these techniques, as measured by decreased symptom burden, improvement in hormone secretion, or radiographic regression, range from ~50-60%, even amongst patients with a high tumour burden. However, the impact on OS remains less definitive.[18,58,59]

1.1.2.3 Systemic therapies

For patients with unresectable metastatic disease, systemic medical therapies that have been used to control hormonal symptoms and stabilise tumour growth include biotherapies, such as somatostatin analogues (SSAs), as well as molecular targeted therapies, such as mechanistic target of rapamycin (mTOR) signalling inhibitors and receptor tyrosine kinase (RTK) inhibitors.[18,60] Cytotoxic chemotherapies (e.g, temozolomide with capecitabine or streptozocin) have been used in patients with progressive disease refractory to other therapies and/or rapidly progressive liver metastases with symptoms secondary to tumour bulk.[61] Platinum-based chemotherapy regimens (e.g., cisplatin or carboplatin) plus etoposide are typically used for PNECs, rather than PNETs.[62] Results of pivotal randomised trials evaluating systemic therapies in patients with NETs are detailed in **Table 1.4**.

Table 1.4. Selected key randomised trials of systemic treatments in NETs

Trial (Year)	Study arms		ORR %		PFS (months)		OS (months)	
	Treatment	Control	Treatment	Control	Treatment	Control	Treatment	Control
PROMID (2009)[63]†	**Octreotide** 30 mg IM every 4 weeks (n=42)	Placebo (n=43)	2.4	0	14.3*	6	84.7	83.7
RADIANT-3 (2011)[64]	**Everolimus** 10 mg PO o.d. (n=207)	Placebo (n=203)	5	2	11*	4.6	44	37.7
NCT00428597 (2011)[65]	**Sunitinib** 37.5 mg PO o.d. (n=44)	Placebo (n=59)	9.3	0	11.4	5.5	38.6	29.1
CLARINET (2014)[66]	**Lanreotide** 120 mg SC every 4 weeks (n=101)	Placebo (n=103)	-	-	NR*	18	-	-
NETTER-I (2017)[67]†	**^{177}Lu-DOTATATE** every 8 weeks plus **octreotide** LAR 60 mg every 4 weeks (n=116)	Octreotide LAR 60 mg every 4 weeks (n=113)	18	3	NR*	8.4	-	-
CABINET (2023)[68]††	**Cabozantinib** 60 mg PO o.d. (n=62)	Placebo (n=31)	18	6	11.4*	3	43.5	31
NETTER-II (2024)[69]††	**^{177}Lu-DOTATATE** plus 30 mg **octreotide** LAR every 8 weeks (n=151)	Octreotide LAR 60 mg every 4 weeks (n=75)	43	9.3	14.3*	8.5	-	-

† Trial limited to patients with small intestinal (midgut) NETs, but results have been extrapolated to PNETs.
†† Trial ongoing. Interim results from trial published as abstract supplement.
* Indicates statistically significant difference between control group. - Indicates data not reported.
IM, intramuscular; LAR, long-acting release; NR, not reached; o.d., once daily; ORR, objective response rate; OS, overall survival (median); PFS, progression-free survival (median); PO, per os (mouth); SC, subcutaneous

Although there is no clear consensus regarding the optimal sequence of therapy, SSAs are typically used as first-line therapy for metastatic unresectable well-differentiated PNETs given their favourable side-effect profile compared to molecular targeted therapies. For patients who develop progressive disease despite SSA therapy and are unsuitable for liver-directed therapy, options for systemic treatment include the mTOR inhibitor everolimus[64] and the RTK inhibitors sunitinib[65] and cabozantinib.[68] Of these, cabozantinib is the most recent targeted therapy to have demonstrated an improvement in median progression free survival (PFS) over placebo (11 months *vs* 3 months) in a randomised controlled trial of 290 patients with treatment refractory NETs, of whom 93 had PNETs **(Table 1.4)**.[68]

Peptide receptor radionuclide therapy (PRRT) offers an alternative for patients whose tumours progress on treatment with somatostatin analogues (SSAs) and

express somatostatin receptors (SSTRs), as confirmed through radiolabelled SSTR imaging. This modality utilises the overexpression of SSTRs on the surface of PNET cells to deliver targeted tumour radiotherapy with radiolabelled somatostatin analogues, such as 177Lu-DOTATATE.[70] The NETTER-1 randomised controlled trial, which focused on patients with progressive metastatic midgut NETs, demonstrated significant improvements in PFS (65.2% *vs* 10.8% at 20 months) and higher response rates (18% *vs* 3%) in patients treated with 177Lu-DOTATATE (with or without long-acting release [LAR] octreotide) compared to those receiving high-dose LAR octreotide alone.[67] Although the trial did not include patients with PNETs, its results formed the basis for US Food and Drug Administration (FDA) and European Medicines Agency (EMA) approval of 177Lu-DOTATATE PRRT for the treatment of SSTR-positive gastroenteropancreatic NETs, including PNETs. Recent interim results form the NETTER-II trial, predominantly involving patients with G2 and G3 PNETs, indicated that 177Lu-DOTATATE as first-line therapy improved PFS to 14.3 months compared to 8.5 months with octreotide LAR alone.[69] Despite these promising data, the drawbacks of PRRT include the requirement for tumour SSTR expression, the lack of widespread availability and a small but significant risk of acute myeloid leukaemia.[71]

While the aforementioned treatments have all been shown to prolong PFS, they are not curative and a beneficial impact on OS has not consistently been demonstrated. This underscores the need for more effective therapies and a better understanding of the molecular pathogenesis of advanced PNETs.

1.1.3 Multiple endocrine neoplasia type 1 (MEN1)

MEN1 is an inherited endocrine tumour syndrome with an estimated prevalence of 1 to 3 per 100,000 individuals.[72] It is characterised by the occurrence of primary hyperparathyroidism (PHPT), pancreatic and duodenal NETs (PD-NETs) and anterior pituitary adenomas, which are commonly referred to as the '3 Ps'.[73,74] Additionally, the spectrum of MEN1–related tumours has expanded as patients

have also been observed to develop, albeit less commonly, adrenocortical neoplasms, bronchial and thymic NETs and other non-endocrine tumours **(Figure 1.2)**.[75,76]

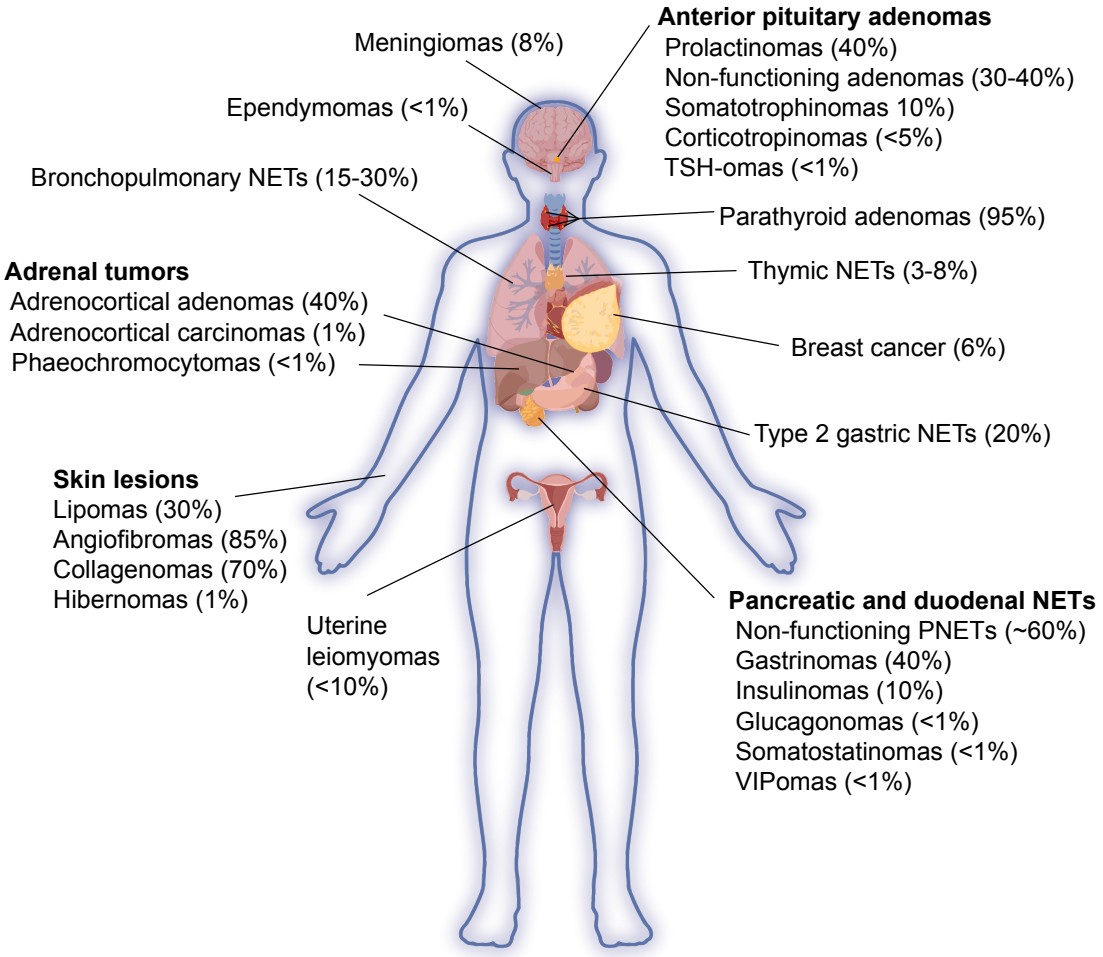

Figure 1.2. Overview of MEN1-related manifestations. Frequencies of individual tumour types are derived from Waguespack et al.[75] and Goudet et al.[77] and are reported in parentheses.

The majority of patients with MEN1 (~80%-90%) harbour a detectable germline pathogenic variant in the coding region of the *MEN1* gene on chromosome 11q13, which encodes menin, a ubiquitously expressed tumor suppressor protein.[74] Menin acts as nuclear scaffold protein that serves multiple roles including transcriptional regulation, genome stability, cell division, cell cycle control and epigenetic regulation.[74] Tumourigenesis in MEN1 is initiated when the remaining wild-type *MEN1* allele is inactivated (known as loss of heterozygosity) in predisposed somatic

cells, consistent with Knudson's 'two-hit' model of hereditary cancer, in which both alleles of a tumor suppressor gene must be affected to contribute to cancer development.[78] In MEN1, the first hit is the germline pathogenic variant and the second hit occurs somatically and typically involves large chromosomal deletions that include 11q13.[79] The syndrome is highly penetrant, such that >95% of *MEN1* pathogenic variant carriers develop manifestations by 50 years of age.[80] MEN1 follows an autosomal dominant pattern of inheritance; therefore, establishing the diagnosis in an individual patient has significant implications for family members, who may have a 50% risk of inheriting the pathogenic variant depending on their familial relationship to the proband.

Patients with MEN1 have a decreased life expectancy compared with that of the general population, predominantly due to malignant PNETs.[76,81] Furthermore, the development of synchronous or metachronous hormonally-active tumours can lead to substantial morbidity. To address this, international clinical practice guidelines (first published in 2001[72] and subsequently updated in 2012[73]) recommend an intensive regimen of surveillance, encompassing clinical, biochemical, and radiological evaluations beginning in childhood to facilitate early detection and treatment. Owing to the rarity and complexity of MEN1, it is recommended that such surveillance be coordinated by dedicated multidisciplinary teams with expertise in managing this syndrome. In the decade that has elapsed since the most recent iteration of the guidelines, several multicenter and large single-center cohort studies have furthered our understanding of the natural course and management of MEN1.[77,82,83] However, the prevalence of MEN1-related manifestations in children and adolescents is not well-characterised. Existing reports from this age group are typically from small cohorts at single institutions,[84–89] or in the case of larger multicenter series,[89,90] consist of historical cohorts of patients for whom screening was initiated late or before modern screening methods were available, likely leading to an underestimation of true incidence. Moreover, there is a a lack of consensus regarding the best management practices for MEN1-related manifestations, such as PHPT and NF-PNETs, in children and adolescents. Thus, there is a need for further

studies that focus on this age group. This is particularly important, becasuse the management of MEN1–related PNETs can be challenging due to their multifocal nature, which can be further complicated by the synchronous occurrence of both functioning and nonfunctioning tumours in the same patient.[18,19]

Similar to MEN1, MEN4, is also an autosomal dominant diorder, but is caused by germline pathogenic variants in the Cyclin-Dependent Kinase Inhibitor 1B (*CDKN1B*) gene, which encodes the cylin-dependent kinase inhibitor, $p27^{Kip1}$, a key regulator of cell cycle progression.[74] MEN4 closely resembles MEN1, although there are notable differences. PHPT in MEN4 typically presents at an older age compared to MEN1 and PD-NETs are less prevalent.[91] The incidence of MEN4 syndrome is reported to be 1.5-3.7% in patients with an MEN1-related phenotype.[74]

1.1.4 Genomic landscape of PNETs

Molecular subtyping with next-generation sequencing (NGS) technologies has been employed in the classification and treatment stratification of a number of solid-organ tumours and now plays a role in clinical practice in certain contexts.[92] For example, while 80% of breast cancers are defined as invasive ductal carcinomas based on pathological evaluation, in-depth molecular profiling has led to the classification of five distinct subtypes, each with different epidemiological risk factors, natural histories and responses to systemic and local therapies.[93,94] Despite the rarity of PNETs, which has posed challenges for conducting large-scale studies, important molecular profiling studies have been published over the past decade that have laid the groundwork for a more nuanced understanding of their molecular basis. These studies will be discussed in the sections below.

1.1.4.1 Insights gained from familial PNET syndromes

Approximately 10-15% of PNETs may occur as part of a complex hereditary syndrome, such as MEN1 or MEN4, von Hippel-Lindau disease (VHL),

neurofibromatosis type 1 (NF1) and tuberous sclerosis complex 1 and 2 (TSC1 and TCS2).[95] Up to 80% of patients with MEN1, 20% of patients with VHL, <10% of patients with NF1 and <1% of patients with TSC1/TSC2 will develop a PNET during their lifetime. Thus, MEN1 is the most common hereditary syndrome associated with an increased susceptibility to PNET development, as outlined above. The *VHL* gene is responsible for producing the protein pVHL, which forms a complex involved in the degradation of hypoxia-inducible factors (HIFs).[96] In the absence of functional pVHL, HIFs accumulate, leading to increased expression of genes that promote angiogenesis, cell proliferation, and survival. The *NF1* gene encodes neurofibromin, a negative regulator of the Rat Sarcoma (*RAS*) proto-oncogenes, the loss of which enhances RAS-dependent activation of the Mitogen-Activated Protein Kinase (MAPK) pathway and the Phosphoinositide 3-Kinase (PI3K)/Protein Kinase B (AKT)/mTOR pathway.[97] The *TSC1* and *TSC2* genes encode for the proteins hamartin and tuberin, respectively, which together form a complex that inhibits the mTOR signalling pathway.[98,99]

1.1.4.2 Molecular profiling of sporadic PNETs

Although the majority (~85-90%) of PNETs arise sporadically, studies of inherited PNET syndromes have provided valuable insights into the genes implicated in sporadic PNET development. Indeed, >40% of non-familial PNETs harbour somatic *MEN1* mutations,[100–102] while up to 25% have non-mutational *VHL* inactivation[103] and ~10% have been found to carry *TSC2* mutations.[100] With the increasing availability of high-throughput NGS technologies and multi-institutional collaborations, the past decade has seen a surge in research aimed at elucidating the molecular landscape of PNETs. Two early landmark studies in this field include a whole-exome sequencing (WES) study by Jiao et al.[100] and the whole-genome sequencing (WGS) study by Scarpa et al.,[34] both of primarily focused on G1 and G2 NF-PNETs. Jiao et al.[100] performed WES on 10 PNETs, followed by directed Sanger sequencing in a further 58 samples. In line with previous targeted sequencing studies, mutations in *MEN1* were identified in 44% of cases and in PI3K/AKT/mTOR

pathway genes in 15% of cases. This study also identified, for the first time, mutations in the chromatin remodelling genes Death-Domain Associated Protein (*DAXX*) and Alpha-Thalassemia/Mental retardation X-linked (*ATRX*), where were present in 25% and 17% of cases, respectively, and mutually exclusive.[100] Scarpa et al.[101] subsequently performed WGS in 160 PNETs (98 in a discovery cohort and 62 in a validation cohort), confirming a high incidence of somatic *MEN1* mutations in 37% of cases, followed by mutations affecting *ATRX/DAXX* in 34% and the PI3K/AKT/mTOR pathway genes, Phosphatase and Tensin Homolog (*PTEN*), *TSC1/2* and DEP Domain Containing 5 (*DEPDC5*), in 12% of cases. These findings reiterated the predominance of chromatin remodelling and mTOR signalling as key pathways implicated in the pathogenesis of PNETs. An unexpectedly high incidence of germline mutations (17%) was also found in patients lacking a family or personal history of cancer, in the DNA damage repair pathways genes MutY DNA Glycosylase (*MUTYH*), Checkpoint Kinase 2 (*CHEK2*) and Breast Cancer Gene 2 (*BRCA2*), as well as the known PNET susceptibility genes *MEN1*, *VHL* and *CDKN1B*.

The genomic landscape of functioning PNETs remains largely unexplored apart from insulinomas, which appear to have a unique genetic background compared to NF-PNETs. While somatic *MEN1* mutations appear to be rare in insulinomas (2%), the most common mutation (10-30%) involves a Threonine to Arginine substitution at codon 372 of the transcription factor gene Ying Yang 1 (*YY1*), enhancing its activity.[104–106] Because YY1 regulates mitochondrial activity and insulin/insulin-like growth factor signalling via the mTOR pathway, mTOR inhibitors may be beneficial for this subset of patients.

Based on the above findings, Scarpa et al.[101] proposed four main molecular pathways in which genetic alterations occur in NF-PNETs. These pathways, along with the involved genes are categorised as follows: 1) altered telomere length: *ATRX/DAXX*; 2) chromatin remodelling: SET Domain Containing 2 (*SETD2*) and Mixed Lineage Leukemia 3 (*MLL3*); 3) mTOR signalling: *TSC1*, *TSC2*, *PTEN* and *DEPDC5* and 4) DNA damage repair: *MUTYH*, *CHEK2* and *BRCA2*. *MEN1*

plays a role in each of these pathways, underlining its significance in the molecular framework of PNETs **(Figure 1.3)**.

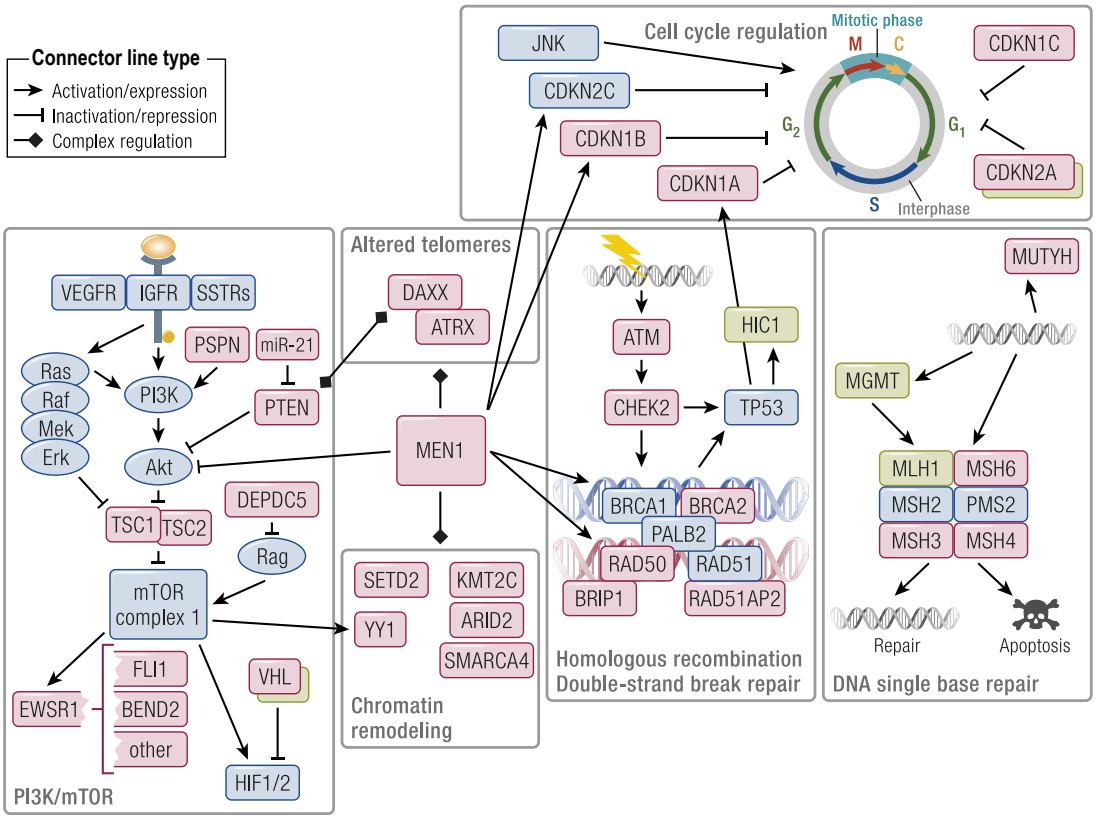

Figure 1.3. Overview of selected altered molecular pathways in PNETs. Genes with demonstrated germline or somatic alterations in the literature are shaded in red, and those inactivated via epigenetic mechanisms are shaded in green. MEN1 encodes menin, which acts as a hub gene that interacts with and modulates all core pathways. The inset legend shows the nature of interactions between molecules, pathways and/or processes, with activation represented by an arrow, inactivation represented by a blunt end line and complex regulation represented by a line ending in a diamond. Figure adapted from Mafficini and Scarpa.[103] Gene abbreviations not defined in the main text: Vascular Endothelial Growth Factor Receptor (*VEGFR*), Insulin Growth Factor Receptor (*IGFR*), Mitogen-Activated Protein Kinase Kinase (*MEK*), Extracellular Signal-Regulated Kinase (*ERK*), Forkhead Box Protein L1 (*FLI1*), BEN Domain Containing 2 (*BEND2*), EWS RNA Binding Protein 1 (*EWSR1*), Mixed Lineage Leukemia 3 (*MLL3*), AT-rich Interaction Domain 2 (*ARID2*), SWI/SNF, Matrix Associated, Actin Dependent Regulator of Chromatin, Subfamily A, Member 4 (*SMARCA4*), Cyclin Dependent Kinase Inhibitor 1A (*CDKN1A*), Cyclin Dependent Kinase Inhibitor 1C (*CDKN1C*), Cyclin Dependent Kinase Inhibitor 2A (*CDKN2A*), Jun N-terminal kinase (*JNK*), O-6-Methylguanine-DNA Methyltransferase (*MGMT*), MutS Protein Homolog 2 (*MSH2*), MutS Protein Homolog 6 (*MSH6*), Postmeiotic Segregation Increased 2 (*PMS2*), MutS Protein Homolog 3 (*MSH3*), MutS Protein Homolog 4 (*MSH4*) [Caption continues on next page...]

Figure 1.3. Overview of selected altered molecular pathways in PNETs. Ataxia Telangiectasia Mutated (*ATM*), Hypermethylated in Cancer 1 (*HIC1*), Partner And Localiser of BRCA2 (*PALB2*), RAD50 Double Strand Break Repair Protein (*RAD50*), RAD51 Recombinase (*RAD51*), RAD51 Associated Protein 1 (*RAD51AP1*) and BRCA1 Interacting Protein C-terminal Helicase 1 (*BRIP1*).

One of the major findings of the WGS and WES studies highlighted above is that PNETs have a low mutational burden (0.82 mutations per megabase)[101] when compared to other tumours such as PDAC (2.64 mutations per megabase).[107] Moreover, classical tumour suppressor genes and oncogenes, such as Tumour Protein P53 (*TP53*), Retinoblastoma (*RB1*) and Kirsten Rat Sarcoma Viral Oncogene Homolog (*KRAS*) are only very infrequently mutated PNETs, whilst >90% of PDACs harbour KRAS mutations.[107] This lack of oncogenic driver mutations suggest the presence of alternative pathogenic mechanisms in PNETs, such as epigenetic modifications.

1.2 Epigenetics

Epigenetics refers to processes that cause heritable changes in gene expression without altering the underlying DNA sequence.[108] In eukaryotic cells, chromosomal DNA is organised into a compact structure known as chromatin, which is composed of nucleosomes. These nucleosomes consist of 147 base pairs of DNA tightly coiled around a core of eight histone proteins (two each of H2A, H2B, H3, and H4). Chromatin transitions between two configurations: an open, transcriptionally active state called euchromatin, and a condensed, transcriptionally silent state known as heterochromatin. Dynamic changes to chromatin structure can be induced through a series of post-translational modifications, including methylation, acetylation, phosphorylation, ubiquitination, and sumoylation.[108] Positively charged lysine residues on the tails of histones can be neutralised via acetylation, thus weakening electrostatic interactions with negatively-charged DNA molecules. As a result, euchromatin assumes a sterically 'relaxed' structure that can more readily be accessed by DNA and RNA polymerases, as well as transcription factors. In contrast,

heterochromatin is highly dense and inaccessible to transcriptional machinery. Both DNA methylation and histone modifications contribute towards a complex network of chemical modifications made to DNA and histones that collectively dictate the transcriptional landscape within a cell.

1.2.1 Histone modifications

The epigenetic landscape is orchestrated by 'writers', 'readers' and 'erasers' **(Figure 1.4)**.[109] Writers are proteins that catalyse the deposition of epigenetic marks, such as methylation or acetylation, to the lysine or arginine residues found on the tails of histones. Acetylation of histone tails, particularly lysines 9 and 14 on histone H3 (H3K9 and H3K14, respectively) by histone acetyltransferases (HATs) is associated with euchromatin and gene activation. Methylation of histone tails by histone methyltransferases (HMTs) can repress or activate transcription, depending on the specific residue that is methylated and the number of methyl moieties attached. For example, whilst trimethylation of lysine 4 on histone H3 (H3K4me3) is associated with active gene transcription, di- and trimethylation of lysine 9 on histone H3 (H3K9me2/3) is associated with transcriptional silencing.[110] Acetylation of lysines not only alters chromatin structure but also creates docking sites for reader proteins that are equipped with specialised motifs to recognise these modifications. This interaction facilitates the assembly of transcription factors at the enhancer and promoter regions of genes.

Reader proteins often feature specific domains, such as bromodomains, chromodomains, plant homeodomain (PHD) fingers, or tudor domains, enabling the precise identification and binding to post-translationally modified histones.[111] In addition to histone modifications, reader proteins such as those with methyl-CpG-binding domains (MBD) specifically recognise methylated CpG islands within the DNA sequence, facilitating the recruitment of additional proteins that contribute to the compaction of chromatin and further gene silencing.[112]

Epigenetic erasers, such as histone deacetylases (HDACs) and histone demethylases (HDMs), remove acetylation and methylation marks from histones, respectively, highlighting the reversible nature of epigenetic marks **(Figure 1.4)**.[109]

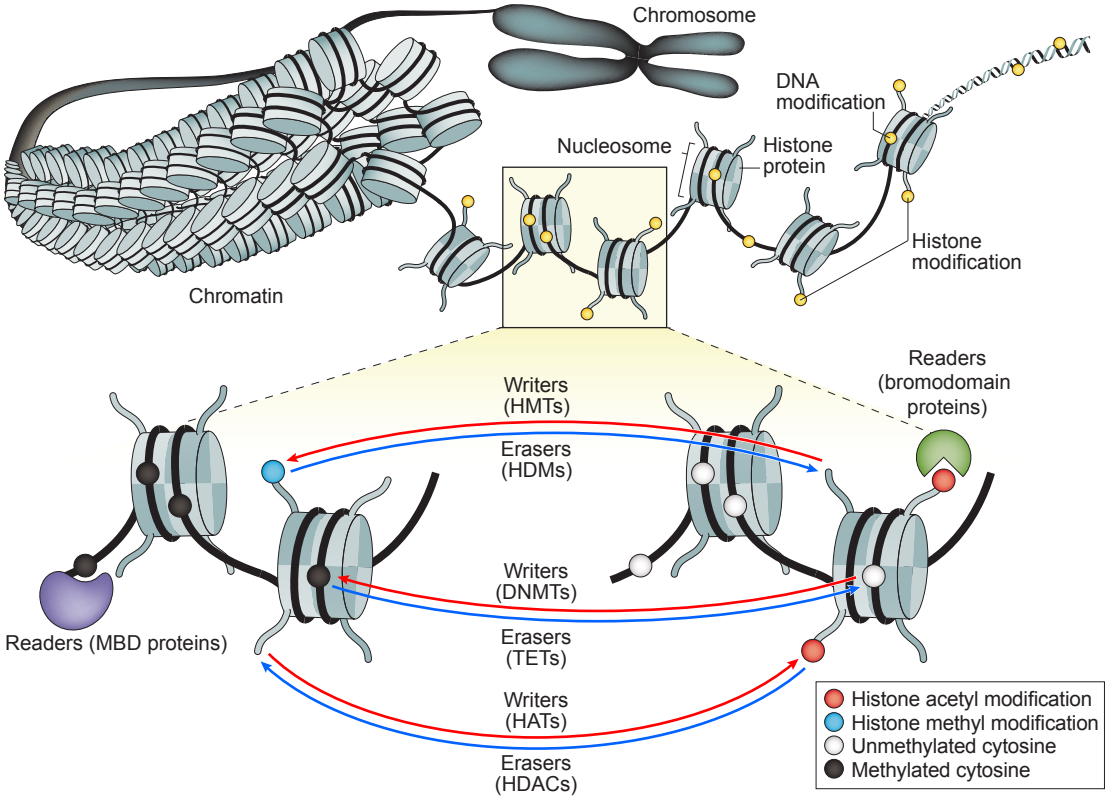

Figure 1.4. Overview of epigenetic modifications. A 147 base pair (bp) segment of DNA is coiled around a core of eight histone proteins, compacting the genome into nucleosomes, which further organise into chromatin and chromosomes. Specific covalent modifications (depicted as yellow circles) on both histone and DNA elements regulate DNA's accessibility to transcription factors and other regulatory proteins. These covalent modifications are applied by epigenetic 'writers', including histone lysine methyltransferases (HMTs), histone acetyltransferases (HATs), and DNA methyltransferases (DNMTs). The modifications are then recognised by 'readers', such as methyl-CpG-binding domain (MBD) proteins for DNA and proteins such as bromodomain-containing proteins for histone modifications. These marks can be reversed by 'erasers', including histone demethylases (HDMs), histone deacetylases (HDACs), and the ten-eleven translocation (TET) family of 5-methylcytosine oxidases. Figure adapted from Jones et al.[111]

1.2.2 DNA methylation

DNA methylation is the most extensively studied epigenetic modification in humans, entailing the transfer of a methyl group from S-adenosylmethionine to the 5'-carbon of cytosine residues, typically within cytosine-guanine (CpG) dinucleotide sequences.[113] This modification results in the formation of 5-methylcytosine (5mC) which is responsible for recruiting transcriptional repressors to DNA promoters, and/or inhibiting transcriptional factor binding, ultimately silencing gene expression, usually of CpG dinucleotides, which can subsequently be removed by ten–eleven translocation (TET) enzymes and base excision repair. The DNA methyltransferase (DNMT) enzymes DNMT3A and DNMT3B mediate de novo DNA methylation patterns, which are maintained by DNMT1.[114,115] The recently discovered TET enzymes—TET1, TET2 and TET3—directly oppose the actions of DNMTs and are responsible for the demethylation process.[116] These enzymes catalyse the conversion of 5mC to 5-hydroxymethylcytosine (5hmC), which is a critical first step in a series of reactions that can further oxidise 5hmC into intermediates such as 5-formylcytosine (5fC) and 5-carboxylcytosine (5caC). These intermediates can eventually be restored to an unmodified or hypomethylated cytosine state through the base excision repair pathway, effectively opposing the methylation effects imparted by DNMTs. The majority of CpGs are clustered in regions termed 'islands' that are located near transcription start sites at approximately 70–80% of gene promoters.[117] Methylation of these regions functionally silences the promoter and its corresponding gene by precluding binding of transcription machinery, or by recruiting MBD proteins that interact with repressive histone-modifying enzymes **(Figure 1.4)**.[118]

1.2.3 Epigenetic dysregulation in PNETs

Although sporadic PNETs are relatively mutationally silent, the most commonly mutated genes, *MEN1*, *ATRX* and *DAXX*, are involved in the epigenetic processes of histone modification and chromatin remodelling.[100,101] For example, menin directly

interacts with the HMTs mixed-lineage leukaemia 1 and 2 (MLL1 and MLL2), which are encoded by Lysine Methyltransferase 2A and B (*KMT2A and KMT2B)*, respectively. Both MLL1 and MLL2 catalyse the addition of a methyl group to lysine 4 of histone protein H3, forming the active histone mark H3K4me3 and open chromatin.[119] This results in the increased transcriptional activity of *CDKN2C* and *CDKN1B*, which encode critical regulators of the cell cycle.[120] Menin is also known to inhibit the activity of the oncogenic transcription factor JunD, by recruiting HDAC complexes to JunD target sites and removing activating acetyl marks.[121] ATRX and DAXX interact to form a chromatin-remodelling complex that deposits histone H3.3-containing nucleosomes at telomeric chromatin, a process that is important for maintaining genomic stability and proper telomere structure.[122] Loss of this pathway enables a repeat process known as alternative lengthening of telomeres (ALT), which allows cancer cells to maintain telomere length without the telomerase enzyme, contributing to their immortality by using homologous recombination to extend telomeres. Together, these findings suggest that the dysregulation of epigenetic mechanisms play a role in PNET development.

Recent studies have begun to reveal the complex epigenetic landscape associated with specific PNET subtypes. For instance, using deep bisulfite sequencing, Karakose et al.[123] uncovered aberrant methylation patterns in human insulinomas within the 11p15.5-p15.4 imprinted region of chromosome 11, a region known for its involvement in other disorders characterised by dysregulated β-cell function, such as Beckwith-Wiedemann Syndrome and Silver-Russell Syndrome.[124] Compared to normal human β-cells, the authors observed that insulinomas consistently exhibit hypermethylation at typical β-cell transcription factor binding sites, rendering them poorly accessible to transcription factors, such as pancreatic and duodenal homeobox 1 (PDX1), that normally regulate insulin gene expression. These epigenetic changes lead to reprogramming of the transcriptional machinery in insulinomas, with the sustained activation of alternative signalling pathways, prominently driven by nuclear factor of activated T-cells (NFAT) transcription factors, that drive insulin (*INS*) gene

expression. This aberrant transcriptional activation circumvents the usual regulatory networks, leading to uncontrolled insulin production that is typical of these tumours.

In addition to DNA methylation, studies have also investigated aberrant patterns of histone modifications in PNETs. Cejas et al.[125] utilised chromatin immunoprecipitation with next-generation sequencing (ChIP-seq) to characterise histone marks in NF-PNETs, focusing on acetylated histone H3 at lysine 27 (H3K27Ac), an active enhancer- and promoter-associated mark.[126–128] By mapping the genome-wide binding patterns of H3K27ac at super-enhancers—regulatory regions crucial for cell identity and function that are characterised by high levels of H3K27ac and an extensive presence of transcriptional co-activators[129]—the authors identified three distinct NF-PNET subtypes. Type A tumours exhibited strong H3K27ac enrichment at the Aristaless-Related Homeobox (*ARX*) and Iroquois Homeobox 2 (*IRX2*), both of which are characteristic of α-cell lineage, and were associated with poorer prognosis. Conversely, Type B tumours showed strong H3K27ac binding at the *PDX1* locus, indicative of β-cell lineage, and correlated with a more favourable prognosis. Type C tumours were a mixed or intermediate category, with enrichment of H3K27ac at both *ARX* and *PDX1* loci.[125] This aberrant enhancer activity suggests that histone acetylation, alongside DNA methylation, may play key roles in the dysregulation of gene expression seen in PNETs.

1.2.4 Bromodomain and extra-terminal domain proteins

Epigenetic readers of acetylated lysine residues do so via an evolutionarily conserved protein module known as a bromodomain.[130] The human genome contains 61 unique bromodomains encoded in 46 proteins, which can be categorised into eight distinct families (I-VIII) based on sequence homology **(Figure 1.5**). The bromodomain and extra-terminal (BET) domain family, which are in family II, are among the best characterised bromodomain-containing (BRD) proteins and include the members BRD2, BRD3, BRD4, and BRDT.[130]

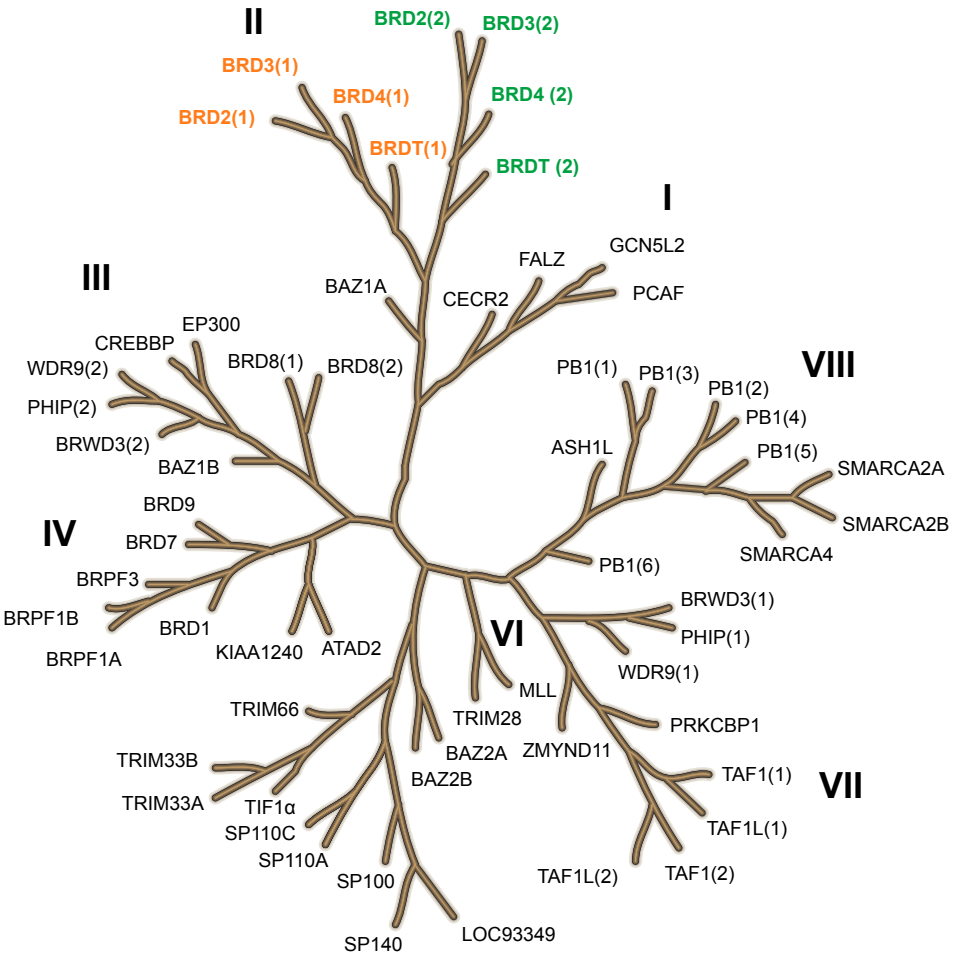

Figure 1.5. Phylogenetic tree of the human bromodomain family. Roman numerals (I–VIII) indicate the major structural classes of bromodomain-containing proteins. Bromodomains BD1 and BD2 of the BET proteins, which are in family II, are highlighted in orange and green text, respectively. For proteins with multiple bromodomains, the domains have been numbered starting from the N-terminus and the number is shown in parentheses. Figure adapted from Filippakopoulos et al.[131] Abbreviations not defined in the main text: ASH1 like histone lysine methyltransferase (ASH1L), ATPase family AAA domain containing 2 (ATAD2), Bromodomain adjacent to zinc finger domain protein (BAZ1), Bromodomain and PHD finger containing (BRPF), BRD and ring domain 3 (BRWD3), Bromodomain testis associated (BRDT), Cat eye syndrome chromosome region, candidate 2 (CECR2), CREB binding protein (CREBBP), E1A binding protein p300 (EP300), Foetal Alzheimer antigen (FALZ), General control non-depressible 5-like 2 (GCN5L2), P300/CBP-associated factor (PCAF), Plant homeodomain finger protein (PHIP), Protein polybromo-1 (PB1), Protein kinase C binding protein 1 (PRKCDBP1), SP100 nuclear antigen (SP100), SP110 nuclear body protein (SP110), SP140 nuclear body protein (SP140), SWI/SNF related, matrix associated, actin dependent regulator of chromatin subfamily A (SMARCA), TATA-box binding protein associated factor 1 (TAF1), Taf1 like (TAF1L), Transcriptional intermediary factor 1 alpha (TIF1α), Tripartite motif containing (TRIM), Tumour protein p53 inducible nuclear protein 1 (TP53INP1), WD repeat domain 9 (WDR9), Zinc finger MYND-type containing 11 (ZMYND11).

Each bromodomain consists of a 110 amino acid chain that arranges into a structure of four left-handed α-helices (αA, αB, αC, and αZ), interconnected by two loops known as the ZA and BC loops **(Figure 1.6)** These loops create a significant hydrophobic cavity that serves as the binding site for acetylated lysine residues, such as those found on H3K27ac.[131,132]

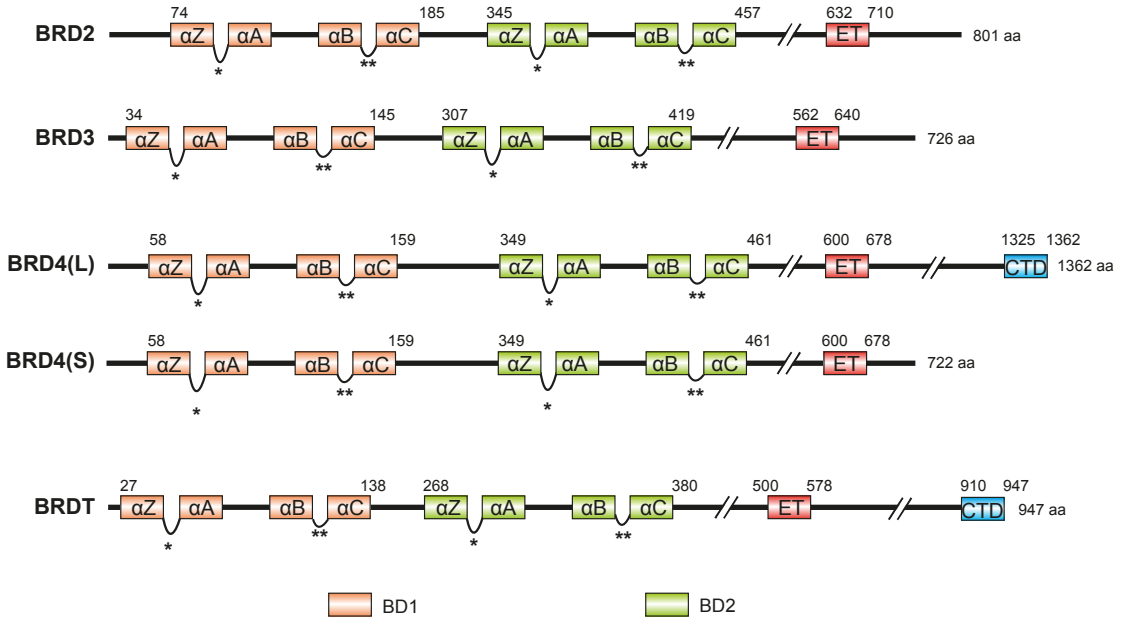

Figure 1.6. Domain organisation of human BET family members. Numbers indicate the amino acid (aa) positions of key functional domains in individual proteins. BET bromodomains BD1 (orange) and BD2 (green) are each composed of 4 α-helices (αZ, αA, αB, and αC) and 2 loops (a ZA loop indicated by * and a BC loop indicated by **). Each BET protein (BRD2, BRD3, BRD4, and BRDT) contains BD1 and BD2 at their N-terminal end and an extra-terminal (ET) domain located at the C-terminal end. BRD4 exists as two isoforms: a long isoform (BRD4(L)), which comprises the complete protein, and a short isoform (BRD4(S)), which corresponds to an alternative splicing variant lacking exons 12–20. Only BRD4(L) and BRDT possess a C-terminal domain (CTD). Figure adapted from Bechter et al.[133]

BET proteins are ubiquitously expressed in all tissues, except for BRDT, whose expression is restricted to the testis, where it plays a vital role in spermatogenesis.[134] BET proteins are characterised by two tandem bromodomains at their N-terminus: BD1 and BD2. They also feature an extra-terminal (ET) domain at their C-terminus, significant for its role in transcriptional activation and chromatin remodelling **(Figure 1.6)**.[135] This domain interacts with various chromatin-modifying enzymes,

including the histone demethylase Jumonji domain-containing protein 6 (JMJD6),[136] methyltransferase nuclear SET domain-containing protein 3 (NSD3),[137] and elements of the BRG1/BRM-associated factor (BAF) complex such as SWI/SNF related, matrix associated, actin dependent regulator of chromatin subfamily A, member 4 (SMARCA4)[138] and chromodomain helicase DNA binding protein 4 (CHD4)[137] through a conserved hydrophobic groove.[135] These interactions are crucial for recruiting BRD4 to chromatin, which facilitates further chromatin remodelling, leading to a transcription-permissive environment. The long isoform of BRD4 (BRD4L) and BRDT additionally contain C-terminal domains (CTD), which serve as docking sites for various transcriptional co-activators and regulatory proteins.[139]

Once bound, BET proteins have multifaceted roles in the regulation of gene transcription. For example, BRD2 is involved in cell cycle progression, through the activation of cell cycle regulatory genes that harbour E2F transcription factor binding sites, such as cyclin A.[140] BRD3 has overlapping functions with BRD2 and also interacts with the acetylated transcription factor GATA1 to regulate target erythroid genes.[141] Meanwhile, BRD4 associates with the positive transcription elongation factor b (P-TEFb), as part of a multiprotein complex that activates RNA polymerase II (RNA Pol II)-mediated transcriptional elongation.[142] BRD4 is also the most extensively studied BET family member in oncology research, as it is particularly enriched at the promoter and enhancer regions of oncogenes such as *MYC*.[143]

1.2.4.1 BET protein inhibition as a treatment for PNETs

Overexpression of BET family members has been observed in solid-organ cancers such as gastric carcinoma,[144] PDAC,[145] and hepatocellular carcinoma;[146,147], and BET protein inhibition with epigenetic modifier compounds has shown promising preclinical efficacy. However, the expression and significance of BET proteins in human PNETs has not yet been characterised. Nonetheless, the BET inhibitors JQ1 and CPI203 have shown *in vitro* and *in vivo* efficacy in preclinical PNET models, suggesting that BET proteins are implicated in PNET tumourigenesis and

that BET inhibition may provide a novel treatment for PNETs in the clinic.[60,148] However, the poor bioavailability and short half-lives of JQ1 and CPI203 render them unsuitable candidates for clinical translation.[149] An alternative BET inhibitor, I-BET151 (also known as GSK1210151A), has been shown to possess superior pharmacokinetic (PK) properties and a longer half-life compared to JQ1 that would make it potentially suitable for clinical use.[150] First generation BET inhibitors (e.g., JQ1, CPI203 and I-BET151) show equal binding affinity for BD1 and BD2 of each BET protein. Although dual-BD BET inhibitors are currently being evaluated in early-phase clinical trials for haematological and solid-organ malignancies, reports of side effects and short-lived efficacy may limit their therapeutic potential.[151]

It has recently been reported that BD1 and BD2 of the BET proteins have distinct functions with differential effects on transcription and cellular phenotypes.[152–155] Therefore, it has been proposed that selective targeting of one of the two bromodomains may mitigate the dose-related toxicities observed with dual-BD BET inhibitors, while maintaining therapeutic efficacy. While the acetyl-lysine binding pockets of BD1 and BD2 are highly conserved (with ~95% sequence similarity), crucial residue differences between them have provided the structural basis for the design of potent next-generation BD1- and BD2-selective inhibitors.[152,156–158] The efficacy of these compounds, however, and the biological implications of domain-specific BET inhibition in PNETs are unknown.

1.3 Thesis objectives

The goal of my thesis is to explore the presentation and treatment outcomes of MEN1-associated tumours in children and adolescents, and also to then investigate current and next-generation BET inhibitors to elucidate their potential therapeutic utility for PNETs in patients with or without MEN1. The specific objectives are to:

1. **Investigate the clinical presentation and treatment outcomes of MEN1-associated endocrine tumours, including PNETs, in children and adolescents.**
2. **Elucidate the expression and clinical relevance of BET family proteins in PNETs.**
3. **Evaluate the efficacy of the current-generation dual-BD BET inhibitor, I-BET151, both *in vitro* and *ex vivo* in PNET models.**
4. **Compare the therapeutic efficacy of next-generation BD1- and BD2-selective BET inhibitors with I-BET151.**
5. **Characterise the transcriptomic and epigenomic alterations induced by selective and dual BD inhibition in PNET cell lines *in vitro*.**

2

Methods

Chapter-specific table of contents

2.1 Multiple endocrine neoplasia type 1 (MEN1) paediatric patient cohort study 32
2.1.1 Ethics approval 32
2.1.2 Study population 32
2.1.3 Surveillance screening 33
2.1.4 Data collection 35
2.2 Histology and immunohistochemistry 36
2.2.1 Medical University of Vienna PNET samples 36
2.2.2 Sectioning and mounting 36
2.2.3 Deparaffinization and rehydration 36
2.2.4 Antigen retrieval and endogenous peroxidase blocking 37
2.2.5 Antibody staining 37
2.2.6 Dehydration 38
2.2.7 Haematoxylin and eosin (H&E) staining 38
2.2.8 Image acquisition and Qupath software analysis . . . 39
2.3 *In vitro* experiments 40
2.3.1 Cell lines 40
2.3.2 Cell counting 41
2.3.3 Epigenetic inhibitors 42
2.3.4 Epigenetic inhibitor screen 42
2.3.5 Proliferation time-course studies 43
2.3.6 Dose-response curves 44
2.3.7 Drug synergy studies 45
2.3.8 Drug washout studies 46
2.3.9 Apoptosis assays 47
2.3.10 Crystal violet assays 48
2.3.11 Propidium iodide (PI) cell cycle analysis 49

2.3.12 Quantitative real-time PCR (qPCR) 51
2.3.13 Western blotting 52
2.4 Next-generation sequencing and bioinformatics 54
2.4.1 RNA sequencing (RNA-seq) of BON1 PNET cells . . 54
2.4.2 RNA-seq of human PNET samples 58
2.4.3 Thiol(SH)-linked alkylation for the metabolic sequencing of RNA (SLAM-seq) 60
2.4.4 Chromatin immunoprecipitation with next-generation sequencing (ChIP-Seq) 66
2.5 Mouse studies 74
2.5.1 Ethics approval 74
2.5.2 Housing and animal husbandry 74
2.5.3 Mouse strains 74
2.5.4 Mouse genotyping 75
2.5.5 Histology and immunofluorescence 77
2.5.6 *Ex vivo* neoplastic mouse islet drug studies 78
2.6 Data visualisation 80
2.7 Statistical analysis 80

2.1 Multiple endocrine neoplasia type 1 (MEN1) paediatric patient cohort study

2.1.1 Ethics approval

This was an international cohort study that was approved by each participating centre's local institutional review board (IRB). More specifically, for the UK-based data, protocols approved by the Multi-Research Ethics Committee (MREC/02/2/93) were used in addition to a protocol approved under the audit and service improvement provision from the Oxford University Hospitals NHS Foundation Trust. Retrospective data collection for this study were additionally approved by IRBs at the Mayo Clinic (#24-003334) and the Medical University of Vienna (#1053/2013).

2.1.2 Study population

Patients with MEN1 who were evaluated and treated at five European and North American centres (University of Oxford, UK; Mayo Clinic, Rochester, USA;

University of Cambridge, UK; Great Ormond Street Hospital for Children, UK; and Medical University of Vienna, Austria) were identified through retrospective review of patent records. The study protocol was approved by local institutional review boards. The diagnosis of MEN1 was based on established criteria that included the presence of a: 1) pathogenic germline *MEN1* variant; 2) ≥2 MEN1-associated endocrine tumours; or 3) at least 1 MEN1-related tumour in a patient with a first-degree relative with MEN1.[73] Patients ≤35 years of age were selected to maximise the likelihood of obtaining childhood data from medical records that would contain information from annual surveillance programs of combined clinical, biochemical, and radiological screening, in accordance with current clinical practice guidelines.[73]

2.1.3 Surveillance screening

Surveillance screening for MEN1 manifestations at each of the five centres participating in the study included annual measurement of serum calcium, parathyroid hormone (PTH), pancreatic and duodenal neuroendocrine tumour (PD-PNET) markers (gastrin, glucagon, pancreatic polypeptide, and chromogranin A) and pituitary tumour markers (prolactin and IGF-1) beginning from ≥5 to 10 years of age. Pituitary-directed magnetic resonance imaging (MRI) of the head was also obtained every 2-3 years beginning at ages 5 to 10 years, and annual abdominal MRI, computed tomography (CT) and/or endoscopic ultrasound (US) was performed from ≥10 years of age. Chest CT scans, obtained every 1-2 years, were commenced from ≥15 years of age. Definitions of each MEN1 manifestation are provided in **Table 2.1**.

Table 2.1. Screening protocol and definitions of MEN1 manifestations

MEN1 manifestation	Criteria for diagnosis
PHPT	Defined as a concomitant elevation in serum calcium with an elevated or inappropriately normal PTH level. **Persistent PHPT:** defined as hypercalcaemia with raised or inappropriately normal PTH levels within 6 months of surgery. **Recurrent PHPT:** defined as a return of hypercalcaemia with raised or inappropriately normal PTH levels after a 6-month period of eucalcaemia.
PD-NETs	Diagnosed based on histology (if available) and/or detection of ≥ 1 lesion on two or more sequential abdominal imaging studies (i.e., CT, MRI, and/or EUS). **Insulinoma:** diagnosis established in the setting of an inappropriately high serum insulin or C-peptide concentration during a spontaneous or induced episode of hypoglycaemia. **NF-PNET:** diagnosed in the absence of a clinical syndrome of hormone hypersecretion. **Gastrinoma:** diagnosed when fasting hypergastrinaemia is present with confirmed positive immunohistochemical staining for gastrin.
Pituitary adenomas	Diagnosed if a lesion is detected on pituitary-directed MRI on at least two sequential imaging studies. **Macroadenoma:** defined as a pituitary adenoma > 1 cm in maximal dimension. **Microadenoma:** defined as a pituitary adenoma < 1 cm in maximal dimension. **Prolactinoma:** presence of an MRI-identifiable pituitary tumour with an elevated serum prolactin (macroprolactin excluded). **Non-functioning pituitary adenoma:** presence of an MRI-identifiable pituitary tumour in the absence of biochemical evidence of hormonal hypersecretion. **Somatotrophinoma:** presence of an MRI-identifiable pituitary tumour with elevated serum IGF-1 levels and/or an OGTT showing lack of growth hormone suppression.

Continued on next page

Table 2.1. Screening protocol and definitions of MEN1 manifestations (Continued)

MEN1 manifestation	Criteria for diagnosis
	Corticotrophinomas: presence of an MRI-identifiable pituitary tumour with biochemical evidence of hypercortisolism and suppression of corticotrophin on a high dose dexamethasone suppression test.
Adrenal tumours	Present on $\geq$ 2 consecutive imaging studies and/or on histology (if available). Functionality was determined by biochemical testing (e.g., plasma renin and aldosterone concentrations, low dose dexamethasone suppression test, urinary catecholamines and/or metanephrines).
Bronchial carcinoids	Present on $\geq$ 2 consecutive imaging studies, and/or on histology (if available).
Thymic carcinoids	Present on $\geq$ 2 consecutive imaging studies, and/or on histology (if available).
Malignancy	Presence of involved lymph nodes or distant metastasis seen on imaging and/or on histopathology.
Cutaneous manifestations	Diagnosed based on physical examination for subcutaneous lipomas, facial collagenomas, and angiofibromas.

CT, computed tomography; EUS, endoscopic ultrasound; IGF-1, insulin-like growth factor-1; MRI, magnetic resonance imaging; NF-PNET, non-functioning pancreatic neuroendocrine tumour; OGTT, oral glucose tolerance test; PHPT, primary hyperparathyroidism; PTH, parathyroid hormone

2.1.4 Data collection

Baseline demographics, age of MEN1 diagnosis and date of genetic testing (if performed) were recorded. For patients who underwent genetic testing, genotype was reported according to the *MEN1* reference sequence NM_130799 using Human Genome Variation Society (HGVS) nomenclature. For each MEN1 manifestation detected at $\leq$ 18 years of age, the date of diagnosis, results of biochemical testing and imaging, treatments received, histopathological findings (if applicable), and disease status at last follow-up were ascertained.

2.2 Histology and immunohistochemistry

2.2.1 Medical University of Vienna PNET samples

Formalin-fixed paraffin-embedded (FFPE) tumour blocks from 53 patients with PNETs who underwent surgical resection were obtained from Dr Andreas Selberherr, Head of the European Neuroendocrine Tumour Society (ENETS) Center of Excellence Vienna, through a material transfer agreement (MTA) with the Medical University of Vienna. Three patients had MEN1-related PNETs while the remainder had sporadic tumours. ENETS stages IIA and IIB were not subdivided, and neither were stages IIIA and IIIB. Therefore, metastatic tumours were considered to be stage III and IV. Details regarding the samples are presented in Chapter 4, in **Table 4.1** on page 105. Prior to sectioning, blocks were stored at 4°C.

2.2.2 Sectioning and mounting

FFPE blocks were trimmed and sectioned into serial sections (5 μm thick) using a Leica RM2255 rotary microtome (Leica Biosystems, Wetzlar, Germany). Sections were mounted on Superfrost™ Plus glass slides (Thermo Fisher Scientific, Paisley, UK) and dried at 37°C overnight.

2.2.3 Deparaffinization and rehydration

Sections were deparaffinized by washing in Histo-Clear® solution (National Diagnostics, Summerville, NJ, USA) for 5 minutes at room temperature, followed by two additional washes of 3 minutes each. The slides were then rehydrated in graded ethanols (100% → 100% → 95% → 95% → 80% → 80%) for 3 minutes each at room temperature, after which they were washed in distilled water (dH_2O).

2.2.4 Antigen retrieval and endogenous peroxidase blocking

Formalin fixation typically results in the formation of methylene bridges that cross-link proteins and mask epitopes, making them inaccessible to antibody binding.[159] Heating the tissue sections in a citrate buffer under high pressure (e.g., in an autoclave) reverses these cross-links by inducing thermal energy that breaks the methylene bridges. This retrieval of antigens restores the ability of antibodies to bind effectively, enhancing the specificity and sensitivity of immunodetection. I performed antigen retrieval by heating slides to 121°C for 15 minutes in 10 mM citrate buffer (pH 6.0), using an Osprey 40L benchtop autoclave (LTE Scientific, Oldham, UK). After cooling down to room temperature, the sections were permeabilised in 1% Triton-X in PBS for 10 minutes. To block endogenous peroxidase, which if left active, could lead to non-specific staining by reacting with chromogens in the absence of target antigen binding, sections were incubated in 3% hydrogen peroxide (Sigma Aldrich) for 10 minutes. Following this, slides were rinsed with dH_2O to remove any residual hydrogen peroxide and washed twice in Tris-buffered saline with 0.1% Tween®-20 detergent (TBS-T) for 10 minutes each time while gently rocking.

2.2.5 Antibody staining

For each antibody, four slides per FFPE block (at least 40 μm apart) were selected for staining. Tissue sections were encircled with a hydrophobic PAP marking pen to reduce the surface area for antibody binding. Slides were then incubated in blocking solution (10% goat serum in PBS) for 30 minutes at room temperature. Subsequently, 100 μL of primary antibodies diluted in blocking serum (according to the concentrations shown in **Table 2.2**) were added to each section and the slides were incubated in a humidified chamber overnight at 4°C. The following day, the slides were washed twice for 10 minutes with TBS-T and then incubated with 100 μL of hydrogen peroxidase-conjugated secondary goat anti-rabbit IgG antibodies (Jackson ImmunoResearch, West Grove, PA, USA) diluted 1:200 in TBS-T for 1

hour at room temperature. Slides were again washed in TBS-T twice for 10 minutes, after which they were developed using the 3,3'-diaminobenzidine (DAB) chromogen (Vector Labs, Peterborough, UK) for 5 minutes, followed by counterstaining with haematoxylin QS (Vector Labs) for 30 seconds.

2.2.6 Dehydration

The slides were washed in running tap water and dehydrated by immersing in graded ethanol solutions (80% → 95% → 95% → 100% → 100%) for 3 minutes each, followed by two 3-minute Histo-Clear® washes and a final 3-minute xylene wash. Coverslips were mounted onto the sections using VectaMount™ medium (Vector Labs), which was left to harden overnight before the slides were imaged.

Table 2.2. List of primary antibodies used for immunohistochemistry

Antibody	Species	Catalogue no.	Dilution	Source
Anti-BRD2	Rabbit	A302-583A	1:100	Bethyl Laboratories Inc., Montgomery, TX, USA
Anti-BRD3	Rabbit	HPA051830	1:100	Atlas Antibodies, Stockholm, Sweden
Anti-BRD4	Rabbit	ab128874	1:100	Abcam, Cambridge, UK
Anti-synaptophysin	Rabbit	ab32127	1:500	Abcam, Cambridge, UK

2.2.7 Haematoxylin and eosin (H&E) staining

H&E-stained slides were prepared from 4 μm thick sections that were cut adjacent to the sections used for antibody staining. The rehydration steps were identical

to those described in Section 2.2.3. Following rehydration, slides were washed with dH_2O, stained with haematoxylin QS for 45 seconds, washed in running tap water for 10 minutes, and rinsed in dH_2O. The slides were then dipped in 95% ethanol, followed by staining with 0.5% Eosin Y (Sigma Aldrich) mixed with 0.25% glacial acetic acid (Scientific Laboratory Supplies, Nottingham, UK) for 7 minutes. Excess stain was removed by dipping the slides in 70% ethanol. The slides were then washed in running tap water and dehydrated by immersing in graded ethanol solutions (95% → 95% → 100% → 100%) for 3 minutes each, followed by two 5-minute Histo-Clear® washes and a final 5-minute xylene wash. Coverslips were mounted onto the sections using VectaMount™ medium, and the slides were left to dry overnight before being imaged.

2.2.8 Image acquisition and Qupath software analysis

Digital images of the stained sections were visualised using an Eclipse E400 microscope (Nikon) and captured at 10x and 40x magnification with a DXM1200 digital camera (Nikon) and NIS-Elements BR software (v2.30, Nikon). Four randomly-selected 40x high-power field (HPF) images (covering an area of approximately 0.25 mm^2 each) from tumour areas and four randomly-selected HPF images of surrounding exocrine pancreas were captured per slide. If the section also contained adjacent non-tumour islets, four randomly selected HPF islets were captured per slide. In slides stained with BRD2, BRD3, and BRD4, staining intensity was calculated using Qupath software (v0.4.3, `https://qupath.github.io/`). First, areas consisting of tumour, stroma, exocrine tissue, and adjacent non-tumour islets were manually annotated in several 'training' images. The software then used this information to train a machine learning classifier to distinguish these features in the remaining images. After the classifier was trained, Qupath formulated a score based on the intensity of the staining within each region, which was used to quantify the amount of protein expression **(Figure 2.1)**.

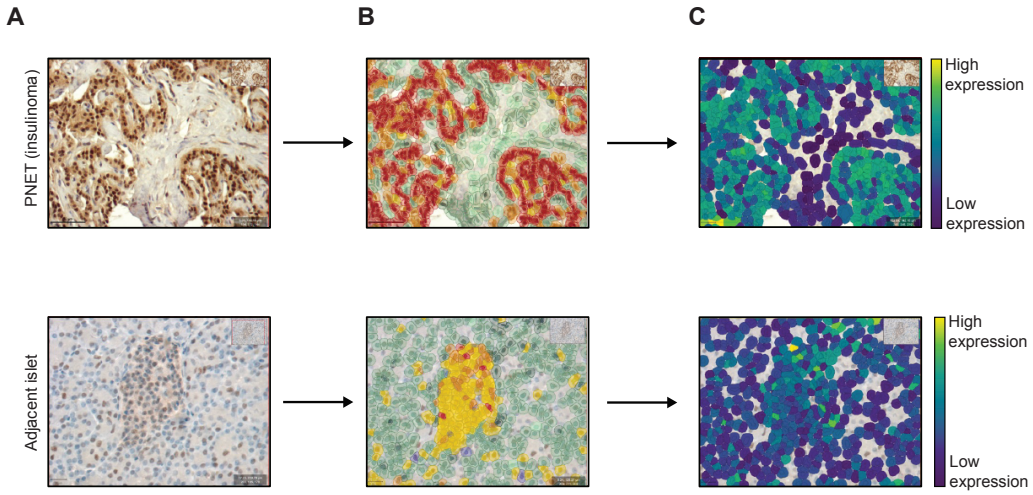

Figure 2.1. Overview of Qupath analysis. (A) High power field (40X) microscopy image of BET protein-stained tumours (upper panel) and adjacent non-tumour pancreatic islets (lower panel) were uploaded into Qupath software. **(B)** A machine-learning based classifier was used to train the software to distinguish between tumour *vs* stroma (top panel) and between pancreatic islet *vs* exocrine tissue (lower panel). **(C)** Intensity of staining was quantified within tumours *vs* islets and expressed as an IHC score as calculated by Qupath software. IHC, immunohistochemistry.

2.3 *In vitro* experiments

2.3.1 Cell lines

The human BON1 cell line, which was originally established from a peripancreatic lymph node metastasis from a non-functioning PNET in a 28-year-old male,[160] were provided as a gift by Dr Simona Grozinsky-Glasberg (Hadassah-Hebrew University Hospital, Israel). The human QGP1 cell line (catalogue no. JCRB0183), which was originally derived from a somatostatin-secreting PNET in a 61-year-old male,[161] was purchased from the Japanese Collection of Research Bioresources Cell Bank (Osaka, Japan). The murine MIN6 cell line, which was derived from a rat insulin promoter (RIP)-Tag mouse insulinoma,[162] was provided as a gift by Professor Patrick Rorsman (University of Oxford, UK). The LNCaP androgen sensitive human prostate adenocarcinoma cell line (catalogue no. CRL-1740), which was

originally derived from a supraclavicular lymph node metastasis in a 50-year-old male, was purchased from American Type Culture Collection (ATCC, Rockville, USA).[163] An overview of the PNET cell lines used in this thesis, and alterations in disease-relevant genes and pathways, are provided in **Table 2.3**.

Table 2.3. Overview of PNET cell lines used in this thesis.

Name	Species	PNET subtype	Alterations in PNET-relevant genes/pathways[164,165]
BON1	Human	NF-PNET	*TP53, TSC2, CHEK2*
QGP1	Human	Somatostatinoma	*TP53, KRAS, MTOR, ATRX, SETD2, CHEK2*
MIN6	Mouse	Insulinoma	p53*, Rb*

*The MIN6 cell line is derived from a RIP-Tag transgenic mouse in which the viral oncogene, SV40 T-antigen, inactivates the p53 and Rb tumour suppressors.

BON1 cells were cultured in Dulbecco's Modified Eagle Medium/F12 (DMEM/F12) (Gibco, Paisley, UK) supplemented with 10% fetal bovine serum (FBS) (Sigma-Aldrich, Gillingham, UK). QGP1 and LNCaP cells were cultured in Roswell Park Memorial Institute (RPMI)-1640 medium (Gibco) supplemented with 10% FBS. MIN6 cells were cultured in DMEM-GlutaMAX™-I media, containing 25 mM glucose and 25 mM HEPES, supplemented with 10% FBS and 55 μM β-mercaptoethanol (Sigma-Aldrich). Cells were cultured in 75 cm^2 flasks (Corning, St. David's Park, UK) at 37°C in a humidified incubator with 5% CO_2. The culture medium was changed every 2 days. When cells reached approximately 80% confluency, they were passaged using 0.05% trypsin-EDTA with phenol red (Thermo Fisher Scientific). Cells up to passage 20 were used for all *in vitro* experiments.

2.3.2 Cell counting

Cells taken from exponential growth phase cultures were trypsinised for 5 minutes at 37°C, gathered in growth medium and centrifuged at 1000 *g* for 3 minutes. The cell pellet was then resuspended in a known volume of medium and 10 μL of the

suspension was mixed with 10 μL of 0.4% trypan blue stain (Sigma-Aldrich). Ten μL of the mixed solution was then pipetted onto a Neubauer improved haemocytometer (Hirschmann Em-Techolor, Eberstadt, Germany) and the number of live cells that do not stain with trypan blue per mL was calculated based on the number of cells per haemocytometer square x dilution factor x 10,000. The cell suspension was then diluted according to the desired concentration.

2.3.3 Epigenetic inhibitors

The small molecule epigenetic inhibitor compounds used in this thesis are shown in **Table 2.4**. Each compound was dissolved in DMSO at a stock concentration of 20 mM and stored at -20°C.

Table 2.4. BET inhibitor compounds used in this thesis

Compound	Target	Source	Catalogue no.
JQ1	BD1 and BD2 non-selective BET inhibitor	Selleck Chemicals	S7110
JQ1(-)	Negative control enantiomer of JQ1	Selleck Chemicals	S2965
I-BET151	BD1 and BD2 non-selective BET inhibitor	Dr R. Prinjha, GSK	N/A
GSK778	BD1-selective BET inhibitor	Dr R. Prinjha, GSK	N/A
GSK789	BD1-selective BET inhibitor	Dr R. Prinjha, GSK	N/A
GSK791	Negative control enantiomer of GSK789	Dr R. Prinjha, GSK	N/A
GSK620	BD2-selective BET inhibitor	Dr R. Prinjha, GSK	N/A
GSK046	BD2-selective BET inhibitor	Dr R. Prinjha, GSK	N/A
ABV-744	BD2-selective BET inhibitor	Selleck Chemicals	S8723

2.3.4 Epigenetic inhibitor screen

The CellTiter-Blue® assay, which utilises the ability of living cells to convert resazurin, a non-fluorescent dye, into resorufin, a fluorescent compound, was used to assess the effects of epigenetic inhibitors on cell proliferation and survival. This assay

serves as an indicator of cellular metabolic activity, which is directly proportional to the number of viable cells.[166]

BON1, QGP1, MIN6, or LNCaP cells were seeded in 96-well black polystyrene microplates (Corning) in 100 μL of media per well. Seeding concentrations were 5×10^4 cells/mL for BON1 and LNCaP cells and 10×10^4 cells/mL for QGP1 and MIN6 cells. The following day, the media was refreshed, and the epigenetic compounds JQ1, I-BET151, GSK789, GSK620, and ABBV-744 were added to the wells at a concentration of 1 μM. Negative control cells were treated with media alone or 0.05% DMSO. All treatments were performed in quadruplicate wells and in three-to-four independent experiments. After 96 hours of treatment, cell viability (as an indicator of cell proliferation) was assessed using the CellTiter-Blue® assay (Promega, Madison, WI, USA), whereby 20 μL of CellTiter-Blue® reagent was added per well. The plates were then incubated for 1 hour at 37°C with 5% CO_2, and the fluorescent outputs were read on a PHERAstar FS microplate reader (BMG LabTech, Aylesbury, UK) at 530 nm excitation and 580 nm emission. Fluorescence values of the wells were corrected for background intensity of the cell culture medium, and the final results were calculated by dividing the fluorescence values of the treated cells by the values of the untreated control cells.

2.3.5 Proliferation time-course studies

To explore the dynamic effects of epigenetic inhibitors on cell growth and proliferation, and to help inform an appropriate timeframe for mechanistic studies, time-course viability experiments were conducted. BON1, QGP1, or MIN6 cells were seeded in 96-well black polystyrene microplates at a concentration of 5×10^4 cells/mL for BON1 cells and 10×10^4 cells/mL for QGP1 and MIN6 cells. A total of 100 μL of media was added per well. The following day, the media was refreshed, and the epigenetic compounds I-BET151, GSK789, or GSK620 were added to the wells at a concentration of 1 μM. To examine the effects of bromodomain 1 (BD1) and bromodomain 2 (BD2)-selective inhibitors in combination, cells were treated with a

50:50 mixture of GSK789 and GSK620, resulting in a combined dose of 1 μM (0.5 μM each). Negative control cells were treated with media alone or 0.05% DMSO. All treatments were performed in quadruplicate wells and in three-to-four independent experiments. Cell viability was assessed using the CellTiter-Blue® cell viability assay (as described in Section 2.3.4) at 0 hours post-treatment and every 24 hours for 4 days. Fluorescence values of the samples at each time point were normalised to 0-hour intensities. Photomicrographs of the cells were also taken at each time point at 20x magnification with an inverted Eclipse TS100 microscope (Nikon, Tokyo, Japan) equipped with a GXCam U3 Pro camera (GT Vision, Wickhambrook, UK).

2.3.6 Dose-response curves

In order to characterise the dose-dependent effects of BET inhibitors on cell viability and to explore compound potency, dose-response experiments were conducted. BON1, QGP1, or MIN6 cells were seeded in 96-well black polystyrene microplates at a concentration of 5×10^4 cells/mL for BON1 cells and 10×10^4 cells/mL for QGP1 and MIN6 cells. A total of 100 μL of media was added per well. The following day, the media was refreshed, and the epigenetic drugs I-BET151, GSK789, or GSK620 were added to the cells in increasing concentrations ranging from 10 nM to 10 μM. Negative control cells were treated with DMSO alone. For BD1- and BD2-selective inhibitor combination treatments, drugs were mixed in a 50:50 ratio, resulting in combined doses of 20 nM, 50 nM, 10 nM, 50 nM, 1 μM, 5 μM and 10 μM. All treatments were performed in quadruplicate wells and in three-to-four independent experiments. After 96 hours of treatment, cell viability was assessed using the CellTiter-Blue® assay (as described in Section 2.3.4). Fluorescence values of the samples were corrected for the background intensity of the cell culture medium, and the final results were calculated by dividing the fluorescence values of the treated cells by the values of the negative control cells. Half maximal inhibitory concentration (IC_{50}) values were calculated using GraphPad Prism v9.5.1 (GraphPad

Software, La Jolla, CA, USA) by fitting the data to the 'log(inhibitor) *vs* response – variable slope (four parameters) fit' equation.

2.3.7 Drug synergy studies

The combined effects of BD1- and BD2-selective inhibition were determined by treating BON1, QGP1, or MIN6 cells with GSK789 and GSK620 in an 8 × 8 matrix grid format **(Figure 2.2)**. Cells were seeded in 96-well black polystyrene microplates at a concentration of 5×10^4 cells/mL for BON1 cells and 10×10^4 cells/mL for QGP1 and MIN6 cells. A total of 100 µL of media was added per well. The following day, the media was refreshed, and cells were co-treated with 7-point serial 2:1 dilutions of both compounds (4 µM – 0.06 µM). Negative control cells were treated with 0.05% DMSO. Treatments were performed in three independent experiments. Cell viability was measured after 96 hours using the CellTiter-Blue® cell viability assay (as described in Section 2.3.4). The fluorescence values of the wells were corrected for the background intensity of the cell culture medium, and the final results were calculated by dividing the fluorescence values of the treated cells by the values of the untreated control cells. To determine the level of drug synergy, cell viability data were analysed using the Bliss independence model in the 'SynergyFinder' (v3.8.2) package for RStudio (v1.4.1717, Posit Software, Boston, MA, USA).[167] The Bliss model is based on the assumption that the effects of two drugs acting together can be predicted by the effects of the drugs acting independently, and that any deviation from this prediction indicates synergy or antagonism.[168] Specifically, the Bliss model calculates the expected effect of the drug combination by multiplying the effects of each drug individually. The observed effect of the drug combination is then compared to this expected effect, and a Bliss score of >10 indicates that the interaction between two compounds is likely synergistic, scores from 10 to -10 indicate additivity, and a score of < -10 indicates antagonism.[167]

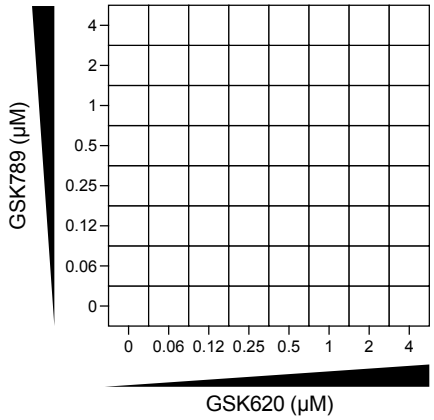

Figure 2.2. Dose-response combination matrix for combination studies with GSK789 and GSK620. Overview of an 8 x 8 dose-response matrix within a 96-well plate showing serial dilutions of GSK789 and GSK620 from 4 μM to 0.06 μM. Each matrix features 49 unique combination points assessing the synergistic effects of combined BD1- and BD2-selective inhibition.

2.3.8 Drug washout studies

To evaluate the reversibility of drug effects and the recovery dynamics of cells post-treatment, compound washout studies were conducted. BON1, QGP1, or MIN6 cells were seeded in 96-well black polystyrene microplates at a concentration of 5×10^4 cells/mL for BON1 cells and 10×10^4 cells/mL for QGP1 and MIN6 cells. A total of 100 μL of media was added per well. The following day, the media was refreshed, and epigenetic drugs were added to the wells at a concentration of 1 μM. For the BD1- and BD2-selective inhibitor combination drug treatments, cells were treated with a 50:50 mixture of the two drugs, resulting in a combined dose of 1 μM (0.5 μM each). Negative control cells were treated with media alone or 0.05% DMSO. All treatments were performed in quadruplicate wells and in three-to-four independent experiments. After 96 hours of treatment, the drug- and DMSO-containing media were aspirated, the cells were rinsed with phosphate-buffered saline (PBS), and 100 μL of culture media was added to the wells to initiate the drug washout period. Cell viability was assessed using the CellTiter-Blue® cell viability assay (as described in Section 2.3.4) at 0 hours and 96

hours post-treatment and every 24 hours for 4 days after drug washout. Fluorescence values of the samples at each time point were normalised to 0-hour intensities.

2.3.9 Apoptosis assays

BET inhibitors have been reported to induce apoptosis in some cancer types,[169,170] via activation of caspases, which are are a family of cysteine proteases that play essential roles in programmed cell death.[171] Executioner caspases such as caspase-3 and caspase-7, cleave key cellular substrates like poly (ADP-ribose) polymerase (PARP) and cytoskeletal proteins, leading to the morphological and biochemical changes characteristic of programmed cell death.[171] To specifically assess the activation of these executioner caspases in response to BET inhibitors, apoptosis assays using the Caspase-Glo® 3/7 assay were conducted. This bioluminescent assay measures the activity of caspase-3 and caspase-7 by detecting the cleavage of a luminogenic caspase-3/7 substrate, which contains a sequence recognised and cleaved specifically by these caspases, releasing a luminescent signal proportional to the level of caspase activation.[172]

BON1, QGP1, or MIN6 cells were seeded in 96-well white-walled polystyrene microplates (Corning) at a concentration of 5×10^4 cells/mL for BON1 cells and 10×10^4 cells/mL for QGP1 and MIN6 cells. A total of 100 µL of media was added per well. The following day, the media was refreshed, and epigenetic drugs were added to the wells at a concentration of 1 µM or 0.5 µM each for the BD1- and BD2-selective inhibitor combination drug treatments. Negative control cells were treated with media alone or 0.05% DMSO. All treatments were performed in quadruplicate wells and in three-to-four independent experiments. After 72 hours of treatment, apoptosis was evaluated using the Caspase-Glo® 3/7 assay (Promega), whereby 100 µL of Caspase-Glo® reagent was added per well, and plates were incubated for 1 hour at room temperature in the dark. The luminescent outputs were read on a microplate luminometer (Turner Biosystems, Sunnyvale, CA, USA). Caspase activity was normalised to cell viability, as determined using

CellTiter-Blue® assays, which were performed in parallel and as described in Section 2.3.4. Final results were calculated by dividing the luminescence signals of the drug-treated wells by those of the untreated control wells.

2.3.10 Crystal violet assays

To confirm the effects of BET inhibitors on apoptosis, crystal violet staining was utilised. This method involves staining cell nuclei with crystal violet dye, a triphenylmethane dye that binds to DNA and protein, providing a measure of cell density.[173] It relies on the detachment of adherent cells from culture plates during cell death. Thus, staining the remaining attached live cell allows for the indirect quantification of cell death and the evaluation of differences in proliferation following treatment.

BON1, QGP1, or MIN6 cells were seeded in 24-well plates (Corning) at a concentration of 1×10^5 cells/mL for BON1 cells and 2×10^5 cells/mL for QGP1 and MIN6 cells, in 500 µL of media per well. The following day, the media was refreshed, and epigenetic drugs were added to the wells at concentrations of either 1 µM or 10 µM. For the BD1- and BD2-selective inhibitor combination drug treatments, cells were treated with a 50:50 mixture of the two drugs, resulting in combined concentrations of 1 µM (0.5 µM each) or 10 µM (5 µM each). Negative control cells were treated with 0.05% DMSO. Treatments were performed in triplicate wells and in three independent experiments. After 96 hours of treatment, the media was aspirated, cells were fixed with 100% ice-cold methanol for 10 minutes, and stained with 0.05% crystal violet (Sigma-Aldrich) in dH_2O for 15 minutes. Following this, the wells were rinsed in tap water and left to air dry overnight. The plates were then photographed using a flatbed scanner, and crystal violet staining area and intensity were quantified using the ColonyArea plugin for ImageJ v1.8.0 (National Institutes of Health, Bethesda, MD, USA).

2.3.11 Propidium iodide (PI) cell cycle analysis

To assess the impact of BET inhibitors on the cell cycle dynamics of human (BON1 and QGP1) PNET cell lines, propidium iodide (PI) staining and subsequent flow cytometric analysis was conducted. PI is a fluorescent dye that binds to DNA, allowing for the measurement of DNA content across different cell cycle phases. As cells progress through G0/G1, S, and G2/M phases, their DNA content varies, and this variation is detected as changes in PI fluorescence intensity during flow cytometry.[174] This method quantifies the proportion of cells in each phase, providing insights into potential arrests or alterations in cell cycle progression induced by drug treatments.

BON1 or QGP1 cells were seeded in 24-well plates at a concentration of 1 $\times$ 10^5 cells/mL and 2 $\times$ 10^5 cells/mL, respectively, in 500 µL of media per well. The following day, the media was refreshed, and epigenetic drugs were added to the wells at a concentration of 1 µM or 0.5 µM each for the BD1- and BD2-selective inhibitor combination drug treatments. Negative control cells were treated with 0.05% DMSO. All treatments were performed in triplicate wells and in four independent experiments. After 48 hours of treatment, cells were trypsinised and collected by centrifugation, washed once with PBS, and then fixed in 100% ethanol overnight at 4°C. The following day, the ethanol was removed by aspiration following centrifugation, the fixed cells were washed with PBS, and stained with PI solution containing 50 µg/mL PI (Abcam, Cambridge, UK), 200 µg/mL RNase A (Sigma-Aldrich), 0.1% NP-40 lysis buffer, and 150 mM sodium chloride in PBS. Cells were incubated in the dark for 30 minutes and analysed on an LSRII flow cytometer (BD Biosciences, San Jose, CA, USA) equipped with a 532-nm laser and a 610/20-nm bandpass filter.

FCS files generated from the flow cytometer were imported into ModFit LT v5.0.9 (Verity Software House, Topsham, ME, USA) for data analysis. Firstly, a gate was drawn on a forward scatter area (FSC-A) *vs* side scatter area (SSC-A) density plot to exclude debris and identify the cell population of interest. Next, a gate was

drawn on an SSC-A vs SSC-Width (SSC-W) plot to exclude aggregates. Plots of PI area (PI-A) vs PI height (PI-H) were used to gate single cells and exclude doublets. The resulting histogram plots of cell number vs PI fluorescence intensity were fitted with two Gaussian distributions to calculate the percentage of cells in the G0/G1 and G2/M phases, while a polynomial distribution was used to model the S phase. The percentage of cells in each of these phases was averaged from four independent experiments. An overview of the gating strategy is shown in **Figure 2.3**.

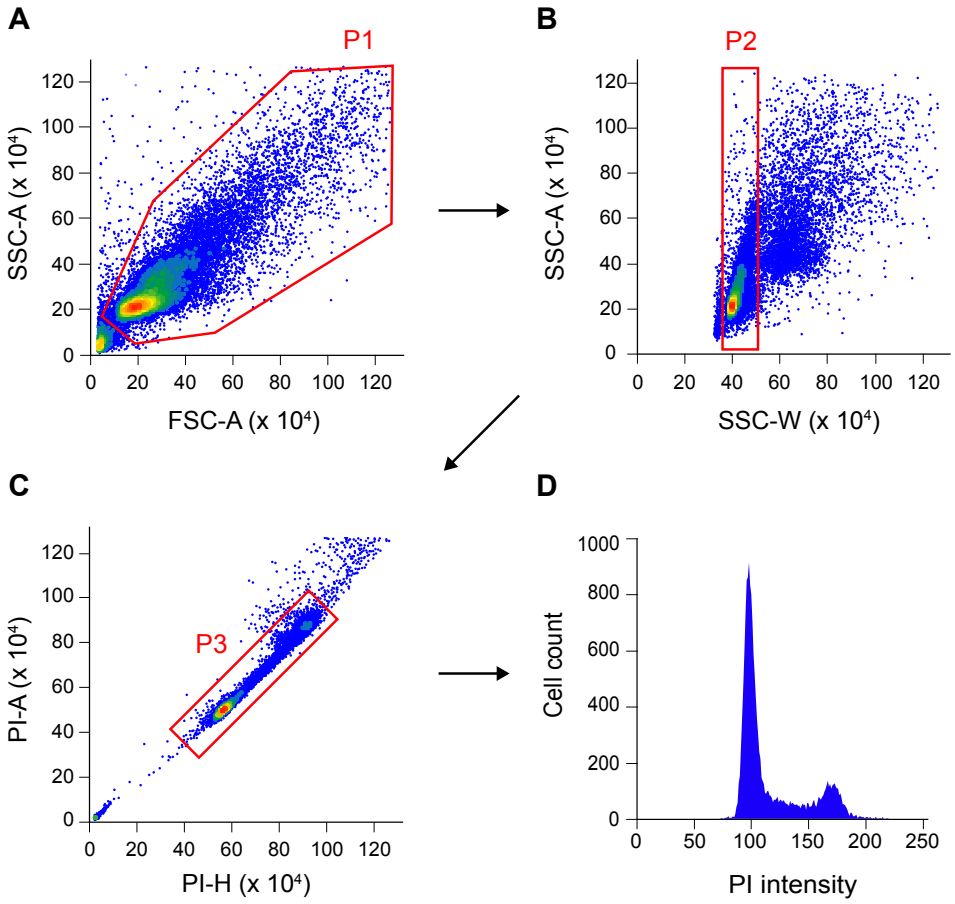

Figure 2.3. Representative flow cytometry density plots indicating gating strategy used for cell cycle analysis. (A) An initial gate (P1) was set on a plot of FSC-A vs SSC-A to exclude debris. **(B & C)** Single cells were gated and doublets excluded based on a plot of SSC-A vs SSC-W (P2) and PI-A vs PI-H (P3). **(D)** The resulting histogram plots of cell count vs PI intensity were used to determine the proportion of cells in the G0/G1, S, and G2/M phases in ModFit LT software. FSC-A, forward scatter area; PI-A, propidium iodide area; PI-H, propidium iodide height; SSC-A, side scatter area; SSC-W, side scatter width

2.3.12 Quantitative real-time PCR (qPCR)

2.3.12.1 RNA extraction

Total RNA was extracted from ~8×10^6 cells/mL using the RNeasy Mini Kit (Qiagen, Hilden, Germany). Briefly, cells were washed twice with PBS and harvested by centrifugation at $1000g$ for 3 minutes. The cells were then lysed in buffer RLT, and the lysates were transferred to silica membrane-lined spin columns that selectively bind RNA. Following two wash steps, the RNA was eluted in nuclease-free water. RNA concentration and purity were quantified using a NanoDrop ND-1000 spectrophotometer (Thermo Fisher Scientific), and the ratio of the absorbance at A_{260}/A_{280} was calculated.

2.3.12.2 Complementary DNA (cDNA) synthesis

For cDNA synthesis, 1 µg of RNA was reverse transcribed using the QuantiTect Reverse Transcription Kit (Quiagen). Briefly, RNA was mixed with gDNA Wipeout Buffer and RNase-free water and incubated at 42°C for 2 minutes to remove genomic DNA contamination. The reaction was then cooled on ice and mixed with reverse transcription mix containing Quantiscript Reverse Transcriptase, Quantiscript RT Buffer and RT Primer Mix. The reaction mixture was incubated at 42°C for 15 minutes to synthesise cDNA, followed by incubation at 95°C for 3 minutes to inactivate the reverse transcriptase. The resulting cDNA was then diluted 1:4 in RNase-free water.

2.3.12.3 qPCR analysis

qPCR was performed using the cDNA templates synthesised in Section 2.3.12.2 and the QuantiTect SYBR Green PCR Kit (Qiagen) with gene-specific QuantiTect Primer assays (Qiagen) **(Table 2.5)**. Briefly, 4 µL of cDNA template was added to a 36 µL of reaction mixture containing 20 µL of 2x QuantiTect SYBR Green PCR Master Mix, 4 µL of 10x QuantiTect primer assay and 12 µL of RNAse-free

water. The PCR reactions were performed on a Rotor-Gene Q cycler (Qiagen) with the following cycling conditions: initial denaturation at 95°C for 15 minutes, followed by 40 cycles of denaturation at 95°C for 15 seconds, annealing at 55°C for 30 seconds and extension at 72°C for 30 seconds. Reactions were performed in triplicate (technical replicates) and repeated in three biological replicates. Mean cycle threshold (Ct) values were calculated for each gene of interest. Relative gene expression levels were determined using the 2-ΔΔCt method,[175] normalised to the geometric mean of the reference genes Glyceraldehyde 3-Phosphate Dehydrogenase (*GAPDH/Gapdh*) and Calnexin (*CANX/Canx*).

Table 2.5. List of human and mouse QuantiTect primers used for qPCR

Gene symbol	Gene name	Qiagen catalogue no.
Human		
BRD2	Bromodomain containing 2	QT00012852
BRD3	Bromodomain containing 3	QT00084154
BRD4	Bromodomain containing 4	QT00044345
BRDT	Bromodomain testis associated	QT00069888
GAPDH	Glyceraldehyde-3-phosphate dehydrogenase	QT00079247
CANX	Calnexin	QT00092995
Mouse		
Brd2	Bromodomain containing 2	QT00197666
Brd3	Bromodomain containing 3	QT00120883
Brd4	Bromodomain containing 4	QT02329040
Brdt	Bromodomain testis associated	QT00141218
Gapdh	Glyceraldehyde-3-phosphate dehydrogenase	QT01658692
Canx	Calnexin	QT00152579

2.3.13 Western blotting

2.3.13.1 Preparation of protein lysates

Cells were lysed in NP-40 lysis buffer (1% NP-40, 1 mM EDTA, 150 mM NaCl, 1 mM EDTA, 50 mM Tris-HCl [pH7.5]) supplemented with cOmplete™ protease inhibitor

cocktail (Sigma-Aldrich) and incubated on ice for 15 minutes. Protein lysates were cleared of insoluble cellular debris by centrifugation at 14,000 *g* for 20 minutes at 4°C, and the supernatant was preserved. Protein concentrations within the supernatant were quantified using the Bradford assay containing Coomassie Plus protein reagent (Bio-Rad, Watford, UK). Briefly, 2 µL of diluted protein lysates (1:10 dilution in PBS) and 200 µL of Quick Start™ Bradford 1x Dye Reagent (Bio-Rad) were added to clear polystyrene 96-well plates (Corning). Protein standards containing 9 different concentrations of bovine serum albumin (BSA) (ranging from 0 to 2 mg/mL) were prepared using the Pierce™ BCA Protein Assay Kit (Thermo Fisher Scientific) and added to the 96-well plate. Absorbance values of each well were then measured at 595 nm on a PHERAstar FS microplate reader. Known concentrations of the BSA protein standards were used to plot a standard curve fitted using linear regression to allow for the calculation of protein concentrations in each sample.

2.3.13.2 Immunodetection of proteins

Prior to electrophoretic separation, protein lysates were prepared in 4x Laemmli buffer (Bio-Rad) containing 10% β-mercaptoethanol and heated at 95°C for 5 minutes. Protein lysates were then separated via sodium dodecyl sulfate polyacrylamide gel electrophoresis (SDS-PAGE) using 4-12% TruPAGE™ Precast Gels (Sigma-Aldrich). The Precision Plus Protein™ Dual Colour standard (Bio-Rad) was used as a molecular weight marker. The separated proteins were then transferred to Immun-Blot® 0.2 µm polyvinylidene fluoride (PVDF) membranes (Bio-Rad) by electroblotting at 100 V for 90 minutes in a Mini Trans-Blot® Cell (Bio-Rad) containing 1x TruPAGE transfer buffer (Sigma-Aldrich). The PVDF membranes were then blocked with blocking buffer (5% dry non-fat milk in TBS-T) for 1 hour at room temperature and then incubated overnight at 4°C in the appropriate primary antibody **(Table 2.6)** diluted in blocking buffer. The following day, membranes were washed three times in TBS-T (5 minutes per wash) and then incubated for 1 hour at room temperature with mouse anti-rabbit IgG-horseradish peroxidase (HRP)-conjugated secondary antibody (Santa Cruz Biotechnology, Santa Cruz,

CA, USA) diluted 1:3000 in blocking buffer. Membranes were washed a further three times in TBS-T (5 minutes per wash) to remove excess secondary antibody and developed using Clarity™ Western ECL substrate (Bio-Rad). Protein bands were visualised on a ChemiDoc MP™ system (Bio-Rad) with Image Lab v6.0.1 software (Bio-Rad).

Table 2.6. List of primary antibodies used for Western blotting

Antibody	Species	Catalogue no.	Dilution	Source
Anti-BRD2	Rabbit	D89B4	1:1000	Cell Signaling Technology, Danvers, MA, USA
Anti-BRD3	Rabbit	61489	1:1000	Active Motif, La Hulpe, Belgium
Anti-BRD4	Rabbit	ab128874	1:1000	Abcam, Cambridge, UK
Anti-GAPDH	Rabbit	ab9485	1:5000	Abcam, Cambridge, UK

2.4 Next-generation sequencing and bioinformatics

2.4.1 RNA sequencing (RNA-seq) of BON1 PNET cells

All *in vitro* next-generation sequencing experiments were performed in BON1 cells. This human cell line was selected for further study as it was derived from a hormonally non-functioning PNET, which represents the most common subtype of these tumours,[160] while the other two cell-lines studied in this thesis (QGP1 and MIN6) were derived from hormonally functioning PNETs,[161,162] which have a lower incidence.

2.4.1.1 Preparation of samples and RNA extraction

BON1 cells were seeded in 75 cm^2 tissue culture flasks at a density of 2×10^6 cells/mL in 30 mL of media. The following morning, the media was refreshed, and cells were treated with 1 μM GSK789, 1 μM GSK620, or 1 μM I-BET151. For the combination treatment group, cells were treated with 0.5 μM of GSK789 plus 0.5 μM of GSK620. Negative control cells were treated with 0.05% DMSO. After 48 hours of treatment, cell pellets were collected, and total RNA was extracted using the RNeasy Mini Kit as described in Section 2.3.12.1. The 48-hour timepoint was chosen based on the premise that it would sufficiently capture downstream gene expression changes while also ensuring sufficient yield for RNA extraction. Samples were prepared in biological triplicates. Prior to sequencing, the concentration and quality of extracted RNA were assessed using the NanoDrop ND-1000 spectrophotometer and Agilent 2200 TapeStation (Agilent Technologies, Santa Clara, CA, USA). Samples selected for library preparation fulfilled the following criteria: A_{260}/A_{280} of 2.0-2.2 and an RNA integrity number (RIN) of > 9.

2.4.1.2 Library preparation and sequencing

Purified RNA at a concentration of 100-125 ng/μL per sample was submitted to the Wellcome Trust Centre for Human Genetics, University of Oxford, where both library preparation and sequencing were performed by staff within the facility. The QuantSeq 3' mRNA-Seq Library Prep Kit (Lexogen, Vienna, Austria) was used to generate libraries, as per the manufacturer's instructions.[176] The QuantSeq library preparation method specifically targets and quantifies the 3' untranslated regions (3'UTRs) of mRNA. The advantages of this method compared to traditional RNA-seq library preparation methods, such as TruSeq (Illumina, San Diego, CA, USA), include a more simplified workflow, a reduction in sequencing depth required to achieve reliable gene expression measurements and compatibility with low quantities of input RNA.[176] In the first step of the QuantSeq protocol, oligo-dT primers containing a 5' Illumina-compatible sequence were hybridised to

the RNA for reverse transcription and synthesis of the first cDNA strand. Following degradation of the RNA template, synthesis of the second cDNA strand was initiated by random primers containing an Illumina-compatible linker sequence at the 5' end and RNA polymerase. The double-stranded library was then purified with magnetic beads, PCR amplified and bar-coded. Sequencing was completed on a NextSeq500 (Illumina) to generate approximately 5 million 75 base pair (bp) single-end reads per sample.

2.4.1.3 *In vitro* RNA-seq bioinformatics analysis

Raw sequencing reads were first demultiplexed using bcl2fastq2 software (v2.2, Illumina) to generate FASTQ format sequence data. I subsequently performed all bioinformatics analyses including quality control, alignment to the human reference genome, quantification of gene expression levels and differential expression analysis, as outlined below. FASTQ files were assessed for quality using FastQC (v0.12.0, `http://bioinformatics.babraham.ac.uk/projects/fastqc/`). Next, Cutadapt (v2.6, `https://github.com/marcelm/cutadapt/`) was used to remove bias introduced by random primers at the 5' end and trim poly(A) tail-derived reads at the 3' end. The resulting reads were mapped to the Genome Reference Consortium Human Genome Build 38 (GRCh38) using STAR software (v2.7.10b, `https://github.com/alexdobin/STAR`) with default parameters, generating binary alignment map (BAM) files. In order to quantify the number of reads mapped to each gene, the 'HTSeq-count' script within the 'HTSeq' package (v2.0.3) was run in Python (v2.7, Python Software Foundation, Beaverton, OR, USA). Normalised read counts and differential gene expression analysis (comparing the DMSO-treated group vs compound-treated groups) were performed using the 'DESeq2' (v1.40.1) R package. Genes were considered to be differentially expressed between two experimental conditions based on an absolute $\log_2$fold-change of > 1 and false discovery rate (FDR)-corrected p-value of ≤ 0.05.

A filtered list of differentially regulated genes for each comparison was generated and used for downstream pathway enrichment analysis using the 'clusterProfiler' (v4.8.1) R package. Several curated pathway databases were utilised for enrichment analysis, including the Gene Ontology Biological Process (GO:BP)[177] dataset, the Pathway Interaction Database (PID),[178] the Kyoto Encyclopedia of Genes and Genomes (KEGG)[179] and Reactome.[180] GO:BP terms describe processes accomplished by multiple molecular activities, typically encompassing broad biological objectives, such as cell cycle regulation, apoptosis and immune response. PID contains curated data on signalling and regulatory pathways in human cells and is particularly useful for exploring the pathways that govern cellular responses to various stimuli.[178] KEGG is a collection of manually curated pathway maps representing molecular interaction and reaction networks. KEGG pathways cover a wide range of biochemical processes that can be grouped into seven broad categories: metabolism, genetic and environmental information processing, cellular processes, bodily systems, human diseases and drug development.[179] Reactome is another curated open-source pathway database that that provides detailed information on molecular events, such as signal transduction, transport, DNA replication and metabolism. Overall, pathway enrichment analysis helps elucidate the specific biological processes associated with the observed gene expression changes, providing insights into the underlying mechanisms of therapeutic effect.[180]

The filtered list of genes was also used to predict upstream regulators using Ingenuity Pathway Analysis (IPA) software.[181] Upstream regulators are molecules, including transcription factors, cytokines, growth factors, kinases and chemicals) that can affect the expression of target genes within a given dataset. The identification of these regulators is based on known interactions derived from a comprehensive, curated database of biological interactions and functional annotations. Predicted activities of upstream regulators are based on directionality of underlying gene expression that is similar to (predicted activation) or inverse (predicted inhibition) of the uploaded differential expression signature. IPA not only predicts which upstream

regulators may be active but also assigns a statistical measure of confidence, known as a z-score, to predict the likelihood of activation or inhibition of these regulators.[181]

Gene set enrichment analysis (GSEA) was also performed on the complete (unfiltered) list of genes from each comparison, using the R package 'fsgea' (v1.26.0). In contrast to pathway enrichment analysis, GSEA evaluates the complete list of genes, ranking them by their expression levels, to determine whether predefined sets of genes show statistically significant, concordant differences between two biological states. This allows GSEA to capture subtle, but coordinated changes in gene expression that might be missed by focusing only on differentially expressed genes. GSEA was performed using Hallmark gene sets were downloaded from the Molecular Signatures Database (MSigDB, `https://www.gsea-msigdb.org/gsea/msigdb`).[182] MSigDB is a comprehensive database that provides curated collections of gene sets representing biological processes, pathways, and molecular signatures. The Hallmarks collection contains gene expression signatures that summarise pathways across MSigDB's various sources. These include molecular processes that are fundamental to cell biology, as well as cancer development and progression.

2.4.2 RNA-seq of human PNET samples

2.4.2.1 Mayo Clinic PNET samples

Frozen tumour specimens from 46 patients with sporadic PNETs who underwent surgical resection at the Mayo Clinic were provided as a gift from Professor Gloria Petersen, Professor of Epidemiology, through an MTA under Mayo Clinic IRB #354-06. Details regarding the samples are presented in Chapter 4, in **Table 4.2** on page 110.

2.4.2.2 Sample preparation and RNA extraction from frozen tissue

RNA extraction from 46 frozen PNET specimens was performed by the Biospecimen Accessioning and Processing Core Facility at Mayo Clinic, using a combination

of mechanical disruption and enzymatic treatment. Initially, the tissue samples were homogenised using a motorised tissue homogeniser. Following homogenisation, Trizol reagent (Invitrogen, Carlsbad, CA, USA) was added to the tissue lysates to dissociate nucleoprotein complexes and the samples were incubated at room temperature for 5 minutes. The homogenate was then mixed with chloroform and centrifuged to separate the mixture into aqueous and organic phases. RNA was precipitated from the aqueous phase using isopropanol, washed with ethanol, and finally dissolved in 40 µL of RNase-free water. This protocol yielded ~300 ng of total RNA per sample. The integrity and concentration of the RNA were assessed using the Agilent Fragment Analyser (Santa Clara, CA, USA) and Qubit® RNA High Sensitivity assay (Thermo Fisher Scientific), respectively. Post-extraction, RNA samples underwent DNase I treatment (Zymo Research, Irvine, CA) to remove any contaminating genomic DNA, followed by purification using RNAClean XP beads (Beckman Coulter, Indianapolis, IN, USA). Samples that met quality standards, including a required RIN of > 9, were selected for further processing.

2.4.2.3 Library preparation and sequencing

Library preparation and sequencing were performed by the Genome Analysis Core Facility at Mayo Clinic. A total of 100 ng of cleaned RNA was processed using the TruSeq Stranded Total RNA reagent kit (Illumina). The concentration and size distribution of the completed libraries were determined using an Agilent 22000 TapeStation and Qubit® fluorometry.

The generated libraries were pooled and sequenced on a NovaSeq 6000 system, employing the NovaSeq XP 4-Lane Kit (Illumina) for individual lane loading. Sequencing was executed to generate an average of 200 million total reads per sample, with each library sequenced as 100 bp paired-end reads.

2.4.2.4 Human PNET samples RNA-seq bioinformatics analysis

Raw sequencing reads were demultiplexed using 'bcl2fastq2' software to generate FASTQ format sequence data. After receiving the FASTQ files, I performed all bioinformatics analyses myself using the same pipeline as outlined in Section 2.4.1.3, although the comparisons in 'DESeq2' were adjusted for this study's objectives. Specifically, gene expression was compared between metastatic tumours, defined as having lymph node or distant metastases (i.e., ENETS stages IIIB-IV), and localised tumours (ENETS stages I-IIIA). Comparisons were also made between functioning and non-functioning tumours, as well as G1 *vs* G2 or G3 tumours.

2.4.3 Thiol(SH)-linked alkylation for the metabolic sequencing of RNA (SLAM-seq)

2.4.3.1 Principles of assay

In order to identify direct gene targets of drugs such as epigenetic modulators, it is important to measure changes in gene expression at an early time point (e.g., within a few hours) after drug treatment, before secondary downstream effects confound the interpretation of results.[183] A limitation to using standard RNA-seq for this purpose is that this technique captures steady-state mRNA levels only and is unable to distinguish between newly transcribed and pre-existing RNA. Thus, while RNA-seq provides an overall snapshot of the transcriptome at a given time point, it is unable to determine changes in *de novo* transcription occurring over short time frames. Moreover, conducting an RNA-seq experiment shortly after drug perturbation can introduce a bias towards transcripts with short half-lives, as they are more rapidly turned over and changes in their transcription rates will be more readily detected.[184] In contrast, transcripts with longer half-lives may exhibit more subtle changes in abundance during the early stages of drug treatment, and their steady-state levels may not fully reflect dynamic changes occurring at the transcriptional level immediately after treatment. To address these limitations,

innovative techniques that specifically capture newly transcribed (nascent) RNA have been developed, such as SLAM-seq.[183,185]

SLAM-seq enables the quantification of nascent transcription through metabolic labelling of RNA using 4-thiouridine (4sU), a nucleotide analogue that differs from regular uridine due to the presence of a sulfur atom (thiol group) instead of the oxygen atom found at the fourth carbon position of the pyrimidine ring.[185] When cells are incubated in media containing 4sU, the 4sU is incorporated into newly synthesised RNA instead of uridine. After RNA isolation, adding iodoacetamide (IAA) modifies the 4-thiol group on the 4sU to a carboxyaminodomethyl group. This modification leads reverse transcriptase to incorporate guanine (G) instead of adenine (A) during cDNA synthesis opposite the modified 4sU. This results in what is read as a T>C substitution in the DNA sequence. This occurs because in DNA, thymine (T) normally pairs with adenine (A); however, in the modified cDNA, where guanine (G) is now present, it pairs with cytosine (C). These T>C conversions in the cDNA serve as the signature of newly synthesised RNA. By mapping the next-generation sequencing reads to a reference genome and quantifying these T>C conversions, nascent transcripts can be distinguished from pre-existing ones. An overview of the SLAM-seq workflow is shown in **Figure 2.4**.

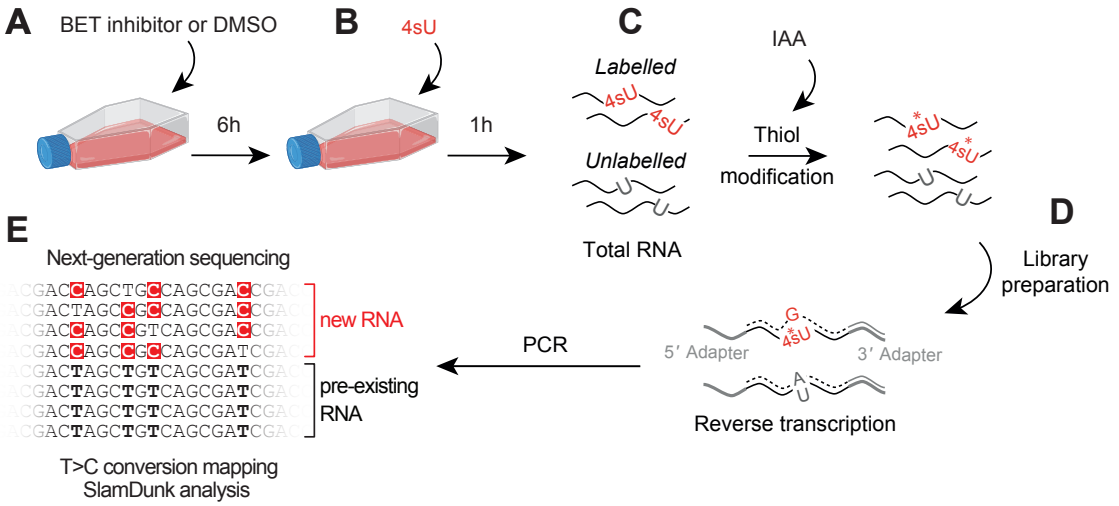

Figure 2.4. Overview of SLAM-seq experiment. **(A)** BON1 cells are treated with BET inhibitor compounds or DMSO control for 6 hours. **(B)** Three hundred µM of 4sU is added to the culture media to allow 4sU nucleotides to become incorporated into newly synthesised RNA. **(C)** After 1 hour of labelling, RNA is extracted and consists of both existing (unlabelled) and newly synthesised (4sU-labelled) RNA. **(D)** The addition of IAA modifies 4sU nucleotides, leading reverse transcriptase to incorporate guanine '(G)' instead of adenine '(A)' at any position where a reduced *4sU nucleotide is encountered during cDNA synthesis. **(E)** This results in the appearance of T>C conversions in sequencing reads from 4sU-labelled transcripts. Bioinformatics analysis using the 'SlamDunk' pipeline[186] allows for the quantification of T>C read counts and downstream differential expression analysis with 'DESeq2'. PCR, polymerase chain reaction.

2.4.3.2 Optimisation of metabolic labelling

Because 4sU has been reported to inhibit cellular proliferation at varying concentrations,[187] and SLAM-seq experiments had not previously been performed in BON1 cells, the SLAM-seq Explorer Kit – Cell Viability Titration Module (Lexogen) was used to evaluate the optimal concentration of 4sU needed to ensure minimal cell toxicity throughout the duration of metabolic labelling. Serial 2:1 dilutions (4 mM - 2 µM) of 4sU were prepared in culture media, according to the manufacturer's instructions. BON1 cells were seeded in 96-well black polystyrene microplates at a concentration of 1×10^5 cells/mL in 100 µL of media per well. The following day, the media was exchanged for the 4sU-containing media while negative control cells were treated with media alone. After 6 hours and 12 hours of incubation, cell viability was assessed using the CellTiter-Blue® assay as described in Section 2.3.4.

These two time points were chosen based on the manufacturer's recommendation to assess cell viability after a duration that exceeds the intended labelling duration (1 hour) for the final SLAM-seq experiment by a factor of at least 2. Fluorescence values of the samples were corrected for the background intensity of the cell culture medium, and the final results were calculated by dividing the fluorescence values of the 4sU-treated cells by the values of the negative control cells. All treatments were performed in quadruplicate wells and in three independent experiments. To minimise light-induced degradation, all steps involving 4sU were performed in the dark under red light, per the manufacturer's recommendations. Dose-response curves were generated using GraphPad Prism by fitting the data to the 'log(inhibitor) vs response – variable slope (four parameters) fit' equation. Based on these experiments, a final 4sU concentration of 300 µM was determined to be optimal, as it did not compromise cell viability beyond 10-15% within time periods that far exceeded the labelling duration intended for the final SLAM-seq experiment **(Figure 2.5)**.

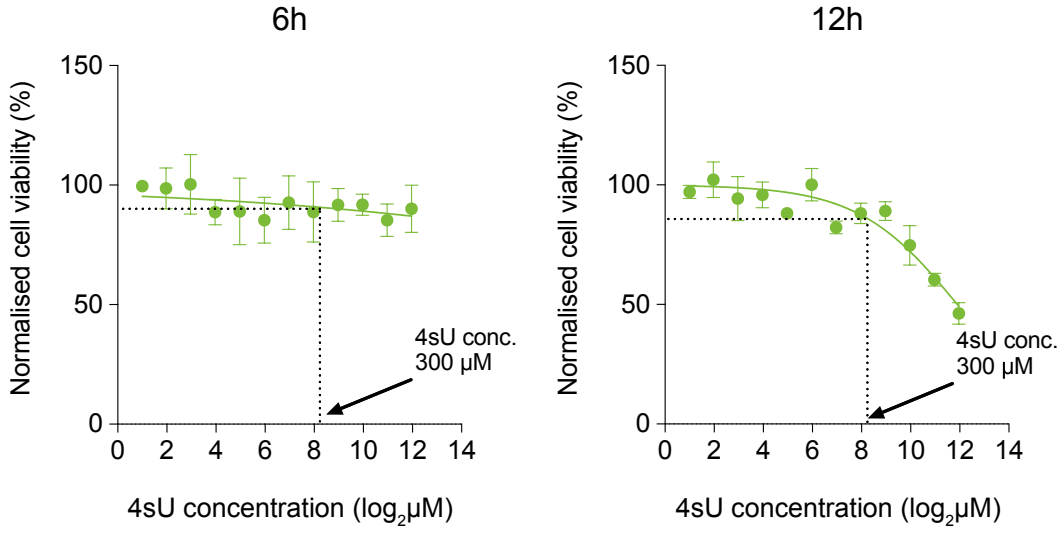

Figure 2.5. Viability of BON1 cells upon treatment with 4sU. Cell viability was assessed using the CellTiter-Blue® assay after 6 hours (left) and 12 hours (right) of exposure to increasing concentrations (2 µM – 4 mM) of 4sU mixed in media. Percentage viability (Y axis) is expressed relative to untreated cells. Concentrations of 4sU (X axis) are reported as $\log_2$µM. The arrows indicate the concentration of 4sU at which 10% of the cells were inhibited in the given time windows. Data are representative of three independent experiments. Error bars denote s.e.m.

2.4.3.3 Preparation of samples, RNA extraction and alkylation

BON1 cells were seeded in 75 cm^2 tissue culture flasks at a density of 2×10^6 cells/mL in 30 mL of media. The following morning, the media was refreshed, and cells were treated with 1 μM GSK789, 1 μM GSK620, or 1 μM I-BET151. For the combination treatment group, cells were treated with 0.5 μM of GSK789 plus 0.5 μM of GSK620. Negative control cells were treated with 0.05% DMSO. After 6 hours of treatment, 300 μM of 4sU was added to the cell culture media, while ensuring protection from light. In addition, a 4sU-untreated non-drug treated control was prepared. After 1 hour of labelling, the media was removed, cells were washed with PBS, and pellets collected by centrifugation at 1000 *g* for 3 minutes. Samples were prepared in biological triplicates. RNA was extracted using the RNeasy Mini Kit as described in Section 2.3.12.1, with the exception that all steps were performed in the dark under red light. Subsequent steps were performed according to the protocol outlined in the SLAM-seq Kinetics Kit—Anabolic Kinetics Module (Lexogen). In brief, 5 μg of RNA per sample was aliquoted for the alkylation reaction and brought up to a volume of 15 μL with nuclease-free water. RNA was alkylated by the addition of 5 μL of 100 mM IAA, 25 μL of DMSO, and 5 μL of sodium phosphate buffer (0.5 M, pH 8), followed by incubation at 50 °C for 15 minutes. The reaction was stopped with the addition of 1 μL of 1 M dithiothreitol (DTT). The alkylated RNA was purified by ethanol precipitation and quantified using a NanoDrop ND-1000 spectrophotometer and Agilent 2200 TapeStation (Agilent Technologies, Santa Clara, CA, USA). Samples selected for library preparation had a RIN of > 9.

2.4.3.4 Library preparation and sequencing

Approximately 50 ng/μL of alkylated RNA per sample was submitted to the Wellcome Trust Centre for Human Genetics for library preparation. The QuantSeq 3′ mRNA-Seq Library Prep Kit was used by staff within the facility to generate sequencing libraries as described in Section 2.4.1.2. Multiplexed libraries were

sequenced on a NextSeq 500 using single-end 75-bp reads, with a mean sequencing depth of ∼30 million reads per sample.

2.4.3.5 SLAM-seq bioinformatics analysis

Raw sequencing files were demultiplexed using bcl2fastq2 software to generate FASTQ files. I subsequently performed all bioinformatics analyses. Read quality assessment was performed using 'FastQC'. 'Cutadapt' was then used to trim adaptors from the 5' end and poly(A) tails from the 3' end of reads. Trimmed FASTQ files were then analysed using 'SlamDunk' (v0.4.3, `http://t-neumann.github.io/slamdunk`),[186] using default settings. 'SlamDunk' is an automated pipeline for the processing of SLAM-seq data and comprises four steps: (1) read mapping; (2) alignment filtering; (3) single nucleotide polymorphism (SNP) calling and correction; and (4) 3'UTR sequence counting. Briefly, reads were aligned to the human genome build GRCh38 using a T>C mismatch-aware aligner. The resulting BAM format files were filtered to remove low-quality and ambiguous alignments aligning to > 1 annotated 3'UTR sequence. Since T>C conversions found in SLAM-seq reads can also be present in genuine SNPs (i.e., false positives), the third step of the pipeline used 'VarScan' software (v2.4, `https://github.com/dkoboldt/varscan`) to identify these SNPs based on a minimum read depth of 10x and variant fraction cut-off of 0.8. Identified SNPs were then excluded from subsequent analyses. In the final step of the pipeline, T>C conversion-containing reads (TcReadCount) and total reads (ReadCount) were determined, and the fraction of labelled transcripts per gene's 3'UTR was calculated. Count matrices were imported into RStudio for downstream analysis using the 'DESeq2' package. Differential expression analysis was performed with an additional step of normalising TcReadCounts to total ReadCounts to account for differences in library sizes and sequencing depth. Genes were considered to be differentially expressed between two experimental conditions based on an absolute $\log_2$fold-change of > 0.5 and false discovery rate (FDR)-corrected p-value of ≤ 0.05.

2.4.4 Chromatin immunoprecipitation with next-generation sequencing (ChIP-Seq)

2.4.4.1 Principles of assay

ChIP-seq is a technique that can be used to investigate genome-wide binding of protein-DNA interactions at bp resolution.[188] Briefly, DNA-binding proteins (e.g., histone modifications, epigenetic readers and transcription factors) and their associated DNA are cross-linked by formaldehyde. The cross-linked chromatin is then sheared into small fragments (typically by sonication). Antibodies specific to the protein of interest are used to immunoprecipitate the protein-DNA complexes. Following this, the DNA is purified and prepared for high-throughput sequencing. The sequencing reads are aligned to a reference genome and the genomic regions where reads are enriched indicate where the protein of interest binds. Comparing ChIP-seq data from different experimental conditions (e.g., drug treatments) allows one to uncover changes in protein-DNA interactions and identify regulatory elements involved in gene expression. An overview of the workflow is shown in **Figure 2.6**.

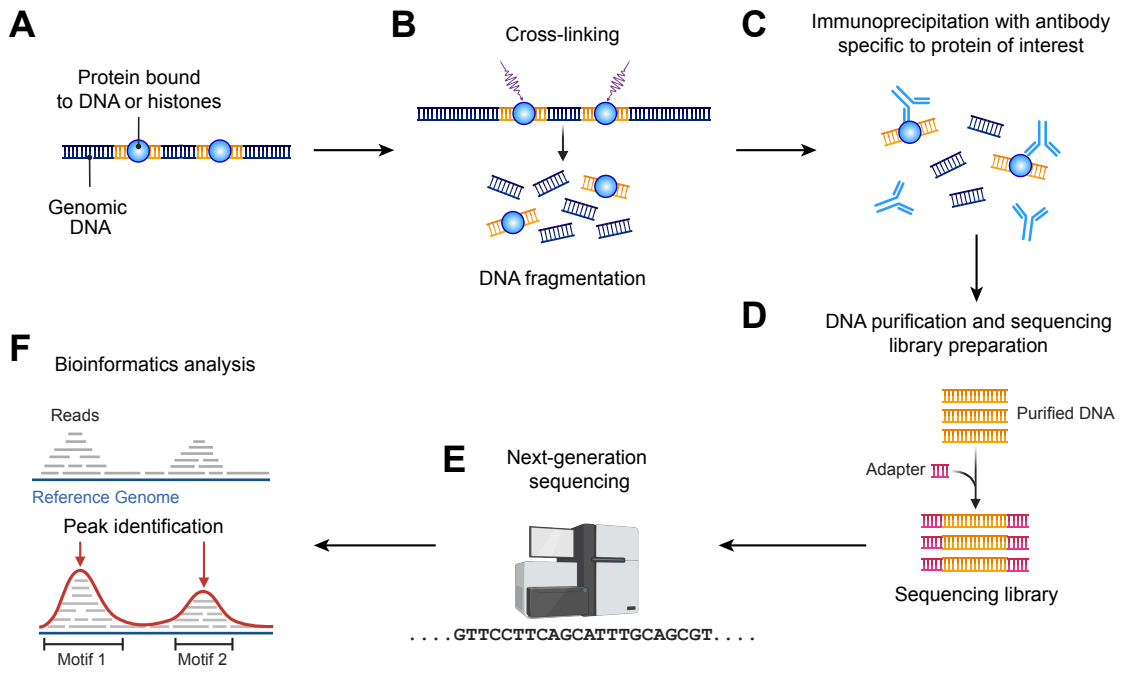

Figure 2.6. Overview of ChIP-seq workflow. [Caption continues on next page...]

Figure 2.6. Overview of ChIP-seq workflow. **(A)** The protein of interest is bound to DNA or histones within the genomic context. **(B)** Cross-linking with formaldehyde stabilises protein-DNA interactions, which is followed by DNA fragmentation through sonication. **(C)** Specific antibodies against the protein of interest are used to immunoprecipitate the protein-DNA complex. **(D)** Cross-links are reversed, and DNA is purified for sequencing library preparation, including the ligation of sequencing adapters. **(E)** The prepared library undergoes next-generation sequencing. **(F)** Bioinformatics analysis involves mapping sequencing reads to a reference genome, identifying peak regions indicative of protein-DNA interactions, and interpreting these regions to understand the binding motifs and functional elements associated with the protein of interest.

Several histone modifications can be investigated using ChIP-seq to gain insights into gene regulation and chromatin dynamics. In this thesis, I chose to focus my studies on acetylated histone H3 at lysine 27 (H3K27ac) because this well-characterised epigenetic mark is associated with active enhancers and promoters and correlates with active gene expression.[126–128] Furthermore, BET proteins have been shown to regulate gene transcription by binding to H3K27ac on active regions of chromatin, and may even modulate the binding activity of H3K27ac itself.[132,189,190] I therefore wished to investigate changes in genome-wide H3K27ac occupancy in response to BET inhibition. In addition, to investigate the functional roles of BET proteins themselves in gene regulation in PNET cells, I conducted ChIP-seq using antibodies against BRD2, BRD3, and BRD4 in DMSO control-treated BON1 cells, aiming to identify the genomic locations where these proteins may influence gene expression.

2.4.4.2 Preparation of chromatin samples and cross-linking

BON1 cells were seeded in 175 cm^2 tissue culture flasks (one flask per treatment group) at a density of 1×10^6 cells/mL in 30 mL of media. The following day, the media was refreshed, and epigenetic drugs were added to the wells at a concentration of 1 μM, or 0.5 μM each for the BD1- and BD2-selective inhibitor combination drug treatments. Negative control cells were treated with 0.05% DMSO. ChIP was performed using the Millipore ChIP Assay Kit (Merck, Watford, UK), according to the manufacturer's protocol. After 6 hours of drug treatment, cells were cross-linked

with cross-linking buffer (1% formaldehyde, 10 mM NaCl, 0.1 mM EDTA, 0.05 mM EGTA, and 5 mM HEPES pH 8.0) (all Sigma-Aldrich) for 15 minutes at room temperature. The cross-linking reaction was quenched with the addition of 125 mM of glycine (Sigma-Aldrich) for 5 minutes with gentle agitation. Following quenching, cells were washed twice in PBS, flash frozen in liquid nitrogen, and stored at -80°C until ready for use.

2.4.4.3 Optimisation of sonication conditions

A prerequisite of ChIP-seq is that chromatin is fragmented to small sizes (approximately 200-600 bp).[191] This is necessary for the successful generation of sequencing libraries that provide high resolution of binding sites. The conditions used to sonicate chromatin require optimisation for each cell line and vary depending on the type and number of cells used, fixation conditions, and model of sonicator. Avoiding over-sonication is also important, as this may lead to stripping of the DNA-binding proteins prior to the immunoprecipitation steps, resulting in loss of signal.[192] Because ChIP-seq data have not previously been reported in BON1 cells, I conducted a series of experiments in which sonication parameters were varied to determine optimal sonication conditions. Briefly, untreated BON1 cells were prepared as described in Section 2.4.4.2. Frozen cell pellets were thawed, resuspended in 1 mL of lysis buffer (1% SDS, 10 mM EDTA, 50 mM Tris, pH 8.1) supplemented with cOmplete™ protease inhibitor cocktail and incubated for 10 minutes on ice. Two hundred µL aliquots of the cell lysate (one per sonication regimen) were transferred into 1.5 mL microcentrifuge tubes (Eppendorf, Stevenage, UK) and were sonicated using an EpiShear™ probe sonicator (Active Motif, Carlsbad, CA). The six tested regimens varied in the number of sonication cycles (0, 4, 8, 12, 16, and 20), with each cycle consisting of 30 seconds of active sonication ('ON') followed by 30 seconds of pause ('OFF'), at an amplitude of 40%. After sonication was complete, 8 µL of 5M NaCl was added to each sample followed by incubation for 4 hours to reverse the crosslinks. DNA was recovered by phenol/chloroform extraction, and 5 µL of each sample was mixed with 6x loading dye (Thermo Fisher

Scientfic) and pipetted into a 2% UltraPure agarose gel (Invitrogen) containing 0.5 μg/mL of ethidium bromide (Sigma-Aldrich). A Hyperladder™ 100 bp molecular weight marker (Bioline, London, UK) was loaded alongside the samples to allow for identification of DNA fragment size. The gel was run for 45 minutes at 110 V in a Mini-Sub® Cell GT Cell tank (Bio-Rad). DNA was visualised on a ChemiDoc MP™ system with Image Lab software. Based on these optimisation experiments, 8 sonication cycles were selected as the optimal regimen **(Figure 2.7)**.

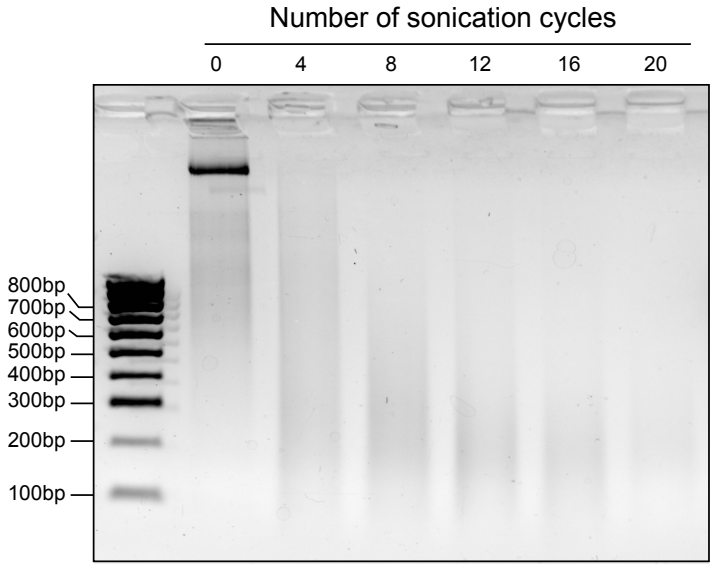

Figure 2.7. Optimisation of ChIP-seq sonication regimen. Samples were sonicated for 4, 8, 12, 16 or 20 cycles of 30 seconds 'ON' and 30 seconds 'OFF' at an amplitude of 40% using an EpiShear™ probe sonicator. The resulting chromatin was de-crosslinked overnight, purified by phenol-chloroform extraction and loaded onto on a 2% agarose gel for electrophoresis. Lane 1 shows a 100 bp DNA ladder marker and lane 2 shows an unsheared DNA control. With increasing number of sonication cycles, the peak of chromatin fragment sizes is shifted towards smaller fragments.

2.4.4.4 Chromatin sonication and immunoprecipitation

Frozen cell lysates prepared in Section 2.4.4.3 were thawed on ice, resuspended in 1 mL of lysis buffer supplemented with cOmplete™ protease inhibitor cocktail and incubated for 10 minutes on ice. 200 μL aliquots of the cell lysates (one per antibody) were transferred to 1.5 mL microcentrifuge tubes and sonicated

using an EpiShear™ probe sonicator to achieve a mean DNA fragment size of 200-600 bps (8 cycles, each consisting of 30 seconds of active sonication followed by 30 seconds of pause, at an amplitude of 40%). Insoluble cellular debris was pelleted by centrifugation at 14,000 *g* for 10 minutes at 4°C. The supernatants were transferred into new tubes and diluted 1:10 in ChIP dilution buffer (0.01% SDS, 1.1% Triton X-100, 1.2 mM EDTA, 16.7 mM Tris-HCl [pH 8.1], 167 mM NaCl) (Merck) supplemented with cOmplete™ protease inhibitor cocktail. One aliquot was set aside to serve as the 'input DNA control' and stored at -20°C. Chromatin in the remaining tubes was pre-cleared using Protein A Agarose/Salmon Sperm DNA (50% slurry) (Merck), for 30 min at 4°C with agitation. Agarose was removed by brief centrifugation (500 *g* at 4°C for 1 minute) and supernatants were incubated overnight with the antibodies listed in **Table 2.7** at 4°C with gentle rotation. Two biological replicates were performed per antibody.

Table 2.7. List of antibodies used for ChIP-seq

Antibody	Species	Catalogue no.	Dilution	Source
BRD2	Rabbit	D89B4	10 µL/IP	Cell Signaling Technology, Danvers, MA, USA
BRD3	Rabbit	61489	10 µL/IP	Active Motif, Carlsbad, CA, USA
BRD4	Rabbit	C15410337	1 µL/IP	Diagenode, Denville, NJ, USA
H3K27ac	Rabbit	C15410196	1 µL/IP	Diagenode, Denville, NJ, USA

H3K27ac, acetylated histone H3 at lysine 27; IP, immunoprecipitation

2.4.4.5 DNA purification

Protein A Agarose/Salmon Sperm DNA (50% slurry) was added to the chromatin-antibody complexes and the samples were incubated for 1 hour at 4°C with gentle rotation. The agarose pellets with bound DNA were collected by gentle centrifugation (500 *g* at 4°C for 1 minute) and the supernatant was removed. The

pellets were then washed for 5 min each with 1 mL of Low Salt Immune Complex Wash Buffer (0.1% SDS, 1% Triton X-100, 2 mM EDTA, 20 mM Tris-HCl [pH 8.1], 150 mM NaCl); 1 mL of High Salt Immune Complex Wash Buffer (0.1% SDS, 1% Triton X-100, 2 mM EDTA, 20 mM Tris-HCl [pH 8.1], 500 mM NaCl); 1 mL of LiCl Immune Complex Wash Buffer (0.25 M LiCl, 1% IGEPAL-CA630, 1% deoxycholic acid, 1 mM EDTA, 10 mM Tris [pH 8.1]) and twice with 1 mL of TE buffer (10 mM Tris-HCl, 1 mM EDTA, [pH 8.0]) (all Merck).

Chromatin was recovered by addition of 250 µL elution buffer (1% SDS and 0.1 M $NaHCO_3$) to the agarose pellets and incubating on a rotator for 15 minutes at room temperature. After gentle centrifugation (1000 *g* for 1 minute), the elutes were transferred to microcentrifuge tubes. The process was repeated, with the addition of another 250 µL of elution buffer, and the elutes were combined. To reverse protein/DNA cross-links, 20 µL of 5 M NaCl was added to the combined elutes and the 'input DNA control' sample (prepared in Section 2.4.4.4), followed by incubation at 65°C for 4 hours. The purified DNA was treated with 10 µL of 0.5 M EDTA, 20 µL of 1 M Tris-HCl (pH 6.5), and 2 µL of 10 mg/mL Proteinase K (Thermo Fisher Scientific) for 1 hour at 45°C. Finally, the DNA was isolated with phenol chloroform extraction and ethanol precipitation.

2.4.4.6 Library preparation and sequencing

ChIP DNA quantity was determined using the Qubit® dsDNA High Sensitivity assay (Thermo Fisher Scientific) and quality was assessed with an Agilent 2200 TapeStation. Approximately 10-15 ng per sample was submitted to the Wellcome Trust Centre for Human Genetics for library preparation and sequencing. Libraries were prepared using the PrepX™ DNA Library Kit and Apollo 324 automatic library prep system (WaferGen, Fremont, CA, USA). The generated libraries were pooled and sequenced on a NovaSeq 6000 system (Illumina) with approximately 40-50 million pair-end 150 bp reads obtained per sample.

2.4.4.7 ChIP-seq bioinformatics analysis

Raw sequencing reads were demultiplexed with bcl2fastq2 software, and FASTQ files were generated. Adapter sequences and low-quality bases were trimmed from the reads using Cutadapt. The processed reads were then aligned to the human reference genome (GRCh38) using the Burrows-Wheeler Alignment (BWA) tool (v0.7.17 `https://github.com/lh3/bwa`). The generated BAM files were indexed and sorted, with unmapped, non-uniquely mapped and duplicate reads filtered and removed using samtools (v1.17 `https://github.com/samtools/samtools`). The 'Model-based Analysis for ChIP-Seq 2' (MACS2, v2.2.8) package for Python was used to call peaks of enriched regions, using the input DNA as a control. An FDR-adjusted p-value threshold of 0.05 was used to call significant peaks using the 'narrowPeak' setting. Overlapping peaks from both replicates in each treatment group were merged into a final peak list using the 'intersect' command in the Bedtools software suite (v2.31.0 `https://github.com/arq5x/bedtools2`). To determine the genomic regions enriched with BRD2, BRD3, BRD4 and H3K27ac ChIP-seq signals, the identified peaks were annotated to genes using the 'ChIPseeker' R package (v1.36.0). Motif analysis was conducted using the 'findMotifsGenome.pl' script in Hypergeometric Optimisation of Motif EnRichment (HOMER) software (v4.11, `http://homer.ucsd.edu/homer/index.html`) to identify enriched transcription factor binding motifs ± 100 bp from the centers of binding peaks.

To normalise read counts and facilitate comparisons across samples, BAM files were converted into BigWig files using the 'bamCoverage' function within the 'DeepTools' (v3.5.2) Python package. Reads were normalised using the reads per kilobase of transcript per million mapped reads (RPKM) method. Normalised BigWig files were then imported into the Integrative Genomics Viewer (IGV) browser (v2.7.0 Broad Institute, Cambridge, MA, USA)[193] for visualisation of binding at specific loci. Heatmaps were generated by computing average read density around peak summits using the 'computeMatrix' and 'plotHeatmap' modules in 'DeepTools'.

To compare changes in H3K27ac occupancy between the DMSO- and drug-treated groups, the R package 'DiffBind' (v3.1.7) was used. MACS2-identified H3K27ac peaks for each condition, along with the respective BAM files for each ChIP experiment and input control, were imported. The 'dba.peakset' function was used to derive a parent consensus peak set of merged peaks present in both biological replicates (minimum overlap 1 bp) in each treatment group. A final consensus peak set was generated by selecting peaks that were common across at least two different treatment groups (minimum overlap 1 bp). This final consensus peak set was then used for differential binding affinity analysis to identify changes in H3K27ac occupancy, employing the 'dba.analyze' function within 'DiffBind', which integrates with 'DESeq2'. Peaks with an absolute $\log_2$ fold-change of ≥ 1 and FDR-corrected p-value of ≤ 0.05 were identified as differentially bound. Annotation of the differential peaks was performed using 'ChIPSeeker'.

Annotation of putative super-enhancer (SE) regions in untreated BON1 cells was performed with the 'Ranking Ordering of Super-Enhancers (ROSE)' algorithm (`https://bitbucket.org/young_computation/rose/src/master/`),[132] run in Python. SEs are large clusters of enhancers that are densely occupied by transcriptional co-activators, driving cell-type specific gene expression.[129,194,195] These regions are marked by high levels of H3K27ac occupancy. 'ROSE' is a widely-used method for computationally identifying SEs from ChIP-seq data.[196] The algorithm first identifies enhancer regions by stitching together H3K27ac peaks that fall within 12.5 kb of one another, ignoring regions 2.5 kb around transcription start sites (TSS). Next, these stitched enhancer regions are ranked based on H3K27ac occupancy over background input. A graph of H3K27ac signal versus enhancer rank is then generated, and a best-fit curve is calculated. Enhancers residing above the inflection point of the curve are designated as SEs, while the rest are designated as typical enhancers.

2.5 Mouse studies

2.5.1 Ethics approval

All animal studies and protocols were approved by the University of Oxford Ethics Committee and were conducted according to the UK Home Office Animals (Scientific Procedures) Act 1986. Regulated procedures were carried out under Procedure Project Licence (PPL) no. 30/2383. Animals were kept in accordance with UK Home Office welfare guidelines and project licence restrictions.

2.5.2 Housing and animal husbandry

Mice were housed in a pathogen-free facility: the Biomedical Services Building, John Radcliffe Hospital (Headington, UK). The facility maintained 12-hour light/dark cycles. Mice were housed in groups of six within individually ventilated cages with woodchip bedding. They were fed a standard diet (Rat and Mouse No. 1, expanded diet, Special Diet Services Ltd., Witham, UK) and had *ad libitum* access to food and water. Atmospheric temperature was maintained at 22°C (range: 21-24 °C) and humidity was maintained at 50% (range: 35-65%). All mice were monitored and cared for on a daily basis by animal technicians in the Biomedical Services Building, and were weighed and examined daily. Once ready for pancreas harvesting, mice were culled humanely using an appropriate Schedule 1 method. Mice used in scientific experiments had not been used for prior experimental procedures or for any other purpose (e.g., breeding).

2.5.3 Mouse strains

The conditional Men1 knockout mouse model (*Men1*$^{L/L/}$*RIP2-Cre*) was generated by crossing two different mouse strains: 129S(FVB)-Men1tm1.2Ctre/J (abbreviated name: *Men1*$^{L/L}$; strain no. 005109; The Jackson Laboratory, Bar Harbor, ME, USA) and B6.Cg-Tg(Ins2-cre)25Mgn/J (abbreviated name: RIP2-Cre; strain no. 003573;

The Jackson Laboratory), as previously described.[197] The Men1$^{L/L}$ strain carries LoxP sites flanking exons 3 to 8 of the *Men1* gene. The RIP2-Cre strain carries the RIP2-Cre transgene, which is under the control of the rat insulin 2 promoter (RIP2) and drives the expression of the Cre recombinase enzyme specifically in pancreatic β cells. Thus, offspring *Men1*$^{L/L/}$*RIP2-Cre* mice inherit both the floxed *Men1* gene and pancreatic β cell-specific Cre recombinase (*Cre*) expression, resulting in excision of *Men1* exons 3 to 8 in a tissue-specific manner. These mice develop insulin-secreting PNETs by 6 months of age. All mice were maintained on a mixed 129S6/SvEv x C57BL/6 genetic background.

2.5.4 Mouse genotyping

Mice were genotyped using genomic PCR to confirm the presence of the floxed *Men1* allele (*Men1*$^{L/L}$) and the presence of the RIP2-Cre transgene. Genomic DNA was extracted from auricular biopsy samples using DNA extraction buffer (10 mM NaCl, 20,mM Tris-HCl [pH 8.0], 1,mM EDTA, 10% SDS) and proteinase K solution at 55°C overnight. Following incubation, the samples were heated to 95°C for 10 minutes to inactivate the proteinase K. The resulting DNA extracts were used as templates for genotyping analyses.

Approximately 0.1 μg of genomic DNA underwent multiplex PCR using three primers for the detection of wild-type (wt) and floxed *Men1* alleles. Primer A (*Men1* common forward: 5'-CCCACATCCAGTCCCTCTTCAGCT-3') is specific to exon 1 of the *Men1* gene and primer B (*Men1* wt reverse: 5'-CCCTCTGGCTATTCAATGGCAGGG-3') is specific for the wt DNA sequence. Primer C (*Men1* LoxP reverse: 5'-CGGAGAAAGAGGTAATGAAATGGC-3') is specific for the LoxP site. The PCR reaction was carried out in a PTC-225 DNA Engine Tetrad thermocycler (MJ Research, Waltham, MA, USA) under the following conditions: initial denaturation at 95°C for 1 minute, followed by 35 cycles of 95°C for 30 seconds, 60°C for 30 seconds, and 72°C for 1 minute, with a final extension step of 72°C for 10 min. PCR products were separated by gel

electrophoresis on a 2% UltraPure agarose gel containing 0.5 μg/mL of ethidium bromide; the combinations of primers A and B yielded a 300 bp wt fragment, whilst primers A and C and C yielded a 236 bp mutant floxed fragment.

For detection of the *Cre* allele, approximately 0.1 μg of genomic DNA was used for multiplex PCR using *Cre* forward primer (CreF; 5'-GCGGTCTGGCAGTAAAAACTATC-3') and *Cre* reverse primer (CreR; 5'-GTGAAACAGCATTGCTGTCACTT3'). Additionally, an internal control gene, Interleukin-2 (*IL-2*), was amplified with control forward primer (5'-CTAGGCCACAGAATTGAAAGATCT-3') and control reverse primer (5'-GTAGGTGGAAATTCTAGCATCATCC -3'). The PCR reaction was carried out in a PTC-225 DNA Engine Tetrad thermocycler under the following conditions: initial denaturation at 95°C for 3 minutes, followed by 35 cycles of: 95°C for 30 seconds, 58°C for 1 minute, and 72°C for 1 minute, with a final extension step of 72°C for 2 minutes. Products were separated by electrophoresis on a 2% UltraPure agarose gel containing 0.5 μg/mL of ethidium bromide. The presence of a 100 bp band indicated the successful amplification of the *RIP2-Cre* transgene, while the presence of the 325 bp expected band for the internal control primer confirmed the reliability of the PCR reaction and DNA quality **(Figure 2.8)**.

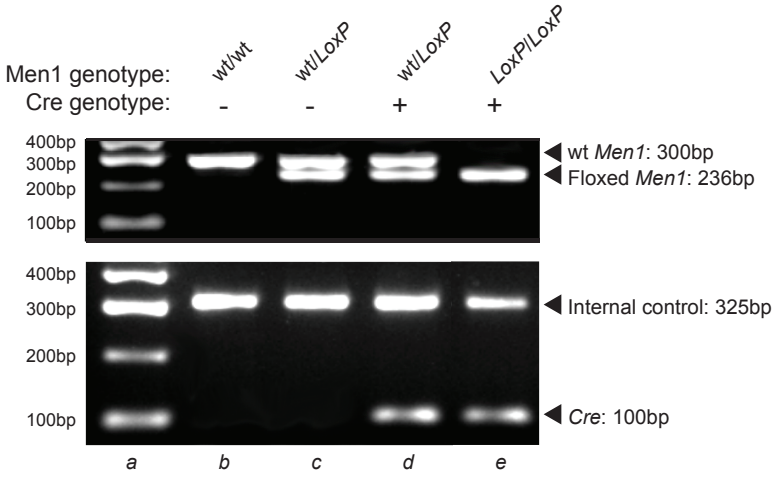

Figure 2.8. Overview of mouse genotyping. [Caption continues on next page...]

Figure 2.8. Overview of mouse genotyping. Representative genotypes of wt and floxed (LoxP) *Men1* mice with and without Cre recombinase expression. Lane *a* corresponds to the molecular weight marker. Lane *b* represents a mouse that is homozygous for the wt *Men1* allele and does not express Cre recombinase. Lanes *c* and *d* represent mice that are heterozygous for both a wt and floxed *Men1* allele. The mouse in lane *c* expresses Cre, whereas the mouse in lane *d* does not. The mouse in lane *e* is homozygous for floxed *Men1* alleles and also harbours Cre recombinase. Thus, the mouse in lane *e* would be expected to develop insulin-secreting PNETs by 6 months of age, due to Cre-recombinase mediated deletion of *Men1* exons 3 to 8 in pancreatic β cells.

2.5.5 Histology and immunofluorescence

2.5.5.1 Tissue preparation and sectioning

To confirm the development of PNETs in *Men1*$^{L/L/}$*RIP2-Cre* mice, a cohort of untreated mice were humanely culled at 8 months of age and their pancreata were harvested and immediately fixed in 4% paraformaldehyde (PFA, Sigma-Aldrich) dissolved in PBS. For control comparisons, pancreata from wt mice aged 6–8 months were similarly processed. After 24 hours, the samples were placed in histology cassettes and subjected to serial dehydration and paraffin embedding using a TP1020 automated semi-enclosed bench top tissue processor (Leica Biosystems). Paraffin-embedded blocks were sectioned, mounted and rehydrated as detailed in Section 2.2.3.

2.5.5.2 Antigen retrieval and blocking

Antigen retrieval was performed by heating slides to 121°C for 10 minutes in 10 mM citrate buffer (pH 6.0) using a 2100-Retriever bench top pressure cooker (Electronic Microscopy Sciences, Hatfield, PA, USA). Once cooled down, the sections were blocked in 3% hydrogen peroxide for 10 minutes, followed by blocking with 10% donkey serum in PBS for 30 minutes at room temperature.

2.5.5.3 Antibody staining

After the blocking step, 50 µL of rabbit anti-Ki-67 (Abcam) and 50 µL of mouse anti-insulin (Abcam) primary antibodies were each diluted 1:100 in PBS to the required volume and then combined and added to each section, followed by incubation in a humidified chamber at room temperature for 1 hour. The slides were then washed twice for 10 minutes with PBS followed by incubation with 50 µL each of Cy2-conjugated donkey anti-rabbit and Cy3-conjugated donkey anti-mouse secondary antibodies (Jackson ImmunoResearch), both diluted 1:100 in PBS, for 1 hour. After two further 10-minute washes in PBS, coverslips were mounted using ProLong® Gold Antifade Reagent with DAPI (Molecular Probes, Eugene, OR, USA).

2.5.5.4 Image acquisition

Sections were examined under fluorescent microscopy using an Eclipse E400 microscope and images captured at 10x and 20x magnifications with a DXM1200 digital camera and NIS-Elements BR software. Representative whole slides were also scanned at 40x magnification using an Aperio CS2 digital pathology slide scanner (Leica Biosystems) to assess pancreatic islet size and Ki-67 staining distribution.

2.5.6 *Ex vivo* neoplastic mouse islet drug studies

2.5.6.1 Pancreas digestion and islet purification

Neoplastic islets were isolated from the pancreata of 9-10 month-old *Men1*$^{L/L}$/*RIP2-Cre* mice following humane culling using a Schedule 1 procedure. After exposing the liver, pancreas and common bile duct, the ampulla of Vater in the duodenum was clamped under a dissecting microscope. Using a 3 mL syringe with 30G needle, ~2 mL of Liberase TM solution (Sigma-Aldrich) at a concentration of 1 mg/mL (diluted 1:5 in 0.2% bovine serum albumin (BSA) in Hanks' buffer [Thermo Fisher Scientific]) was injected into the common bile duct. The clamp on

the ampulla prevented leakage of Liberase solution into the intestine. The distended pancreas was then harvested and placed in a falcon tube containing ice-cold 0.2% BSA in Hanks' buffer to inhibit further enzymatic activity.

The harvested pancreas was incubated at 37°C for 13 minutes with gentle shaking to facilitate digestion. After incubation, the tissue was mechanically dissociated by shaking the tube ~65 times. The digested tissue was washed three times with cold 0.2% BSA in HBSS, each time discarding the supernatant containing exocrine tissue, while the denser islets settled at the bottom of the tube. After the final wash, the tissue was resuspended in 10 mL of Ficoll-Paque solution (Sigma-Aldrich) and thoroughly mixed. The suspension was then centrifuged at 1200 revolutions per minute (rpm) for 20 minutes and the supernatant (containing islets) was decanted into 25 mL of 0.2% BSA in Hanks' buffer. The mixture was then centrifuged at 1500 rpm for 4 minutes so that the islets formed a pellet. After decanting the supernatant, the pellet was resuspended in 10 mL of 0.2% BSA in Hanks' buffer followed by centrifugation at 1200 rpm for 3 minutes. Finally, the supernatant was carefully removed, and the islets were resuspended in RPMI-1640 medium supplemented with 10% FBS, 100 U/mL penicillin and 100 µg/mL streptomycin (Sigma-Aldrich), and 10 mM glucose.

2.5.6.2 Islet plating and compound treatments

Islets were individually hand-picked using a P200 micropipette under an inverted microscope and plated at a density of 10 islets per well in black-walled 96-well plates, with each well containing 100 µL of culture medium. Compound treatments were conducted similarly to those applied to the cell lines, as described in Section 2.3.4. Treatments included 1 µM each of GSK789, GSK620 or I-BET151, or a combination of GSK789 and GSK620 at 0.5 µM each. Wells treated with 0.05% DMSO served as negative controls. After 96 hours of treatment, cell viability was assessed using the CellTiter-Blue® assay (as described in Section 2.3.4).

2.6 Data visualisation

Figures were prepared in Illustrator (v27.5, Adobe Inc., San Jose, CA, USA), Photoshop (v 24.5, Adobe Inc.), GraphPad Prism and in RStudio using the packages 'ggplot2' (v3.4.2) and 'RColorBrewer' (v1.1-3).

2.7 Statistical analysis

Unless otherwise specified, all statistical analyses were performed in GraphPad Prism. Numerical data were assessed for normality using the Shapiro–Wilk test and normally distributed (parametric) data were analysed using a two-tailed unpaired t-test or one-way analysis of variance (ANOVA) with Tukey's *post-hoc* test for multiple comparisons. Non-normally distributed (non-parametric) data were analysed using the Mann-Whitney U test or the Kruskal-Wallis test. The Chi-squared test was used to analyse categorical data. For the clinical study of MEN1 in children and adolescents, Kaplan-Meier curves were generated to estimate the cumulative age-specific penetrance of each manifestation and disease-free outcome after surgery. Comparisons between Kaplan-Meier curves were made using the log-rank test. The specific analysis undertaken is stated in the corresponding figure legend. All numerical data are expressed as mean ± standard error of the mean (s.e.m.) unless otherwise indicated. A p-value of ≤ 0.05 was considered to be statistically significant.

3

Multiple endocrine neoplasia type 1 in children and adolescents: clinical features and treatment outcomes

Chapter-specific table of contents

3.1 Aims **81**
3.2 Results **84**
3.2.1 Clinical features of cohort and tumour development . 84
3.2.2 Primary hyperparathyroidism (PHPT) 87
3.2.3 Pancreatic and duodenal neuroendocrine tumours (PD-NETs) 89
3.2.4 Pituitary tumours 93
3.2.5 Adrenal tumours 95
3.2.6 *MEN1* genetic analysis and genotype-phenotype correlations 95
3.3 Discussion **97**

3.1 Aims

Multiple endocrine neoplasia type 1 (MEN1)-related tumours have been reported to occur as early as 5 years of age.[73] Thus, current guidelines recommend that patients with MEN1 undergo comprehensive screening for endocrine neoplasms from

childhood, to enable early tumour recognition and ensure timely intervention before the development of adverse sequelae, such as metastatic disease.[73] However, there is no consensus regarding the age at which screening should start, as the benefits are offset by concerns about burden of testing, potential radiation exposure and cost.[198] Moreover, some studies have indicated that clinically-significant or symptomatic MEN1 manifestations are rare before 16 years of age,[86] although it is of note that these reports consist of either small numbers of paediatric and adolescent patients from single institutions,[84,85,87,88] or in the case of larger multi-centre series,[89,90] include historical cohorts of patients seen prior to the introduction of contemporary screening methods or in whom screening began relatively late in childhood **(Table 3.1)**. Thus, the incidence of MEN1-related manifestations in this age group is not well-characterised, and may have been underestimated.[84–90] Furthermore, there is also a lack of consensus regarding the optimal management of MEN1 manifestations, such as primary hyperparathyroidism (PHPT) and non-functioning PNETs (NF-PNETs) in children and adolescents.

The aims of this chapter were therefore to evaluate the occurrence of MEN1-related manifestations by $\leq$ 18 years of age, their treatment outcomes, and genotype-phenotype correlations. I was particularly interested in ascertaining whether MEN1 patients in this age group present with malignant pancreatic or duodenal NETs (PD-NETs), as these are the leading cause of MEN1-related mortality[76,81] This focus on early-onset MEN1 manifestations is crucial, as earlier detection and management can potentially alter the course of the disease and improve long-term outcomes.

Table 3.1. Studies in the literature that describe paediatric and adolescent MEN1 cohorts

Study (reference in parenthesis)	Newey et al. (2009)[84]	Gonçalvez et al. (2014)[85]	Goudet et al. (2015)[90]	Manoharan et al. (2017)[86]	Vannucci et al. (2018)[87]	Marini et al. (2018)[88]	Herath et al. (2019)[89]	Current study
Country/countries	UK	Brazil	France, Belgium	Germany	Italy	Italy	Australia	UK, USA, Austria
Patients (n=)[a]	12	8	924	166	22	19	180	80
Upper age limit for paediatric and adolescent group	19 yrs	19 yrs	20 yrs	18 yrs	31 yrs	19 yrs	21 yrs	18 yrs
Patients with MEN1 manifestation below upper age limit (n=)b	5 (42%)	8c	160 (17%)	20 (12%)	12 (55%)	19e	53 (29%)	56 (70%)
Patients with PHPT (n=)[c]	4 (80%)	N/A	122 (76%)	9 (45%)	11 (92%)	19e	42 (79%)	46 (82%)
Patients with NF-PNET (n=)[c]	2 (40%)	8d	14 (9%)	3 (15%)	2 (17%)	N/A	9 (17%)	15 (27%)
Patients with insulinoma (n=)[c]	0	2d	20 (13%)	5 (25%)	0	N/A	3 (6%)	8 (14%)
Patients with PA (n=)[c]	1 (20%)	N/A	55 (34%)	6 (30%)	7 (58%)	N/A	13 (25%)	18 (32%)
Patients with other tumours (n=)[c]	0	N/A	Gastrinoma (n = 3, 2%), ACC (n = 2, 1%), Thymic NET (n = 1, <1%)	Bronchial NET (n = 1, 5%)	0	N/A	Bronchial NET (n = 1, 2%)	Gastrinoma (n = 1, 2%), AA (n = 1, 2%)
Patients without any manifestations below upper age limit (n=)[b]	7 (58%)	N/A	764 (83%)	146 (88%)	10 (45%)	N/A	127 (71%)	24 (30%)

[a]Total includes MEN1 patients of all ages. [b]Percentage refers to total number of patients (with and without manifestations) included in study. [c]Percentage refers to total number of patients who developed an MEN1 manifestation before the paediatric/adolescent upper age limit. [d]Study only described patients with NF-PNETs and insulinomas so percentages not reported. [e]Study only included patients with PHPT so percentages not reported. AA, adrenal adenoma; ACC, adrenocortical carcinoma; N/A, not applicable; PA, pituitary adenoma; PHPT, primary hyperparathyroidism. Table reproduced from Shariq et al.[199]

3.2 Results

3.2.1 Clinical features of cohort and tumour development

A total of 118 patients with MEN1 (median age = 25 years, range = 6–35 years) were ascertained, and 38 patients were excluded because: screening was not commenced until after 18 years of age (n = 34); follow-up was not continued after their initial visit (n = 3); and surveillance abdominal imaging had not been performed at the time of last follow-up (n = 1) **(Figure 3.1)**. The remaining 80 patients, from 60 unrelated families, consisted of 50 females (63%) and 30 males (38%), who had MEN1 diagnosed at a median age of 11.5 years (range = 0.8–18 years), with the median duration of follow-up being 92.5 months (range = 7–306 months). Eighteen percent (14/80) of patients had not reached 18 years of age at the time of inclusion. Details regarding the screening protocol are provided in Section 2.1.3 (see **Table 2.1** on page 34).

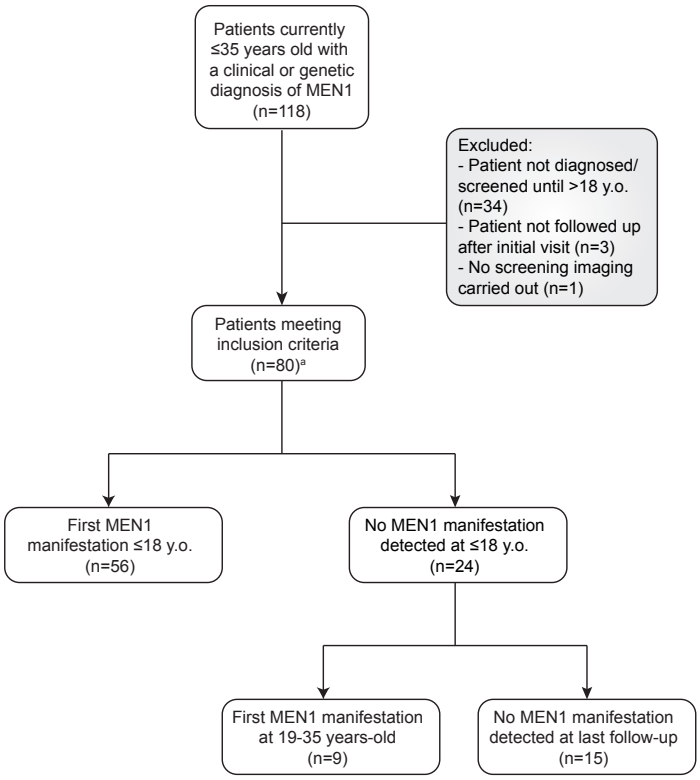

Figure 3.1. Flow chart of the study population. [a]Fourteen patients had not yet reached 18 years of age at the time of study inclusion. Figure reproduced from Shariq et al.[199]

Seventy percent (56/80) of patients (37 females and 19 males) developed at least one MEN1-related manifestation at ≤ 18 years of age, with the first manifestation detected at a median age of 14 years (range = 6–18 years) **(Table 3.2)**. Of these 56 patients, 68% (38/56) had prospective screening that preceded the development of the first MEN1 manifestation, whereas 32% (18/56) had commenced screening only after the first manifestation was detected and, of these, 12 had a known family history and had either not been referred for screening or were referred and declined further participation, while the remaining 6 were index cases.

Table 3.2. Details of 56 MEN1 patients with manifestations detected at ≤ 18 years of age

	Overall (n = 56)	**Male (n = 19)**	**Female (n = 37)**
Median age at MEN1 diagnosis, yrs [range]	13 [2 – 18]	11 [6 – 18]	13 [2 – 17]
Median age at first MEN1 manifestation, yrs [range]	14 [6 – 18]	14 [6 – 18]	14.5 [6 – 18]
Median age at last follow-up, years [range][a]	22.5 [6 – 35]	24 [6 – 35]	22 [6 – 34]
Index case	4 (7 %)	3 (16%)	1 (%)
Genetic testing performed	53 (95%)	17 (90%)	36 (97%)
MEN1 screening started before first manifestation detected	38 (68%)	10 (53%)	28 (76%)
Initial MEN1 manifestation(s) detected			
PHPT only	29 (52%)	9 (47%)	20 (54%)
Pituitary adenoma only	12 (21%)	3 (16%)	9 (24%)
NF-PNET only	5 (9%)	1 (6%)	4 (11%)
Insulinoma only	3 (5%)	0	3 (8%)
PHPT + pituitary adenoma	2 (4%)	1 (5%)	1 (3%)
PHPT + NF-PNET	2 (4%)	2 (11%)	0
PHPT + insulinoma	2 (4%)	2 (11%)	0

Continued on next page

Table 3.2. Details of 56 MEN1 patients with manifestations detected at ≤ 18 years of age (Continued)

	Overall (n = 56)	Male (n = 19)	Female (n = 37)
Pituitary adenoma + NF-PNET	2 (4%)	1 (5%)	1 (3%)
PHPT ≤ 18 years old	46 (82%)	17 (90%)	29 (78%)
PD-NET ≤ 18 years old			
NF-PNET	15 (27%)	5 (28%)	10 (27%)
Insulinoma	8 (14%)	3 (17%)	5 (13%)
Gastrinoma	1 (2%)	0	1 (2%)
PA ≤ 18 years old	18 (32%)	5 (36%)	13 (54%)
Adrenal tumour ≤ 18 years old	1 (2%)	0	1 (2%)

[a]No deaths occurred during the follow-up period. PA, pituitary adenoma; PD-NET, pancreatic or duodenal neuroendocrine tumour; PHPT, primary hyperparathyroidism. Table reproduced from Shariq et al.[199]

Out of the overall cohort of 80 patients, by the age of 18 years ~70% had PHPT, ~35% had PD-NETs, ~30% had pituitary tumours, 1% had adrenal adenomas **(Figure 3.2A)** and no patients had developed bronchial or thymic carcinoids. Thus, PD-NETs were the second most common MEN1 manifestation during childhood and adolescence. By PD-NET subtype, ~25% had NF-PNETs and ~15% had insulinomas by 18 years of age **(Figure 3.2B)**.

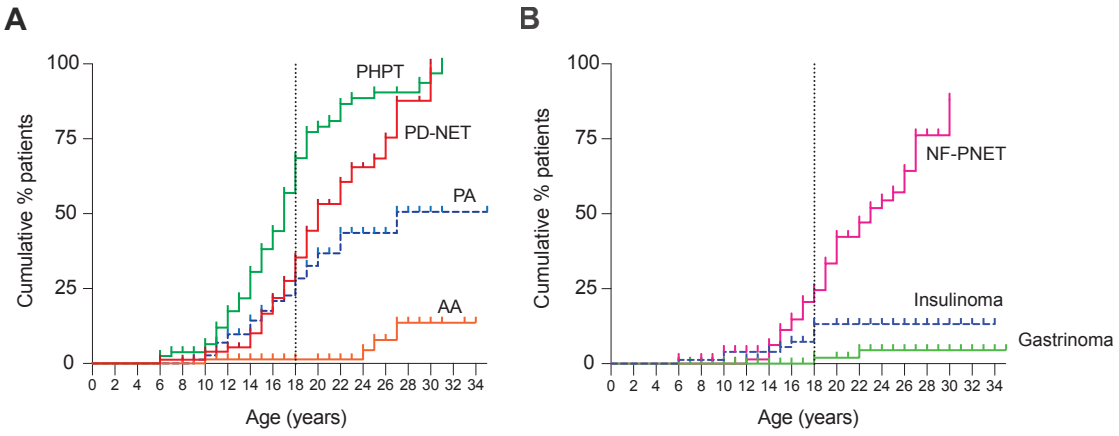

Figure 3.2. Age-related penetrance of MEN1-related manifestations [Caption continues on next page...]

Figure 3.2. Age-related penetrance of MEN1 manifestations in the overall cohort of 80 patients. (A) The dashed vertical line indicates the age threshold of 18 years for paediatric and adolescent patients in this study. **(B)** Age-related penetrance of NF-PNETs, insulinomas, and gastrinomas. New development of insulinomas was not observed in patients above 18 years of age, whereas NF-PNETs continued to develop in patients above 18 years of age, and gastrinomas developed only in those who were 18 years of age and older. AA, adrenal adenoma; NF-PNET, non-functioning pancreatic neuroendocrine tumour; PA, pituitary adenoma. Figure adapted from Shariq et al.[199]

3.2.2 Primary hyperparathyroidism (PHPT)

PHPT at ≤ 18 years of age was diagnosed in > 80% (46/56) of patients who had an MEN1 manifestation in childhood or adolescence, and was the first manifestation of MEN1 disease (either alone or synchronously with another manifestation) in ~60% (33/56) of patients **(Table 3.2)**. The median age of PHPT diagnosis was 15 years (range = 6–18 years), with 3 patients diagnosed before 10 years of age. PHPT occurrence was similar in males and females (89% males vs 78% females, p = 0.467). Symptomatic disease or end-organ manifestations of PHPT were present in 20% (9/46) of patients) and these comprised: nephrolithiasis (n = 3), bone pain (n = 2), gastrointestinal dysfunction (n = 2), muscle weakness (n = 1), and ischaemic stroke (n = 1), which occurred in an index case who, at 14 years of age, presented with a generalised seizure, with magnetic resonance imaging (MRI) revealing a right-sided cortical infarct.[200]

Over 70% (33/46) of patients with PHPT underwent parathyroidectomy, which was performed at ≤ 18 years of age in ~70% (23/33) of cases (median age = 15 years, range = 6–18 years), with the remaining ~30% (10/33) of patients having surgery as adults (median age = 20.5 years, range = 19–028 years). Less than 10% (3/33) of patients had total parathyroidectomy, TPTX, (i.e., resection of 4 glands) with auto-transplantation of parathyroid tissue into the non-dominant forearm or sternocleidomastoid muscle; > 40% (14/33) of patients had subtotal parathyroidectomy, SPTX, (i.e., resection of 3–3.5 glands, leaving a remnant *in situ*); and > 45% (16/33) of patients had less than SPTX, <SPTX (i.e., resection of <3 glands). Transcervical thymectomy was performed in > 65% (22/33) of

patients. Post-operatively (median follow-up = 62 months, range = 1-290 months), > 50% (17/33) of patients developed persistent or recurrent PHPT, and these comprised > 85% (14/16), > 20% (3/13), and 0% (0/13) of patients having <SPTX, SPTX, and TPTX, respectively ($p < 0.001$). Thus, patients who underwent <SPTX had significantly worse disease-free outcome compared with those who underwent SPTX/TPTX (median 27 months *vs* not reached, log-rank hazard ratio 4.3; 95% confidence interval 1.8 – 12.6; $p = 0.005$) **(Figure 3.3)**. Eleven of 17 (~65%) patients with persistent or recurrent PHPT following SPTX (n = 2) and <SPTX (n = 9) had further surgery (median time following the first procedure = 61 months, range = 3-262 months), which resulted in normocalcaemia in only 4 patients, with the remaining 7 patients continuing to have persistent/recurrent disease. Two patients underwent a third operation (leading to completion TPTX) which failed to restore normocalcaemia. Less than 10% (3/33) of patients developed post-surgical permanent hypoparathyroidism, and these comprised a patient who had TPTX as the only surgery, and 2 patients who initially had <SPTX followed by completion TPTX.

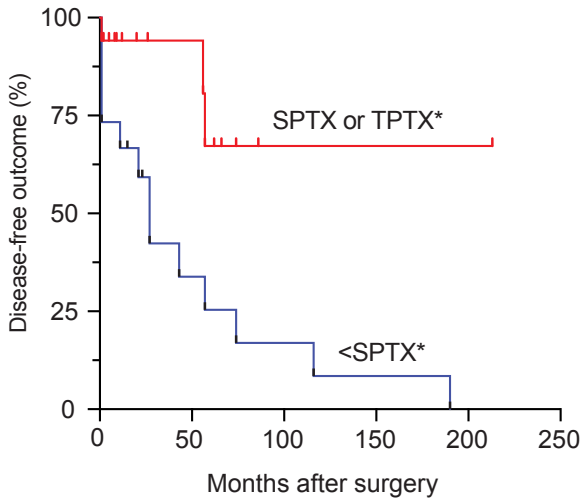

Figure 3.3. Postoperative outcomes after parathyroidectomy. Kaplan-Meier curves showing disease-free outcome and time to recurrence in 33 patients with PHPT who underwent <SPTX compared to those who had SPTX or TPTX. *p = 0.005 indicating a statistically significant difference between the survival curves on log-rank test. Figure reproduced from Shariq et al.[199]

3.2.3 Pancreatic and duodenal neuroendocrine tumours (PD-NETs)

PD-NETs were identified at ≤ 18 years of age in ~40% (21/56) of patients, with similar occurrences in males and females (42% males *vs* 35% females, p = 0.772). Synchronous or metachronous NF-PNETs and functioning PD-NETs developed in ~10% (2/21) of patients, with NF-PNETs only occurring in ~60% (13/21) of patients, and insulinomas only occurring in ~30% (6/21) of patients (**(Figure 3.2B)**). One patient had gastrinomas, and no patients had glucagonomas or vasoactive intestinal peptide-omas (VIPomas). MRI, computed tomography (CT), and endoscopic ultrasound (EUS) were used as the initial imaging modality for diagnosis in ~50% (11/21), ~25% (5/21), and ~25% (5/21) of patients, respectively.

Insulinomas, which were found at a median age of 15.5 years (range = 6-18 years, n = 8), and were the first manifestation of MEN1 in > 10% (6/56) of patients, were associated with neuroglycopaenic symptoms, which included loss of consciousness in 1 patient and seizures in another patient **(Table 3.3)**. Diagnosis was established by demonstrating hypoglycaemia and hyperinsulinaemia during a 72-hour fast in 75% (6/8) of patients. Insulinoma occurrence was similar in males and females (17% males *vs* 14% females, p = 0.99). In > 85% (7/8) of patients, the insulinomas were located in the pancreatic body/tail, while the remaining patient had multifocal insulinomas in the pancreatic head. Surgical resection by distal pancreatectomy (n = 7) or completion pancreatic head resection (n = 1), at median age 16 years (range = 6-19 years) resulted in successful resolution of hypoglycaemia without recurrence in all patients (median follow-up = 101 months, range = 14-293 months).

Table 3.3. Characteristics and treatment outcomes of 8 patients with insulinomas at ≤ 18 years of age

Case ID	Sex	Germline pathogenic variant[a]	Age at diagnosis of insulinoma	Other MEN1 features ≤ 18 years old (age, years)	Tumours on imaging (n =)	Size of largest tumour on imaging, mm	Location of largest tumour	Disease extent at diagnosis	Type of surgery	Tumours on pathology (n =)	Grade, stage, and size of largest insulin-positive tumour	Status at last F/U	Duration of F/U, months
36	F	c.421C>T; p.Gln141X	15	PHPT (18 yrs)	1	60	Tail	Localised	DP	Unknown	Unknown	No recurrence of hypoglycaemia	158
38	F	Unknown	18	PHPT (18 yrs)	2	11	Body	Localised	DP	9	G2, T1N0M0 (18 mm)	No recurrence of hypoglycaemia	71
43	F	c.1045C>T; p.Gln349X	18	NF-PNET (12 yrs), PRL (12 yrs), GA (18 yrs)	3	5	Head	Localised	CP	7	G1, T1N0M0 (15mm)	No recurrence of hypoglycaemia New liver mets from NF-PNET (age 24)	137
44	F	c.1045C>T; p.Gln349X	10	NF-PNET (10 yrs) PRL (10 yrs) AA (10 yrs)	2	13	Tail	Solitary liver met from NF-PNET	DP	2	G2, T1N0M0[b] (17mm)	No recurrence of hypoglycaemia Progresion of liver mets from NF-PNET (age 13)	45
61	M	c.549G>A; p.Trp183X	10	None	1	10	Tail	Localised	DP	Unknown	Unknown	No recurrence of hypoglycaemia New NF-PNETs (x2) in remnant (age 24): stable at last F/U	293
68	M	c.1204_1208del; p.Ser402fsX5	6	PHPT (6 yrs)	3	4	Body	Localised	DP	25 (micro-adenomatosis)	G1, T1N0M0 (4.1mm)	No recurrence of hypoglycaemia	14
71	M	c.1075_1077del; p.Glu359del	18	PHPT (18 yrs)	1	20	Tail	Localised	DP	1	G1, T1N1M0 (6mm)	No recurrence of hypoglycaemia	106
75	F	Unknown	16	PHPT (17 yrs)	2	21	Tail	Localised	DP	2	G2, T1N0M0 (21mm)	No recurrence of hypoglycaemia	96

[a]Further details of germline variants are provided in Figure 3.5.
[b]Classified as "M0" as liver lesion thought to represent metastasis from synchronous NF-PNET, not insulinoma.
AA, adrenal adenoma; CP; completion pancreatectomy; DP, distal pancreatectomy; F, female; F/U, follow-up; G, grade; GA, gastrinoma; M, male; PRL prolactinoma; Table adapted from Shariq et al.[199]

NF-PNETs, which were detected at a median age of 15 years (range = 10-18 years, n = 15) and were the first detected MEN1 manifestation in > 15% (9/56) of patients, occurred as solitary lesions in ~55% (8/15) of patients (median size = 9 mm, range = 4-38 mm) and as multifocal lesions in ~45% (7 /15) of patients (median size of the largest tumour 10 mm, range = 7-17 mm). NF-PNET occurrence was similar in males and females (27.8% males *vs* 25% females, p = 0.99). In ~75% (11/15) of patients, NF-PNETs were located in the pancreatic body/tail, and in the remaining ~25% (4/15) of patients they were located in the head/uncinate process. Approximately 75% (8/11) of patients had tumour growth ≥ 2 mm, by a median follow-up of 81 months (range = 13-125 months) **(Figure 3.4**). Distal pancreatectomy was performed in 33% (5/15) of patients, all of whom had NF-PNETs that were > 20 mm in diameter at diagnosis or during follow-up (median age at surgery = 16 years, range = 12-20 years). The remaining 10/15 patients had tumours that did not exceed the 20 mm threshold during follow-up. Surgery was not followed by recurrence in 3 patients, but 2 patients developed new tumours in the pancreatic remnant (median follow-up = 72.5 months, range = 40-135 months). Three patients developed metastases, with lymph node metastasis occurring in 1 patient with insulinoma, and hepatic metastases occurring in 2 patients with NF-PNETs, both of whom also had metachronous functioning PD-NETs **(Table 3.4)**

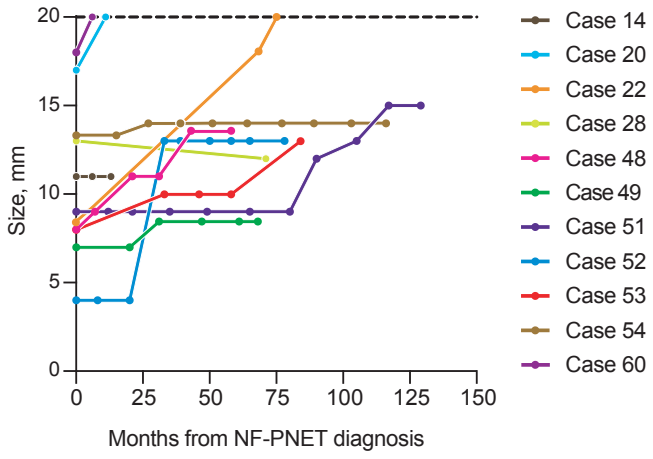

Figure 3.4. Tumour growth trajectories in patients with NF-PNETs. Tumour growth curves in 11/15 MEN1 patients with NF-PNETs that developed during childhood/adolescence. [Caption continues on next page...]

Figure 3.4. Tumour growth trajectories in patients with NF-PNETs. Approximately 75% (8/11) of patients had tumour growth $\geq$ 2 mm, by a median follow-up of 81 months (range = 13-125 months). The horizontal dashed line indicates the 20 mm size threshold that was used as an indication1 for surgical resection at centres included in this study. In patients with multiple NF-PNETs, the maximal diameter of the largest tumour was plotted. Four out of 15 patients were excluded from this analysis: two patients (cases 43 and 24) who underwent surgery at the time of NF-PNET diagnosis; one patient (case 44) who had hepatic metastases at the time of diagnosis; and one patient (case 79) who had $<$ 2 abdominal imaging scans. Figure adapted from Shariq et al.[199]

Table 3.4. Characteristics and treatment outcomes of 15 patients diagnosed with NF-PNETs at $\leq$ 18 years old

	NF-PNET $\leq$ 18 years (n = 15)
Age at MEN1 diagnosis, years, median [range]	14 [4 – 17]
Sex, female	9 (64%)
Age at last follow-up, median [range]	22 [16 – 27]
Age at NF-PNET diagnosis, years, median [range]	15 [10 – 18]
Imaging modality for diagnosis	
CT	2 (13%)
MRI	10 (67%)
EUS	3 (20%)
Multifocality	7 (47%)
Number of tumours on imaging, median [range]	1 [1 – 6]
Size of largest tumour at diagnosis, mm, median [range]	9 [4 - 38]
Location of largest tumour on imaging	
Head/uncinate	4 (27%)
Body/tail	11 (73%)
Metastasis at time of diagnosis	1 (7%)
Surgical resection	5 (36%)
Age at surgery, median [range]	16 [12-20]
Number of tumours on pathology, median [range]*	2 [1 – 5]
Size of largest tumour on pathology, mm, median [range]*	22 [18 – 40]
Tumour grade	
G1	1 (20%)
G2	2 (40%)
G3	1 (20%)
Missing	1 (20%)
Positive lymph nodes on pathology	0
Recurrence in pancreatic remnant after surgery	2 (40%)
Development of metastases during follow-up	1 (7%)
Duration of follow-up, months, median [range]	79 [6-131]

*Pathology data were missing for 1 patient. Table reproduced from Shariq et al.[199]

3.2.4 Pituitary tumours

Pituitary tumours occurred in > 30% (18/56) of patients at ≤ 18 years of age and were the first detected MEN1 lesion in ~30% (16/56) of patients (median age of pituitary adenoma diagnosis = 14 years, range = 9-18 years) **(Table 3.5)**. Pituitary tumour occurrence was similar in males and females (26% males *vs* 35% females, p = 0.56). Clinical symptoms included amenorrhoea/galactorrhoea in > 45% (6/13) of female patients, and headaches in 17% (3/18), visual field defects in > 10% (2/18), and delayed puberty in > 5% (1/18) of all patients, with ~45% (8/18) remaining asymptomatic. Prolactinomas were found in ~85% (15/18) of patients and non-functioning adenomas were found in ~15% (3/18) of patients. Somatotrophinomas or corticotrophinomas were not found in any patients. Over 66% (12/18) of patients had microadenomas, while the remaining ~35% (6/18) of patients (1 male and 5 females) had macroadenomas (median size = 15 mm, range = 12-55 mm), all of which were prolactinomas.

Treatment was required in ~70% (12/18) of patients and of the remaining ~30% (6/18) who did not require treatment, all had microadenomas (3 prolactinomas and 3 non-functional adenomas) that remained stable during a median follow-up of 61 months (range = 23-135 months). In 80% (12/15) of patients with prolactinomas, dopamine agonists were first-line therapy, and were successful in > 80% (10/12). The two patients who failed dopamine agonist therapy had macroprolactinomas and comprised: a male diagnosed with a 55 mm prolactinoma at age 11 years,[201] that initially responded to cabergoline, but subsequently required two transcranial debulking procedures (at 12 years of age) and proton beam irradiation (at 13 years of age); and a female diagnosed with a 13 mm prolactinoma at 16 years of age, who experienced persistent amenorrhoea and galactorrhoea despite cabergoline and underwent successful transsphenoidal resection at 26 years of age. In another female patient, who presented with bitemporal hemianopia and amenorrhoea at 14 years of age due to a macroprolactinoma (33 mm), transsphenoidal surgery was used as first-line therapy; she remained disease-free after 12 months of follow-up.

Table 3.5. Characteristics of 18 patients diagnosed with pituitary adenomas at ≤ 18 years of age

Case ID	Sex	Germline pathogenic variant[a]	Age at MEN1 diagnosis, years	Age at PA diagnosis, years	Type of PA	Micro or macro-adenoma at diagnosis	Size at diagnosis, mm	Presenting symptoms	Management
9	F	c.1400_1413del; p.Ala467fsX59	5	9	PRL	Microadenoma	4	None	Observation
46	F	c.1008dup; p.Ala337fsX30	6	10	PRL	Microadenoma	7	None	Cabergoline
16	M	c.658TC; p.Trp220Arg	7	11	NF	Microadenoma	5	None	Observation
6	F	c.503TC; p.Leu168Pro	2	11[b]	PRL	Macroadenoma	12	None	Cabergoline
63	M	c.784-9GA; p.Lys262fsX10	11	11[c]	PRL	Macroadenoma	55	BH, headaches	Cabergoline, debulking surgery x2, adjuvant proton beam irradiation
48	F	c.1204_1208del; p.Ser402fsX5	6	12	PRL	Microadenoma	9	Galactorrhea	Cabergoline
43	F	c.1045CT; p.Gln349X	8	12	PRL	Microadenoma	6	None	Cabergoline
74	F	c.1546dup; p.Arg516fsX15	15	14[d]	PRL	Macroadenoma	17	Delayed puberty	Cabergoline
22	M	Unknown[e]	14	14	NF	Microadenoma	9	None	Observation
23	F	Unknown[f]	14	14[d]	PRL	Macroadenoma	33	BH, amenorrhoea	Tran-sphenoidal surgery
34	F	c.668T>C; p.Leu223Pro[g]	14	15	PRL	Microadenoma	6	None	Bromocriptine
14	M	c.770_775dup; p.Leu259_Gln260dup	15	15	PRL	Microadenoma	7	Headache	Observation
29	F	Unknown[e]	16	16	PRL	Microadenoma	5	Galactorrhea	Cabergoline
25	F	c.654+3AG	16	16[d]	PRL	Macroadenoma	13	Amenorrhea	Cabergoline, trans-sphenoidal surgery
51	F	c.668T>C; p.Leu223Pro[g]	15	17[b]	PRL	Macroadenoma	12	None	Cabergoline
31	F	c.1243CT; p.Arg415X	7	18	PRL	Microadenoma	7	None	Bromocriptine
78	F	Unknown[h]	10	18	NF	Microadenoma	4	None	Obervation
37	M	Unknown[h]	8	18	PRL	Microadenoma	4	None	Observation

[a]Further details of germline variants are provided in Figure 3.5. [b]Patient was enrolled in an MEN1 surveillance screening program before macroadenoma was detected. [c]Patient is an index case who had not undergone prior screening for MEN1 manifestations before the diagnosis of macroprolactinoma was made. [d]Patient had a family history of MEN1, but had not yet commenced screening at the time that the macroadenoma was detected. [e]Germline variant unknown as family declined genetic testing. [f]Patient's first-degree relative tested positive for *MEN1* germline pathogenic variant, but specific variant unknown. [g]Unrelated patients with an identical genotype (e.g. c.668T>C; p.Leu223Pro) noted to have variable aggressiveness of pituitary tumours. [h]Patient tested positive for *MEN1* germline pathogenic variant but specific variant unknown. BH, bitemporal hemianopsia; NF, non-functioning; PRL, prolactinoma. Table reproduced from Shariq et al.[199]

3.2.5 Adrenal tumours

A 20 mm non-functioning left adrenal adenoma was detected as an incidentaloma on MRI in 1 female patient at 10 years of age, who was being investigated for an insulinoma **(Table 3.3)**. Repeat MRI 6 months later showed the mass to have increased in size to 25 mm, and open adrenalectomy was therefore performed at the same time that the patient underwent a laparotomy and hepatic wedge resection for a metastatic NF-PNET. Pathological assessment showed a benign adrenal adenoma.

3.2.6 *MEN1* genetic analysis and genotype-phenotype correlations

Genetic analysis, which was performed in 96% (77/80) of the overall cohort, revealed 38 different pathogenic germline *MEN1* variants, which occurred throughout the length of the *MEN1* gene, with > 70% (27/38) of these occurring in patients who developed an MEN1 manifestation by ≤ 18 years of age. The majority of these pathogenic variants (~70%, 26/38) are predicted to result in a loss of function through premature truncation of the encoded menin protein[202] (i.e. nonsense variants (> 25%, 10/38); frameshift variants (> 30%, 12/38) with predicted premature truncations; splice site variants (~8%, 3/38); and exonic deletions (~3%, 1/38)). The remaining ~30%, which are predicted in-frame variants (~5%, 2/38) and missense variants (> 25%, 10/38), are also likely to disrupt menin function.[202] Three of these pathogenic variants have not been previously reported: p.Ala337fs*30; p.Ile247Asn; and p.Lys362fs*6. Ten variants occurred in members of ≥ 2 unrelated families, and the remaining 28 variants each occurred in only one family, six of which had multiple affected members **(Figure 3.5)**.

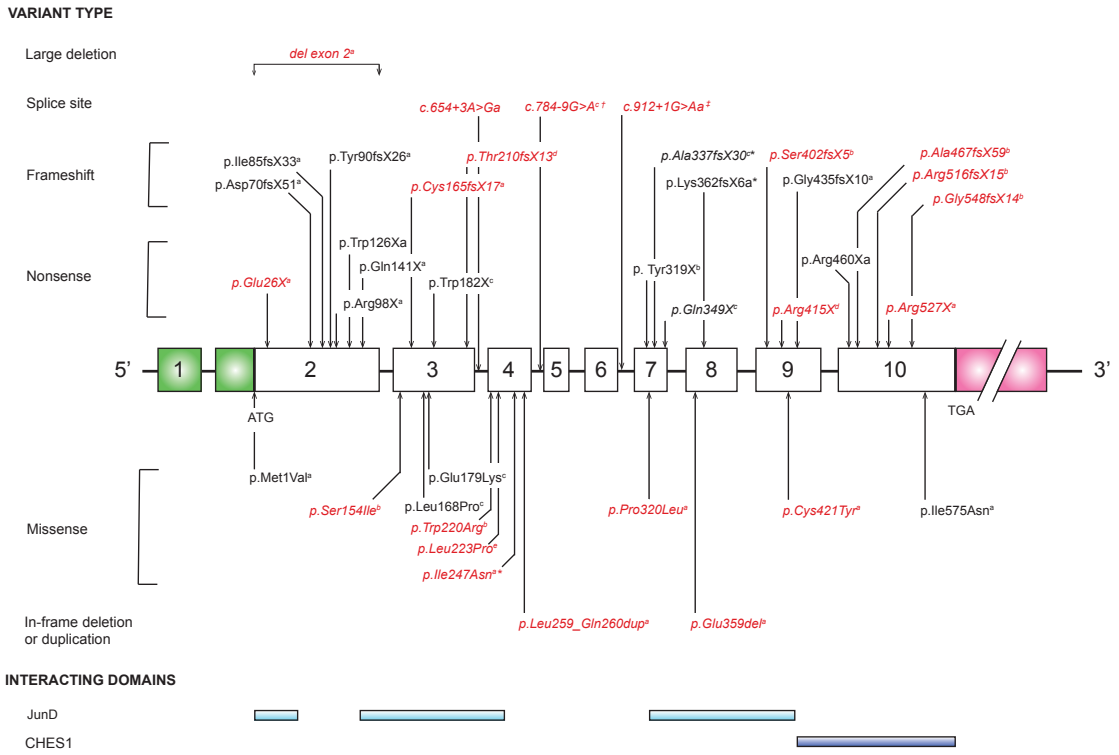

Figure 3.5. Schematic representation of the genomic organisation of the *MEN1* gene. The human *MEN1* gene consists of 10 exons that span more than 9 kilobases (kb) of genomic DNA and encodes a 610–amino-acid protein, menin. The 1.83-kb coding region (open boxes) is organised into 9 exons (exons 2 to 10) and 8 introns (indicated by a line but not to scale). The sizes of the exons (boxes) range from 41 to 1297 base pairs (bp), and that of the introns range from 80 to 1564 bp. The start (ATG) and stop (TGA) codons in exons 2 and 10, respectively, are indicated. Exon 1, the 5' part of exon 2, and the 3' part of exon 10 are untranslated (green and purple boxes, respectively). The sites of 38 germline variants which were found in the 60 unrelated families are represented with the affected codon number(s) shown. The locations of the predicted mutations are reported with reference to the transcript encoding the 610 amino acid menin protein (*MEN1* reference sequence NM_130799 using Human Genome Variation Society (HGVS) nomenclature). Variants that occurred: in patients who developed an MEN1 manifestation by $\leq$ 18 years of age, are shown in red; and in more than one patient are indicated in superscript (a = variant occurred in 1 patient, b = variant occurred in 2 patients; c = variant occurred in 3 patients; d = variant occurred in 4 patients, and e = variant occurred in 7 patients †The splice site variant c.784-9G>A has been shown experimentally to result in a frame shift (p.Lys262fsX10) and menin protein truncation.[203] ‡The splice site variant c.912+1G>A has been shown experimentally to result in a frameshift (p.Tyr276fsX63) and menin protein truncation.[204] Figure reproduced from Shariq et al.[199]

Menin, which is a scaffold protein, has roles in regulating transcription, genome stability, cell division, and proliferation through direct associations with interacting protein partners, such as the transcription factor JunD and checkpoint kinase 1

(CHES1) **(Figure 3.5)**.[82,205] Moreover, *MEN1* variants affecting the menin-JunD interacting domains (i.e. codons 1-40, 139-242, and 323-428) are reported to be associated with an increased risk of premature death,[82] while those involving the menin-CHES1 interaction domain (i.e. codons 428-610) are reported to be associated with a higher frequency of aggressive PD-NETs and death.[205] An examination for such correlations revealed a higher occurrence of *MEN1* variants affecting the menin-JunD interaction domain in patients developing PD-NETs at $\leq$ 18 years of age, compared to those without PD-NETs (80% *vs* 51.9%; p = 0.046) **(Table 3.6)**. Other statistically significant genotype-phenotype correlations were not observed.

3.3 Discussion

The findings of this chapter illustrate that morbidity from MEN1-related manifestations occurred during childhood and adolescence in 70% of patients, and that PD-NETs, which developed in ~35% of patients at ~18 years of age, may be metastatic in ~15% of cases. Furthermore, pituitary tumours occurred in > 30% of these children and adolescents with MEN1 and ~35% of these were macroprolactinomas. These findings are of clinical importance because PD-NETs are the leading cause of mortality and reduced life-expectancy in patients with MEN1;[206] and pituitary macroadenomas are an important cause of morbidity due to local compressive effects, such as visual loss, and systemic effects from alterations in hormone secretion. Thus, our study underscores the importance of establishing an early genetic diagnosis of MEN1 with timely initiation of surveillance screening in childhood. Other studies have reported that screening in children with MEN1 is associated with diminished health-related quality of life (HR-QOL) because of the burden of frequent physician visits and life-long surveillance,[207] and that screening tests could be postponed until the age of 16 years.[86] However, ~50% of the 80 patients in this study developed manifestations at ~16 years of age, some of which were life-threatening, metastases, and/or required surgical intervention. These findings would therefore caution against delaying screening until the end of adolescence.

Table 3.6. Frequency of MEN1 manifestations at 18 years of age according to genotype

	Truncating variant, yes[a,b]	Nonsense or frameshift variant in exons 2, 9, 10, yes[c]	Variant affecting JunD interacting domain, yes[d]	Variant affecting CHES1 interacting domain, yes[e]
Any manifestation at 18 years				
Yes	30 (68%)	11 (24%)	28 (62%)	7 (16%)
No	14 (58%)	6 (25%)	12 (50%)	4 (17%)
p-value	0.438	0.590	0.234	0.579
PHPT at 18 years				
Yes	26 (70%)	11 (29%)	22 (60%)	7 (19%)
No	18 (58%)	6 (19%)	28 (67%)	4 (13%)
p-value	0.320	.220	0.334	0.0348
PD-NET at 18 years				
Yes	10 (67%)	3 (20%)	12 (80%)	0
No	34 (64%)	14 (2%)	28 (52%)	20 (20%)
p-value	0.999	0.461	**0.046**	0.105
PA at 18 years				
Yes	7 (58%)	3 (23%)	8 (62%)	2 (15%)
No	37 (66%)	14 (25%)	32 (57%)	9 (16%)
p-value	0.741	0.598	0.513	0.660

[a]Patients who did not undergo genetic testing (n = 3) or did not have information available regarding their specific *MEN1* germline pathogenic variant (n = 8) were excluded.

[b]Truncating germline variants were defined as nonsense, frame shifts, and gross deletions. Non-truncating variants were defined as missense, in-frame deletions, or insertions. The splice site variants c.784-9G>A (n = 3 patients) and c.912+1G>A (n = 1 patient) have been shown experimentally result in menin protein truncation so these patients were included in the truncating variants group.[24,25] The impact of the splice site variant c.654+3A>G (n = 1 patient) on menin protein structure has not been experimentally validated; therefore, this patient was excluded from this analysis.

[c]All known variants included in analysis.

[d]JunD interaction domain: codons 1-40, 139-242, and 323-428

[e]CHES1 interaction domain: codons 428–610

Table reproduced from Shariq et al.[199]

The observed ~35% penetrance of PD-NETs at $\leq$ 18 years of age is comparable to a study that showed a penetrance of $>$ 40% by 20 years of age in 19 patients with MEN1 who also underwent screening using a combination of MRI/CT and/or EUS,[85] but contrasts with the $<$ 5%[90] and $<$ 15%[89] reported from 2 other studies of patients aged $<$ 21 and $<$ 22 years, respectively **(Table 3.1)**. The lower penetrances in the latter 2 studies may be partly explained by the limitations of the imaging modalities that were used, as ~66% of patients in one study had been screened prior to 1999, and before the advent of modern MRI technology and high-resolution EUS,[90] and in the other study,[89] patients were screened only with transabdominal US, which has limited sensitivity for the detection of pancreatic lesions, when compared to MRI, CT and EUS.[208]

The finding that a third of pituitary adenomas were macroadenomas at diagnosis is consistent with other studies describing MEN1-related pituitary tumours in patients of all ages.[209,210] All macroadenomas in our study were prolactinomas, and this differs from findings in adults with MEN1, in whom microprolactinomas are more likely.[209] Moreover, $>$ 80% of patients with macroadenomas in our study were female, and this contrasts with the occurrences of sporadic macroprolactinomas in children and adolescents, which are more common in males.[211] Furthermore, ~50% of patients with macroadenomas did not respond to medical therapy and required surgical treatment. This is consistent with a report of pituitary adenomas in MEN1 patients, compared to non-MEN1 pituitary tumours, being less responsive to medical therapy and more aggressive,[212] although another study, which excluded paediatric patients, reported that MEN1-related prolactinomas rarely required surgery.[210] Further studies are required to determine the underlying differences in the biological behaviour of MEN1-related pituitary tumours in children and adolescents.

PHPT occurred in $>$ 80% of patients who had an MEN1 manifestation at ~18 years of age, with $>$ 70% having parathyroidectomy, in which <SPTX was associated with significantly worse disease-free outcome and a higher incidence of reoperations compared to SPTX or TPTX. Although current clinical practice guidelines generally

recommend SPTX or TPTX (with or without auto-transplantation),[73] some groups recommend <SPTX in selected MEN1 patients, e.g. those with localised disease on preoperative imaging, as a treatment that provides an acceptable outcome while obviating the risk of permanent hypoparathyroidism.[213] However, the proposed benefits of <SPTX are negated by the increased incidence of persistent or recurrent disease and reoperations, which pose a higher risk of complications.[213] Notably, of the 3 patients who developed permanent postoperative hypoparathyroidism in our cohort, 2 underwent <SPTX as their initial procedure, followed by reoperative parathyroidectomy due to recurrent disease, and 1 patient underwent TPTX as their only procedure. In contrast, none of the 14 patients who underwent SPTX developed hypoparathyroidism and only 3 of these patients had PHPT persistence or recurrence. Thus, my findings suggest that <SPTX should be avoided in children and adolescents with MEN1-related PHPT. However, the small number of patients who underwent TPTX (n = 3) may have led to an underestimation of the risk of hypoparathyroidism in the SPTX/TPTX group, and precluded statistical comparisons between subgroups.

My genetic analyses identified 38 pathogenic *MEN1* germline variants, of which 3 are previously unreported, and a correlation between variants located at the menin domains that interact with JunD and the occurrence of PD-NETs at $\leq$ 18 years of age. An association between pathogenic variants affecting the menin-JunD interaction domain and a higher risk of death secondary to MEN1-related tumours, the majority of which were PD-NETs, has been reported by one study,[82] although another study of patients with PD-NETs did not find such an association.[205] Further such studies may help to elucidate the roles, if any, of these genotype-phenotype correlations in patients with MEN1.

This study has several limitations, which include: its retrospective nature, which may have introduced bias because of ascertaining historical data that may be incomplete; selecting ~35 years of age for study inclusion, that may have missed identifying some patients who had documented MEN1 manifestations in childhood

or adolescence; and having ~33% of patients who did not have prospective screening prior to the development of their first manifestation. Nevertheless, this study provides a detailed overview of MEN1 manifestations and treatment outcomes in children and adolescents.

In conclusion, 70% of children and adolescents with MEN1 develop parathyroid, pancreatic, and pituitary tumours. These data have implications for the counselling of young MEN1 patients and their families, and underscore the importance of initiating surveillance screening early in childhood. Importantly, the finding that 1 in 3 patients in this age group will develop PNETs, some of which may behave aggressively, suggests that effective systemic treatments are needed in the setting of metastatic disease.

4

Characterisation of BET expression in PNETs

Chapter-specific table of contents

4.1 Aims **103**
4.2 Results **104**
4.2.1 BET proteins are overexpressed in human PNETs compared to normal pancreatic islets 104
4.2.2 BET expression remains consistent across PNET subtype, stage and grade 108
4.2.3 *BRD2* is the highest expressed BET gene in PNET cell lines and in human tumours 112
4.2.4 RNA-seq and pathway analysis reveals dysregulation of E2F signalling in metastatic PNETs 114
4.2.5 Cell cycle master regulators are activated in metastatic PNETs 118
4.2.6 The transcriptome of metastatic PNETs is enriched with BET inhibitor target genes 121
4.2.7 Mapping of the BET protein cistrome in PNET cells reveals enrichment of cancer-related and neuronal lineage pathways 122
4.2.8 E2F transcription factor binding motifs are enriched within BRD2 and BRD4 peak regions 127
4.2.9 BET proteins bind to the promoter regions of key cell cycle regulators 128
4.3 Discussion **129**
4.3.1 BET proteins are overexpressed in human PNETs . . 130
4.3.2 *BRD2* is the most abundant BET gene in PNETs . . 131

4.3.3 BET mRNA and protein expression does not vary by PNET stage or grade 132
4.3.4 Dysregulation of cell cycle-related pathways may link BET protein activity to aggressive PNET behaviour 133
4.3.5 Genes associated with oxidative phosphorylation are upregulated in metastatic PNETs 135
4.3.6 CTLA4 is an inhibited upstream regulator in metastatic PNETs 136

4.1 Aims

BET proteins, including BRD2, BRD3 and BRD4, have been shown to play a pivotal role in the orchestration and regulation of transcriptional activity, cell cycle progression, and DNA damage repair.[130,214] Their broad functional repertoire is achieved through diverse interactions with various cellular proteins, including chromatin-remodelling complexes, transcription factors and histone modifying enzymes.[139] Recognising that dysregulated transcriptional programmes are a known hallmark of cancer, the potential role of BET proteins in this context has become an area of considerable scientific interest over the last decade.[215–217]

Various solid-organ cancers such as gastric,[218] hepatocellular,[146,147] colorectal[219] and pancreatic adenocarcinoma[220,221] have been associated with overexpression of BRD2, BRD3 and BRD4 at both the mRNA and protein level, compared to normal adjacent tissue. The consequences of this overexpression may include aberrant expression of downstream genes that contribute towards cancer development and progression.

Pharmacological inhibition of the BET proteins and genetic knockdown studies, both *in vitro* and *in vivo*, have provided further evidence in support of their role in the pathogenesis of a myriad of solid-organ malignancies. The Thakker group has previously demonstrated that treatment with the BET inhibitor JQ1 reduces proliferation in both the BON1 human PNET cell line and in a mouse model of insulinomas.[60] However, no studies to date have evaluated the expression of BRD2,

BRD3, or BRD4 in human PNETs. Thus, the clinical relevance of BET proteins in these tumours remains unclear, especially given the inherent biological differences that can arise between preclinical models and human disease.

This chapter aims to bridge the aforementioned gaps in the literature by investigating the expression profile of BET family members in human PNETs. Specifically, the expression of BRD2, BRD3 and BRD4 was evaluated across different subtypes of PNETs and compared to normal adjacent pancreatic islets using immunohistochemistry. BET expression was also characterised in three PNET cell lines to determine whether these represented suitable *in vitro* models for utilisation in subsequent experiments described later in this thesis. Furthermore, the landscape of genome-wide BET protein binding was characterised using chromatin immunoprecipitation with next-generation sequencing (ChIP-seq) in a PNET cell line, aiming to identify their potential genomic targets. An additional objective of this chapter was to compare gene expression profiles between metastatic and non-metastatic PNETs, with the goal of determining whether downstream targets of BET inhibitors are upregulated in metastatic cases.

4.2 Results

4.2.1 BET proteins are overexpressed in human PNETs compared to normal pancreatic islets

To determine whether BET proteins represent a clinically-relevant therapeutic target in human PNETs, the expression of BRD2, BRD3 and BRD4 was assessed using immunohistochemistry in a cohort of 52 functioning and non-functioning PNETs that were surgically resected at the Medical University of Vienna, Austria (see Section 2.2.1). **Table 4.1** provides details regarding this cohort.

Table 4.1. Overview of human PNET FFPE blocks from the University of Vienna cohort (n = 53)

Variable	Number of patients (%)
Median age at surgery, yrs [range]	50 [15 – 94]
Sex	
Male	22 (41.5%)
Female	22 (41.5%)
Unknown	9 (17%)
Subtype of PNET	
Non-functioning	24 (45.3)
Insulinoma	14 (26.4%)
Gastrinoma	10 (18.8%)
VIPoma	4 (7.5%)
Somatostatinoma	1 (1.9%)
Extent of surgery	
PD	17 (32.1%)
DP	21 (39.6%)
Enucleation	12 (22.6%)
CP	1 (1.9%)
Unknown surgery type	2 (2.8%)
WHO grade	
G1	35 (66%)
G2	14 (26.4%)
G3	4 (7.5%)
ENETS stage	
I	21 (39.6%)
II	11 (20.8%)
III	17 (32.1%)
IV	4 (7.5%)

CP, central pancreatectomy; DP, distal pancreatectomy; ENETS, European Neuroendocrine Tumour Society; PD, pancreaticoduodenectomy, VIPoma, vasoactive intestinal peptide-oma; WHO, World Health Organisation

The neuroendocrine nature of the samples was confirmed by staining for synaptophysin, a synaptic vesicle membrane protein that is expressed in both

PNETs and islet cells. Diffuse granular cytoplasmic staining of synaptophysin was observed in normal pancreatic islets and in all PNET cell types, confirming the neuroendocrine features of the samples. A nuclear staining pattern was observed for BRD2, BRD3 and BRD4, consistent with their role as epigenetic readers that act on chromatin context within the nucleus **(Figure 4.1)**.

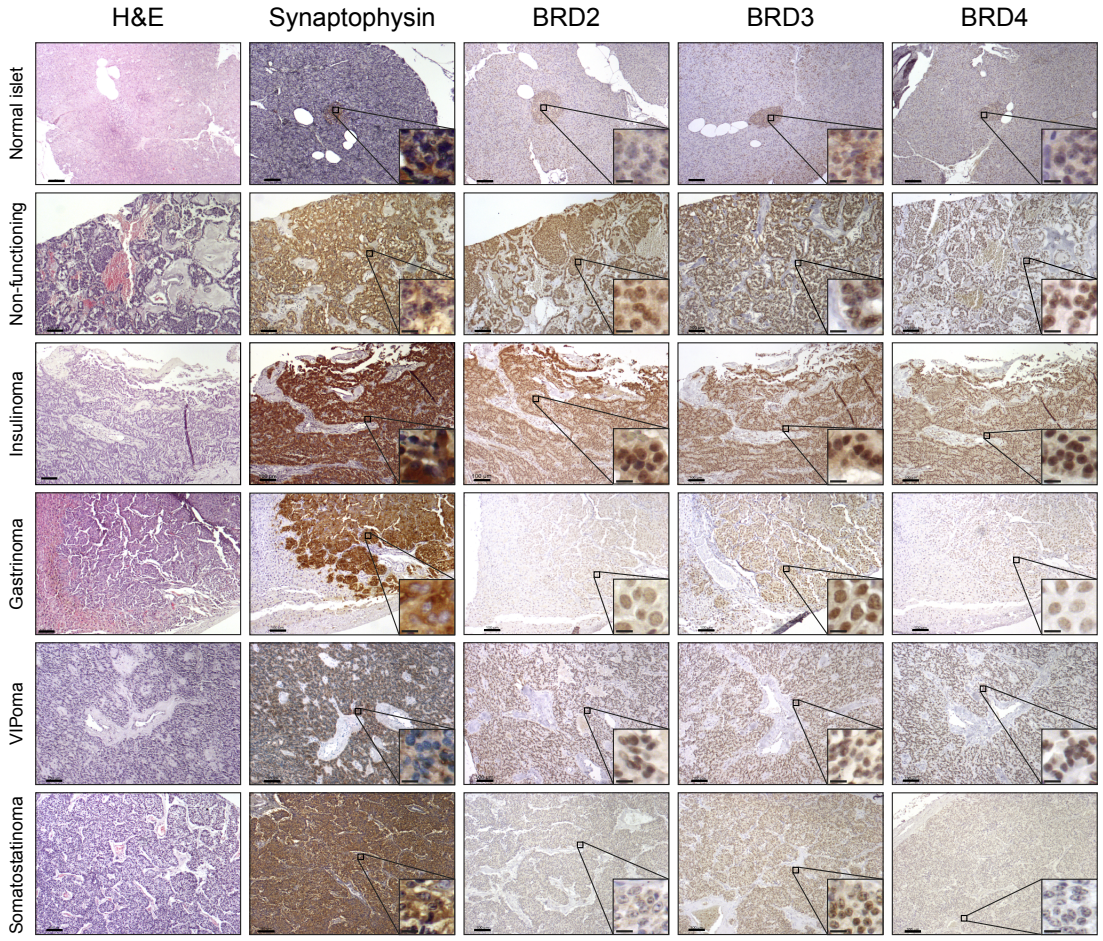

Figure 4.1. Nuclear staining of BET protein family members is observed in human PNETs. Representative images of non-functioning and functioning PNET samples and adjacent normal pancreatic islets stained with antibodies specific for BRD2, BRD3 and BRD4. Haematoxylin and eosin (H&E) and synaptophysin staining were used to confirm the histopathological diagnosis of PNET. Scale bars represent 100 µm in main images (at 10x magnification) and 10 µm in insets (at 40x magnification).

Sixteen of the Vienna PNET samples included adjacent pancreatic islets, which were used as a comparator group for analysing BET protein expression between tumour tissues and normal islets. The intensity of nuclear DAB staining was

quantified using QuPath digital pathology software and H-scores were calculated for each antibody per sample (as described in section 2.2.8). Initially, H-scores were compared between normal islets and adjacent tumours in the 16 samples that contained both tissue types only. This showed that the H-scores of BRD2, BRD3 and BRD4 were significantly higher in PNETs compared to matched adjacent normal islets with median differences of 67.7 ($p = 0.0004$), 59.3 ($p = 0.0008$) and 58.7 ($p = 0.0009$), respectively **(Figure 4.2A)**. Furthermore, when BET protein H-scores were compared between PNETs in the overall cohort of 52 samples (which included 36 samples without adjacent normal islets) and the 16 samples with adjacent normal islets, the median H-scores for BRD2, BRD3 and BRD4 were significantly higher in the tumours, with increases of 2.1-fold ($p = 0.003$), 1.5-fold ($p = 0.03$), and 2.5-fold ($p = 0.004$) compared to islets, respectively **(Figure 4.2B)**.

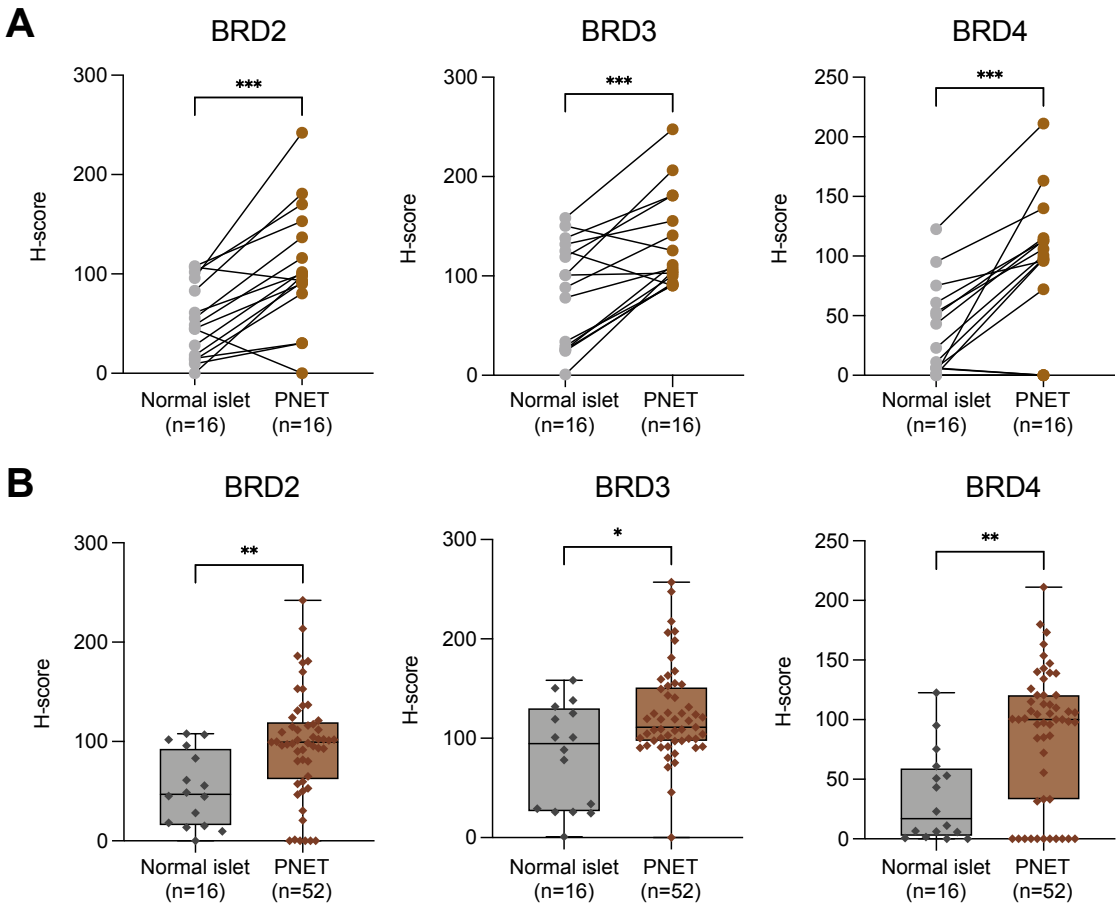

Figure 4.2. BET proteins are over-expressed in human PNETs compared to normal pancreatic islets. [Caption continues on next page...]

Figure 4.2. BET proteins are over-expressed in human PNETs compared to normal pancreatic islets. (A) Paired dot plot comparisons of H-scores for BRD2, BRD3 and BRD4 in 16 matched samples of PNETs and normal adjacent islets. Individual samples are connected with lines to highlight the paired nature of the comparison. **(B)** Box plots comparing H-scores for BRD2, BRD3 and BRD4 in normal islets (n = 18) and in all PNET subtypes (n = 52). Horizontal lines within each box plot represent the median, with the upper and lower bounds of the box corresponding to the upper and lower quartiles, respectively. The whiskers outside each box extend to the maximum and minimum values. Data analysed using Wilcoxon signed rank tests and Mann Whitney tests in panels A and B, respectively. *p $\leq$ 0.05, **p $\leq$ 0.01, *** p $\leq$ 0.001

4.2.2 BET expression remains consistent across PNET subtype, stage and grade

To explore subtype-specific variations in BET protein expression, H-scores were compared across various PNET subtypes (n = 24 NF-PNETs, n = 14 insulinomas, n = 10 gastrinomas, n = 4 VIPomas and n = 1 somatostatinoma). Owing to the limited number of patients in the VIPoma and somatostatinoma groups, these samples were pooled into a single group, referred to as 'other'. These subgroup analyses showed that the mean H-scores for BRD2, BRD3 and BRD4 did not differ significantly by PNET subtype **(Figure 4.3)**.

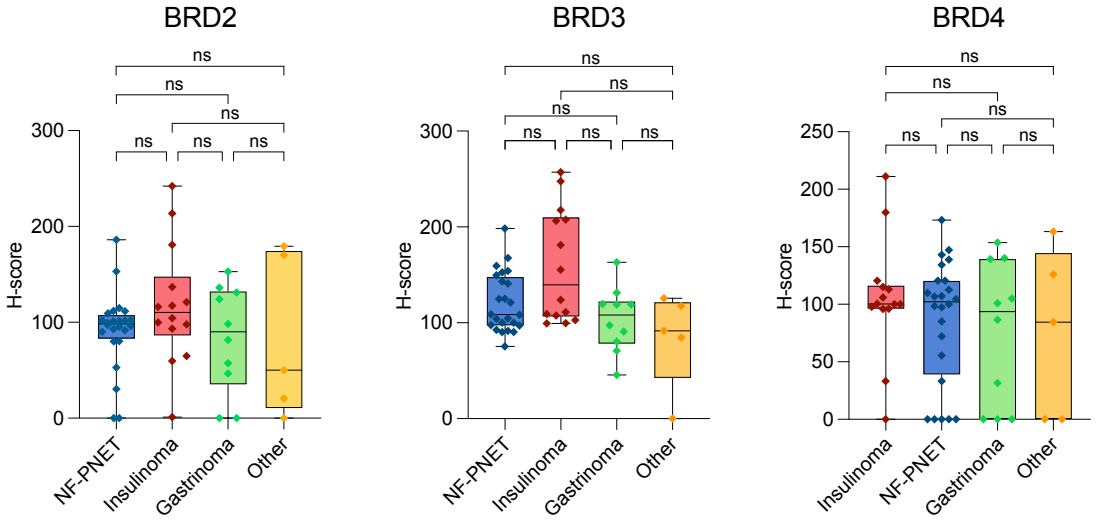

Figure 4.3. BET protein expression does not vary by PNET subtype. [Caption continues on next page...]

Figure 4.3. BET protein expression does not vary by PNET subtype. Box plots showing BET protein H-scores in NF-PNETs (n = 24), insulinomas (n = 14), gastrinomas (n = 10), and other functioning subtypes (n = 5). The horizontal line within each box plot represents the median value of the data, with the upper and lower bounds of the box corresponding to the upper and lower quartiles, respectively. The whiskers outside each box extend to the maximum and minimum values. Statistical analysis was performed using Kruskal-Wallis tests. ns, not significant.

Moreover, no significant differences in BET protein expression were observed when tumours were compared by disease stage (metastatic *vs* non-metastatic) **(Figure 4.4A)** and grade (G1 *vs* G2 or G3) **(Figure 4.4B)**.

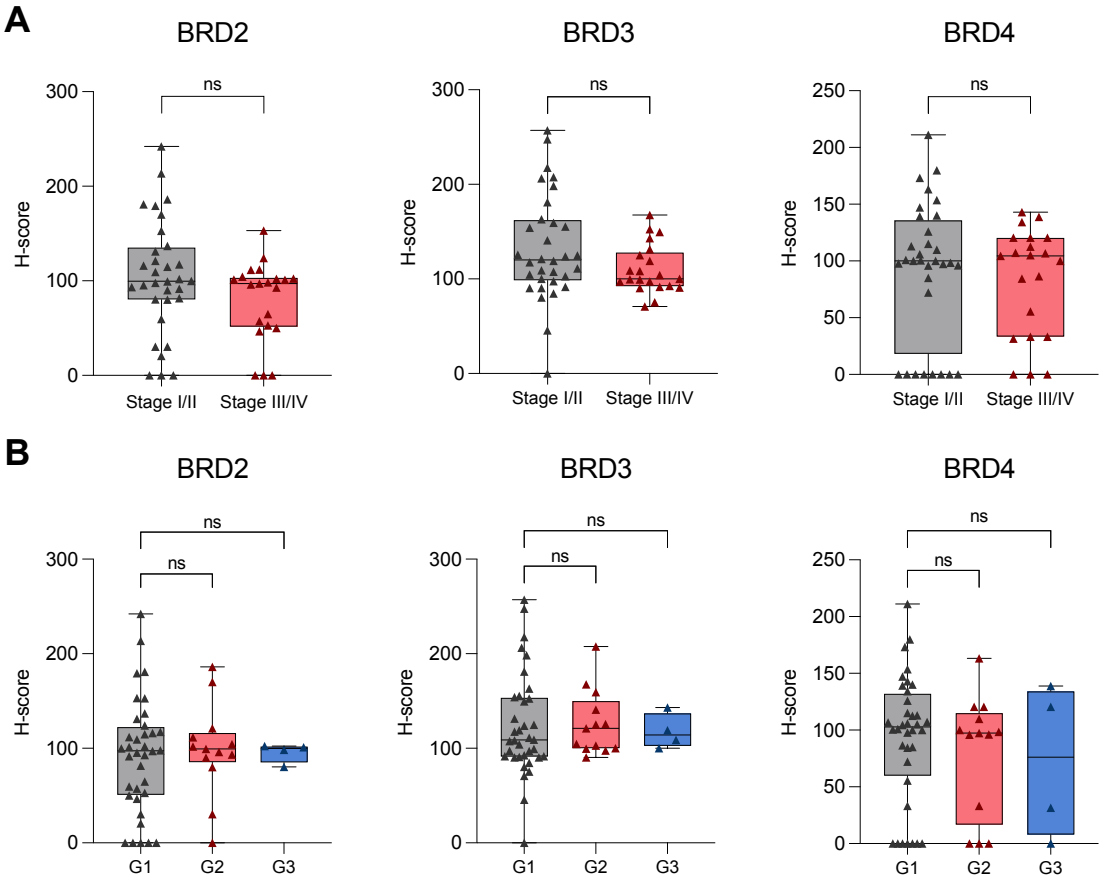

Figure 4.4. BET protein expression does not vary by PNET subtype. **(A)** Box plots showing BET protein H-scores in patients with metastatic (stage III/IV; n = 21) *vs* non-metastatic (stages I-II; n = 32) disease. **(B)** Box plots showing BET protein H-scores in PNETs histopathologically classified as grade 1 (G1; n = 36), grade 2 (G2; n = 13) and grade 3 (G3; n = 4). The horizontal line within each box plot represents the median value of the data with the upper and lower bounds of the box corresponding to the upper and lower quartiles, respectively. The whiskers outside each box extend to the maximum and minimum values. Statistical analysis was performed using the Mann Whitney test in panel A and the Kruskal-Wallis tests in panel B. ns, not significant.

These immunohistochemistry findings in the Vienna cohort were then validated using a novel RNA sequencing (RNA-seq) dataset that was generated from 46 surgically resected PNETs at the Mayo Clinic (see Section 2.4.2.1). **Table 4.2** provides details regarding this cohort.

Table 4.2. Overview of human PNET frozen samples from the Mayo Clinic cohort (n = 46)

Variable	Number of patients (%)
Median age at surgery, yrs [range]	60 [20 – 78]
Sex	
Male	21 (45.7%)
Female	25 (54.3%)
Subtype of PNET	
Non-functioning	25 (54.3%)
Insulinoma	14 (30.4%)
Gastrinoma	7 (15.2%)
Extent of surgery	
PD	8 (17.4%)
DP	33 (71.7%)
Enucleation	5 (10.9%)
WHO grade	
G1	19 (41.3%)
G2	24 (52.2%)
G3	3 (6.5%)
T stage	
T1	8 (17.4%)
T2	18 (39.1%)
T3	10 (21.7%)
T4	10 (21.7%)
N stage	
N0	33 (71.7%)
N1	13 (28.3%)
M stage	
M0	37 (80.4%)
M1	9 (19.6%)

Continued on next page

Table 4.2. Overview of human PNET frozen samples from the Mayo Clinic cohort (n = 46) (Continued)

Variable	Number of patients (%)
ENETS stage	
I	8 (17.4%)
IIA	13 (28.3%)
IIB	5 (10.9%)
IIIA	3 (6.5%)
IIIB	7 (15.2%)
IV	10 (21.7%)

Analysis of the Mayo Clinic dataset confirmed no significant differences in the mRNA expression levels of *BRD2*, *BRD3* and *BRD4* by PNET subtype **(Figure 4.5A)**, stage or grade **(Figure 4.5B)**. These findings suggest that BET protein overexpression is a common characteristic of PNETs, independent of tumour type or aggressiveness.

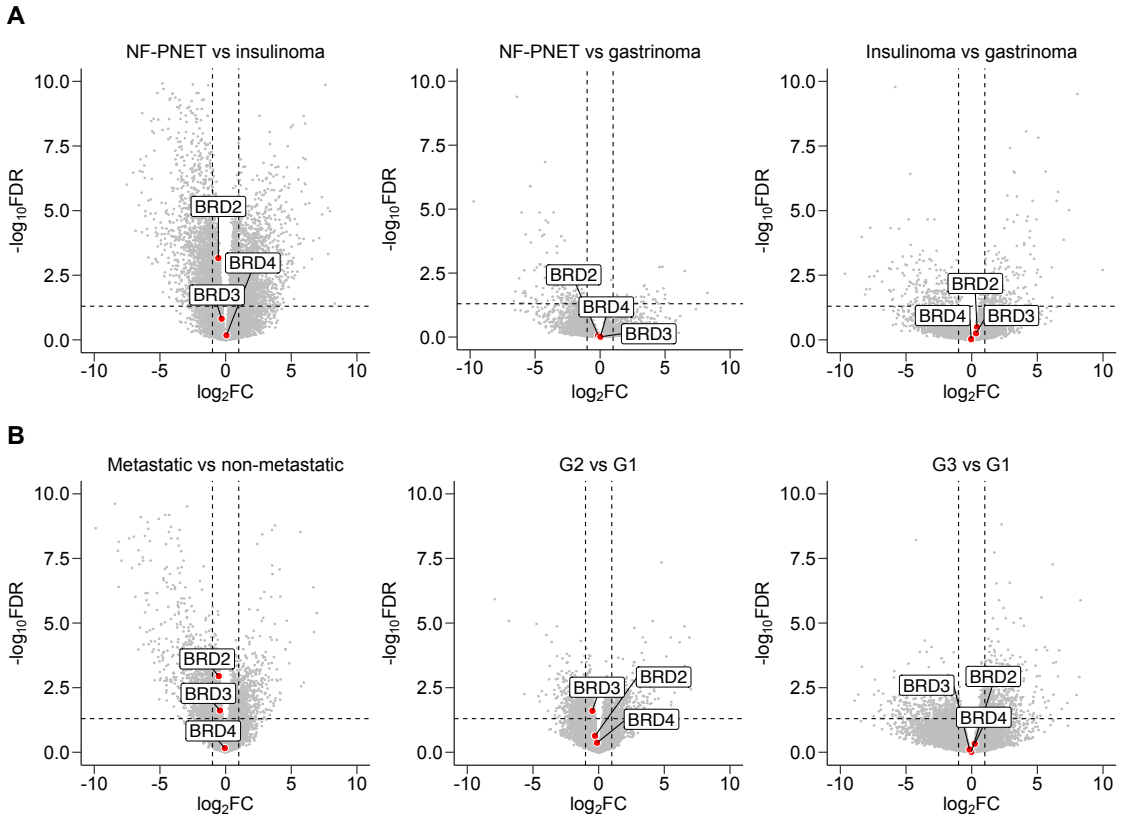

Figure 4.5. BET gene expression does not vary by PNET subtype, stage or grade [Caption continues on next page...].

Figure 4.5. BET gene expression does not vary by PNET subtype, stage or grade. Volcano plots illustrating differences in gene expression across **(A)** PNET subtypes and **(B)** tumour stage and grade. Each gray dot represents an individual gene identified by RNA-seq, with those corresponding to *BRD2*, *BRD3* and *BRD4* highlighted in red and labelled. The x-axis displays the $\log_2$ fold change ($\log_2$FC), which represents the magnitude of differential expression for each gene between two groups. The left and right vertical dashed lines mark the thresholds for significant differential expression with a $\log_2$FC < -1 (downregulation) and > 1 (upregulation), respectively. The y-axis represents the negative logarithm (base 10) of the false discovery rate-adjusted p-value (-$\log_{10}$FDR).

4.2.3 *BRD2* is the highest expressed BET gene in PNET cell lines and in human tumours

In order to ascertain the applicability of PNET cell lines as a suitable *in vitro* model for studying BET protein biology and the effects of BET inhibitors, expression levels of *BRD2*, *BRD3*, *BRD4* and *BRDT* were measured in two human cell lines (BON1 and QGP1) using qRT-PCR. Expression levels of *Brd2*, *Brd3*, *Brd4* and *Brdt* were also evaluated in a mouse PNET cell line (MIN6) **(Figure 4.6A)**. These analyses revealed *BRD2* as the most abundant BET family member in BON1 cells, exhibiting expression levels 10-fold and 8-fold higher than *BRD3* and *BRD4*, respectively (both $p \leq 0.0001$). No significant difference was observed between expression levels of *BRD3* and *BRD4*. Similarly, *BRD2* was the most abundant BET gene in QGP1 cells, with ~4-fold and ~20-fold higher expression than *BRD3* and *BRD4*, respectively, (both $p \leq 0.0001$). Unlike BON1 cells, QGP1 cells had a significantly higher expression of *BRD3* compared to BRD4, by 1.3-fold ($p \leq 0.0001$). In MIN6 cells, *Brd2* remained the most prominently expressed BET family member, with ~3-fold and ~2-fold higher expression than *Brd3* and *Brd4*, respectively (both $p \leq 0.01$) while the expression difference between *Brd3* and *Brd4* was not significant. Notably, expression of *BRDT/Brdt*, which is testis-specific, was not detected after 40 cycles of qRT-PCR, confirming its absence in PNET cell lines. To verify if patterns of BET mRNA expression observed in cell lines mirrored those in human tumours, the Mayo RNA-seq dataset was analysed. **(Figure ??B)**. This confirmed that *BRD2* was the most abundant BET gene in human tumours,

with a 12-fold and 14-fold increase in expression compared to *BRD3* and *BRD4*, respectively (both $p \leq 0.0001$). There was no significant difference between the expression levels of *BRD3* and *BRD4*. As expected, *BRDT* expression was not detectable in any of the human tumour samples.

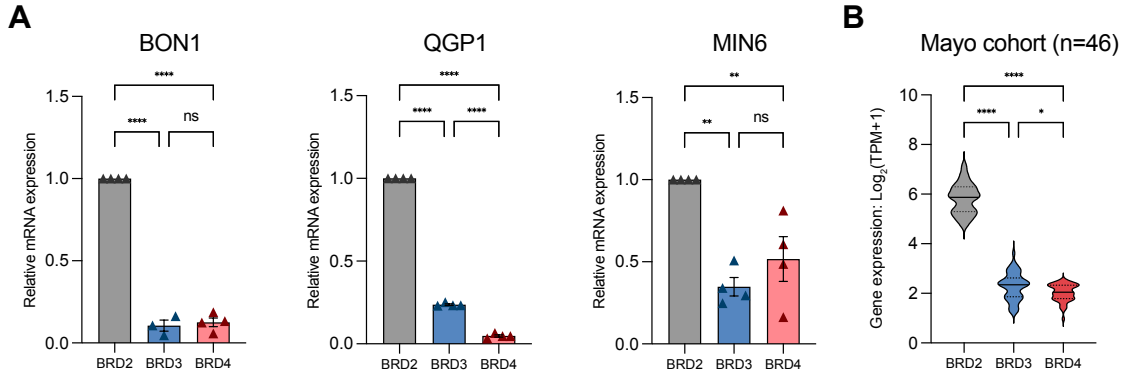

Figure 4.6. mRNA expression patterns of BET family members in PNET cell lines are consistent with those of human tumours. (A) Evaluation of mRNA expression of BET genes in human and mouse PNET cells by qRT-PCR. Data are presented relative to *BRD2*/*Brd2* expression and represent the mean ± SEM of four independent experiments. **(B)** Violin plots showing BET gene expression levels (normalized by TPM and $\log_2$ transformed) from RNA sequencing of 46 human PNETs from the Mayo Clinic cohort. Solid horizontal line indicates median, dotted lines indicate upper and lower quartiles. Statistical analysis was performed using one-way ANOVA with Tukey's test for multiple comparisons. ns, not significant, TPM, transcripts per million, **$p \leq 0.01$, ***$p \leq 0.001$, ****$p \leq 0.0001$

To evaluate the expression of BRD2, BRD3 and BRD4 in PNET cell lines at the protein level, Western blotting was performed. This confirmed that all three family members were expressed in all three PNET cell lines **(Figure 4.7A)**. Although the blots shown in the figure are cropped, no additional bands were seen, consistent with the antibodies being highly specific. Densitometry analysis showed that MIN6 cells had the highest expression of BRD2 compared to BON1 ($p \leq 0.05$) and QGP1 cells ($p \leq 0.0001$). Conversely, BON1 cells exhibited the highest expression of BRD3 compared to QGP1 cells ($p \leq 0.001$) and MIN6 cells ($p \leq 0.0001$). BRD4 expression was also significantly higher in BON1 cells than in QGP1 cells ($p \leq 0.01$) and MIN6 cells ($p \leq 0.01$) **(Figure 4.7B)**.

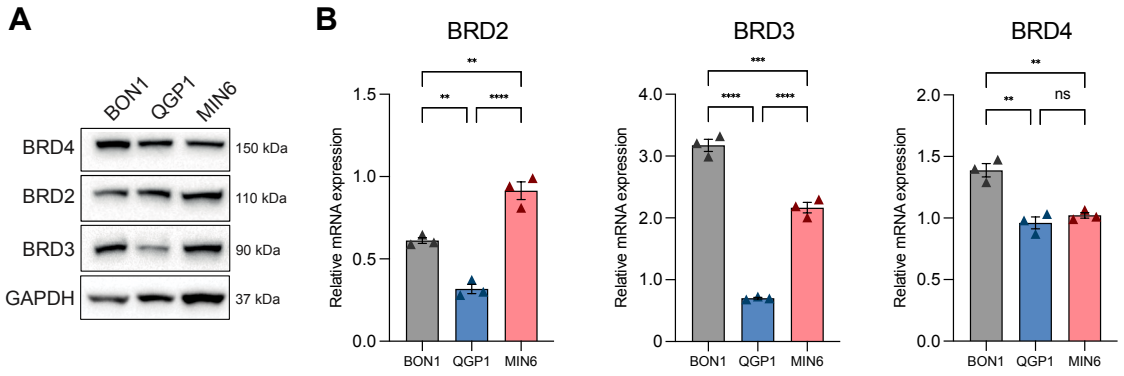

Figure 4.7. Western blot analysis of BET protein expression in PNET cell lines. (A) Representative Western blots showing BET protein expression in PNET cell lines. GAPDH was used as a loading control. **(B)** Densitometry analysis of Western blots. Data are presented relative to GAPDH and represent the mean ± SEM of three independent experiments. Statistical analysis was performed using one-way ANOVA with Tukey's test for multiple comparisons. kDa, kilodalton; ns, not significant, TPM, transcripts per million, **p ≤ 0.01, *** p ≤ 0.001, ****p ≤ 0.0001

4.2.4 RNA-seq and pathway analysis reveals dysregulation of E2F signalling in metastatic PNETs

Building upon the finding that BET proteins are over-expressed in PNETs, I undertook a more comprehensive analysis of the previously mentioned RNA-seq dataset, which was generated from 46 PNETs resected at the Mayo Clinic. This analysis was aimed at elucidating the biological pathways upregulated in metastatic tumours and their potential relevance to BET proteins. Genes that showed a significant difference in expression levels in metastatic *vs* localised tumours (n = 3,706; adjusted p ≤ 0.05) were scaled to Z-scores and visualised as a heatmap **(Figure 4.8A)**. Euclidean k-means clustering was used to group together similar gene expression profiles, resulting in a clear distinction between the metastatic and non-metastatic samples. Specifically, non-metastatic insulinoma samples clustered together in the heatmap, while gastrinomas did not exhibit distinct clustering from other tumour subtypes. Principal component analysis (PCA) further revealed a distinct separation of samples by tumour subtype and stage along the first principal component (PC1), which accounted for 26% of the total variance **(Figure 4.8B)**.

To validate the representativeness of the gene expression profiles observed in the Mayo Clinic cohort, I employed gene set enrichment analysis (GSEA) to align these profiles with transcriptomic signatures from other well-documented PNET cohorts reported in the literature.[101,222,223] As described by Sadanandam et al.,[222] metastasis-like primary (MLP)-1 and MLP-2 tumours are enriched for genes associated with hypoxia, angiogenesis and pancreatic β-cell precursors, and have a higher propensity to metastasise. Conversely, the insulinoma-like subtype is characterised by the expression of mature β-cell-specific genes and exhibits a less aggressive phenotype.[222] Correspondingly, the MLP-1 and MLP-2 signatures were found to be significantly enriched in metastatic PNETs in the Mayo Clinic cohort, while the insulinoma-like signature was enriched in non-metastatic tumours **(Figure 4.8C)**. To identify biological pathways upregulated in metastatic PNETs, GSEA was additionally performed using 50 predefined gene sets from the Human Molecular Signatures Database (MSigDB) Hallmark gene set collection (see Section 2.4.1.3).[182] These gene sets are specifically curated to condense complex gene expression data into biologically meaningful patterns, thus providing a more interpretable summary of the underlying cellular processes. This analysis revealed that the 'E2F_TARGETS' gene set from the Hallmark collection was the most highly enriched gene set in metastatic PNETs **(Figure 4.8D)**, a notable finding given the role of E2F transcription factors as key regulators of cell cycle progression and the known co-activation function of BET proteins in oncogenic E2F signalling.[224–226] Examination of normalised RNA-seq mRNA expression levels revealed that *E2F2* was the only significantly upregulated E2F family member in metastatic PNETs, with 2.2-fold higher expression than in localised tumours (adjusted $p = 0.03$). Other Hallmark gene sets upregulated in metastatic PNETs included 'MTORC1_SIGNALING', consistent with the well-documented role of the mechanistic target of rapamycin (mTOR) pathway in PNET growth and progression,[227] as well as 'OXIDATIVE_PHOSPHORYLATION', suggesting increased metabolic demands and energy production in metastatic cells.

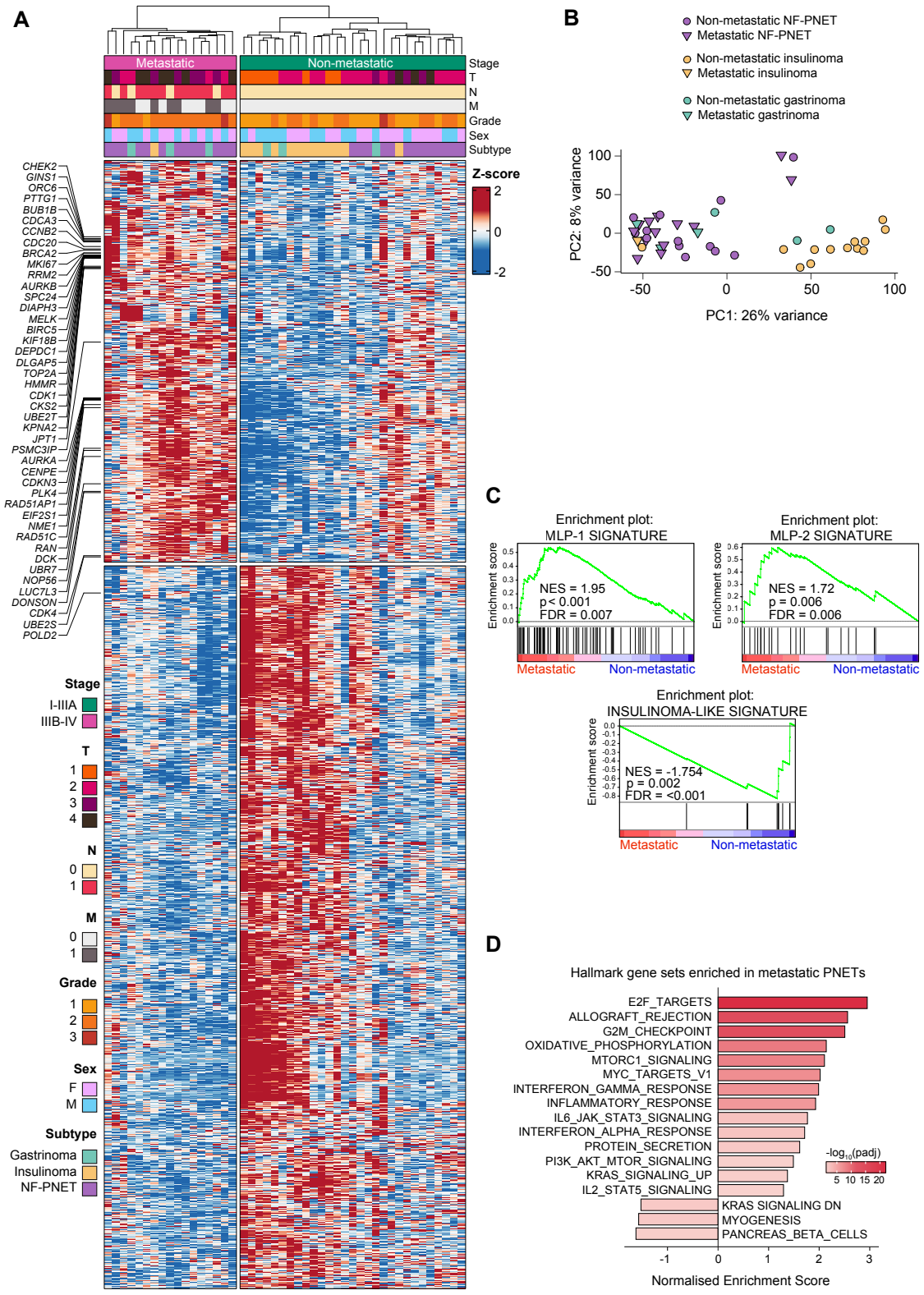

Figure 4.8. RNA-seq in human PNETs reveals upregulation of BET-protein relevant transcriptional programs in metastatic tumours. [Caption continues on next page...]

Figure 4.8. RNA-seq in human PNETs reveals upregulation of BET-protein relevant transcriptional programs in metastatic tumours. **(A)** Heatmap showing differentially expressed genes in 17 metastatic *vs* 29 non-metastatic primary PNETs from the Mayo Clinic cohort. The coloured annotation bars above the heatmap denote patient and tumour characteristics. Each column within the heatmap represents a unique sample and each row represents a unique gene. The intensity of the red or blue colour reflects higher or lower gene expression, respectively, standardized to Z-scores. Genes belonging to the Hallmark 'E2F_TARGETS' gene set have been indicated and labelled on the left. **(B)** PCA plot showing distribution of samples along principal component 1 (PC1, x-axis) and 2 (PC2, y-axis), which represent the two dimensions of maximum variability in the gene expression data. Each dot on the PCA plot corresponds to an individual sample, with clustering indicating similarity in gene expression profiles. **(C)** GSEA plots of gene sets derived from the molecular PNET subtypes described by Sadanandam et al.[222] The x-axis represents genes from the Mayo Clinic RNA-seq dataset ranked by differential expression, with the most upregulated genes in metastatic tumours on the left (red) and the most downregulated genes on far right (blue). Vertical black bars at the bottom of each plot mark the positions of genes from the corresponding gene signature ('MLP-1', 'MLP-2' and 'INSULINOMA-LIKE') within the ranked list of all genes. The green line represents the running enrichment score, showing the degree of over-representation of the gene set at the extremes (top or bottom) of the entire ranked list. A high positive peak, as seen with the 'MLP-1' and 'MLP-2' gene sets, indicates a positive correlation with metastatic PNETs. Conversely, a negative peak, observed in the 'INSULINOMA-LIKE' plot, indicates over-representation of this gene set in non-metastatic PNETs. **(D)** Bar plot indicating significantly enriched (adjusted $p \leq 0.05$) MSigDB Hallmark and gene sets identified by GSEA. Enrichment in metastatic *vs* non-metastatic samples is indicated by a positive or negative normalised enrichment score (NES), respectively. The colour gradient represents the significance level of enrichment ($-\log_{10}$ of the adjusted p-value). FDR, false discovery rate.

GSEA was also performed using 7,751 gene sets from the Gene Ontology Biological Process (GO:BP) collection, a comprehensive and systematically organised collection of annotated gene sets that describe the biological objectives to which each gene contributes.[177] These analyses revealed enrichment of GO:BP terms related to the cell cycle and cell division, such as 'cell cycle DNA replication', 'mitotic sister chromatid separation' and 'chromosome segregation', in metastatic tumours **(Figure 4.9)**. This suggests that genes involved in these processes are systematically upregulated in metastatic PNETs, which may contribute to the higher proliferation rates and genomic instability in these tumours. GSEA also highlighted a significant downregulation of GO:BP terms associated with hormone secretion in metastatic PNETs, such as 'regulation of insulin secretion' and 'catecholamine

secretion', which may reflect the fact that the majority of metastatic tumours were NF-PNETs. Furthermore, downregulation of GO:BP terms related to the cellular response to metal ions (e.g., 'cellular response to copper ion' and 'cellular response to zinc ion') in metastatic tumours might reflect a broad reprogramming of cellular priorities to favour processes that support tumour growth and metastasis over those that maintain metal ion homeostasis.

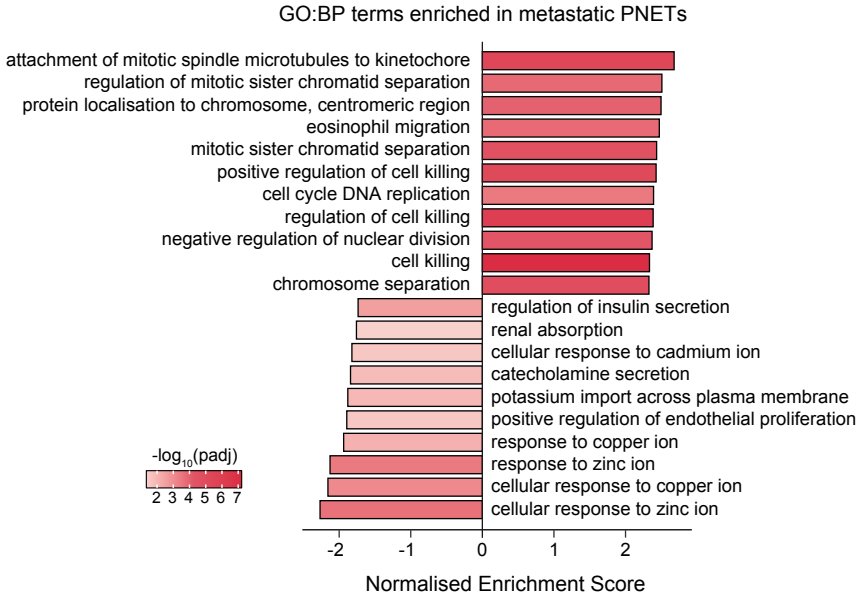

Figure 4.9. Gene set enrichment analyses identifies enrichment of cell cycle-related pathways in metastatic tumours. Bar plots indicating significantly enriched (adjusted $p \leq 0.05$) GO:BP gene sets identified by GSEA. Enrichment in metastatic *vs* non-metastatic samples is indicated by a positive or negative normalised enrichment score (NES), respectively. The colour gradient represents the significance level of enrichment ($-\log_{10}$ of the adjusted p-value).

4.2.5 Cell cycle master regulators are activated in metastatic PNETs

Ingenuity Pathway Analysis (IPA) was applied to the RNA-seq data to predict upstream regulators implicated in the gene expression alterations observed in metastatic PNETs **(Figure 4.10A)**. IPA identifies potential upstream regulators using its knowledge base of biological interactions and functional annotations (see Section 2.4.1.3).[181] The software calculates a Z-score for each upstream regulator

that reflects the similarity between the observed expression changes in the input dataset and the known biological effects of each regulator. This analysis identified cytoskeleton associated protein 2 like (CKAP2L), a mitotic spindle protein that plays a key role in cell cycle progression,[228] as the most significantly activated regulator in metastatic PNETs **(Figure 4.10A & B)**. Furthermore, inspection of normalised *CKAP2L* mRNA levels in the RNA-seq dataset showed that its expression was > 2-fold higher in metastatic PNETs compared to non-metastatic ones (adjusted p = 0.05). The forkhead box protein M1 (FOXM1) transcription factor, a known master regulator of the cell cycle,[229] also emerged as a highly activated regulators in metastatic PNETs **(Figure 4.10A & C)**. This finding was corroborated with GSEA, which showed enrichment of the "FOXM1_PATHWAY" gene set from the National Cancer Institute (NCI) Pathway Interaction Database (PID)[178] in metastatic PNETs **(Figure 4.10D)**. However, *FOXM1* mRNA levels did not significantly differ between metastatic and non-metastatic tumours, suggesting that its activation in metastatic PNETs might be influenced by post-transcriptional mechanisms or interactions with other proteins, rather than changes in mRNA levels. Conversely, the top 10 significantly inhibited regulators in metastatic PNETs included p53 and the cyclin dependent kinase inhibitor 1A (CDKN1A), both of which are known regulators of cell cycle progression **(Figure 4.10A)**.[230,231] Collectively, these results implicate the dysregulation of cell cycle-related pathways in metastatic PNETs. Notably, cytotoxic T-lymphocyte Antigen 4 (CTLA4) was identified as the top inhibited upstream regulator in metastatic PNETs, suggesting a possible adaptive immune mechanism against metastatic tumours, whereby the inhibition of CTLA4 may enhance T-cell activity and promote a more robust immune response against the tumour cells.

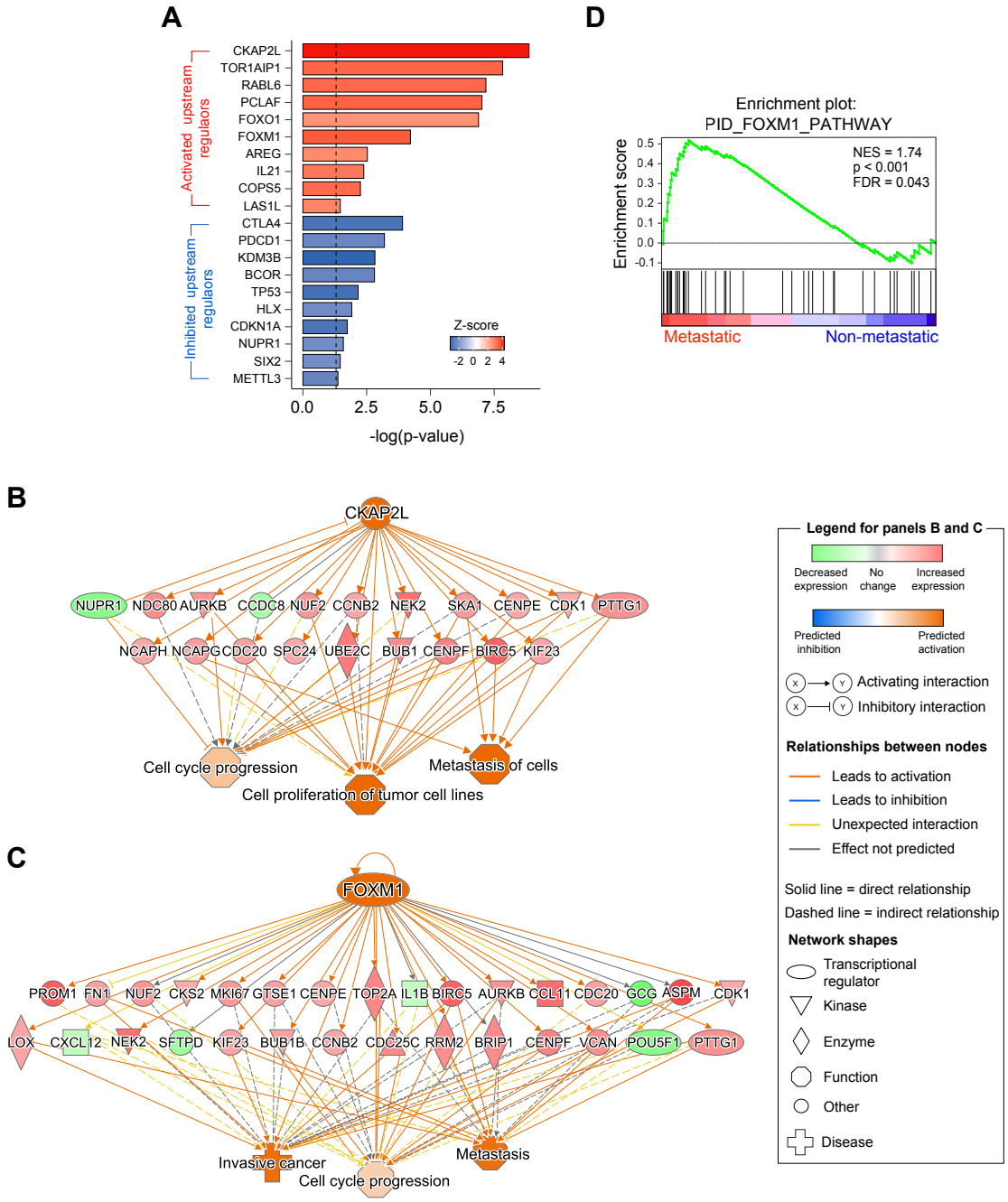

Figure 4.10. Pathway analysis identifies activation of cell cycle master regulators in metastatic PNETs. (A) Bar plot showing IPA upstream regulator analysis results. Bar colours represent Z-score, indicating the degree to which a regulator is predicted to be activated (red) or inhibited (blue). The top 10 activated/inhibited regulators are ranked by -$\log_{10}$p-value. The dashed vertical line marks the threshold for p ≤ 0.05 (-$\log_{10}$p-value > 1.3). p-values were calculated using Fisher's exact test by IPA software. Network diagrams generated by IPA showing genes regulated by **(B)** CKAP2L and **(C)** FOXM1 in metastatic PNETs. Red nodes represent upregulated genes, while green nodes indicate downregulated genes on RNA-seq. The inset legend on the right of the diagrams explains the symbols and colours used within the network. [Caption continues on next page...]

Figure 4.10. Pathway analysis identifies activation of cell cycle master regulators in metastatic PNETs. **(D)** GSEA plot for the "PID_FOXM1_PATHWAY" gene set compared to the entire RNA-seq gene list, ranked by differential expression in metastatic *vs* non-metastatic PNETs. The green line indicates the enrichment score across the ranked list of genes. NES, normalised enrichment score, FDR, false discovery rate.

4.2.6 The transcriptome of metastatic PNETs is enriched with BET inhibitor target genes

To explore the potential relevance of my RNA-seq findings to BET proteins and their inhibitors, GSEA was conducted against a signature of BET-inhibitor target genes. This signature was curated from BET inhibitor targets recorded in the IPA database and literature-reported genes downregulated by BET inhibition in various cancer cell lines.[232] This analysis verified that the expression of BET inhibitor target genes was significantly enriched in metastatic PNETs **(Figure 4.11A)**, supporting the notion that BET inhibitors could be of therapeutic benefit in these tumours. The 'Analysis Match' module in IPA was then used to compare the gene expression profiles of metastatic PNETs to expression changes induced by > 20,000 compounds across different cell lines catalogued in the Library of Integrated Network-Based Cellular Signatures (LINCS) database.[233,234] Remarkably, BET inhibitors constituted four of the top five compounds predicted to reverse the gene expression alterations in metastatic PNETs **(Figure 4.11B)**. Furthermore, these compounds were ranked higher than the mechanistic target of rapamycin (mTOR) inhibitor everolimus (rank #26) and the tyrosine kinase inhibitor sunitinib (rank #27), both of which are currently approved by the US Food and Drug Administration (FDA) and European Medicines Agency for the treatment of metastatic PNETs.

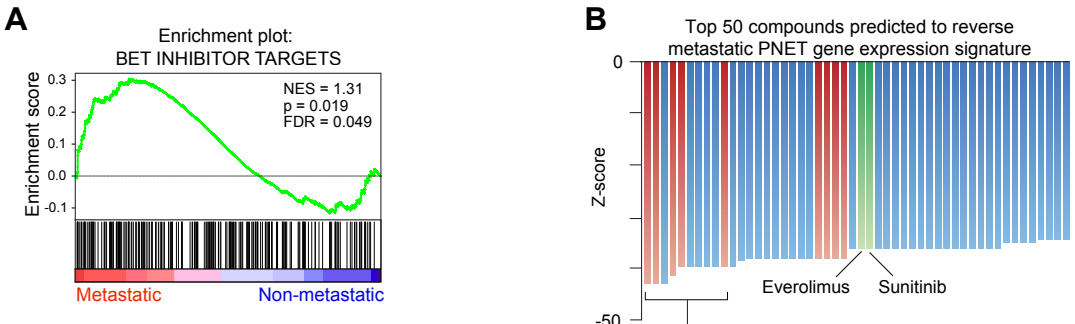

Rank	Compound	Target (s)	Tissue	Z-score	p-value
1	I-BET762	BRD2, BRD3, BRD4	Kidney	-42.92	4.33×10^{-14}
2	JQ1	BRD2, BRD3, BRD4	Kidney	-42.92	4.33×10^{-14}
3	BI2536	PLK1	Breast	-42.92	4.33×10^{-14}
4	I-BET151	BRD2, BRD3, BRD4	Lung	-41.36	1.01×10^{-12}
5	XMD8-92	BMK1; BRD4	Kidney	-39.74	5.63×10^{-14}
6	Saracatinib	Src; BCR-ABL	Breast	-39.74	7.81×10^{-12}
7	TWS119	GSK-3β	Breast	-39.74	2.15×10^{-11}
8	TPCA-1	IKK-β	Kidney	-39.74	2.15×10^{-11}
9	XMD-1150	LRRK2	Kidney	-39.74	2.15×10^{-11}
10	I-BET151	BRD2, BRD3, BRD4	Kidney	-39.74	2.15×10^{-11}

Figure 4.11. BET-inhibitor target gene expression is enriched in metastatic PNETs. (A) GSEA plot for the 'BET INHIBITOR TARGETS' gene set compared to the entire RNA-seq gene list ranked by differential expression in metastatic *vs* non-metastatic PNETs. The green line indicates the enrichment score across the ranked list of genes. **(B)** Bar plot of top 50 compounds predicted by the 'IPA Analysis Match' module to reverse the gene expression signature of metastatic PNETs. Compounds are ranked by their Z-score, with a more negative score indicating a higher predicted efficacy in reversing the gene expression pattern. BET inhibitors (red bars), sirolimus and sunitinib (green bars), and other drug classes (blue bars) are highlighted. The table (below) details the top 10 compounds, including their molecular targets and the tissue types where a similar reversal of gene expression signature has been observed in the IPA database. p-values calculated using Fisher's exact test by IPA software.

4.2.7 Mapping of the BET protein cistrome in PNET cells reveals enrichment of cancer-related and neuronal lineage pathways

After establishing that BET protein targets were upregulated in metastatic human PNETs in the Mayo Clinic cohort, I performed ChIP-seq to characterise the genome-wide binding sites of BRD2, BRD3 and BRD4 in the BON1 cell line, a widely used *in vitro* PNET model.[235,236] The term 'cistrome' refers to the complete set of *cis*-regulatory targets, such as enhancers and promoters, bound by a particular protein or complex of proteins (i.e, *trans*-acting factors) across the genome.[237] Thus, mapping the BET protein cistrome involves identifying all

genomic regions that are bound by BET proteins, providing insights into their regulatory roles in gene expression. This analysis identified ~74,000 BRD2 peaks, ~32,900 BRD3 peaks and ~64,800 BRD4 peaks **(Figure 4.12A)**. These peaks were annotated using the 'ChIP-seeker'[238] R package, which showed that all three BET protein peaks were most frequently found near the transcription start sites (TSS) of individual genes (~36-46%), indicating a significant role in transcription regulation at promoter regions **(Figure 4.12B)**. Additional enrichment was noted at intronic and distal intergenic regions, consistent with the involvement of BET proteins in cis-regulatory elements, such as enhancers. The distribution of peaks across the various genomic regions was similar amongst BRD2, BRD3 and BRD4, suggesting potential functional similarities among these proteins in regulating gene expression.

The CistromeDB toolkit (http://dbtoolkit.cistrome.org/) was used to assess the similarity of the identified BET protein binding loci with over 10,000 datasets in the ENCODE ChIP-seq database,[239] and the degree of similarity was quantified as a 'GIGGLE' score. This analysis provided validation of my ChIP-seq data by confirming that the identified BRD2, BRD3, and BRD4 binding sites overlap with published BET protein cistromes as well as the cistromes of other factors that are known to co-localise with BET proteins (e.g., RNA Polymerase II Subunit A [POLR2A][142] and Mediator Complex Subunit 1 [MED1][240]) **(Figure 4.12C)**. Interestingly, both BRD2 and BRD4 peaks showed the highest similarity with BRD4 datasets, suggesting potential functional redundancies between these two BET protein family members. In contrast, BRD3 peaks showed similarities with a distinct set of peak sets in the CistromeDB toolkit, suggesting unique regulatory roles for BRD3 that may be distinct from those of BRD2 and BRD4.

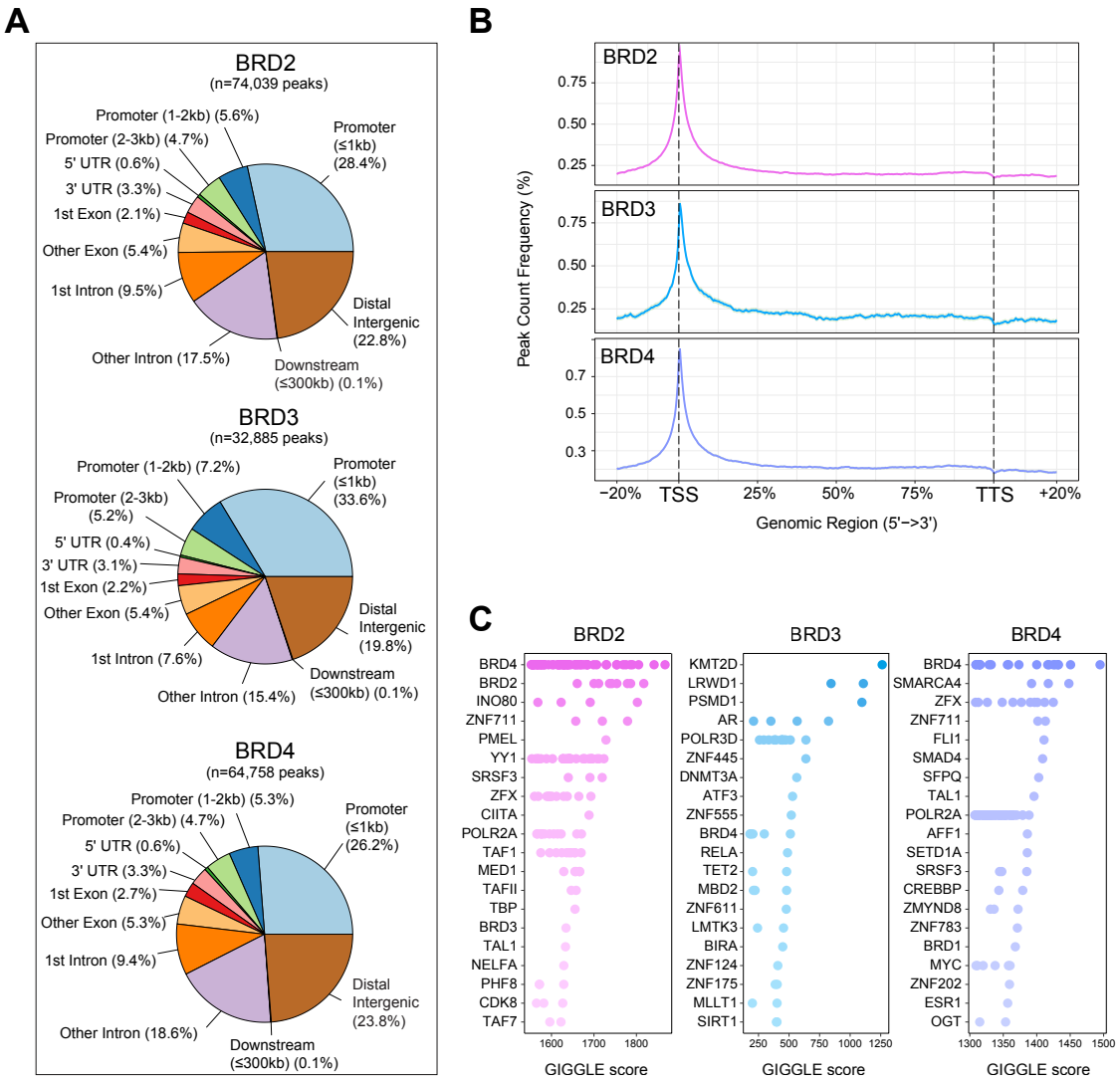

Figure 4.12. ChIP-seq maps the BET protein cistrome in BON1 PNET cells. **(A)** Pie charts depicting the genomic distribution of BRD2, BRD3 and BRD4 protein binding sites across different genomic regions, including promoters, introns, exons, and distal intergenic regions. The percentage of peaks identified in each region is indicated for each BET protein. **(B)** Metagene plots showing aggregate BET protein ChIP-seq signal enrichment across the entirety of the genome relative to the transcriptional landmarks of all annotated genes. The x-axis spans from 20% upstream of the transcription start sites (TSS) to 20% downstream of the transcription termination sites (TTS), reflecting a genome-wide view from the 5' to the 3' regions. The y-axis denotes the frequency of binding peaks, indicating the likelihood of BET protein association at various genomic intervals. **(C)** Dot plots showing GIGGLE scores, which represent similarity between BET protein peak sets identified in this chapter and deposited ChIP-seq profiles in the CistromeDB toolkit. Each point represents a separate ChIP-seq dataset.

The 'ChIP-seeker' package was then used to annotate BRD2, BRD3 and BRD4 peaks to 15,487, 10,566 and 15,183 genes, respectively. Over-representation analysis

was performed using the 'clusterProfiler' R package to determine Kyoto Encyclopedia of Genes and Genomes (KEGG) pathways enriched in the list of genes mapped to each BET peak set.[179] This analysis identified 'pathways in cancer' as the highest enriched KEGG pathway in genes associated with BRD3 and BRD4 peaks, and the second-highest ranked pathway in genes associated with BRD2 peaks **(Figure 4.13A)**. Other significantly enriched cancer-related KEGG pathways common to all three BET peak-associated genes included 'proteoglycans in cancer', 'MicroRNAs in cancer' as well as pathways related to mitogen-activated protein kinase (MAPK) and rat sarcoma (Ras) signalling. While the enrichment of KEGG pathways was broadly similar among all three BET peak-related genes, one notable difference was the presence of 'calcium signalling pathway' as the second-highest ranked pathway in BRD3 peak-associated genes, a prominence not observed in the gene sets associated with BRD2 and BRD4 peaks.

To further characterise biological processes central to BET protein function in PNETs, Reactome pathway[180] over-representation analysis was conducted on 9,277 genes identified as common to BRD2, BRD3 and BRD4 peaks **(Figure 4.13B)**. This revealed the upregulation of pathways related to the neuronal lineage, such as 'neuronal system', 'axon guidance' and 'transmission across chemical synapses', reflecting the shared evolutionary heritage of neuroendocrine tumours and neuronal cells **(Figure 4.13C)**. The second highest enriched Reactome pathway was 'signalling by receptor tyrosine kinases', which is relevant in the context of neuroendocrine tumours, as tyrosine kinases such as the vascular endothelial growth factor (VEGFR) and the insulin-like growth factor-1 receptor (IGF1R) have been shown to be expressed and promote cell proliferation via activation of phosphoinositide 3-kinase (PI3K)/protein kinase B (AKT) signalling. These findings suggest that BET proteins play a multifaceted role in the maintenance of neuroendocrine lineage-specific biology as well as the promotion of tumourigenic processes through their involvement in critical signalling pathways.

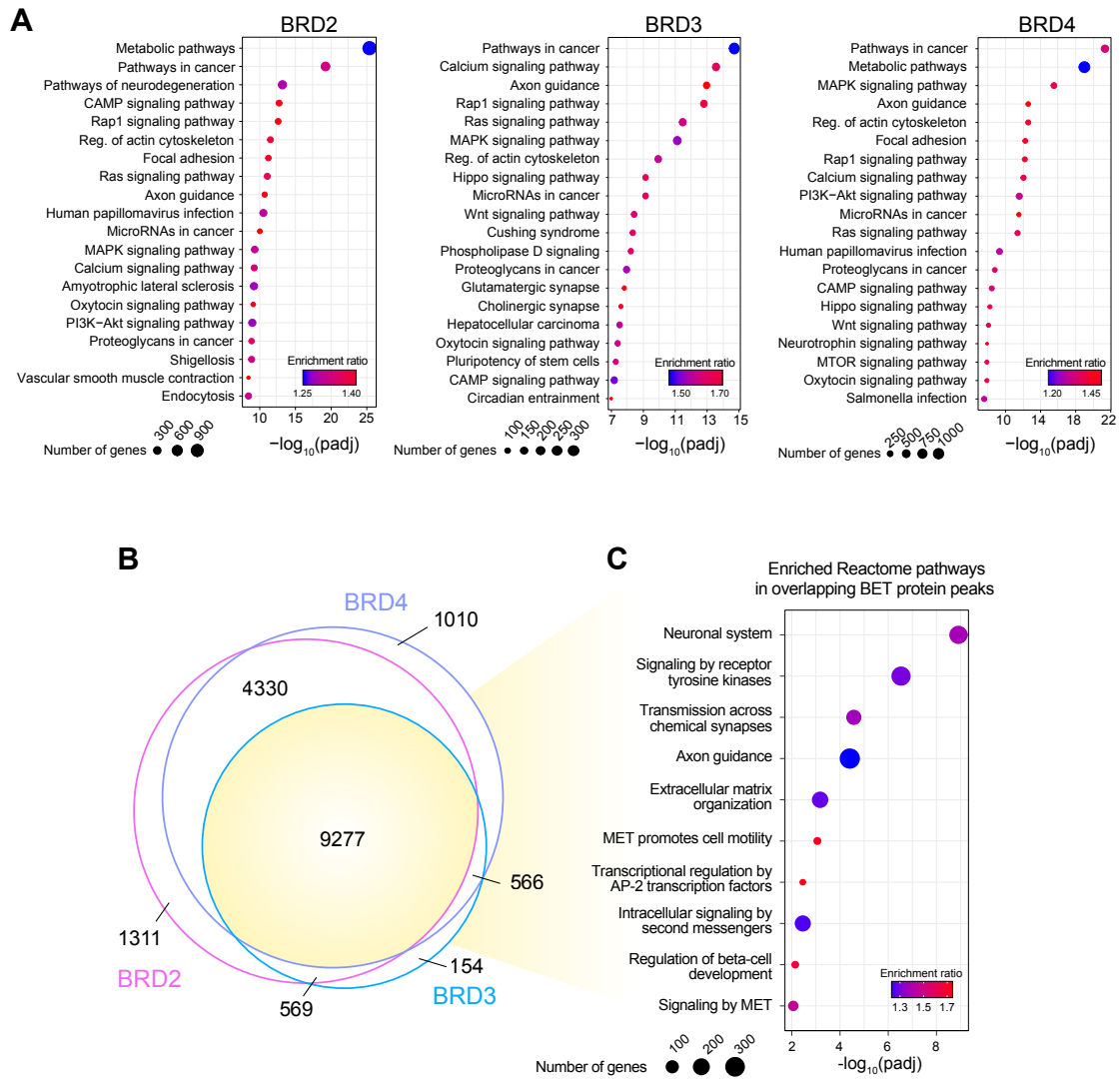

Figure 4.13. Pathway analysis reveals enrichment of cancer-related and neuronal lineage pathways in BET protein peaks. (A) Bubble plots displaying KEGG pathway enrichment analysis for genes associated with BRD2, BRD3, and BRD4 protein binding. The size of each bubble corresponds to the number of genes involved in the pathway, while the colour gradient indicates the enrichment ratio (i.e., the proportion of genes within the dataset that are associated with a given pathway compared to the expected proportion if there was no enrichment). The x-axis shows the negative logarithm of the adjusted p-value ($-\log_{10}(\text{padj})$), signifying the statistical significance of enrichment in various biological processes and pathways. Pathways are ranked by their degree of enrichment and the number of genes involved, underscoring the potential functional impact of BET protein interactions. **(B)** Area-proportional Venn diagram illustrating the overlap of genes associated with BRD2, BRD3 and BRD4 peaks. **(C)** Bubble plot displaying enriched Reactome pathways in 9,277 genes associated with overlapping BRD2, BRD3 and BRD4 peaks. Bubble size corresponds to the number of genes within each pathway, and the colour intensity reflects the enrichment ratio, while x-axis shows the negative logarithm of the adjusted p-value ($-\log_{10}(\text{padj})$).

4.2.8 E2F transcription factor binding motifs are enriched within BRD2 and BRD4 peak regions

To identify transcription factors and regulatory proteins that may co-localise with BET proteins and participate in the modulation of gene expression in PNETs, *de novo* motif analysis was performed on the BRD2, BRD3 and BRD4 peak sets using the HOMER motif discovery software suite.[241] This analysis revealed MED1 as the highest enriched binding motif in BRD2 **(Figure 4.14A)** and BRD3 peaks **(Figure 4.14B)**, and the second-highest enriched motif in BRD4 peaks **(Figure 4.14C)**. This finding is consistent with the role of MED1 as a key component of the Mediator complex, which is known to physically interact with BET proteins and activate RNA Polymerase II (Pol II)-dependent transcription.[142,240] E2F transcription factor motifs were also highly enriched at peaks associated with BRD2 and BRD4, which aligns with the known role of these BET proteins as co-activators of E2F-dependent transcriptional programs.[189,224,225]

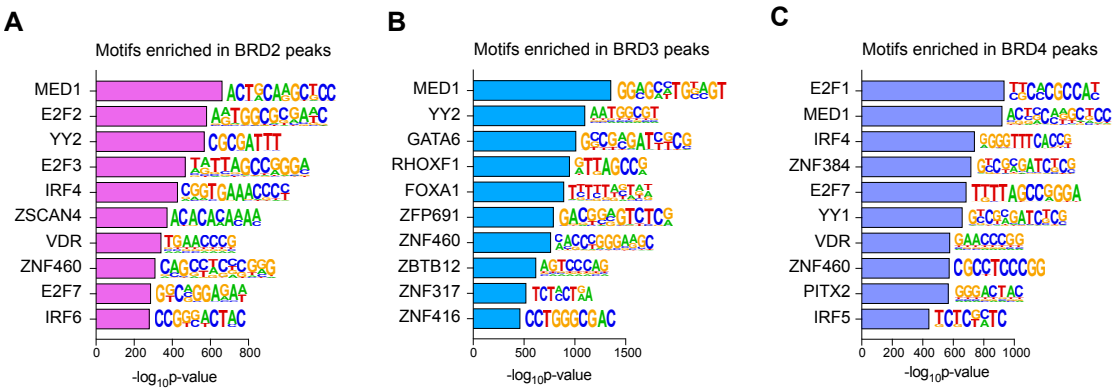

Figure 4.14. E2F transcription factor binding motifs are enriched within BRD2 and BRD4 peak regions. Top 10 *de novo* transcription factor motifs identified by HOMER software as being enriched within the peak regions of **(A)** BRD2, **(B)** BRD3 and **(C)** BRD4. Each motif is ranked based on the negative logarithm of the p-value ($-\log_{10}$(p-value)), which is calculated using a binomial test to evaluate the likelihood of the motif's occurrence being higher than expected by chance in randomly selected genomic regions. The sequence logos next to the bars represent the consensus binding sequences for each transcription factor, with the height of each letter proportional to the frequency of the corresponding nucleotide at that position.

4.2.9 BET proteins bind to the promoter regions of key cell cycle regulators

Based on the findings presented earlier in this chapter, such as the upregulation of E2F targets and the enrichment of E2F motifs at BET protein peaks, I hypothesised that BET proteins themselves may regulate the expression of E2F family members through binding to acetylated histones at their promoters. To investigate this, the Integrated Genomics Viewer (IGV)[193] was used to visualise BRD2, BRD3, and BRD4 peaks at the promoter regions of *E2F1* **(Figure 4.15A)**, *E2F2* **(Figure 4.15B)** and *E2F3* **(Figure 4.15C)**. This analysis revealed distinct peaks for BRD2 and BRD4, indicating strong binding affinity at these genomic loci. BRD3 enrichment was also observed, albeit to a lesser extent. These findings support the notion that BET proteins, particularly BRD2 and BRD4, play a role in the transcriptional regulation of E2F family members, potentially driving the gene expression patterns observed in metastatic PNETs. I additionally examined the enrichment of BRD2, BRD3 and BRD4 at the loci of *CKAP2L* **(Figure 4.15D)** and *FOXM1* **(Figure 4.15E)**, given their identification as activated upstream regulators by IPA, and observed distinct BET peaks at the promoter regions of both genes. Finally, BET protein binding at the *MYC* locus **(Figure 4.15F)** was examined, given the well-described role of *MYC* as a BET protein target gene. This also showed BRD2, BRD3 and BRD4 enrichment (at relatively similar levels) at the *MYC* locus, suggesting that *MYC* transcription is also under BET regulation in PNET cells.

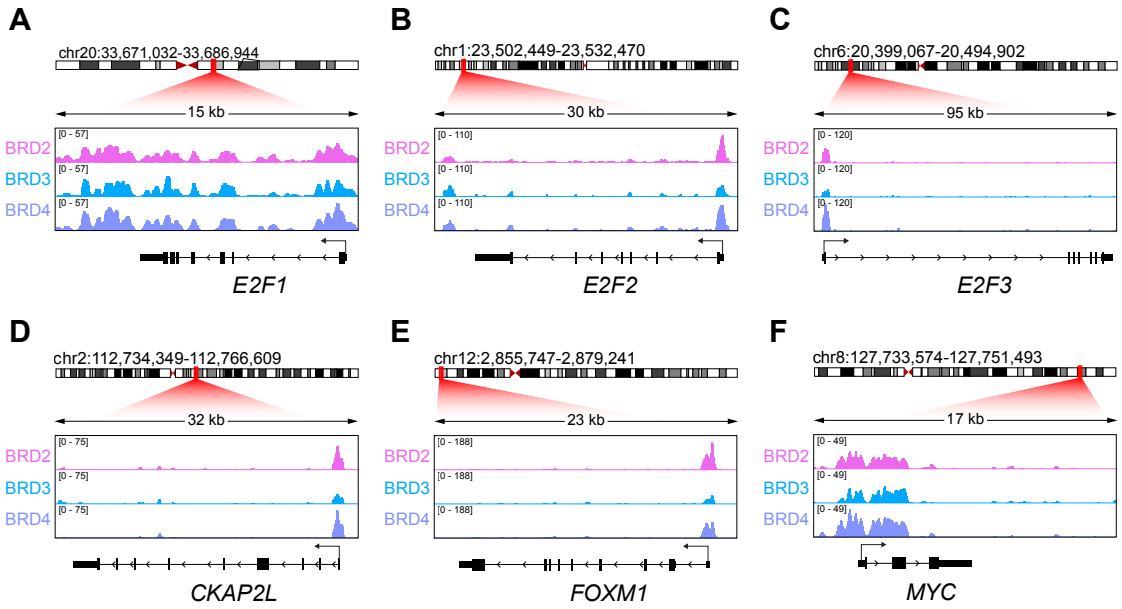

Figure 4.15. BET proteins bind to the promoter regions of cell cycle regulators. IGV genome browser tracks showing the binding profiles of two merged biological replicates of BRD2, BRD3, and BRD4 ChIP-seq reads at the promoter regions of **(A)** *E2F1*, **(B)** *E2F2*, **(C)** *E2F3*, **(D)** *CKAP2L*, **(E)** *FOXM1* and **(F)** *MYC*. Genomic coordinates and gene loci are indicated above and below each track, respectively. The y-axis denotes the range of read counts within square brackets.

4.3 Discussion

In this chapter, expression of the BET proteins—BRD2, BRD3 and BRD4— was characterised in a cohort of human PNETs relative to normal adjacent pancreatic islets, with consistent over-expression observed across various tumour subtypes, stages and grades. Through RNA-seq and ChIP-seq analyses, this chapter also highlights the complex regulatory roles of BET proteins in PNETs, including the enrichment of BET inhibitor target genes in metastatic tumours and the binding of BET proteins to the promoter regions of key cell cycle master regulators. Collectively, these findings suggest that BET proteins may play a role in the molecular pathogenesis of PNETs and support the exploration of BET inhibitors as a therapeutic approach for these tumours.

4.3.1 BET proteins are overexpressed in human PNETs

The oncogenic role of BET proteins was first identified in the context of nuclear protein in testis (NUT) midline carcinoma (NMC), a rare subtype of squamous cell carcinoma, wherein chromosomal translocations lead to the fusion of the carboxy terminus of the NUT protein, which is normally only expressed in mature spermatogonia, with the amino terminus of BRD4 or BRD3.[242] The most common translocation, designated as t(15;19)(q14;p13.1), fuses the *NUT* gene on chromosome 15 at band q14 with the *BRD4* gene on chromosome 19 at band p13.1, resulting in the BRD4-NUT fusion oncoprotein. A less frequent translocation, designated as t(9;15)(q34.2;q14), fuses the *NUT* gene with the *BRD3* gene located on chromosome 9 at band q34.2, leading to formation of the BRD3-NUT fusion oncoprotein. These oncoproteins attract various transcriptional coactivators, such as the histone acetyltransferase p300, which facilitates local chromatin hyperacetylation. This mechanism establishes a positive feedback loop that promotes further recruitment of BRD4 and the aberrant expression of pro-survival genes, such as *MYC*. Beyond the context of NMC, however, chromosomal translocations involving BET protein-encoding genes are rare and no recurrent genomic alterations (e.g., hot spot mutations) that confer gain of function have been identified.[243] Indeed, an analysis of the coding sequence of *BRD4* across diverse cancer genomes revealed predominantly missense mutations dispersed throughout its reading frame, without discernible patterns or mutation types that suggest oncogenic alterations in bromodomain functionality.[244] Nonetheless, overexpression of BET family members has been noted in various cancer types, where mechanistic studies have demonstrated a dependence on BET bromodomain function.[245–247] Copy number amplifications at the BRD4 locus have been observed in approximately 18% of patients with high grade serous ovarian cancer[248] and in 50% of melanoma cell lines.[249] Moreover, an analysis of copy number aberrations in 9,445 tumours across 20 cancer types in The Cancer Genome Atlas (TCGA) dataset revealed recurrent amplifications of *BRD4* in breast, liver, and endometrial cancers.[243] However, the mechanisms driving

BRD4 overexpression outside these contexts, and the overexpression of *BRD2* and *BRD3* in cancer in general are not well understood. Furthermore, studies that include copy-number variation analysis in PNETs have not identified amplification at BET gene loci,[101,106,250,251] suggesting that overexpression of BET proteins in these tumours may be regulated through alternative mechanisms that warrant further study. Nevertheless, given the established role of BRD4-NUT and BRD3-NUT fusion proteins in NUT midline carcinoma, and the observation that these tumours may rarely arise from the pancreas,[252] it would be prudent to investigate whether a subset of highly aggressive PNETs harbour similar rearrangements. Immunostaining with a NUT monoclonal antibody can be employed to detect the presence of NUT fusion proteins in these tumours. If identified, fluorescence *in situ* hybridisation (FISH) and next-generation sequencing (NGS) could be utilised to confirm the specific chromosomal translocations and provide further molecular characterisation. Detecting and characterising NUT rearrangements in PNETs could uncover unique transcriptional programs driven by these fusions, offering insights into their aggressive behaviour and revealing potential therapeutic targets.

4.3.2 *BRD2* is the most abundant BET gene in PNETs

Analysis of BET mRNA levels revealed *BRD2/Brd2* as the most abundantly expressed BET gene across three human and mouse PNET cell lines, exhibiting significantly higher expression than *BRD3/Brd3* and *BRD4/Brd4*. This expression pattern, which was consistent with findings from the Mayo Clinic RNA-seq dataset of human PNETs, suggests a potentially important role for BRD2 in PNET biology. Furthermore, these results underscore the suitability of the BON1 cell line as a representative model for investigating BET protein biology and evaluating the efficacy of BET inhibitors. Importantly, in PNETs derived from *Men1*$^{L/L}$*/RIP2-Cre* mice, *Brd2* expression significantly exceeded that of *Brd3* and *Brd4*,[60] corroborating its prevalent expression across PNET models. BET proteins have been shown to play a role in the differentiation of pancreatic endocrine progenitors,[253] with *BRD2*

specifically implicated in inducing insulin resistance through the mTOR/PI3K signalling pathway,[254] which is known to be dysregulated in PNETs.[100] Although BRD4 is arguably the most extensively studied BET protein, BRD2 was in fact the earliest described human BET family member and was initially reported in the context of its interactions with E2F transcription factors.[224] Thus, BRD2 forms a multi-protein complex with Pol II, E2F1 and E2F2, activating the transcription of genes that encode proteins necessary for the cell cycle G1/S phase transition, such as Cyclin A.[140] Moreover, the presence of 'E2F_TARGETS' as the highest enriched Hallmark gene set in metastatic PNETs supports a role for BRD2 in the pathogenesis and aggressiveness of these tumours.

4.3.3 BET mRNA and protein expression does not vary by PNET stage or grade

Despite their upregulated expression in PNETs relative to normal islets, there was no significant difference in the intensity of BET protein staining across various stages and grades of tumours in the Vienna cohort. This pattern of uniform expression was corroborated using RNA-seq data from the Mayo Clinic cohort. These findings indicate that BET proteins may play a central role in the pathogenesis of PNETs, irrespective of the tumour's specific histological or clinical attributes. Thus, BET inhibition could serve as a universally applicable treatment strategy across the spectrum of PNET cases, obviating the need for stratification by tumour subtype, stage, or grade. That being said, if BET proteins are postulated to play a role in cancer-related pathways in this context, then one might expect that their expression would be higher in more aggressive/advanced tumours. Conversely, transcriptional regulation of BET proteins may not be the driving factor behind the differential aggressiveness observed between metastatic and localised PNETs. Instead, existing literature points to alternative regulatory mechanisms for BET activity, including post-translational modifications such as phosphorylation, acetylation and ubiquitination.[255] For example, phosphorylation

of BRD4 by casein kinase 2 (CK2) has been shown to control the activity of BRD4 by increasing its binding capacity to acetylated chromatin, as well as to human p53 and viral E2 transcription factors[256] As CK2 activity is frequently upregulated in cancer cells[257] and has been shown to regulate pancreatic and duodenal homeobox 1- (PDX1)-mediated transcription in pancreatic β-cells,[258] this mechanism could be responsible for dysregulation of BET protein activity in metastatic PNETs and requires further study.

4.3.4 Dysregulation of cell cycle-related pathways may link BET protein activity to aggressive PNET behaviour

Unlike more common cancers, which are well represented in large repositories such as TCGA,[259] there is a paucity of publicly-available PNET gene expression data annotated with detailed clinical information. Thus, the generation of novel RNA-seq data from 46 PNET samples from the Mayo Clinic provided an invaluable resource for studying their transcriptional landscape. Furthermore, the corroboration of the Mayo Clinic gene expression profiles with previously defined molecular prognostic subtypes of PNETs[222] provided external validation of the representativeness of this dataset. My bioinformatics analyses of these data uncovered significant upregulation of gene sets associated with cell cycle control, DNA replication and mitotic processes in metastatic PNETs, pointing towards aberrant acceleration of the cell cycle as a feature that underpins aggressiveness of these tumours. Among the most prominently enriched pathways were those related to E2F signalling and mitotic spindle assembly, highlighting critical junctures at which BET proteins, particularly BRD2, may exert their influence. The prominent role of E2F and cell-cycle related pathways in metastatic tumours is supported by a recent study that utilised transcriptomic and proteomic profiling to define four molecular subtypes of PNETs: 1) PDX1-high; 2) Alpha cell-like; 3) Stromal/Mesenchymal and 4) Proliferative.[260] PDX1-high and Alpha cell-like tumours were characterised by high expression of PDX1 and the transcription factor Aristaless-related homeobox (ARX), respectively, while the

Stromal/Mesenchymal subgroup was enriched in stromal and immune cell markers. Notably, the Proliferative subtype, which was associated with the poorest survival outcomes, exhibited significant enrichment of 'E2F targets' and 'G2M checkpoints', which is similar to what I observed in the metastatic Mayo Clinic PNET samples. The authors also profiled BON1 and QGP1 cells, and observed that these cell lines clustered with the Proliferative subgroup.[260] The role of E2F and cell-cycle pathways in metastatic tumours is further evidenced by a study that applied single-cell RNA-seq (scRNA-seq) to over 24,000 cells from a primary G2 PNET and its matched liver metastasis.[261] The study delineated seven distinct malignant cell subtypes, with subtype 6 identified as the most aggressive and characterised by increased expression of E2F family members and pathways related to cell cycle progression. Collectively, these findings support the notion that aggressive PNETs are characterised by dysregulated cell cycle signalling and confirm that the human PNET cell lines used in this thesis are an appropriate model for evaluating potential therapeutic strategies in aggressive PNETs.

IPA analysis of the gene expression profiles of PNETs in the Mayo Clinic cohort identified CKAP2L as the most significantly activated upstream regulator in metastatic tumours. Moreover, significantly elevated mRNA expression levels of *CKAP2L* in metastatic tumours indicate that its role as a crucial upstream regulator may stem from dysregulated expression patterns. CKAP2L is a microtubule-associated protein required for cell-cycle progression in neural progenitor stem cells.[228] Beyond its structural role at the spindle pole, CKAP2L has also been revealed as a key orchestrator of cell division in non-small cell lung cancer, via direct interaction with Pol II and regulation of transcription elongation of key genes involved in chromosome segregation and E2F signalling.[262] Recent studies have also implicated elevated CKAP2L expression levels as a poor prognostic factor in hepatocellular carcinoma[263] and prostate cancer,[264] among others.[265] The precise role of BET proteins in CKAP2L upstream regulator activity in PNETs is yet to be elucidated. Nonetheless, evidence from my ChIP-seq analyses, which highlights the enrichment of neuronal lineage genes at overlapping BET peaks and

the binding of BRD2, BRD3 and BRD4 with the *CKAP2L* promoter points towards a potential regulatory interaction. IPA analysis and GSEA also identified FOXM1 as a significantly activated upstream regulator in metastatic PNETs. FOXM1 is an oncogenic transcription factor that plays a key role in cell cycle progression (via the regulation of G2/M phase-specific genes) and DNA damage response. Interestingly, E2F family members have been shown to bind to and activate the FOXM1 promoter.[266] Moreover, in a preclinical study of ovarian cancer, BET inhibition led to downregulation of FOXM1 and its putative transcriptional targets *in vitro* and *in vivo*, while exogenous overexpression of FOXM1 partially rescued tumour cells from the growth-inhibitory effects of JQ1.[267]

4.3.5 Genes associated with oxidative phosphorylation are upregulated in metastatic PNETs

GSEA revealed that the 'OXIDATIVE_PHOSPHORYLATION' gene set was one of the top enriched Hallmark pathways in metastatic PNETs, suggesting a shift in metabolic phenotype towards oxidative phosphorylation (OXPHOS). This shift is notable given the established link between metabolic reprogramming and cancer progression.[268] Traditionally, OXPHOS, the primary pathway through which normal cells produce ATP in the mitochondria, has been viewed as downregulated in cancer cells, which often favour glycolysis for energy generation even in the presence of oxygen - a phenomenon known as the Warburg effect.[269] This occurs because cancer cells reprogram their metabolism to prioritise rapid growth and proliferation (via glycolysis) over efficient energy production (via OXPHOS), leading to increased glucose uptake and lactate production. However, a growing body of evidence indicates that OXPHOS may actually be upregulated in certain cancers, including subtypes of leukaemia, lymphoma, pancreatic ductal adenocarcinoma (PDAC) and melanomas.[270] Studies also indicate metabolic heterogeneity within tumours such as PDAC, where cancer stem cells with high metastatic potential are more reliant upon OXPHOS than the non-stem bulk of the tumour.[271] Understanding

the specific role of OXPHOS in PNETs could guide the exploration of targeted treatments that exploit the metabolic vulnerabilities of these tumours, particularly since OXPHOS inhibitors have been observed to sensitise liver cancer cell lines to the anti-proliferative effects of BET inhibitors.[272]

4.3.6 CTLA4 is an inhibited upstream regulator in metastatic PNETs

CTLA4, a critical immune checkpoint molecule that negatively regulates T-cell activation and proliferation,[273] was identified as the top inhibited upstream regulator in metastatic PNETs by IPA. In the context of cancer, CTLA4 is often upregulated to help tumours evade immune surveillance by inhibiting the activation of anti-tumour T-cells.[273,274] Therefore, the seemingly counterintuitive finding that this upstream regulator was significantly downregulated in metastatic PNETs is intriguing and warrants further exploration. The reduced expression of CTLA4 in metastatic PNETs may help explain the limited effectiveness of immune checkpoint inhibitor therapy in these tumours.[275] Indeed, in other tumour types, such as melanoma[276,277] and head and neck squamous cell carcinoma,[278] low CTLA4 expression has been associated with reduced survival and poor response to immune checkpoint blockade.

A limitation of the RNA-seq profiling study described in this chapter is that bulk RNA-seq was used to analyse the gene expression profiles of PNETs. Bulk RNA-seq averages the gene expression signals from all cells within a tumour sample, potentially masking the contributions of distinct cellular subpopulations.[279] This can obscure important biological insights, particularly in heterogeneous tumours such as PNETs, where different cell types, including cancer cells, stromal cells, and immune cells, may exhibit unique stochastic gene expression patterns. For example, aggressive subpopulations or rare cell types, such as cancer stem cells or infiltrating immune cells, may play critical roles in tumour progression and response to therapy but could be underrepresented or undetectable in bulk RNA-seq data.[279] Instead, scRNA-seq offers a more granular view of the tumour transcriptome, allowing

for the dissection of cellular heterogeneity and the identification of distinct cell types and states within the tumour microenvironment.[280] This approach could reveal specific cellular subpopulations that drive metastatic behaviour or exhibit differential expression of BET family members. Despite the limitations of bulk RNA-seq, the data presented in this chapter have provided valuable insights into the overall gene expression landscape of PNETs and highlighted key pathways and regulators that may drive aggressive tumour behaviour.

In conclusion, this chapter highlights the significant overexpression of BET proteins in PNETs compared to normal pancreatic islets, indicating their potential role in PNET pathology. An over-arching theme from my RNA-seq analyses is that dysregulated cell cycle progression is a hallmark of metastatic tumours, with ChIP-seq showing that BET proteins are enriched at the promoters of key genes in this process. Collectively, these findings suggest that BET proteins play a role in orchestrating a complex regulatory network that facilitates PNET development and progression. This lays the groundwork for the subsequent chapter, in which I explore the phenotypic effects of BET inhibitors in PNET cell lines.

5

Phenotypic effects of current and next-generation BET inhibitors in PNET cell lines

Chapter-specific table of contents

5.1 Aims **139**
5.2 Results **140**
5.2.1 I-BET151 shows comparable efficacy to JQ1 in reducing viability in PNET cell lines 140
5.2.2 BD1- and BD2-selective BET inhibitors have differing effects on PNET cell viability 141
5.2.3 Simultaneous BD1 and BD2 inhibition synergistically reduces PNET cell viability 144
5.2.4 Simultaneous BD1 and BD2 inhibition increases apoptosis in PNET cell lines 150
5.2.5 Simultaneous BD1 and BD2 inhibition alters PNET cellular morphology and decreases viability in a time-dependent manner 151
5.2.6 The effects of simultaneous BD1 and BD2 inhibition on cell viability persist after compound washout . . . 154
5.2.7 Simultaneous BD1 and BD2 inhibition causes cell cycle arrest in human PNET cell lines 155
5.2.8 Effects of BET inhibitors on neoplastic pancreatic islets *ex vivo* 157
5.3 Discussion **157**
5.3.1 First-generation BET inhibitors are effective in PNET cell lines 158

5.3.2 MIN6 cells are relatively resistant to the effects of BET inhibition 159
5.3.3 BD1- and BD2-selective BET inhibitors have differential effects in PNET cell lines 160

5.1 Aims

In the previous chapter, I demonstrated that BET proteins are overexpressed in human PNETs relative to adjacent normal pancreatic islets. Furthermore, I elucidated that BET protein-related biological pathways, namely those related to cell cycle progression, are amongst the most highly upregulated in metastatic PNETs. These findings support the rationale for exploring BET inhibition as a treatment strategy for PNETs.

BET inhibitors have shown promise in early-phase clinical trials for treating both haematological and solid-organ malignancies. However, the occurrence of dose-limiting toxicities may limit their utility.[151] A promising strategy to mitigate these adverse effects involves selective targeting of the BET family's bromodomains (BD), BD1 or BD2.[281] Distinct residue differences between BD1 and BD2 have provided the structural basis for the recent development of potent next-generation inhibitors that are selective for each BD.[152,153] Emerging evidence also suggests that targeting either BD1 or BD2 specifically could exploit their differential roles in gene expression regulation.[155] This approach seeks to leverage aspects of BET biology that rely more heavily on one domain over the other, potentially yielding improved efficacy and a better tolerability profile compared to current-generation dual BD inhibitors. There is ongoing debate, however, surrounding whether this approach offers similar anti-cancer efficacy to dual BD inhibition.[282] Moreover, the implications of BD-selective inhibition in PNETs have not yet been explored. sxxx

The aims of this chapter were to investigate the phenotypic effects of first-generation (i.e. BD non-selective) and next-generation (i.e. BD-selective)

BET inhibitors on both human and murine PNET cell lines, focusing on changes in cell viability, morphology, apoptosis, and cell cycle alterations.

5.2 Results

5.2.1 I-BET151 shows comparable efficacy to JQ1 in reducing viability in PNET cell lines

To assess the efficacy of the BD non-selective inhibitors I-BET151 and JQ1 in reducing cell viability, BON1, QGP1 and MIN6 PNET cell lines were treated with 1 μM of each compound or 0.05% DMSO as a negative control. After 96 hours, I-BET151 significantly reduced cell viability by ~80%, ~81% and ~48% in BON1, QGP1 and MIN6 cells, respectively ($p \leq 0.0001$ *vs* DMSO for all comparisons) **(Figure 5.1)**. JQ1 had similar effects on cell viability in all three cell lines, with no significant differences observed in the degree of inhibition compared with I-BET151 **(Figure 5.1)**.

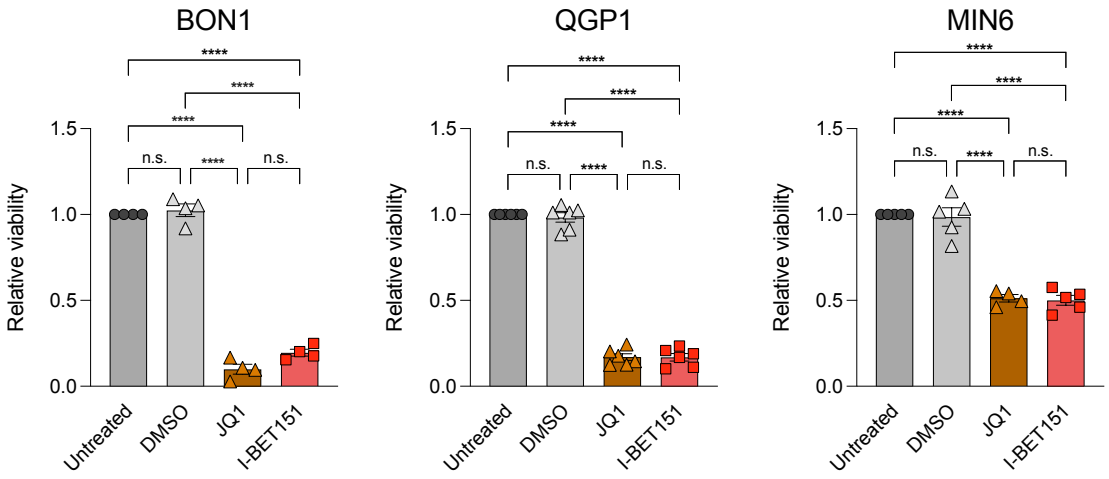

Figure 5.1. I-BET151 is as effective as JQ1 in reducing viability in PNET cell lines. Cell viability, relative to untreated cells, measured using CellTiter-Blue® cell viability assays, after 96 hours of treatment with 1 μM JQ1, 1 μM I-BET151 or 0.05 % DMSO control. Data are presented as mean ± SEM of 4-6 independent experiments and analysed using ordinary one-way ANOVA with Tukey's multiple comparisons test. n.s., not significant, ****$p \leq 0.0001$

5.2.2 BD1- and BD2-selective BET inhibitors have differing effects on PNET cell viability

To assess the impact of BD1- and BD2-selective inhibition on PNET cell line viability, the following next-generation BET inhibitors were selected for testing based on their reported selectivity for BD1 or BD2: GSK789, a BD1-selective inhibitor with > 1000-fold reported selectivity over BD2;[156] GSK620, a BD2-selective inhibitor with > 200-fold reported selectivity over BD1;[157] and ABBV-744 (another BD2-selective inhibitor with > 100-fold reported selectivity over BD1)[158] **(Figure 5.2)**.

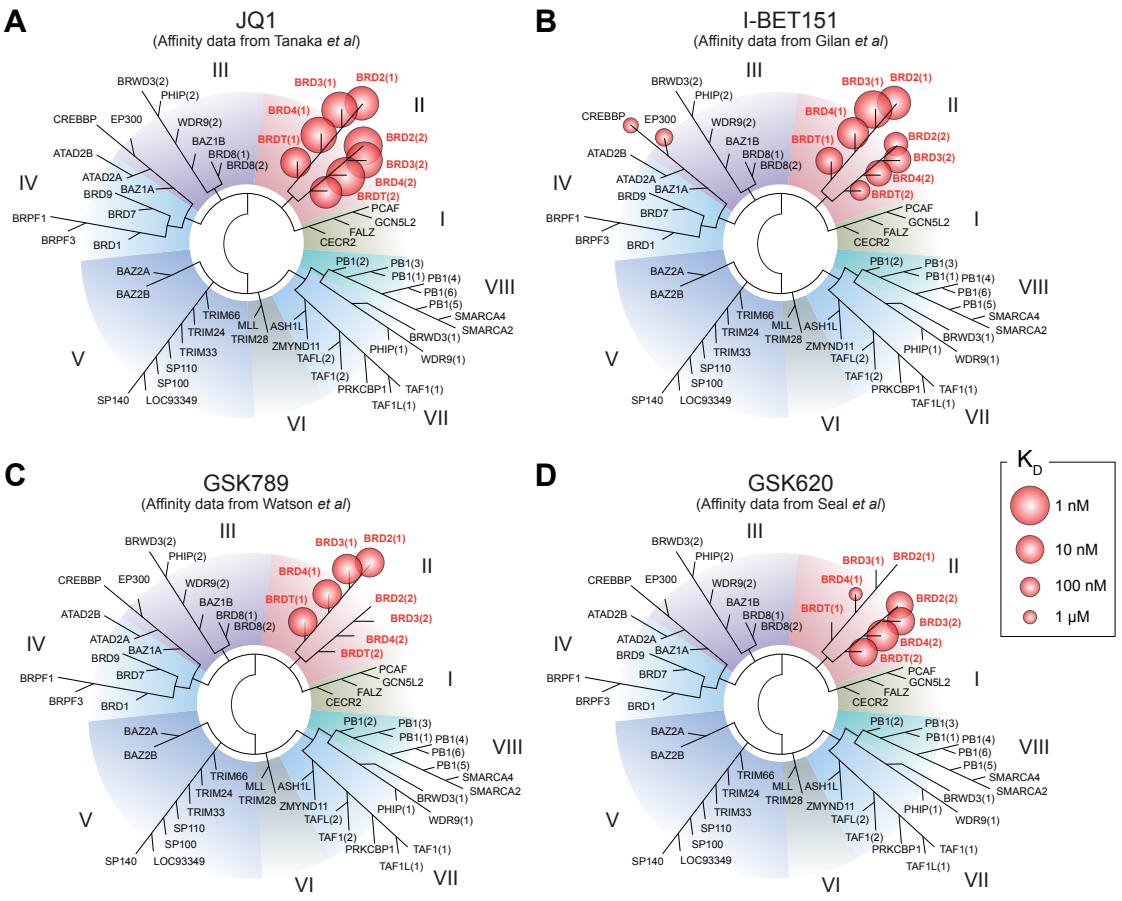

Figure 5.2. Affinity and selectivity profiles of current and next-generation BET inhibitors. Circular dendrograms showing affinity and selectivity profiles of **(A)** JQ1, **(B)** I-BET151, **(C)** GSK789 and **(D)** GSK620 across 40 different BDs. The eight major BD families are designated by Roman numerals (I-VIII) with the BET family (II) highlighted in red. Binding affinity (K_D) values are indicated by the size of the circles and are derived from BROMOscan competition binding assay data adapted from Tanaka et al.[283], Wellaway et al.[284] and Gilan et al.[152]. No publicly available BROMOscan K_D data were available for ABBV-744.

BON1, QGP1 and MIN6 cell lines were exposed to 1 μM of each compound, and cell viability was measured after 96 hours relative to DMSO control **(Figure 5.2B)**. GSK789 significantly decreased cell viability by 50% ($p \leq 0.0001$), 64% ($p \leq 0.0001$) and 21% ($p = 0.001$) in BON1, QGP1 and MIN6 cells, respectively. However, the degree of inhibition in all three cell lines was significantly less than that achieved by I-BET151. In contrast, GSK620 exhibited a negligible effect on cell viability after 96 hours. Intriguingly, treatment with ABBV-744 led to a reduction in cell viability comparable to that observed with I-BET151, highlighting an unexpected difference in efficacy between GSK620 and ABBV-744, despite both being reported as BD2-selective compounds.[150,153].

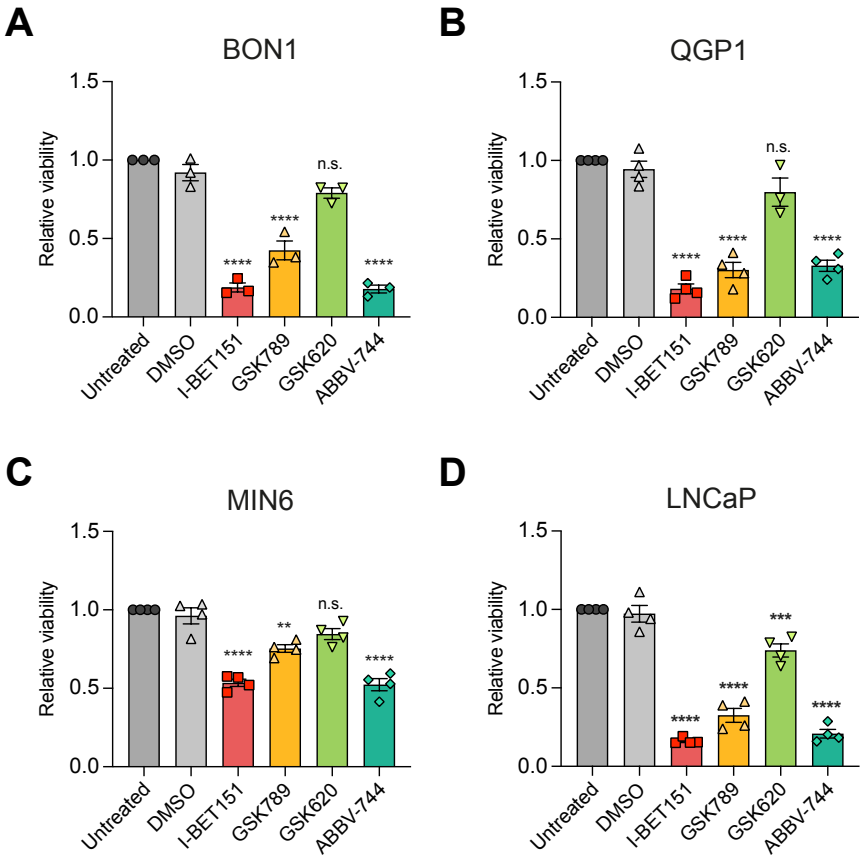

Figure 5.3. BD1- and BD2-selective BET inhibitors have differing effects on PNET cell viability. Bar graphs depicting relative cell viability of BON1, QGP1, MIN6, and LNCaP cells treated with 1 μM of the indicated BET inhibitors for 96 hours, measured by CellTitre Blue assays relative to DMSO control. Data are presented as mean ± SEM of 3-4 independent experiments and analysed using ordinary one-way ANOVA with Dunnett's test for multiple comparisons. n.s., not significant, *$p \leq 0.05$, **$p \leq 0.01$, *** $p \leq 0.001$, ****$p \leq 0.0001$

This discrepancy prompted further investigation into the effects of all four compounds on the LNCaP metastatic prostate cancer cell line,[163] which is reported to be highly sensitive to BD2 inhibition, especially by ABBV-744.[153] Consistent with the effects observed in the PNET cell lines, treatment of LNCaP cells with GSK620 resulted in minimal reduction in cell viability, while ABBV-744 exhibited an inhibitory effect comparable to I-BET151 **(Figure 5.4C)**. Recent mechanistic studies by Gilan et al.[152] suggest that the anti-proliferative effects of ABBV-744 may, in fact, be mediated through BD1 in addition to BD2 engagement. These findings, alongside my own observations, led to a reconsideration of the mechanism of action of this compound, and ultimately its exclusion from subsequent experiments in this chapter.

Crystal violet assays **(Figure 5.2D)** were used to confirm the differential effects of BET inhibitors on cell viability. Treatment with 1 μM of I-BET151 significantly reduced crystal violet staining intensity by 55%, 71% and 44% in BON1, QGP1 and MIN6 cells, respectively ($p \leq 0.0001$ for all). In contrast, the same concentration of GSK789 led to a moderate reduction in staining intensity by 26%, 41%, and 36% in BON1, QGP1 and MIN6 cells, respectively ($p \leq 0.0001$ for all), while GSK620 had minimal impact. A high concentration (10 μM) of each compound was also tested to delineate the upper limits of biological response. At this concentration, I-BET151 showed no additional decrease in cell viability compared to the 1 μM concentration. However, the 10 μM concentration induced cytotoxic effects in MIN6 cells, suggesting cell line-specific responses. GSK789, when administered at 10 μM, achieved a reduction in staining intensity in BON1 and QGP1 cells that was comparable to the effect observed with 1 μM of I-BET151. This suggests that at higher concentrations, GSK789 may engage both BD1 and BD2 domains. Conversely, 1 μM of GSK620 only slightly decreased crystal violet intensity in all three cell lines, reaffirming its specificity for BD2 even at higher concentrations. Collectively, these findings show that selective BD inhibition does not phenocopy the anti-proliferative effects of dual BD targeting in PNET cell lines, contrary to what has previously been reported in prostate cancer[153], leukaemia[152] and MYC-driven paediatric cancer.[285].

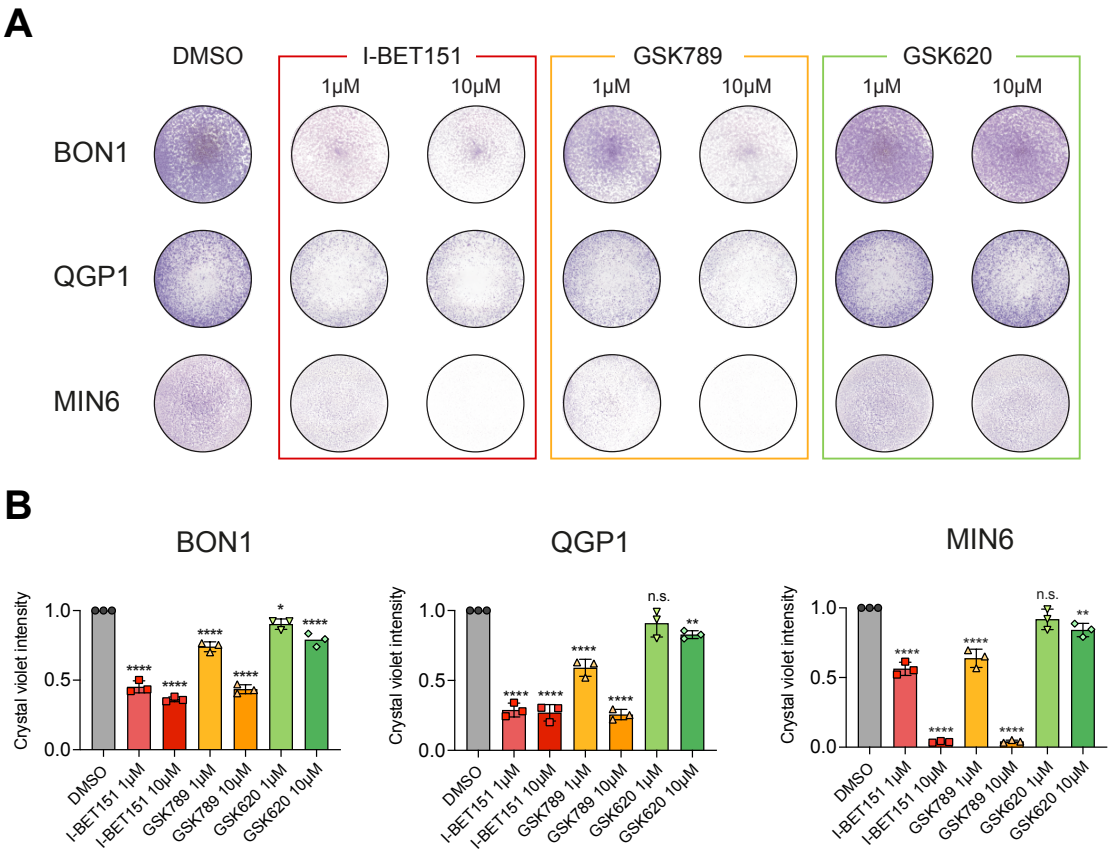

Figure 5.4. BD1- and BD2-selective BET inhibitors have differing effects on crystal violet staining in PNET cell lines. **(A)** Representative crystal violet staining images and **(B)** quantification of BON1, QGP1 and MIN6 cells after treatment with 1 μM and 10 μof the indicated BET inhibitors. Data are normalized to DMSO control and represent mean ± SEM of three independent experiments. Statistical analysis was performed using ordinary one-way ANOVA with Dunnett's test for multiple comparisons. n.s., not significant, *p ≤ 0.05, **p ≤ 0.01, *** p ≤ 0.001, ****p ≤ 0.0001

5.2.3 Simultaneous BD1 and BD2 inhibition synergistically reduces PNET cell viability

Although treatment with 1 μM of GSK789 led to a moderate decrease in PNET cell line viability, the effect was less pronounced than expected. I therefore hypothesised that simultaneous inhibition of BD2 alongside BD1 could lead to a stronger therapeutic effect. To explore this, dose-response studies were conducted where PNET cell lines were exposed to increasing concentrations of GSK789 and/or GSK620 (individually or in a 50:50 mixture) or I-BET151 for 96 hours,

with subsequent assessment of cell viability. These experiments showed that, at the majority of concentrations tested, the combination of GSK789 and GSK620 significantly decreased cell viability beyond the individual effect of either compound alone, with similar half-maximal inhibitory concentration (IC_{50}) values to I-BET151 **(Figure 5.5)**.

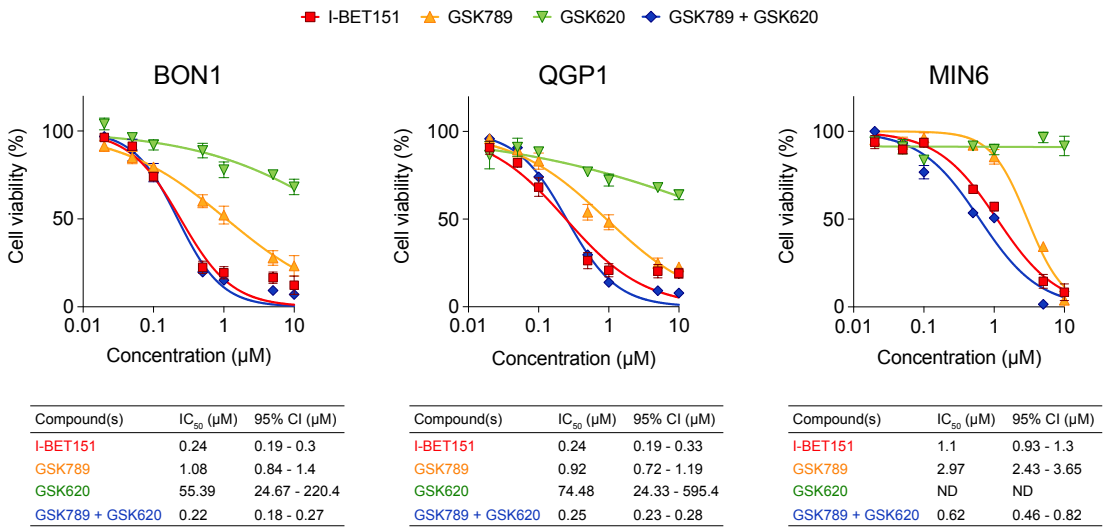

Compound(s)	IC_{50} (μM)	95% CI (μM)
I-BET151	0.24	0.19 - 0.3
GSK789	1.08	0.84 - 1.4
GSK620	55.39	24.67 - 220.4
GSK789 + GSK620	0.22	0.18 - 0.27

Compound(s)	IC_{50} (μM)	95% CI (μM)
I-BET151	0.24	0.19 - 0.33
GSK789	0.92	0.72 - 1.19
GSK620	74.48	24.33 - 595.4
GSK789 + GSK620	0.25	0.23 - 0.28

Compound(s)	IC_{50} (μM)	95% CI (μM)
I-BET151	1.1	0.93 - 1.3
GSK789	2.97	2.43 - 3.65
GSK620	ND	ND
GSK789 + GSK620	0.62	0.46 - 0.82

Figure 5.5. Combined BD1 and BD2 inhibition by GSK789 and GSK620 demonstrates superior efficacy in reducing PNET cell viability compared to either compound alone. Dose-response curves of PNET cell lines treated for 96 hours with increasing concentrations (0.02 μM - 10 μM) of I-BET151, GSK789, GSK620 and a 50:50 mixture of GSK789/GSK620. Cell viability percentage is depicted relative to DMSO control. Data points and error bars represent mean ± SEM from at least n = 3 independent experiments. The accompanying tables provide the calculated IC_{50} values for each compound along with their 95% confidence intervals (CI). ND, not determinable.

In order to confirm that the observed impact of the tested compounds on cell viability was attributable to BET protein inhibition rather than off-target effects or peculiarities inherent to the cell lines, control experiments with inactive enantiomers were performed. These enantiomers possess the same molecular structure as their active counterparts but have a mirrored spatial arrangement, which eliminates or significantly reduces their ability to bind to and inhibit BET proteins effectively. Because a negative control stereoisomer of I-BET151 has not been developed, the inactive enantiomer of JQ1, JQ1(-),[149] was employed as a

surrogate control. GSK620 lacks an enantiomer to serve as a control, while GSK789 is complemented by a corresponding inactive enantiomer known as GSK791.[286] Treatment of all three PNET cell lines with JQ1(-) and GSK791 at concentrations up to 1 μM did not affect viability **(Figure 5.6)**. At concentrations higher than this, however, a dose-dependent reduction in viability was observed, suggesting off-target engagement or non-specific toxicity arising from factors such as the chemical scaffold of the compounds used.

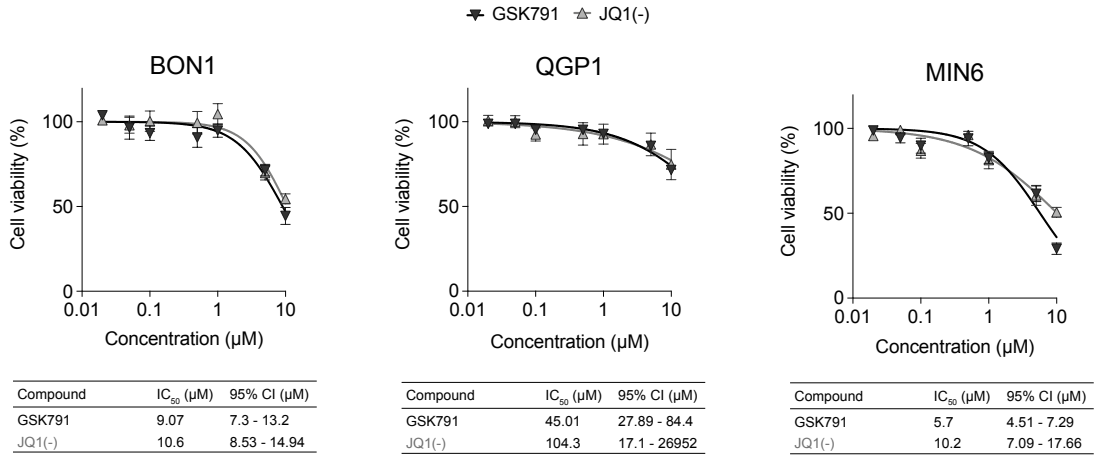

Compound	IC_{50} (μM)	95% CI (μM)
GSK791	9.07	7.3 - 13.2
JQ1(-)	10.6	8.53 - 14.94

Compound	IC_{50} (μM)	95% CI (μM)
GSK791	45.01	27.89 - 84.4
JQ1(-)	104.3	17.1 - 26952

Compound	IC_{50} (μM)	95% CI (μM)
GSK791	5.7	4.51 - 7.29
JQ1(-)	10.2	7.09 - 17.66

Figure 5.6. PNET cell viability is unaffected by negative enantiomer BET inhibitor compounds at concentrations below 1 μM. Dose-response curves of PNET cell lines treated for 96 hours with increasing concentrations (0.02 μM - 10 μM) of GSK791 or JQ1(-). Cell viability percentage is depicted relative to DMSO control. Data points and error bars represent mean ± SEM from at least n = 3 independent experiments.

In another set of control experiments, cells were treated with a fixed concentration (0.5 μM) of GSK620 along with increasing concentrations (0.02 μM - 1 μM) of either GSK789 or GSK791. This showed that the addition of GSK789 to GSK620, which constitutes combined BD1 and BD2 inhibition, resulted in a dose-dependent reduction in cell viability compared to cells treated with GSK620 alone. Conversely, the addition of GSK791 to GSK620, which effectively represents BD2 inhibition alone, had no discernible effect on viability **(Figure 5.7)**.

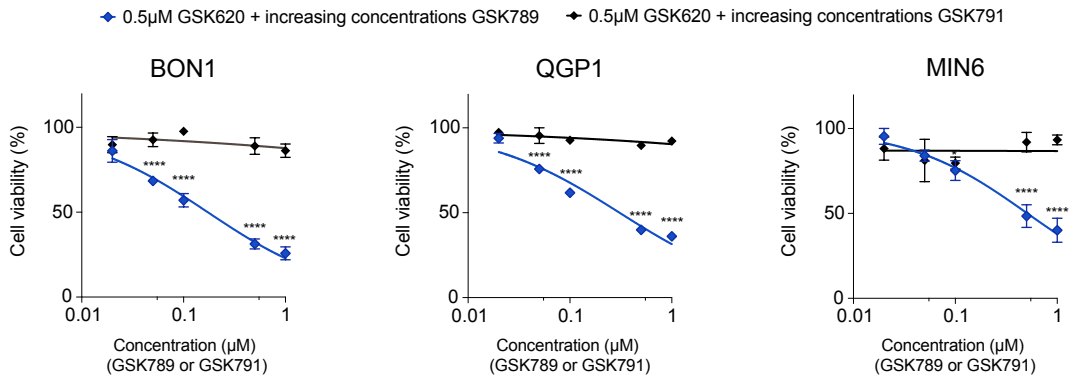

Figure 5.7. The addition of a negative enantiomer BD1 inhibitor (GSK791) to GSK620 does not affect PNET cell viability. Dose-response curves of PNET cell lines treated with 0.5 μM of GSK620 and increasing concentrations of either GSK789 or GSK791 for 96 hours. Data are normalised to cells treated with 0.5 μM of GSK620 alone. Data points and error bars represent the mean ± SEM of at least three independent experiments. Statistical significance was determined using two-way ANOVA with Dunnett's multiple comparisons test, comparing each concentration to the 0.5 μM GSK620 baseline. *p ≤ 0.05, ****p ≤ 0.0001

To further validate the enhanced efficacy observed when targeting BD1 and BD2 simultaneously in PNET cells, I used two additional BD-selective inhibitors that have recently been disclosed by GSK: GSK778, a BD1-selective inhibitor with >130-fold selectivity over BD2[158] and GSK046, a BD2-selective inhibitor with 1,000-fold selectivity over BD1.[287] These compounds were evaluated for their individual impact on cell viability, as well as in combination with each other and with the previously assessed BD-selective inhibitors, GSK789 and GSK620. My experiments confirmed that the effects of targeting BD1 and BD2 individually were consistent across the various compounds and cell lines tested, with combined inhibition yielding the greatest decrease in cell viability. Overall, BON1 and QGP1 cells exhibited a similar sensitivity to combination therapy, with sub-micromolar IC_{50} values ranging from 0.22–0.31 μM and 0.11–0.34 μM, respectively. In contrast, MIN6 cells were the least responsive to combined BD1 and BD2 inhibition, with IC_{50} values of 0.62–1.22 μM **(Figure 5.8)**.

The significant reduction in PNET cell viability observed when GSK789 and GSK620 were used in combination prompted an analysis to determine whether

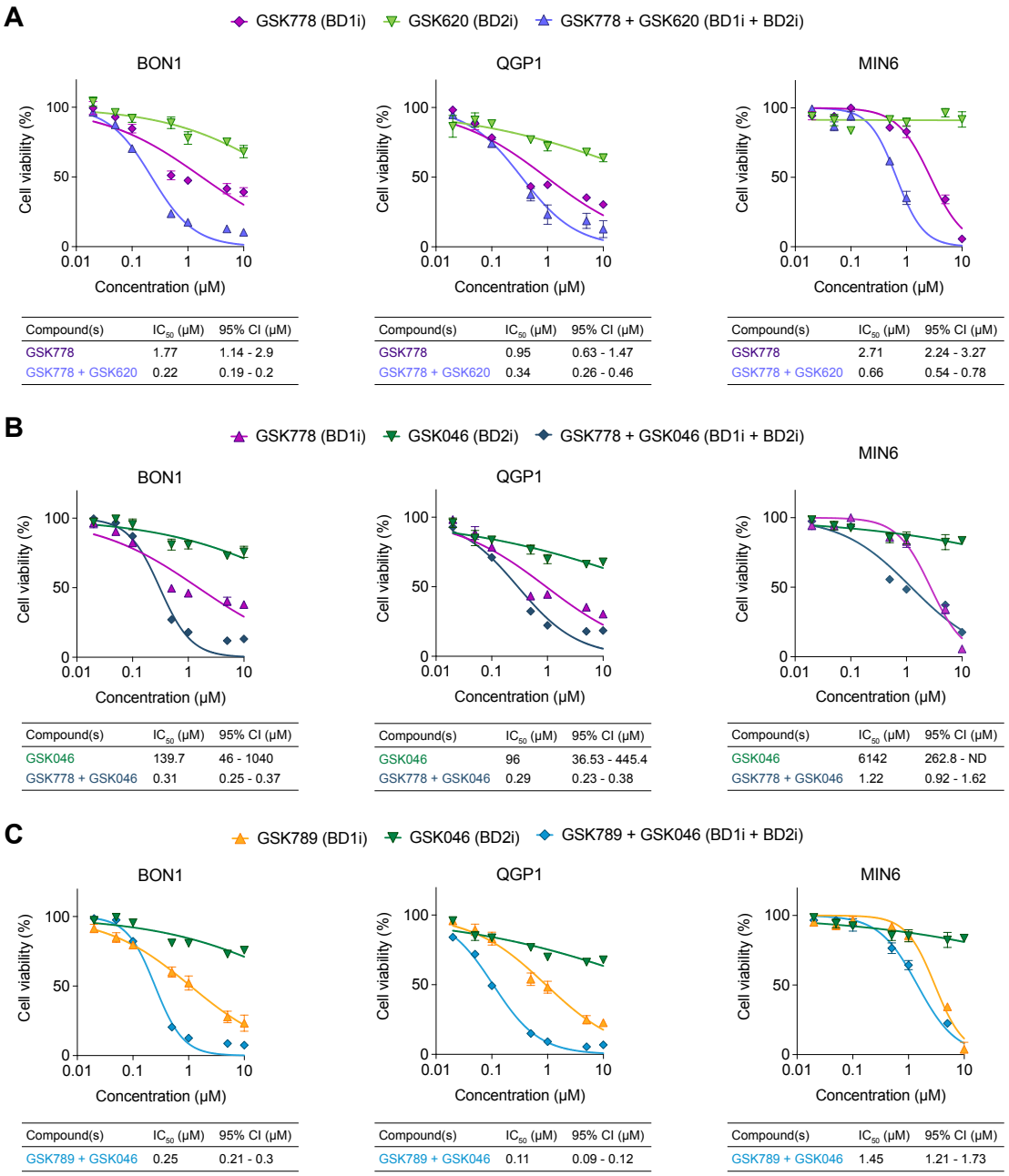

Compound(s)	IC_{50} (μM)	95% CI (μM)
GSK778	1.77	1.14 - 2.9
GSK778 + GSK620	0.22	0.19 - 0.2

Compound(s)	IC_{50} (μM)	95% CI (μM)
GSK778	0.95	0.63 - 1.47
GSK778 + GSK620	0.34	0.26 - 0.46

Compound(s)	IC_{50} (μM)	95% CI (μM)
GSK778	2.71	2.24 - 3.27
GSK778 + GSK620	0.66	0.54 - 0.78

Compound(s)	IC_{50} (μM)	95% CI (μM)
GSK046	139.7	46 - 1040
GSK778 + GSK046	0.31	0.25 - 0.37

Compound(s)	IC_{50} (μM)	95% CI (μM)
GSK046	96	36.53 - 445.4
GSK778 + GSK046	0.29	0.23 - 0.38

Compound(s)	IC_{50} (μM)	95% CI (μM)
GSK046	6142	262.8 - ND
GSK778 + GSK046	1.22	0.92 - 1.62

Compound(s)	IC_{50} (μM)	95% CI (μM)
GSK789 + GSK046	0.25	0.21 - 0.3

Compound(s)	IC_{50} (μM)	95% CI (μM)
GSK789 + GSK046	0.11	0.09 - 0.12

Compound(s)	IC_{50} (μM)	95% CI (μM)
GSK789 + GSK046	1.45	1.21 - 1.73

Figure 5.8. Combined BD1 and BD2 inhibition demonstrates consistent efficacy across different inhibitors in PNET cell lines. Dose-response curves of PNET cell lines treated for 96 hours with increasing concentrations (0.02 μM - 10 μM) of BET inhibitors (individually or in a 50:50 mixture): **(A)** GSK778 (BD1i) and GSK620 (BD2i); **(B)** GSK778 (BD1i) and GSK046 (BD2i); **(C)** GSK789 (BD1i) and GSK046 (BD2i). Cell viability percentage is depicted relative to DMSO control. Data points and error bars represent mean ± SEM from at least n = 3 independent experiments. The accompanying tables provide the calculated IC_{50} values for each compound along with their 95% confidence intervals (CI). BD1i, BD1 inhibitor; BD2i, BD2 inhibitor; ND, not determinable.

their interaction was additive or synergistic. Additivity refers to a situation where the overall effect of a drug combination equals the sum of the pharmacological effects of each agent, with consideration given to their potency and efficacy.[288] In contrast, synergy occurs when the combined effect of the compounds exceeds the expected additive effect.[168] Inhibition data from the treatment of three PNET cell lines with serial dilutions of GSK789 and GSK620 **(Figure 5.9A)** were analysed using the Bliss independence model,[168] a commonly used statistical model to evaluate drug combination efficacy that assumes a stochastic process in which two drugs exert their effects independently. The average Bliss score in each cell line exceeded 10, a value which indicates a synergistic interaction according to the Bliss independence model **(Figure 5.9B)**.[167]

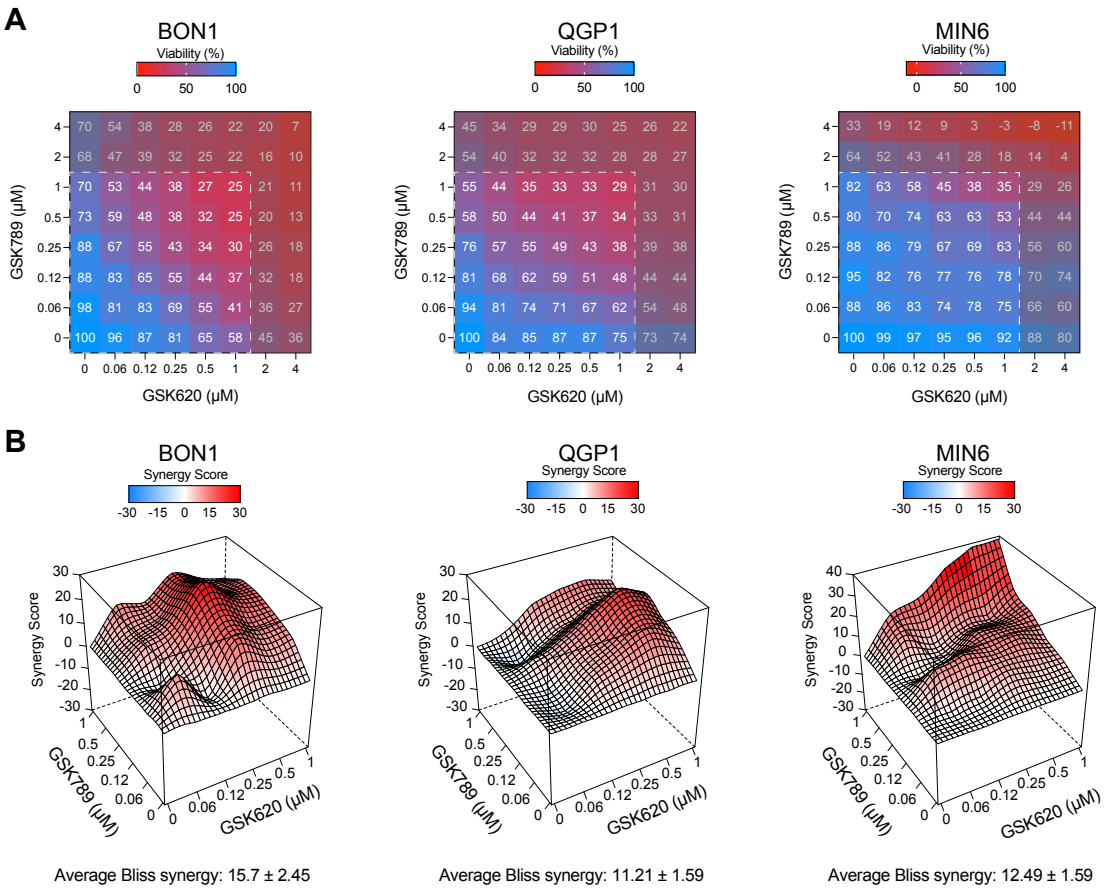

Figure 5.9. The combination of GSK789 and GSK620 synergistically inhibits viability in PNET cell lines. [Caption continues on next page...]

Figure 5.9. The combination of GSK789 and GSK620 synergistically inhibits viability in PNET cell lines. (A) GSK789 and GSK620 were combined in 8 × 8 matrices, with concentrations of each compound serially diluted along the Y and X axes, respectively. Numbers in each cell of the matrix correspond to the mean percentage of cell viability (calculated from four independent experiments) in BON1, QGP1 and MIN6 cells after 96 hours of treatment compared to DMSO. Grey-shaded cells indicate concentrations above 1 μM, where off-target effects were observed in control experiments (Figure 5.6), and thus were excluded from Bliss synergy score calculations. **(B)** Three-dimensional synergy maps of Bliss scores (averaged from four independent experiments) plotted against concentrations of GSK789 and GSK620 (0–1 μM). Areas in red, white and blue indicate regions of synergy, additivity and antagonism, respectively. The overall Bliss synergy score is the mean for the entire matrix, with scores < -10 indicating an antagonism, -10 to 10 indicating additivity and > 10 indicating synergy.[167]

5.2.4 Simultaneous BD1 and BD2 inhibition increases apoptosis in PNET cell lines

Given the observed reduction in cell viability, I hypothesised that combined inhibition of BD1 and BD2 would also enhance apoptotic pathways in PNET cell lines. To investigate this, caspase 3/7 activity, a hallmark of apoptosis, was measured after 48 hours of treatment with BET inhibitors **(Figure 5.10)**. These experiments revealed that GSK789 individually did not significantly alter apoptosis levels at doses of 0.5 μM and 1 μM. However, a higher non-selective concentration (10 μM) led to a significant increase in apoptosis by ~2.1, ~1.6, and ~4.1-fold in BON1 ($p \leq 0.0001$), QGP1 ($p = 0.002$) and MIN6 ($p \leq 0.0001$) cells, respectively. GSK620, when administered individually, did not affect apoptosis at any tested concentration in all cell lines. In contrast, the combination of GSK789 and GSK620 (in a 50:50 mixture) significantly increased apoptosis in all cell lines at all concentrations tested, including the low BD-selective concentration of 0.25 μM per compound, which increased apoptosis by μ~1.7-fold in BON1 ($p \leq 0.0001$) and QGP1 ($p = 0.0002$), and ~2.6-fold in MIN6 ($p \leq 0.01$) cells. A similar dose-dependent increase in apoptosis was observed with I-BET151 across all three cell lines **(Figure 5.10)**. These findings demonstrate that simultaneous targeting of both BD1 and BD2 is critical for the activation of apoptosis in PNET cell lines, supporting the notion that

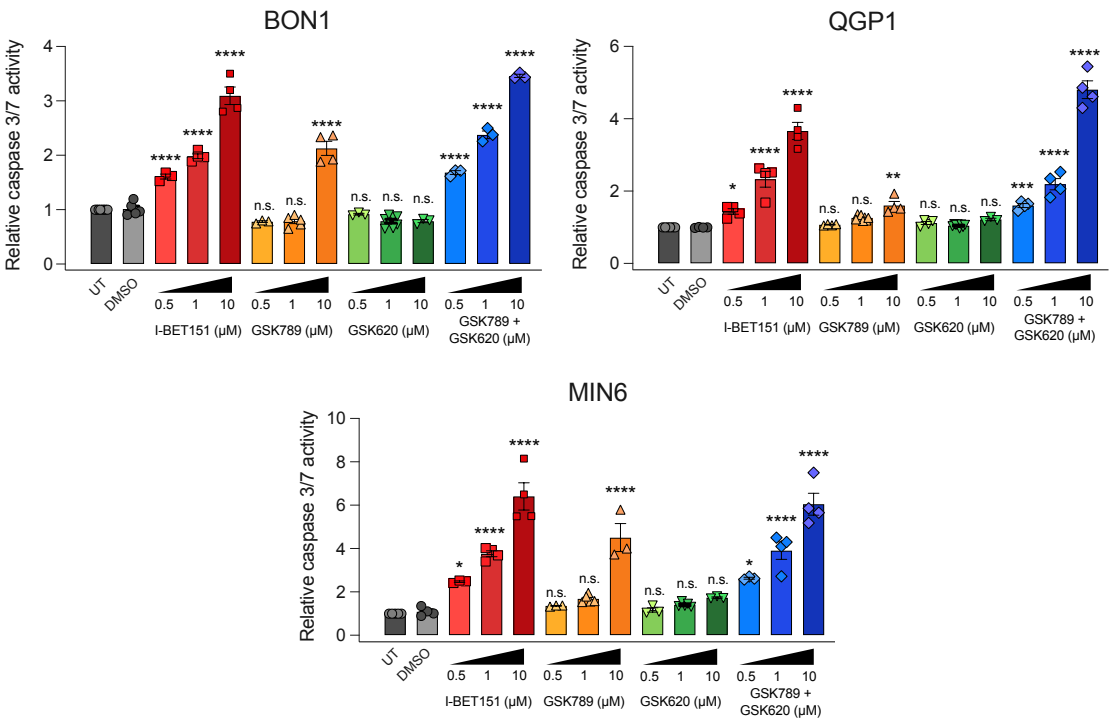

Figure 5.10. Inhibition of both BDs is required for induction of apoptosis in PNET cell lines. Bar plots showing caspase 3/7 activity (relative to untreated cells) in BON1, QGP1 and MIN6 PNET cell lines following 48 hours of treatment with the indicated BET inhibitors. Data points and error bars represent mean ± SEM from n = 4-6 independent experiments. Statistical significance relative to DMSO vehicle was assessed using ordinary one-way ANOVA with Dunnett's test for multiple comparisons. n.s., not significant, *p ≤ 0.05, **p ≤ 0.01, *** p ≤ 0.001, ****p ≤ 0.0001; UT, untreated.

dual BD inhibition may represent a more effective therapeutic strategy compared to targeting each BD individually.

5.2.5 Simultaneous BD1 and BD2 inhibition alters PNET cellular morphology and decreases viability in a time-dependent manner

To gain further insights into the phenotypic effects of single- and dual-BD inhibition in PNET cell lines, light microscopy was used to evaluate changes in morphology. Images were captured at 24 hour intervals over a course of 96 hours after treatment with a single dose of 1 μM of I-BET151, GSK789, GSK620 or a combined dose of 0.5 μM each of GSK789/GSK620. After 48 hours after treatment with I-BET151

and the GSK789/GSK620 combination, discernible changes in cellular morphology were visible in BON1 **(Figure 5.11A)**, QGP1 **(Figure 5.11B)** and MIN6 **(Figure 5.11C)** cells. These changes were also observed, albeit less pronounced, in cells treated solely with GSK789. Specifically, BON1 cells exhibited a flattened and elongated appearance with a spindle-like morphology, indicative of cell cycle arrest and senescence.[289] QGP1 cells, which typically grow in cohesive clumps under normal conditions, assumed a rounded shape with fewer cell-cell contacts, suggesting alterations in cellular adhesion properties. In MIN6 cells, a rounded morphology was also observed, in addition to instances of cells becoming shrunken and detached from the culture flask, indicative of apoptosis. In contrast, treatment with GSK620 alone did not lead to any changes in cellular morphology compared to untreated and DMSO vehicle-treated cells. Collectively, these findings suggest that targeting both BD1 and BD2 of the BET proteins may provide a more effective strategy for inducing phenotypic changes associated with tumour suppression in PNETs.

Concurrent time-course viability assays were performed to determine if morphological changes corresponded with reduced PNET cell viability **(Figure 5.11D)**. In BON1 cells, a time-dependent decrease in viability became significant after 72 hours of treatment with the GSK789 and GSK620 combination (by 2.3-fold *vs* DMSO control; $p = 0.003$). Similarly, a 2.1-fold decrease was seen with I-BET151 ($p = 0.004$) after 72 hours. GSK789 alone led to a significant anti-proliferative effect only after 96 hours, with a 1.8-fold reduction in viability ($p = 0.03$). In QGP1 cells, a small but significant decrease in viability was detected at 24 hours post-treatment with both the GSK789 and GSK620 combination and I-BET151, each reducing viability by 1.2-fold ($p = 0.01$). GSK789 alone also resulted in a 1.1-fold reduction in viability at this time point ($p = 0.03$). In MIN6 cells, a significant decrease in viability was only evident after 96 hours with the combination and I-BET151 treatments, with both showing a 1.5-fold decrease ($p = 0.004$–0.006), but not with GSK789 alone. GSK620 did not affect cell viability at any time point in any of the cell lines examined.

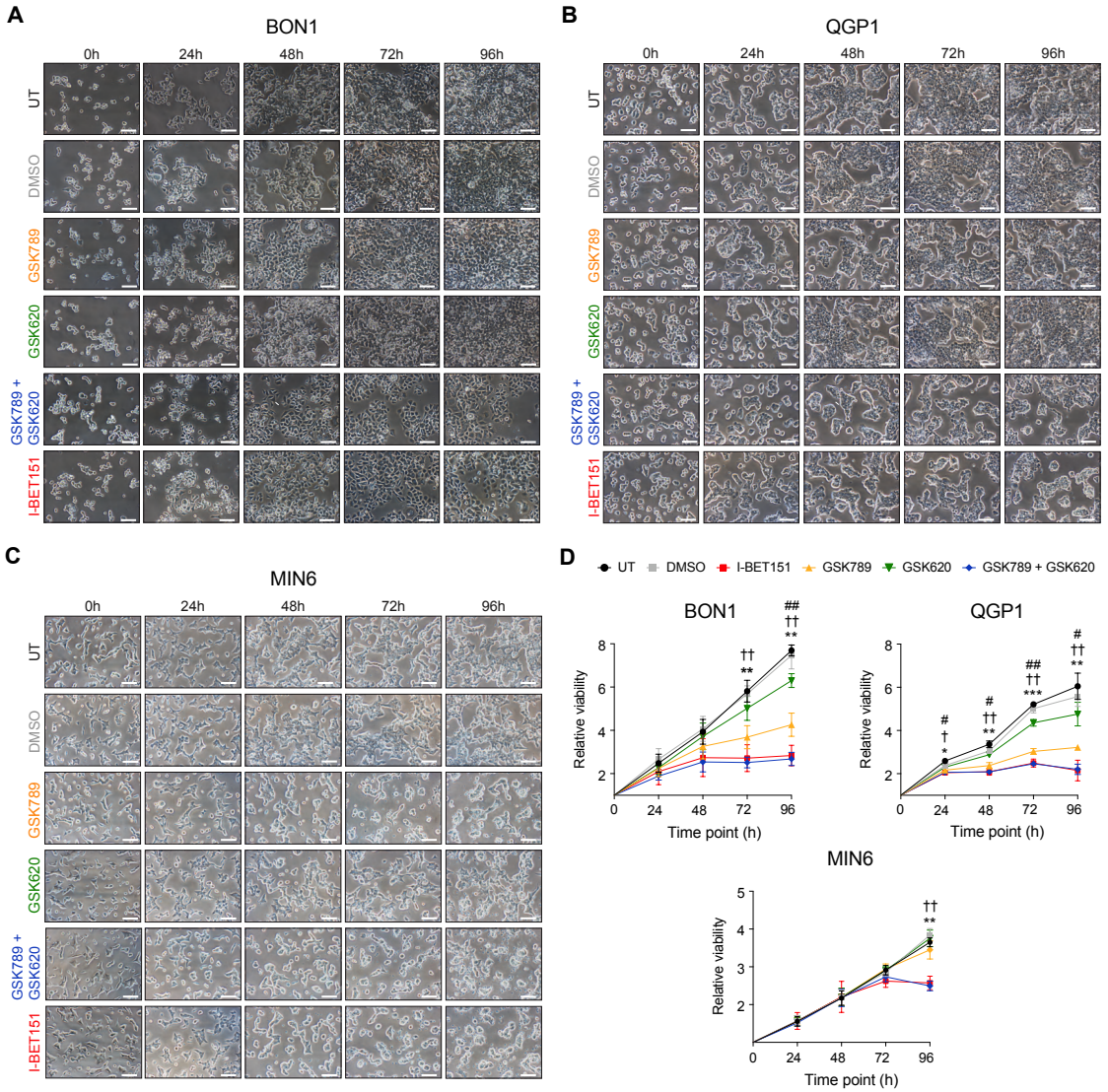

Figure 5.11. Simultaneous BD1 and BD2 inhibition alters PNET cellular morphology and decreases viability in a time-dependent manner. Light microscopy images of PNET cell lines **(A)** BON1, **(B)** QGP1, and **(C)** MIN6 captured at 0, 24, 48, 72, and 96 hours following treatment with 1 μM of I-BET151, GSK789, GSK620, or a combination of 0.5 μM each of GSK789 and GSK620. Images captured at 20x magnification with scale bars representing 100 μm. **(D)** Line graphs showing cell viability of PNET cell lines measured every 24 hours, using CellTiter-Blue® assays, during 96 hours of treatment with the indicated BET inhibitors. Values are shown relative to the 0-hour time point. Data points and error bars represent mean ± SEM from n = 4 independent experiments. Statistical significance relative to DMSO control at each time point was determined using two-way ANOVA with Dunnett's multiple comparisons test. Significance is denoted by (#) for GSK789, (†) for I-BET151 and (*) for the GSK789/GSK620 combination, with single, double and triple symbols indicating $p \leq 0.05$, $p \leq 0.01$ and $p \leq 0.001$, respectively.

5.2.6 The effects of simultaneous BD1 and BD2 inhibition on cell viability persist after compound washout

To examine the longer term effects of BET inhibition, cells were treated with 1 μM of GSK789, GSK620, I-BET151, or a combination of 0.5 μM each of GSK789 and GSK620 for 96 hours. Following treatment, the compound-containing media was washed out and replaced with regular culture media, with viability assessed every 24 hours over a five-day period. All three cell lines treated exclusively with GSK789 demonstrated recovery of proliferative capacity after the compound was eliminated, with the most rapid recovery observed in MIN6 cells (24 hours post-washout), followed by BON1 cells (48 hours post-washout) and QGP1 cells (96 hours post-washout). The viability of cells treated with GSK620 was comparable to that of DMSO vehicle-treated and untreated controls throughout the washout period. In contrast, all three cell lines treated with either the GSK789/GSK620 combination or I-BET151 exhibited a sustained reduction in viability for up to 96 hours post-compound removal **(Figure 5.12)**. Thus, simultaneous targeting of BD1 and BD2 induces a lasting alteration in PNET cell behaviour that is not observed when either BDs are targeted individually.

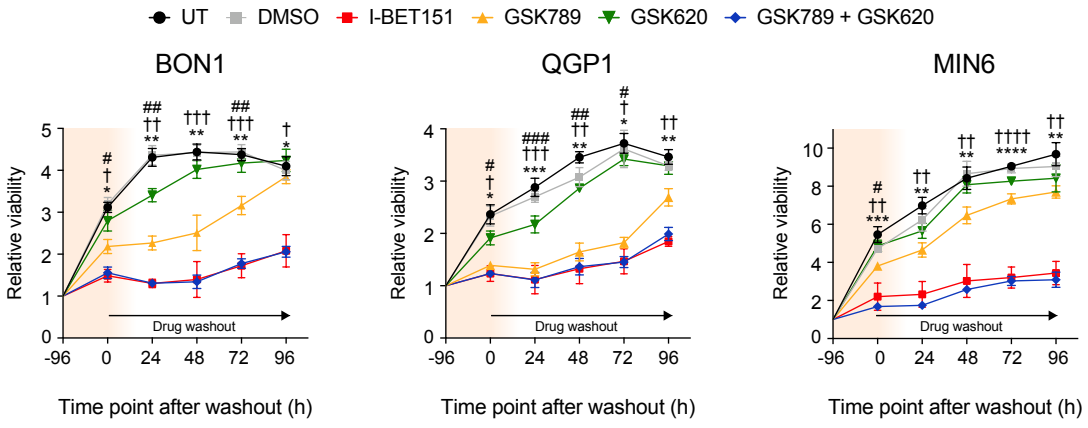

Figure 5.12. The effects of simultaneous BD1 and BD2 inhibition on cell viability persist after compound washout. Relative viability of BON1, QGP1, and MIN6 cell lines assessed over a 96-hour washout period following 96-hours of treatment with 1 μM of GSK789, GSK620, I-BET151, or a combination of 0.5 μM each of GSK789 and GSK620. [Caption continues on next page...]

Figure 5.12. The effects of simultaneous BD1 and BD2 inhibition on cell viability persist after compound washout. Viability was assessed using CellTiter-Blue® assays and values are shown relative to the 0 hour time-point. Data points and error bars represent mean ± SEM from n = 4 independent experiments. Statistical significance relative to DMSO control at each time point was determined using two-way ANOVA with Dunnett's multiple comparisons test. Significance is denoted by (#) for GSK789, (†) for I-BET151, and (*) for the GSK789/GSK620 combination, with single, double, triple and quadruple symbols indicating $p \leq 0.05$, $p \leq 0.01$, $p \leq 0.001$ and $p \leq 0.0001$, respectively.

5.2.7 Simultaneous BD1 and BD2 inhibition causes cell cycle arrest in human PNET cell lines

The findings presented in this chapter thus far suggested that cell cycle arrest could be a key consequence of BET inhibition. To directly assess this, cell cycle analyses were performed on BON1 and QGP1 cells using flow cytometry. In BON1 cells, the percentage of cells in the G_0/G_1 phase increased significantly from ~60% in DMSO vehicle-treated controls to ~86% and ~90%, respectively, following treatment with GSK789/GSK620 and I-BET151 ($p \leq 0.0001$). GSK789 and GSK620 alone also induced G0/G1 arrest to a lesser extent (to ~81% and ~69%, respectively; $p \leq 0.0001$). The percentage of cells in the S phase decreased across all treatments, from ~29% in DMSO controls, to as low as 4.4% and 3.8% with GSK789/GSK620 and I-BET151 ($p \leq 0.0001$), respectively **(Figure 5.13A)**.

For QGP1 cells, the percentage of cells in the G_0/G_1 phase increased from ~58% in DMSO controls to ~79%, ~76% and ~69% after treatment with GSK789/GSK620 ($p \leq 0.0001$), I-BET151 ($p \leq 0.0001$) and GSK789 ($p = 0.04$), respectively. The percentage of cells in the S phase decreased from ~29% in DMSO-treated cells to ~12% and ~13% in cells treated with GSK789/GSK620 and I-BET151, respectively ($p \leq 0.001$). GSK620 showed no significant effect on QGP1 cell cycle phases. G_2/M phase changes were minimal in both cell lines. Collectively, these results demonstrate that simultaneous BD1 and BD2 inhibition causes cell cycle arrest by preventing the G_1-to-S phase transition in human PNET cell lines, to a greater extent than when individual BDs are targeted alone **(Figure 5.13B)**.

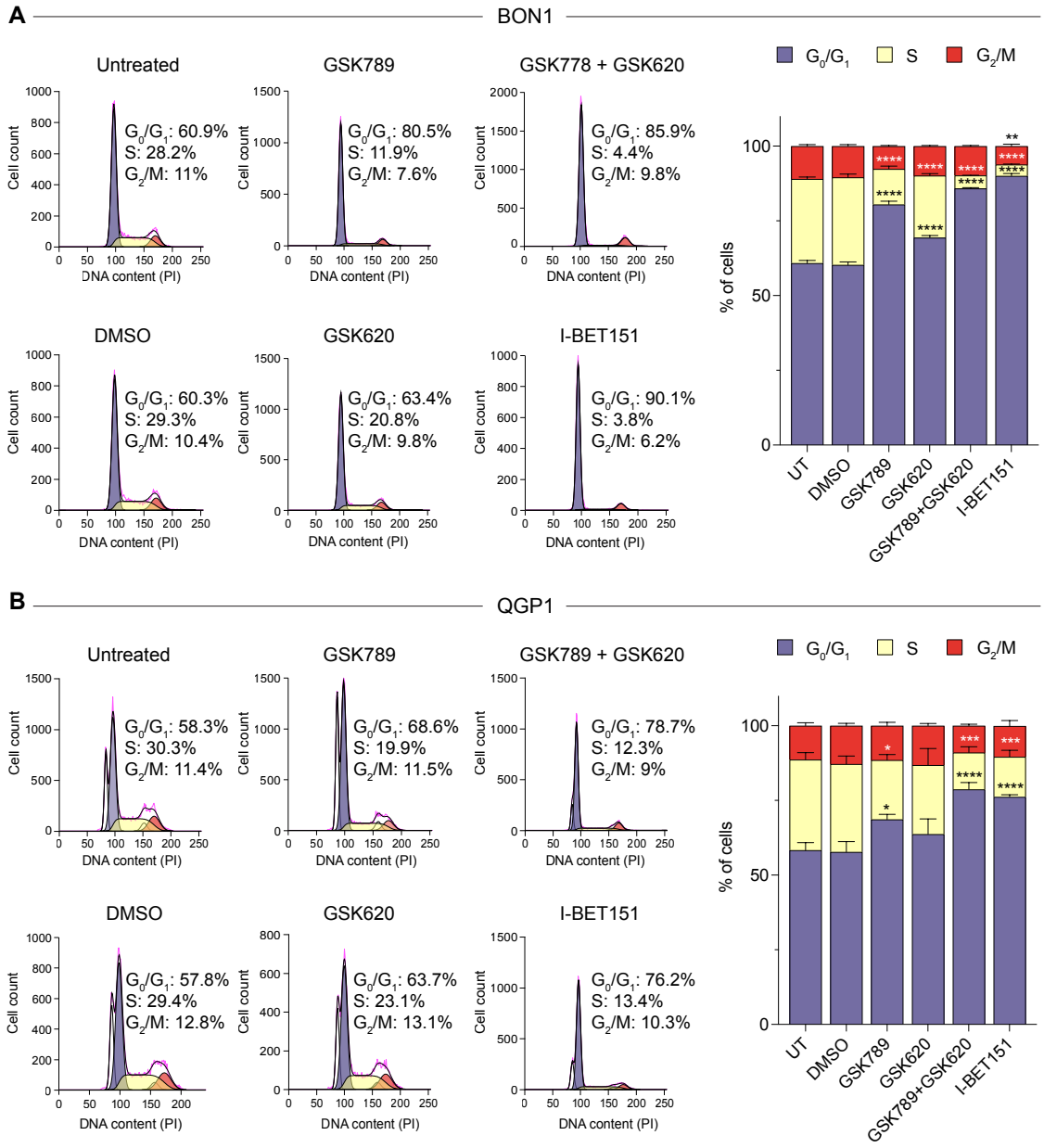

Figure 5.13. Dual BD inhibition induces cell cycle arrest by preventing G_1-to-S phase transition in human PNET cell lines. Representative cell cycle histograms of DNA content analysis via propidium iodide (PI) staining and flow cytometry in **(A)** BON1 and **(B)** QGP1 cells. Cells were treated for 48 hours with 1 µM of I-BET151, GSK789, GSK620 or a combination of GSK789/GSK620 at 0.5 µM each. Untreated and DMSO vehicle-treated cells served as negative controls. Adjacent numbers and bar graphs (right) show the mean percentage of cells in G_0/G_1, S, and G_2/M phases. Error bars represent SEM from n = 4 independent experiments Statistical significance relative to DMSO was assessed using two-way ANOVA with Tukey's multiple comparisons test. *p $\leq$ 0.05, **p $\leq$ 0.01, *** p $\leq$ 0.001, ****p $\leq$ 0.0001

5.2.8 Effects of BET inhibitors on neoplastic pancreatic islets *ex vivo*

To perform *ex vivo* drug studies on neoplastic mouse islets, *Men1*$^{L/L}$/*RIP2-Cre* mice were bred and generated as previously described,[60,197] and detailed in Section 2.5. To verify the development of PNETs, a group of these mice was humanely euthanised at 9 months of age. Their pancreata were then harvested, embedded, and sectioned for immunofluorescence analysis, staining specifically for insulin and the proliferation marker Ki-67. wild-type mice served as controls. The staining of the *Men1*$^{L/L}$/*RIP2-Cre* mouse islets exhibited enlargement and morphological abnormalities, with higher levels of Ki-67 staining compared to those in wild-type mice, confirming the presence of proliferating PNETs **(Figure 5.14A)**.

Neoplastic islets were cultured *ex vivo* and treated with 1 μM of I-BET151, GSK789, GSK620 or a combined dose of 0.5 μM each of GSK789/GSK620. These experiments showed that, after 96 hours of treatment, cell viability was reduced by < 30% with GSK620 ($p \leq 0.005$), ~40% with GSK789 ($p \leq 0.0001$), and ~60% with the combination of GSK789/GSK620 ($p \leq 0.0001$) **(Figure 5.14B)**.

5.3 Discussion

In this chapter, I explored the phenotypic effects of current and next-generation BET inhibitors on PNET cell lines, uncovering important findings regarding the differential efficacy of these compounds. The work outlined herein not only corroborates previous reports of the anti-tumour activity of first-generation BET inhibitors, such as JQ1 and I-BET151, in PNET models but also extends these insights by elucidating the differential impacts of BD1- and BD2-selective inhibition on cell viability, apoptosis, and cell cycle dynamics. Importantly, my findings highlight the synergistic potential and superior efficacy of simultaneous BD1 and BD2 inhibition over individual domain targeting in PNET cell lines.

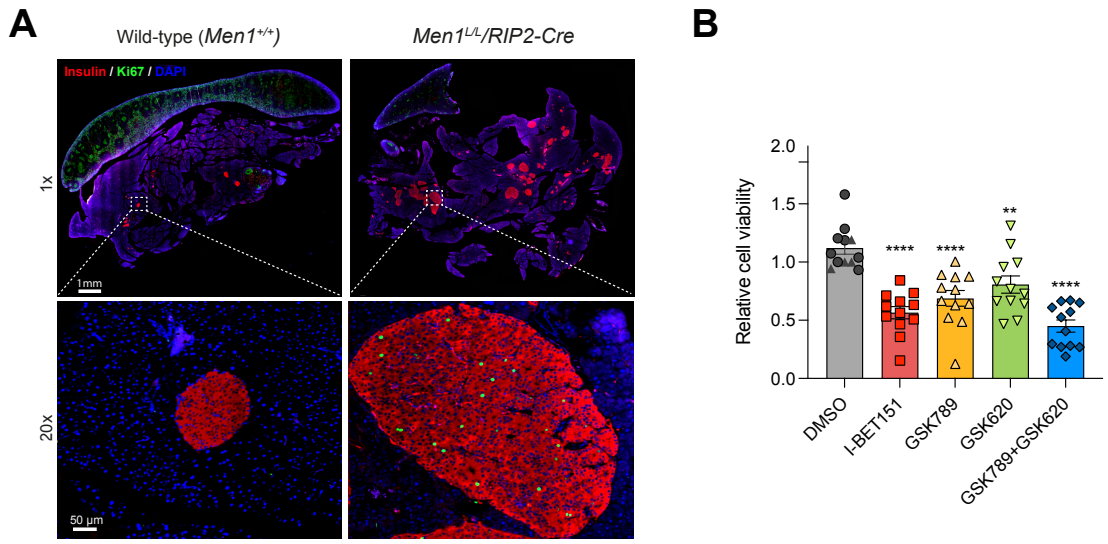

Figure 5.14. Immunofluorescence staining of islets from *Men1*$^{L/L}$*/RIP2-Cre* and wild-type mice and results of *ex vivo* drug studies. **(A)** Left panel: representative fluorescence microscopy image of a pancreatic section from a wild-type (*Men1*$^{+/+}$) mouse, stained for insulin (red), Ki-67 (green), and nuclei (DAPI, blue) at 1x magnification. The inset below shows a higher magnification (20x) view of a single islet of Langerhans, highlighting the presence of insulin-producing beta cells, with proliferative cells marked by Ki67. Right panel: Representative fluorescence microscopy image of a pancreatic section from an *Men1* knockout (*Men1*$^{L/L}$*/RIP2-Cre*) mouse, stained for insulin (red), Ki-67 (green), and nuclei (DAPI, blue) at 1x magnification. The inset shows a higher magnification (20x) view of a single islet, indicating abnormal islet architecture and increased beta-cell proliferation in the absence of functioning *Men1*. Scale bars in the upper and lower panels represent 1 mm and 50 µm, respectively. **(B)** CellTiter-Blue® cell viability assays of *ex vivo* cultures neoplastic islets treated with BET inhibitor compounds for 96 hours. Statistical significance relative to DMSO vehicle was assessed using ordinary one-way ANOVA with Dunnett's test for multiple comparisons. n.s., not significant, *p $\leq$ 0.05, **p $\leq$ 0.01, *** p $\leq$ 0.001, ****p $\leq$ 0.0001

5.3.1 First-generation BET inhibitors are effective in PNET cell lines

Consistent with the findings reported in this chapter, three published studies to date have reported anti-tumour effects of first-generation BET inhibitors in pre-clinical PNET models.[60,148,290] In a study published by the Thakker group, treatment with JQ1 was shown to significantly decrease proliferation and increase apoptosis in the BON1 cell line.[60] Similar effects were also observed *in vivo* in PNET-bearing *Men1*$^{L/L}$*/RIP2-Cre* mice. However, this study only utilised one PNET cell line. Furthermore, the poor bioavailability and short half-life of JQ1 preclude this

compound from clinical translation. Chemical modifications to JQ1 (specifically, the liberation of its carboxylic acid group followed by the synthesis of a primary amide bond) gave rise to CPI203 (also known as RO6870810, TEN-010 or JQ2), a derivative BET inhibitor with significantly enhanced oral bioavailability and pharmacokinetic properties.[291] Wong et al.[148] evaluated the effects of CPI203 on BON1 and QGP1 cells, as well as in BON1 xenografts, observing a significant decrease in proliferation *in vitro* and *in vivo*, and synergistic efficacy when administered with the mTOR inhibitor rapamycin. Despite the compound's promising pharmacokinetic attributes leading to its evaluation in phase I umbrella trials, further development has since been halted due to suboptimal efficacy rates, particularly in solid organ cancers.[292,293]

I-BET151, an alternative first-generation BET inhibitor developed by GSK,[245] not only demonstrates superior pharmacokinetic properties compared to JQ1 but also features a distinct chemical structure, with an isoxazole-based scaffold as opposed to JQ1's thieno-triazolo-1,4-diazepine scaffold.[150] Although the use of I-BET151 in PNETs *in vitro* has previously been described, this study was limited in scope as only one cell line (BON1) was used.[290] Furthermore, an assessment of I-BET151's effects on other cellular phenotypes such as apoptosis, morphology and cell cycle progression was not performed. Thus, the findings of this chapter contribute additional insights into the effects of I-BET151 across a broader spectrum of PNET cell lines and set the stage for further in-depth mechanistic studies in the next chapter.

5.3.2 MIN6 cells are relatively resistant to the effects of BET inhibition

The response patterns to current and next-generation BET inhibitors were consistent across the three evaluated PNET cell lines in this chapter. However, MIN6 cells exhibited the highest IC_{50} values (0.62–1.45 μM), even with combined BD1 and BD2 inhibition, indicating relative resistance compared to BON1 and QGP1 cells. This resistance may be attributed to the unique origin of MIN6 cells, which were derived from an insulinoma in a transgenic mouse line which expresses the Simian virus 40

(SV40) large tumour antigen (TAg) under control of the insulin promoter.[162] SV40 TAg causes oncogenic transformation through inactivation of two well-known tumour suppressors, p53 and the retinoblastoma protein (RB), resulting in uncontrolled cell cycle progression.[294] Interestingly, a recent study has shown that RB acts as an intrinsic inhibitor of BRD4, via binding to its BD1 domain and limiting its interactions with chromatin.[295] Moreover, RB-knockdown cell lines were found to be more resistant to the effects of BET inhibitors.[295] Given the role of SV40 Tag in inhibiting RB activity, it could be postulated that MIN6 cells are more resistant to the effects of BET inhibition due to constitutively active BET protein activity. In contrast, BON1 and QGP1 cells were derived from with sporadic PNETs in humans.[161,235] Whole exome sequencing studies have mapped out the genetic composition of these cell lines, revealing a lack of oncogenic driver mutations or specific alterations in BET protein genes, factors that might influence their sensitivity to BET inhibition.[164,165,296]

5.3.3 BD1- and BD2-selective BET inhibitors have differential effects in PNET cell lines

One of the key findings of this chapter is the distinct impact of BD1- and BD2-selective inhibition on PNET cell lines, highlighting the nuanced role that these domains may play in modulating the cellular response to BET inhibition. My experiments revealed that BD1-selective inhibition led to a moderate reduction in cell viability, whereas BD2-selective inhibition had minimal impact. Most notably, combined BD1- and BD2-selective inhibition not only markedly reduced cell viability in a synergistic fashion, but also significantly increased caspase-mediated apoptosis and cell cycle arrest. Thus, while the role of BD2 appears to be less critical in the context of PNETs, BD1 emerges as a key player whose inhibition alone can moderate tumour cell behaviour. Yet, it is the concurrent targeting of both domains that fully unlocks the therapeutic potential of BET inhibition in this context. These findings challenge recent, sometimes contradicting, assertions that

selectively targeting either BD1 or BD2 could yield equivalent therapeutic outcomes as dual-BD inhibition across various cancer types. For instance, it was reported by Gilan et al.[152] that BD1-selective inhibition with GSK778 phenocopied the effects of I-BET151 in reducing proliferation, inducing cell cycle arrest and upregulating apoptosis in different human cancer cell lines. However, the generalisability of these findings to all cancer types may be limited, as four of the six cell lines used in their study were myeloid leukaemia cell lines, with the remaining two being breast cancer cell lines. Moreover, closer examination of the data indicates that the effect of GSK778 on these breast cancer cell lines was not as pronounced as that of I-BET151, nor did it match the effects observed in the leukaemia cell lines.[152] These observations, combined with the findings presented in this chapter, suggest that the therapeutic efficacy of BD1-selective inhibitors may differ significantly between haematological malignancies and solid tumours.

Recent studies have also proposed that targeting BD2 alone may be sufficient to elicit anti-proliferative effects in certain cancer-related contexts. For example, the BD2-selective inhibitor ABBV-744 has been shown to be effective in reducing proliferation in a subset of acute myeloid leukaemia (AML) cell lines and in the LNCaP prostate cancer cell line with IC_{50} values in the low nanomolar range.[153,297] In contrast, my experiments with the BD2-selective inhibitor GSK620 in LNCaP cells revealed limited efficacy. Gilan et al.[152] similarly observed limited effects of GSK620 in AML cell lines, while the efficacy profile of ABBV-744 was closer to that of I-BET151. To resolve this discrepancy, the authors performed a series of mechanistic studies in which AML cells were genetically modified to carry BD2 mutations involving critical amino acid residues known to interact with ABBV-744. Despite these mutations, the anti-proliferative effects of ABBV-744 remained unchanged, indicating that the compound's anti-cancer effects may largely be mediated through inhibition of BD1, not BD2 as previously thought. Another recent study reported that ABBV-744 was efficacious in gastric cancer models;[298] however, the high concentrations used (2-5 μM) are known to be associated with non-selective BD engagement, reinforcing the view that ABBV-744's anti-tumour

effects cannot solely be attributed to BD2 inhibition. These studies highlight the need for cautious evaluation of BD-selective compound concentrations to ensure that domain-selectivity is maintained at the concentrations tested.

Another key finding of this chapter is the synergistic impact of combining GSK789 and GSK620 on reducing PNET cell viability, as demonstrated by Bliss synergy scores. This synergy may play an important role in mitigating the dose-related toxicities commonly associated with BET inhibitors in clinical settings. Notably, the combination of 0.5 μM each of GSK789 and GSK620 achieved a reduction in cell viability comparable to that observed with 1 μM of I-BET151. This suggests that employing lower doses of BD-selective compounds in tandem could offer a toxicity profile that is more favourable, while preserving the same therapeutic efficacy as dual BD inhibitors. For instance, while I-BET151 was efficacious at 1 μM, binding affinity data (see **Figure 5.2**) suggest that this compound may also engage non-BET BDs, specifically those of CREB-binding protein (CREBBP) and E1A binding protein p300 (EP300), at this concentration, unlike GSK789 or GSK620. This promising strategy warrants further investigation to optimise dosage regimens and to understand the mechanistic basis of the observed synergistic effects.

In conclusion, this chapter has explored the efficacy of a number of current and next-generation BET inhibitors in PNET cell lines, revealing that simultaneous targeting of BD1 and BD2 offers a superior therapeutic strategy than single-domain inhibition alone. This synergistic effect suggests a promising route for enhancing treatment effectiveness and expanding the therapeutic window for PNETs. The insights gained from this chapter pave the way for further investigation into the molecular mechanisms underpinning BET inhibitor efficacy.

6

Characterisation of transcriptomic and epigenomic responses to BET inhibition *in vitro*

Chapter-specific table of contents

6.1 Aims **164**
6.2 Results **165**
6.2.1 Simultaneous BD1 and BD2 inhibition induces more extensive gene expression changes than targeting either domain individually 165
6.2.2 Simultaneous BD1 and BD2 inhibition downregulates a broad range of Hallmark pathways, including those implicated in metastatic PNETs 168
6.2.3 Simultaneous BD1 and BD2 inhibition disrupts RNA and protein synthesis machinery while BD1-selective inhibition predominantly affects cell cycle pathways . 170
6.2.4 The upstream regulator CKAP2L is inhibited by BD1-selective and combined BD1/BD2 inhibition . . 172
6.2.5 I-BET151 has a broader impact on modulating downstream gene expression than combined treatment with GSK789 and GSK620. 175
6.2.6 SLAM-seq identifies direct transcriptional targets of BD-selective and non-selective inhibition 177
6.2.7 I-BET151 and GSK789/GSK620 have distinct and overlapping effects on the nascent transcriptome . . . 182
6.2.8 Integrated analysis of SLAM-seq and RNA-seq identifies *E2F2* and *CKAP2L* as early and late targets, respectively, of dual BD inhibition 184

6.2.9 ChIP-seq reveals alterations in genome-wide H3K27ac enrichment after BET inhibition 187
6.2.10 Regions of H3K27ac loss following BET inhibition coincide with genome-wide BET protein binding sites 193
6.2.11 BET inhibitors regulate the expression of PNET-relevant genes by reducing H3K27ac occupancy at super-enhancers 193
6.2.12 Integrated ChIP-seq and transcriptomic analyses identify BET inhibitor candidates with clinical relevance in PNETs 201
6.3 Discussion **206**
6.3.1 The rationale for domain-selective BET inhibitors . . 207
6.3.2 BD1-selective, BD2-selective and dual BD inhibition are each associated with distinct transcriptional changes in BON1 cells 208
6.3.3 Differences in transcriptomic response between I-BET151 and combination GSK789/GSK620 treatment 210
6.3.4 *CKAP2L* and *E2F2* are clinically-relevant BET inhibitor targets in patients with PNETs 212

6.1 Aims

In the previous chapter, I investigated the phenotypic effects of both current- and next-generation BET inhibitors on human and murine PNET cell lines, focusing on changes in cell viability, morphology, apoptosis and cell cycle dynamics. These experiments revealed variations in efficacy between targeting BD1 or BD2 individually versus simultaneous targeting of both domains.

First-generation BET inhibitors, such as I-BET151 and JQ1, show near equal affinity for both bromodomains located at the N-terminus of each BET protein. As discussed previously, however, their non-selective nature has led to toxicities that limit dose-escalation to the extent required to achieve efficacy in early-phase clinical trials.[151,299] Given the broad role of BET proteins in regulating tissue-specific gene expression, the emergence of such pleiotropic effects is not entirely unexpected. Consequently, there has been a concerted effort within the field of BET inhibitor

development to design compounds with greater selectivity and fewer adverse effects, without compromising efficacy.[281,300,301]

A high degree of sequence conservation (> 75%) exists between BD1 and BD2 across the BET protein family, which has complicated the development of inhibitors specific to a single BET protein.[301] However, there is far less homology (< 40%) between BD1 and BD2 within the same protein, which offers avenues for the development of domain-specific ligands.[301] Emerging evidence suggests that BD1 is primarily responsible for attaching BET proteins to chromatin, and thus plays a key role in the maintenance of established tissue-specific gene expression programs.[152,154,155,302] In contrast, BD2 seems to interact with acetylated non-histone proteins, such as transcription factors, enhancing gene expression in response to external stimuli, such as inflammation.[141,152,303–306] Nonetheless, the mechanistic consequences of dual BD inhibition in PNETs are not well understood and selective inhibitors for BD1- and BD2 have yet to be studied in this setting.

It has been argued that a reason for the lacklustre success of first-generation BET inhibitors in early-phase trials has been the rapid translation of these compounds into the clinic without a robust understanding of their mechanism of action.[151,299] Thus, the aims of this chapter are to mechanistically investigate the effects of I-BET151 as well as novel BD1- and BD2-selective BET inhibitors in PNETs by characterising the transcriptomic and epigenomic alternations induced by these compounds *in vitro*.

6.2 Results

6.2.1 Simultaneous BD1 and BD2 inhibition induces more extensive gene expression changes than targeting either domain individually

To understand the effects of current and next-generation BET inhibitors on PNET cell transcriptional programs, RNA sequencing (RNA-seq) was performed in BON1 cells after 48 hours of exposure to 1 μM of GSK789, GSK620, I-BET151

or a combination of 0.5 μM each of GSK789 and GSK620. As discussed previously, The BON1 cell line was specifically chosen for mechanistic experiments because it originates from a NF-PNET, which reflects the most common PNET subtype encountered in clinical practice.[235] Hierarchical clustering of RNA-seq data demonstrated that cells treated with the combination of GSK789/GSK620 and I-BET151 clustered closely together, indicating similar transcriptional responses to these treatments. Conversely, the GSK620 samples clustered near the vehicle samples, indicating minimal impact on gene expression. The GSK789 group also clustered closer to the DMSO and GSK620 samples, reinforcing observations from the preceding chapter that BD1 inhibition alone in PNET cells does not phenocopy the effects seen with dual-BD targeting **(Figure 6.1A)**.

Principal component analysis (PCA) further supported these findings by quantitatively summarising the gene expression variations across treatments. The first principal component (PC1) captured 78% of the variance, suggesting that the predominant factor distinguishing the samples was the type of BET inhibitor treatment applied **(Figure 6.1B)**.

Differential expression analysis was performed to identify genes that were significantly upregulated or downregulated (absolute $\log_2$FC ≥ 1 and false discovery rate (FDR)-adjusted p-value ≤ 0.05) in response to BET inhibitor treatment. This revealed that GSK620 affected the expression of only a small number of genes (n = 33 downregulated and n = 18 upregulated) when administered alone. GSK789 treatment led to a greater number of differentially expressed genes (n = 196 downregulated and n = 158 upregulated). A more profound effect was seen, however, with the combined GSK789/GSK620 treatment, which resulted in 987 upregulated and 752 upregulated genes. Interestingly, I-BET151 treatment induced the most substantial change, with the upregulation of 1,543 genes and downregulation of 1,173 genes **(Figure 6.1C)**.

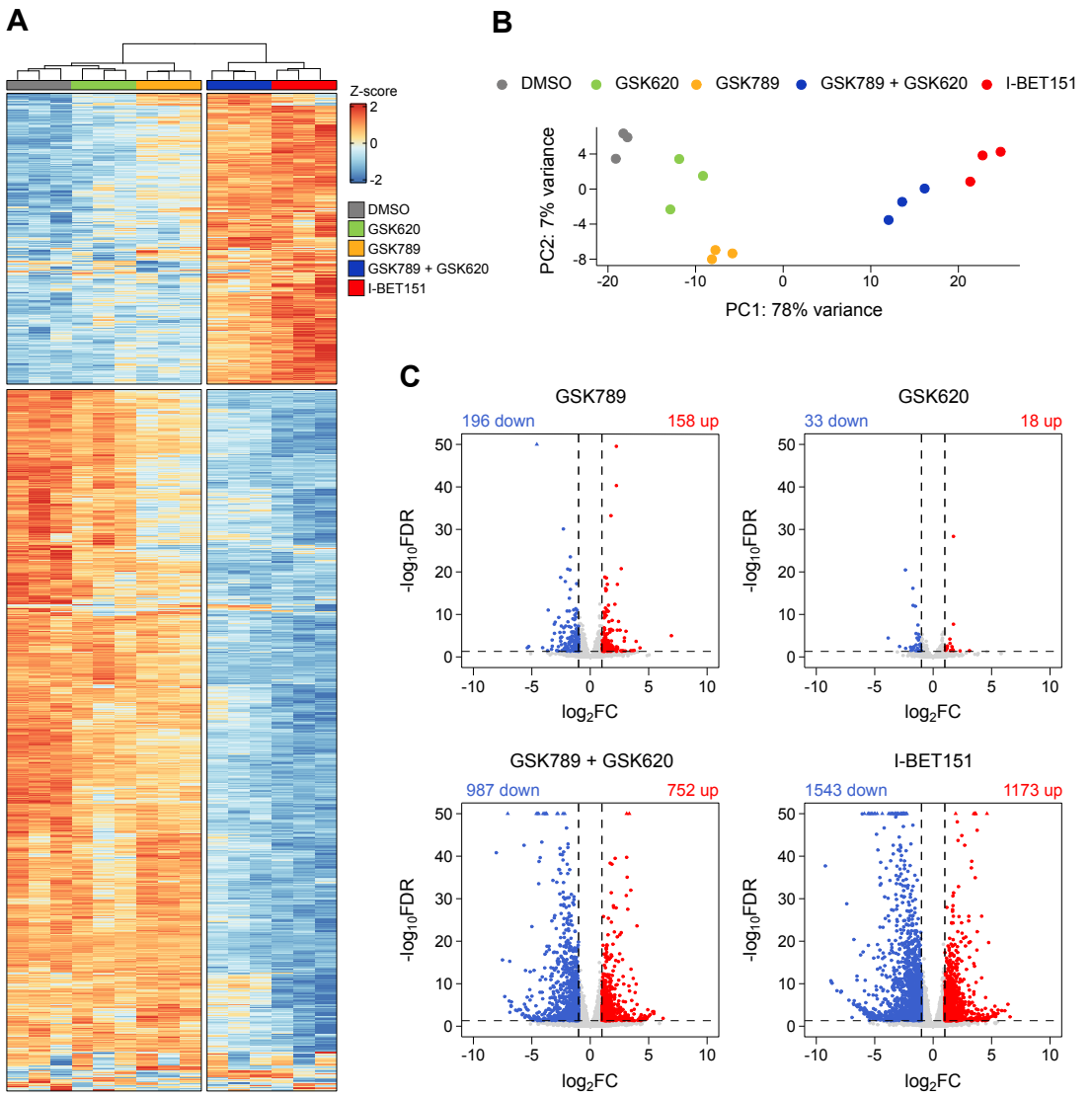

Figure 6.1. Simultaneous BD1 and BD2 inhibition induces more extensive gene expression changes than targeting either domain individually. (A) Heatmap displaying the top 500 most variable genes in BON1 cells post 48-hour treatment with DMSO (negative control), 1 μM GSK620, GSK789, I-BET151 or a combination of 0.5 μM each of GSK789 and GSK620. Z-scores indicate normalised expression levels (high in red, low in blue), with treatments clustered based on similarity in gene expression patterns. **(B)** PCA plot highlighting separation of samples (n=3 per group) based on variance in gene expression profiles. **(C)** Volcano plots showing differentially expressed genes per treatment. The x-axis represents $\log_2$FC in expression between indicated compound and DMSO. The y-axis represents the negative logarithm (base 10) of the FDR-adjusted p-value ($-\log_{10}$FDR). Dashed lines mark thresholds for significance, defined by $\log_2$FC $\geq$ 1 for upregulation, $\leq$ -1 for downregulation, and an FDR-adjusted p-value $\leq$ 0.05 (represented as $-\log_{10}$FDR $\geq$ 1.3 on each volcano plot). Significantly upregulated genes appear as red dots while downregulated genes appear as blue dots.

6.2.2 Simultaneous BD1 and BD2 inhibition downregulates a broad range of Hallmark pathways, including those implicated in metastatic PNETs

Genes identified via RNA-seq were ranked by their $\log_2$ fold change ($\log_2$FC) and gene set enrichment analysis (GSEA) was used to identify the biological pathways impacted in each treatment group. Of the 50 Hallmark pathways in the MSigDB collection,[182] 36 were significantly affected in at least one treatment group, with the majority being downregulated. Treatment with I-BET151 led to the downregulation of the most number of pathways (n = 25) followed by the GSK789/GSK620 combination (n = 24). In comparison, treatments with GSK789 and GSK620 alone resulted in fewer altered pathways (n = 17 and n = 15, respectively) **(Figure 6.2**).

Pathways related to inflammation and immune responses that were downregulated by GSK620, but not GSK789, included 'TNFA_SIGNALING_VIA_NFKB' (normalised enrichment score [NES]: -2.3, adjusted p $\leq$ 0.0001); 'TGF_BETA_SIGNALING' (NES: -1.7, adjusted p = 0.01), 'INTERFERON_ALPHA_RESPONSE' (NES: -2.1, adjusted p $\leq$ 0.0001) and 'INFLAMMATORY_RESPONSE' (NES: -1.6, adjusted p = 0.01). Pathways related to oncogenic processes that were downregulated by GSK789, but not GSK620, included 'MYC_TARGETS_V1' (NES: -2.8, adjusted p $\leq$ 0.0001) and 'MTORC1_SIGNALING' (NES: -2.2, adjusted p $\leq$ 0.0001) **(Figure 6.2)**. Notably, 12 of the 14 Hallmark pathways observed to be upregulated in metastatic PNETs (**Figure 4.5** on page 111) were downregulated after treatment with either GSK789/GSK620 or I-BET151 in BON1 cells, highlighting the potential for simultaneous BD1 and BD2 treatments to counteract clinically-relevant key oncogenic processes in this context.

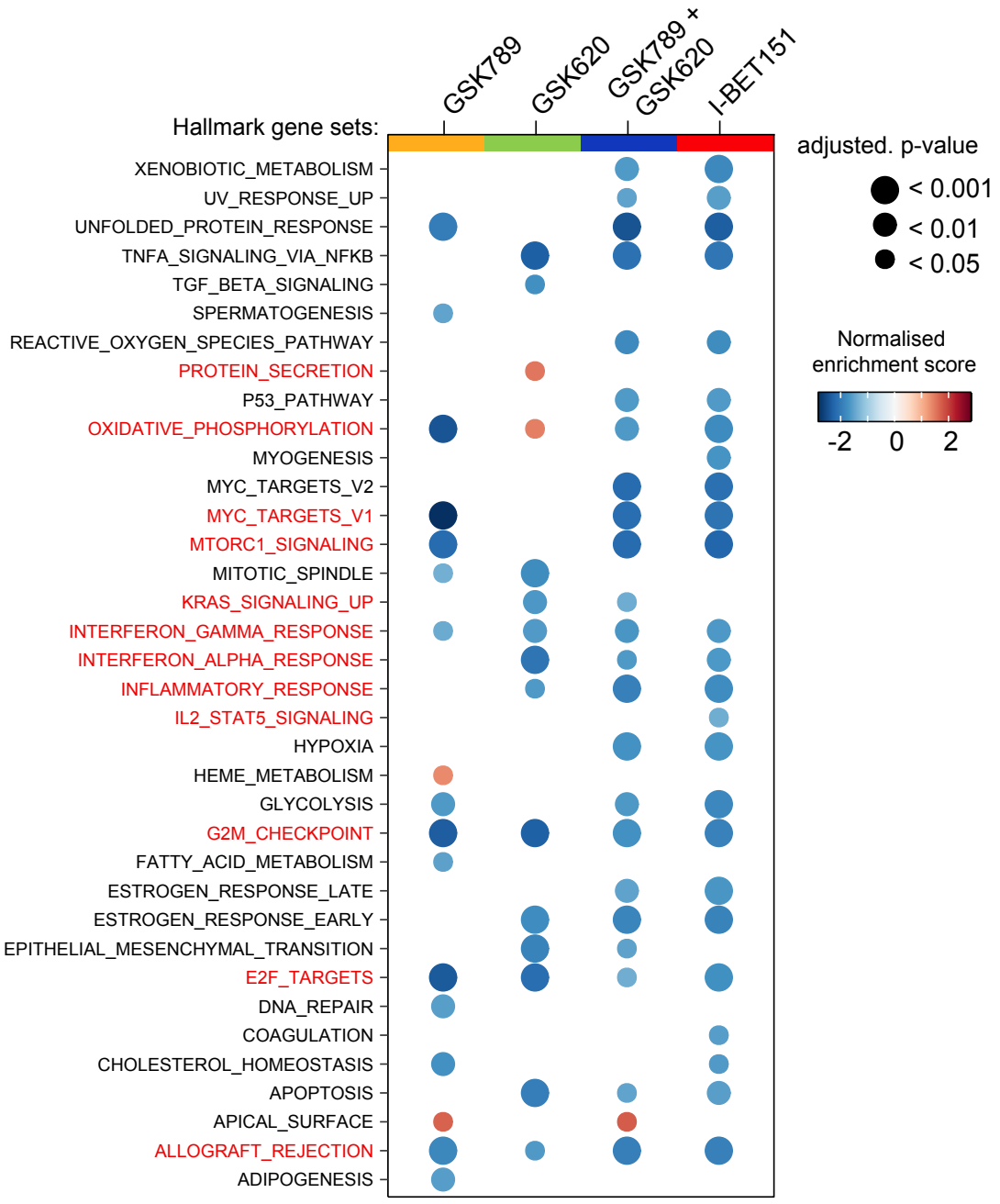

Figure 6.2. Simultaneous BD1 and BD2 inhibition downregulates Hallmark pathways implicated in metastatic PNETs. Dot plot showing Hallmark pathway enrichment, as determined by GSEA of RNA-seq data from BON1 cells treated for 48 hours with the indicated compounds. Dot size indicates the level of statistical significance of the pathway enrichment, with larger dots denoting a lower adjusted p-value. The colour of the dots reflects the normalised enrichment score (NES): red shading indicates a positive NES (upregulation) and blue shading indicates negative NES (downregulation). Pathway names highlighted in red indicate those found to be significantly upregulated in metastatic PNETs in Figure 4.5. GSEA, gene set enrichment analysis.

6.2.3 Simultaneous BD1 and BD2 inhibition disrupts RNA and protein synthesis machinery while BD1-selective inhibition predominantly affects cell cycle pathways

The preceding analyses showed that dual inhibition of BD1 and BD2 led to more extensive gene expression alterations and downregulation of a broader array of Hallmark pathways compared to inhibiting either domain individually. To distinguish the processes uniquely impacted by BD1- or BD2-selective targeting from those altered by the combined effect of dual-BD inhibition, Gene Ontology (GO)[177] enrichment analysis was performed on genes differentially expressed following treatment with GSK789 and GSK620, individually and in combination. GO:biological process (BP) terms *downregulated* by GSK789 treatment were predominantly associated with cell division and growth regulation, encompassing 'intracellular signal transduction', 'mitotic cell cycle' processes, and 'cell population proliferation' mechanisms **(Figure 6.3**). Conversely, no GO:BP terms were enriched in the 33 genes downregulated by GSK620 treatment. Notably, GO:BP terms downregulated by the combined GSK789 and GSK620 treatment were related to RNA and protein synthesis and processing. These included 'transfer RNA (tRNA) metabolism' and 'ribosomal RNA (rRNA) metabolism', essential for protein translation, 'ribosome biogenesis' for protein assembly and 'non-coding RNA (ncRNA) processing' for gene expression regulation **(Figure 6.3**). Thus, simultaneous BD1 and BD2 inhibition disrupts crucial cellular machinery necessary for cell survival and growth, whereas BD1 inhibition alone more specifically affects pathways related to cell proliferation and the cell cycle, with BD2 inhibition alone showing minimal transcriptional impact.

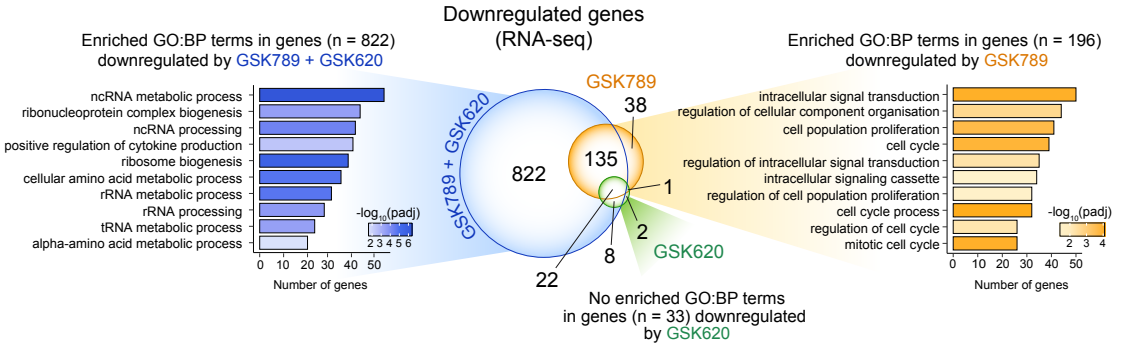

Figure 6.3. Dual bromodomain inhibition disrupts RNA and protein synthesis machinery while BD1-selective inhibition downregulates cell cycle pathways. Venn diagram showing number of overlapping and unique genes downregulated after 48-hours of treatment with 1 μM GSK620, 1 μM GSK789, or a combination of 0.5 μM GSK789 and GSK620. Bar plot on the left shows enriched GO:BP terms in 822 genes exclusively downregulated after treatment with the GSK789/GSK620 combination. Bar plot on the right shows enriched GO:BP terms in 196 genes downregulated by GSK789. Shading intensity of each bar represents the statistical significance of the enrichment, represented as $-\log_{10}$ of the adjusted p-value ($-\log_{10}$padj), with darker shading indicating higher statistical significance of the GO:BP terms.

GO:BP terms *upregulated* by GSK789 treatment encompassed those related to nucleosome assembly and organisation, indicating that BD1 inhibition facilitates chromatin remodelling **(Figure 6.4)**. Moreover, the upregulation of processes such as 'axon development' and 'axonogenesis' suggests an impact on neuroendocrine differentiation patterns. Combined treatment with GSK789 and GSK620 not only upregulated GO:BP terms associated with nervous system development, but additionally enriched processes related to cellular architecture and morphogenesis. These terms included 'cilium organisation', 'cilium assembly' and 'cell projection organisation', which are important in modulating tumour cell signalling and their interaction with the surrounding environment **(Figure 6.4)**. No GO:BP terms were upregulated in response to GSK620 treatment alone. Collectively, these findings highlight the distinct cellular mechanisms targeted by BD1 and combined BD1/BD2 inhibition in BON1 cells, revealing disruption of essential cellular processes and cell cycle dynamics, with potential reprogramming towards a more differentiated, less tumourigenic state.

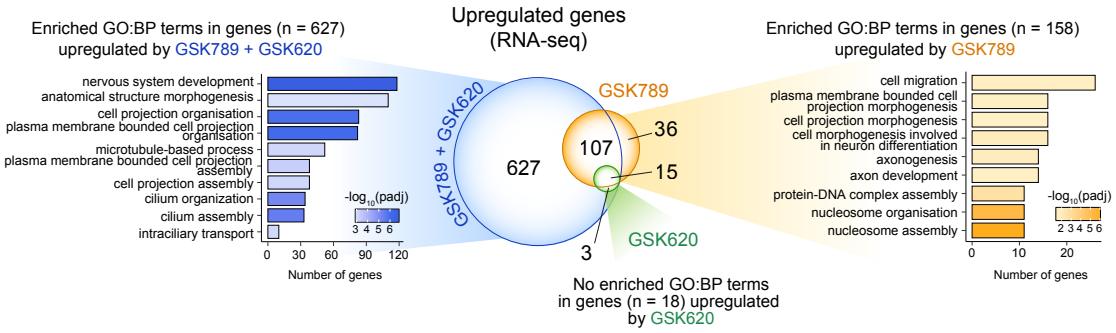

Figure 6.4. Differential effects of BD1-selective and dual BD inhibition on neuronal development and cell architecture. Venn diagram showing number of overlapping and unique genes upregulated after 48-hours of treatment with 1 µM GSK620, 1 µM GSK789, or a combination of 0.5 µM GSK789 and GSK620. Bar plot on the left shows enriched GO:BP terms in 627 genes exclusively upregulated after treatment with the GSK789/GSK620 combination. Bar plot on the right shows enriched GO:BP terms in 158 genes downregulated by GSK789. Shading intensity of each bar represents the statistical significance of the enrichment, represented as $-\log_{10}$padj, with darker shading indicating higher statistical significance of the GO:BP terms.

6.2.4 The upstream regulator CKAP2L is inhibited by BD1-selective and combined BD1/BD2 inhibition

Ingenuity Pathway Analysis (IPA)[181] was applied to RNA-seq data from BET inhibitor-treated BON1 cells to predict altered upstream regulators. While GSK620 treatment alone did not yield enough differentially expressed genes to identify altered regulators, treatments with GSK789, the GSK789/GSK620 combination and I-BET151 resulted in the prediction of multiple activated and inhibited upstream regulators. For GSK789 alone, *activated* regulators included inner membrane mitochondrial protein (IMMT), tetratricopeptide repeat domain 1 (TPRS1), ubiquitin specific peptidase 22 (USP22), and transforming growth factor beta 2 antisense RNA 1 (TGFB2-AS1). When GSK789 was combined with GSK620, however, a different pattern of activated upstream regulators emerged, with somatostatin receptor 2 (SSTR 2) and glioma-associated oncogene homolog 1 (GLI1) being the most significantly activated. A similar pattern of activated upstream regulators was also observed with I-BET151 treatment **(Figure 6.5A)**.

Inhibited upstream regulators after GSK789 treatment included forkhead box O1 (FOXO1) and PDZ and LIM domain 2 (PDLIM2), while the combination

of GSK789 with GSK620 inhibited a number of additional regulators including activating transcription factor 4 (ATF4), GATA binding protein 4 (GATA4), BRD4, breakpoint cluster region protein (BCR) complex and interferon regulatory factor 2 (IRF2) **(Figure 6.5A)**. This pattern of inhibited regulators was largely similar after treatment with I-BET151. Cytoskeleton associated protein 2 like (CKAP2L) and forkhead box M1 (FOXM1) were predicted to be downregulated across all three treatments, a notable finding given their activation in metastatic PNETs in the Mayo Clinic cohort (see **Figure 4.10** on page 120). Furthermore, inspection of differential gene expression analysis data revealed that the expression of *CKAP2L* was ~3 and ~4 times lower after treatment with the GSK789/GSK620 combination and I-BET151, respectively, compared to DMSO control (adjusted $p < 0.0001$), but was not significantly downregulated by GSK789 alone. Despite FOXM1 being predicted as an inhibited upstream regulator by IPA software, its mRNA expression was not significantly reduced in any treatment group. IPA network analysis showed that genes within the CKAP2L regulatory network were involved in cell cycle progression, proliferation of tumour cell lines and metastasis, with each of these processes inhibited by GSK789, GSK789/GSK620 in combination and I-BET151, but not GSK620 **(Figure 6.5B)**.

Interestingly, while IPA predicted that BRD4 was an inhibited upstream regulator in response to combination treatment with GSK789/GSK620 and I-BET151, this was not the case for GSK789 alone, supporting the notion that simultaneous targeting of both BD1 and BD2 domains is required to achieve the maximum transcriptional effect of BET protein inhibition **(Figure 6.5B)**.

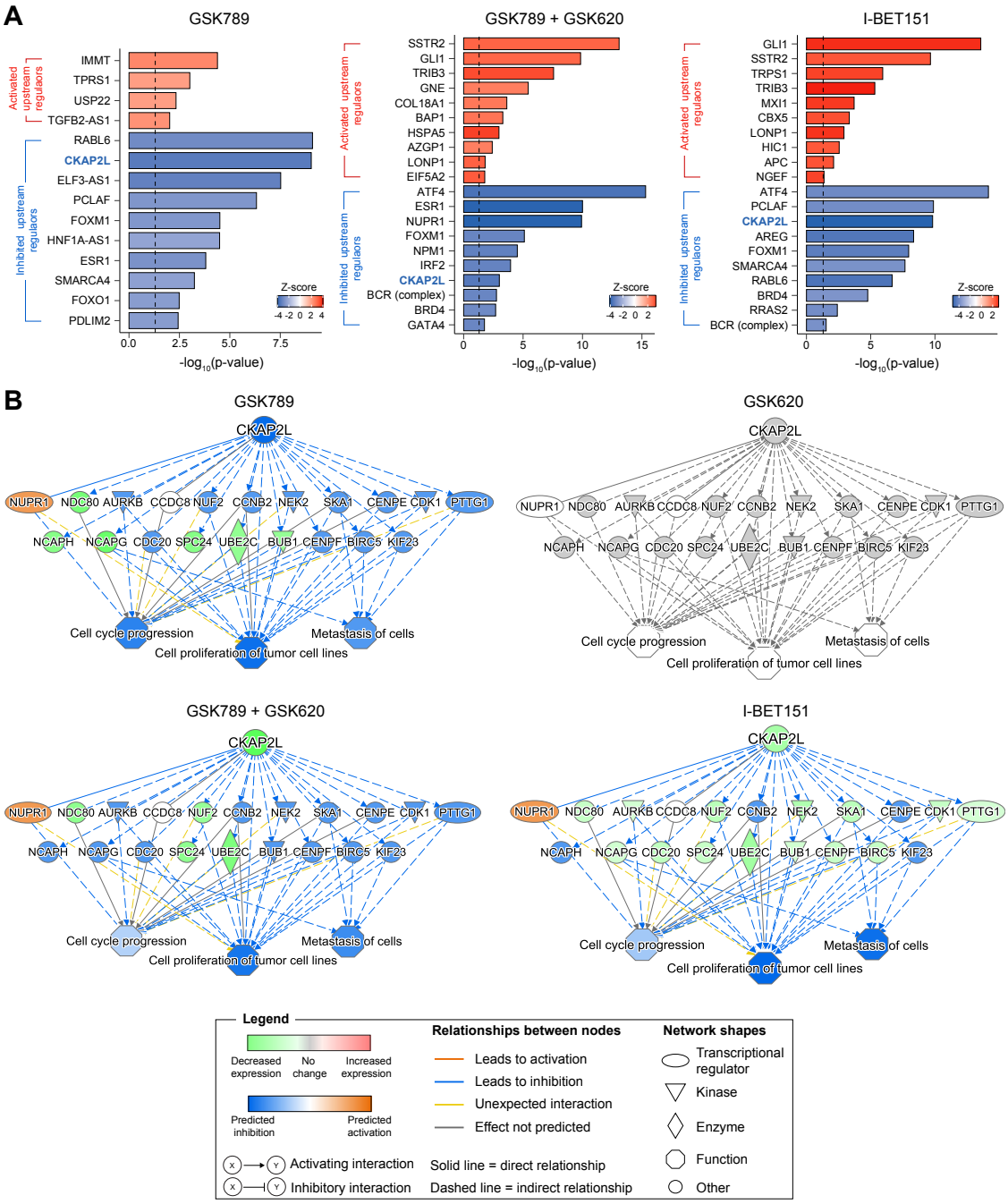

Figure 6.5. CKAP2L is a key upstream regulator that is inhibited by BD1-selective and combined BD1/BD2 inhibition. (A) IPA upstream regulator analysis shown as bar plots, where Z-scores indicate degree of predicted activation (red) or inhibition (blue) of upstream regulators, ordered by -$\log_{10}$ p-value). The dashed vertical line marks the threshold for $p \leq 0.05$ (-$\log_{10}$ p-value > 1.3). CKAP2L is blue-highlighted. **(B)** IPA network diagram showing genes regulated by CKAP2L and the effect of indicated BET inhibitors on each regulatory network. Green nodes represent genes with downregulated expression in the RNA-seq dataset, while blue and orange nodes indicate genes or biological processes that IPA predicts to be inhibited or activated, respectively. Grey/white nodes indicate no changes in gene expression or predicted activity. Inset legend below the diagram further explains the symbols and colours used within the network.

6.2.5 I-BET151 has a broader impact on modulating downstream gene expression than combined treatment with GSK789 and GSK620.

After demonstrating that simultaneous BD1 and BD2 inhibition resulted in more extensive changes in gene expression compared to targeting either domain individually, I next explored transcriptomic differences and similarities between I-BET151 and the combination of GSK789/GSK620.

A comparison of significantly *downregulated* genes between the GSK789/GSK620 combination and I-BET151 revealed 857 genes that were commonly affected by both treatments **(Figure 6.6)**. However, there were distinct differences: 686 genes were exclusively downregulated by I-BET151, while GSK789/GSK620 uniquely downregulated 130 genes. GO:BP enrichment analysis of the genes downregulated by both treatments highlighted terms such as 'regulation of signal transduction', 'intracellular signal transduction' and 'regulation of cell population proliferation', indicating a suppression of crucial signalling pathways essential for cell communication and growth. Interestingly, downregulation of apoptosis-related terms such as 'programmed cell death' and 'apoptotic process' was also observed, suggesting a possible compensatory response to BET inhibition. While no enriched GO:BP terms were found in the genes uniquely downregulated by GSK789/GSK620, analysis of genes exclusively downregulated by I-BET151 identified 'regulation of cellular component organisation' as the most significantly enriched GO:BP term. This term encompasses processes crucial for maintaining cell structure and function, such as the arrangement of organelles and the cytoskeleton. Disruptions here could lead to adverse outcomes including impaired cell polarity and motility, affecting both tumour and normal tissue functionality. Such disturbances might manifest as tissue dysfunction or organ abnormalities, indicative of off-target side effects. Together, these results suggest that downregulation of cellular signalling and proliferation are a common consequence of simultaneous BD1 and BD2 targeting (with either

I-BET151 or GSK789/GSK620), although I-BET151 appears to have a broader impact on fundamental cellular organisational processes.

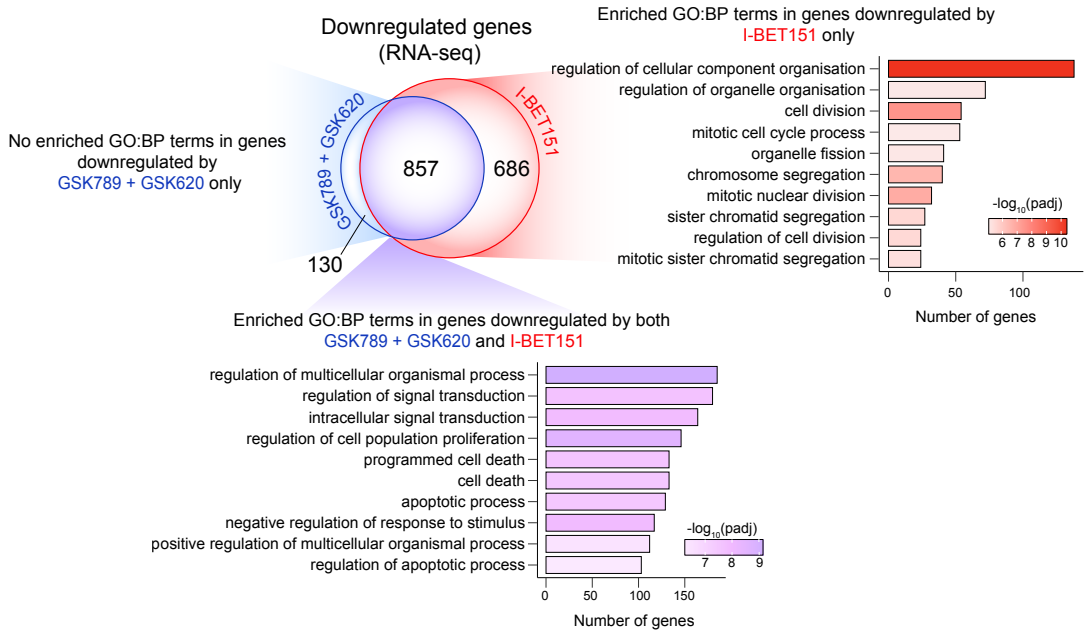

Figure 6.6. I-BET151 has a more pronounced effect on downregulating gene expression compared to combined treatment with GSK789 and GSK620. Venn diagram illustrating number of overlapping and unique genes downregulated after 48 hours of treatment with 1 μM of I-BET151 or 0.5 μM each of GSK789 and GSK620. Bar plot on the right (red) shows GO:BP terms enriched in genes exclusively downregulated by I-BET151. Bar plot below (purple) shows GO:BP terms enriched in genes downregulated by both GSK789/GSK620 and I-BET151. Shading intensity of each bar represents the statistical significance of the enrichment, represented as $-\log_{10}$padj, with darker shading indicating higher statistical significance of the GO:BP terms.

A comparison of significantly *upregulated* genes between the GSK789/GSK620 combination and I-BET151 identified 597 genes commonly upregulated by both treatments **(Figure 6.7)**. Additionally, 576 genes were uniquely upregulated by I-BET151, in contrast to 150 genes exclusively upregulated by GSK789/GSK620. GO:BP enrichment analysis of the genes upregulated by both treatments revealed terms associated with neuronal development and cellular structure, such as 'nervous system development', 'neuron differentiation', 'cilium organisation' and 'cell projection organisation'. A very similar set of GO:BP terms were enriched amongst genes exclusively upregulated by I-BET151. However, the genes uniquely upregulated by the GSK789/GSK620 combination were associated with just two

GO:BP terms: 'response to xenobiotic stimulus' and 'DNA replication', pointing towards another possible mechanism of adaptation or stress response to BET inhibition **(Figure 6.7)**. These findings suggest a more profound downstream impact of I-BET151 on the transcriptomic landscape within BON1 cells, with broader downstream effects compared to GSK789/GSK620.

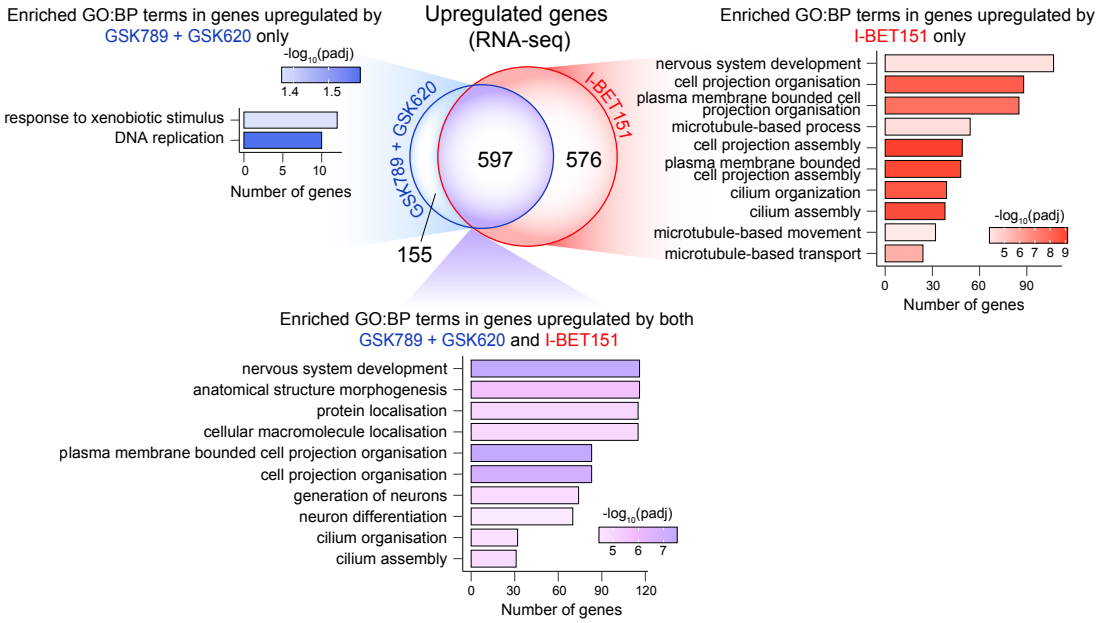

Figure 6.7. I-BET151 has a more pronounced effect on upregulating gene expression compared to combined treatment with GSK789 and GSK620. Venn diagram illustrating number of overlapping and unique genes upregulated after 48 hours of treatment with 1 μM of I-BET151 or 0.5 μM each of GSK789 and GSK620. Bar plots on the right (red) and left (blue) show GO:BP terms enriched in genes exclusively upregulated by I-BET151 and GSK789/GSK620, respectively. Bar plot below (purple) shows GO:BP terms enriched in genes downregulated by both GSK789/GSK620 and I-BET151. Shading intensity of each bar represents the statistical significance of the enrichment, represented as $-\log_{10}$padj, with darker shading indicating higher statistical significance of the GO:BP terms.

6.2.6 SLAM-seq identifies direct transcriptional targets of BD-selective and non-selective inhibition

Whilst RNA-seq data from the preceding sections provided insights into the downstream transcriptional changes following BET inhibitor treatment, to discern the early and direct transcriptional impacts of BD-selective and non-selective

inhibition, the thiol(SH)-linked alkylation for the metabolic sequencing of RNA (SLAM-seq)[185] method was utilised. This technique allows for the quantification of newly transcribed mRNAs by incorporating 4-thiouridine (4sU) into RNA molecules, which are detectable as thymine-to-cytosine (T>C) conversions in 3' mRNA-sequencing. To capture these initial changes, an early time point of 6 hours post-treatment with BET inhibitors was selected. Labelling of culture media with 300 μM 4sU for 1 hour prior to RNA extraction resulted in an excess of T>C conversions relative to a non-4sU control group, confirming that the experimental setup was successful **(Figure 6.8A)**. Consistent with the RNA-seq PCA data **(Figure 6.1B)**, PCA of the SLAM-seq data showed that the samples clustered by treatment type, although a greater degree of overlap was seen between I-BET151 and the GSK789/GSK620 combination samples compared to RNA-seq **(Figure 6.8B)**.

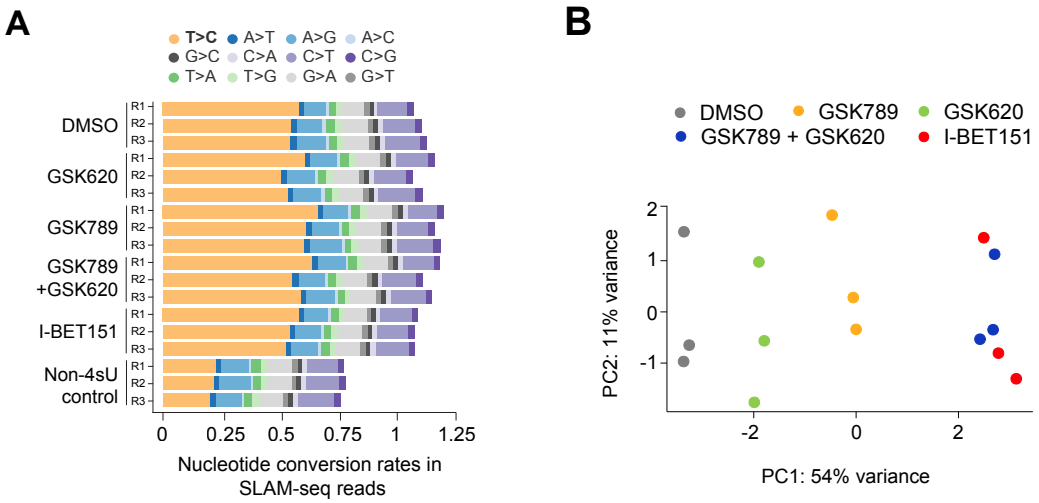

Figure 6.8. Metabolic RNA labelling with SLAM-seq reveals distinct effects of BD-selective and non-selective BET inhibition on nascent transcription. (A) Bar plot showing nucleotide conversion rates in SLAM-seq 3' mRNA-Seq reads. Each bar represents an independent biological replicate (R1-R3) per treatment group. An increase in T>C conversion rates (orange bars) is seen in samples labelled with 4sU relative to non-4sU controls. **(B)** PCA plot highlighting separation of samples (n=3 per group) based on variance in SLAM-seq gene expression profiles.

Differential expression analysis was used to detect significantly altered nascent transcripts, identifying those that were either up- or downregulated (absolute $\log_2$FC ≥ 0.5 and FDR-adjusted p-value ≤ 0.05) after 6 hours of BET inhibitor treatment. GSK620 treatment resulted in the downregulation of only 2 genes and upregulation

of 8 genes, while GSK789 had a slightly larger impact, downregulating 11 genes and upregulating 49 **(Figure 6.9)**. A more pronounced effect was seen with the combined GSK789/GSK620 treatment, which upregulated 207 genes and downregulated 168 genes. In contrast to RNA-seq data, which showed substantially more differentially expressed genes following I-BET151 treatment, SLAM-seq analysis showed that the numbers of nascent transcripts upregulated (n = 180) and downregulated (n = 130) by I-BET151 were similar to those altered by the combined GSK789/GSK620 treatment **(Figure 6.9)**.

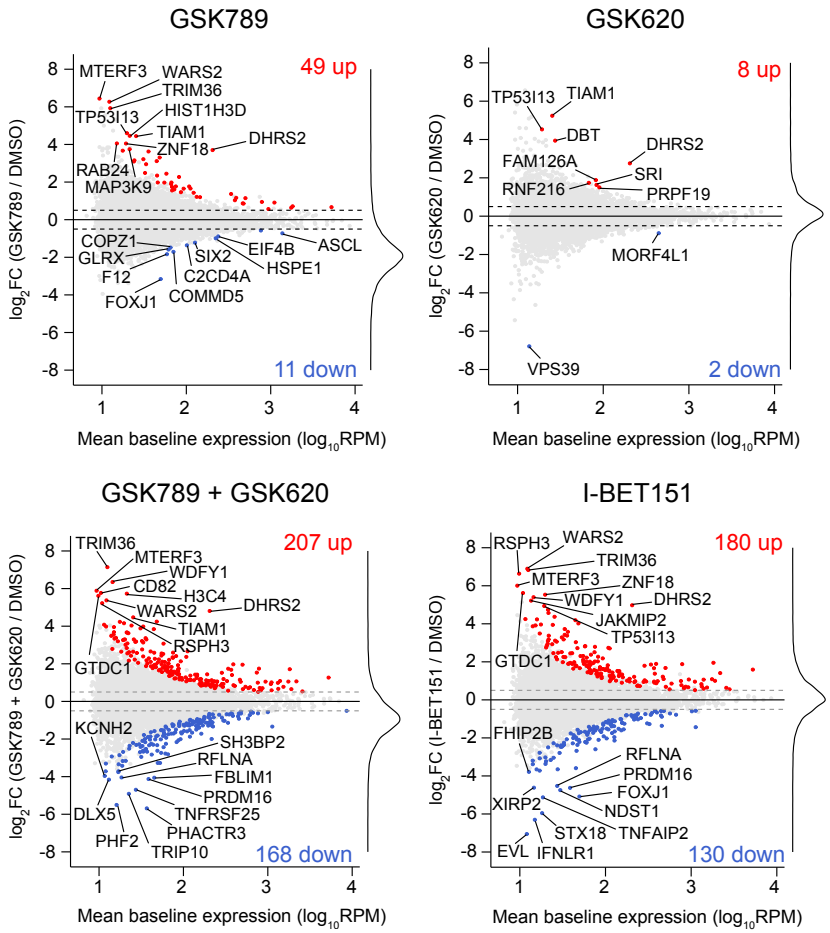

Figure 6.9. SLAM-seq identifies direct transcriptional targets of BD-selective and non-selective inhibition. MA plots of nascent mRNA changes detected by SLAM-seq, where 'M' represents the $\log_2$FC in gene expression between treated and DMSO control samples (y-axis) and 'A' denotes the average gene expression level, expressed as $\log_{10}$ reads per million (RPM) (x-axis). Each point corresponds to an individual gene, with upregulation coloured in red and downregulation in blue. For each MA plot, up to 10 of the most significantly altered genes, according to adjusted p-value, are labelled.

Examination of genes *downregulated* in response to GSK789, GSK620 and their combination revealed none that were downregulated across all three treatment groups. Moreover, only 6 genes were commonly downregulated by both GSK789 and the GSK789/G620 combination, whereas only one gene was downregulated by both GSK620 and the combination treatment **(Figure 6.10)**. Conversely, 161 additional nascent transcripts were uniquely downregulated in response to the combined GSK789/GSK620 treatment. These findings suggest that achieving comprehensive inhibition of direct BET protein targets requires simultaneous targeting of both BD1 and BD2 domains. GO:BP enrichment analysis was conducted on the 161 genes downregulated by the GSK789/GSK620 combination, revealing an inhibitory effect on key cellular processes involved in gene expression, protein synthesis and metabolic activity. In contrast, no GO:BP terms were enriched in the small number of genes downregulated by GSK789 and GSK620 alone **(Figure 6.10)**.

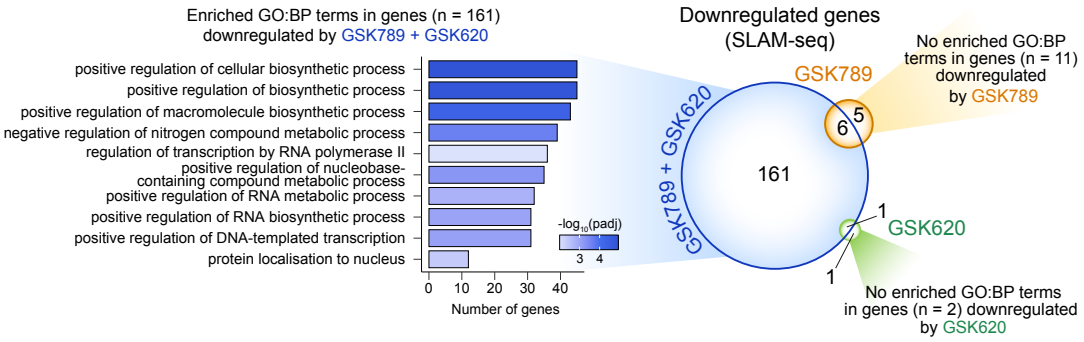

Figure 6.10. Maximal inhibition of direct BET protein targets requires simultaneous targeting of both BD1 and BD2 domains. Venn diagram showing number of overlapping and unique nascent mRNA transcripts downregulated after 6-hours of treatment with 1 μM GSK620, 1 μM GSK789, or a combination of 0.5 μM GSK789 and GSK620. Bar plot on the left shows enriched GO:BP terms in 161 genes exclusively downregulated after treatment with the GSK789/GSK620 combination. Shading intensity of each bar represents the statistical significance of the enrichment, represented as $-\log_{10}$padj, with darker blue shading indicating higher statistical significance of the GO:BP terms.

Evaluation of genes *upregulated* by GSK789, GSK620 and their combination revealed five nascent transcripts that were upregulated across all three treatment groups: Dehydrogenase/Reductase 2 (*DHRS2*), Hydroxycarboxylate Carrier 1

(*HYCC1*), Ring Finger Protein 216 (*RNF216*), T-Cell Lymphoma Invasion And Metastasis 1 (*TIAM1*) and Tumor Protein P53 Inducible Protein 13 (*TP53I13*) **(Figure 6.11)**. Unlike the minimal overlap observed with downregulated genes **(Figure 6.10)**, a substantial portion of transcripts upregulated by GSK789 or GSK620 individually were also elevated when these inhibitors were used in tandem. Regardless, an additional 158 nascent transcripts were upregulated in response to the GSK789/GSK620 combination only. GO:BP enrichment analysis of this subset of genes highlighted processes related to chemical stimulus and hormonal responses. Conversely, the 4 genes upregulated by GSK789 were associated with nucleosome assembly and organisation, further supporting a role for BD1 in chromatin remodelling. Consistent with the limited transcriptional impact of GSK620, no enriched GO:BP terms were found in the 8 genes downregulated by this compound **(Figure 6.11)**. Therefore, while BD1 inhibition appears to play an important role in gene activation following BET inhibition, the unique upregulation of additional genes by the combination treatment suggests that concurrently targeting BD2 inhibition modulates a separate set of biological pathways inaccessible through single-domain targeting.

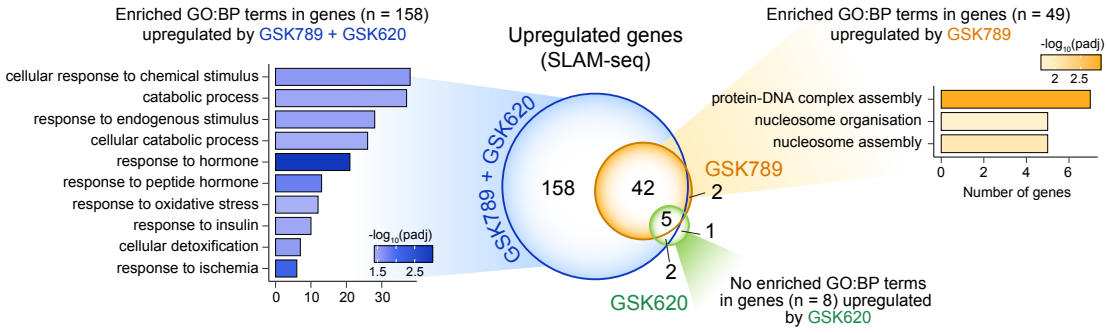

Figure 6.11. BD1-selective inhibition upregulates chromatin remodelling genes while combined BD1 and BD2 inhibition triggers cellular stress response pathways. Venn diagram showing number of overlapping and unique nascent mRNA transcripts upregulated after 6-hours of treatment with 1 μM GSK620, 1 μM GSK789, or a combination of 0.5 μM GSK789 and GSK620. Bar plot on the left shows enriched GO:BP terms in 161 genes exclusively downregulated after treatment with the GSK789/GSK620 combination. Shading intensity of each bar represents the statistical significance of the enrichment, represented as $-\log_{10}$padj, with darker shading indicating higher statistical significance of the GO:BP terms.

6.2.7 I-BET151 and GSK789/GSK620 have distinct and overlapping effects on the nascent transcriptome

Although PCA showed that the nascent transcriptional profiles of BON1 cells treated with I-BET151 and the GSK789/GSK620 combination clustered closely together **(Figure 6.8B**), a detailed comparison of genes significantly altered by both treatments revealed notable differences.

A comparison of significantly *downregulated* nascent transcripts between the GSK789/GSK620 combination and I-BET151 revealed 57 genes that were commonly affected by both treatments. GO:BP enrichment analysis of these genes identified processes predominantly related to transcriptional regulation and biosynthesis, including 'DNA-templated transcription' and 'regulation of RNA biosynthetic processes', consistent with the role of BET proteins in transcriptional activation **(Figure 6.12)**. In contrast to RNA-seq findings that suggested a more pronounced transcriptional impact by I-BET151, SLAM-seq analysis indicated a broader suppression of nascent gene transcription by the combined GSK789/GSK620 treatment. Enrichment analysis of the 111 genes uniquely downregulated by GSK789/GSK620 revealed additional GO:BP terms associated with biosynthetic processes, while the 73 genes uniquely downregulated by I-BET151 were not associated with any enriched GO:BP terms **(Figure 6.12)**. These findings illustrate that whilst both I-BET151 and GSK789/GSK620 combination treatment initially downregulate gene expression programs integral to transcription and synthesis of cellular components, the impact of the GSK789/GSK620 combination is more extensive.

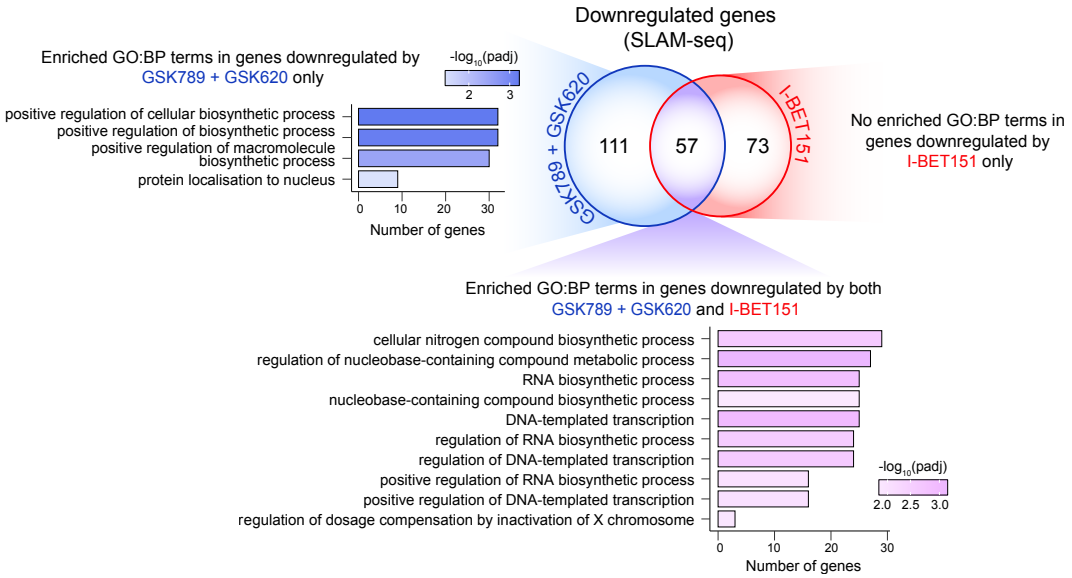

Figure 6.12. Combined treatment with GSK789/GSK620 downregulates nascent transcription to a greater extent than I-BET151. Venn diagram illustrating number of overlapping and unique nascent transcripts downregulated after 6 hours of treatment with 1 μM of I-BET151 or 0.5 μM each of GSK789 and GSK620. Bar plots on the and left (blue) show GO:BP terms enriched in genes exclusively downregulated by GSK789/GSK620. Bar plot below (purple) shows GO:BP terms enriched in genes downregulated by both GSK789/GSK620 and I-BET151. Shading intensity of each bar represents the statistical significance of the enrichment, represented as $-\log_{10}$padj, with darker shading indicating higher statistical significance of the GO:BP terms.

A comparison of significantly *upregulated* nascent transcripts between the GSK789/GSK620 combination and I-BET151 identified 130 genes altered by both treatments, with enrichment of GO:BP terms linked to the mechanics of chromatin architecture, such as 'protein-DNA complex assembly' and 'nucleosome assembly' **(Figure 6.13)**. The GSK789/GSK620 combination also led to a greater number of uniquely upregulated nascent transcripts compared to I-BET151, albeit less markedly than the difference observed in the downregulated genes. The GO:BP terms 'establishment of localisation in cell' and 'intracellular transport,' enriched in the 77 genes upregulated solely by the GSK789/GSK620 combination, suggests an additional impact on cellular behaviour that extends beyond transcriptional regulation. Meanwhile, the 50 genes upregulated by I-BET151 alone were enriched in GO:BP terms genes involved in catalytic activity and cellular responses to hypoxia **(Figure 6.13)**.

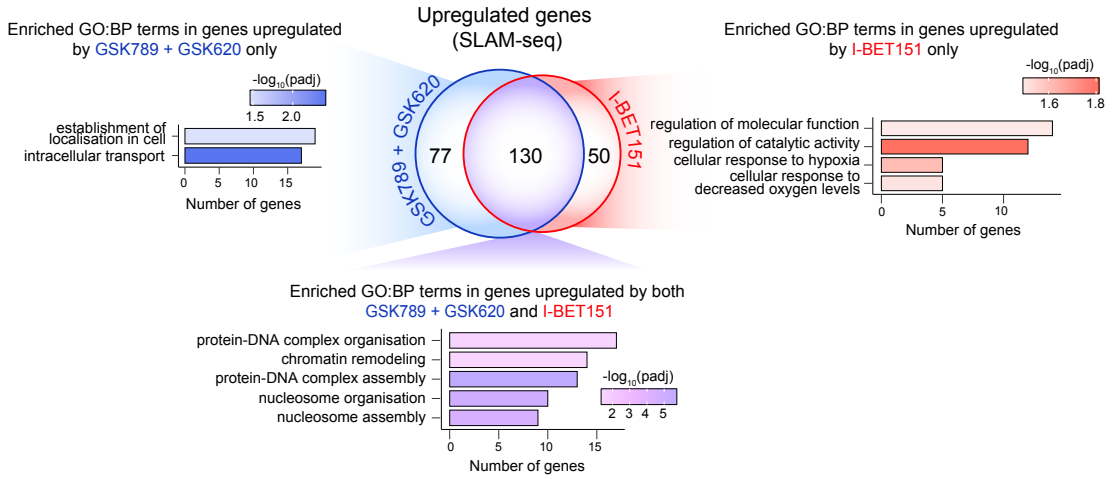

Figure 6.13. Both GSK789/GSK620 and I-BET151 upregulate nascent transcription of genes involved in chromatin remodelling. Venn diagram illustrating number of overlapping and unique nascent transcripts upregulated after 6 hours of treatment with 1 μM of I-BET151 or 0.5 μM each of GSK789 and GSK620. Bar plots on the left (blue) and right (red) show GO:BP terms enriched in genes exclusively upregulated by GSK789/GSK620 and I-BET151, respectively. Bar plot below (purple) shows GO:BP terms enriched in genes upregulated by both GSK789/GSK620 and I-BET151. Shading intensity of each bar represents the statistical significance of the enrichment, represented as $-\log_{10}$padj, with darker shading indicating higher statistical significance of the GO:BP terms.

6.2.8 Integrated analysis of SLAM-seq and RNA-seq identifies *E2F2* and *CKAP2L* as early and late targets, respectively, of dual BD inhibition

To identify genes consistently affected at both early and late phases of BET inhibition, as well as those uniquely responsive at either time point, SLAM-seq and RNA-seq analyses were integrated by plotting the $\log_2$FC values of overlapping genes from both datasets against each other **(Figure 6.14)**. Only one gene, C2 Calcium Dependent Domain Containing 4A (*C2CD4A*) was significantly downregulated according to both SLAM-seq and RNA-seq after GSK789 treatment, while no genes were downregulated at both time-points following GSK620 treatment. In contrast, 50 and 51 genes were downregulated in response to the GSK789/GSK620 combination and I-BET151, respectively, at both time points. Nineteen of these downregulated genes were common to both I-BET151 and the GSK789/GSK620

combination, suggesting a high degree of sensitivity to BET inhibition. These included Aurora Kinase A (*AURKA*) and Cyclin D1 (*CCND1*), both key cell cycle regulators that have been linked to cancer progression,[112,303] and genes encoding the S100 protein family members *S100A2* and *S100A16*, which have been used as specific immunohistochemical markers for PNETs.[307]

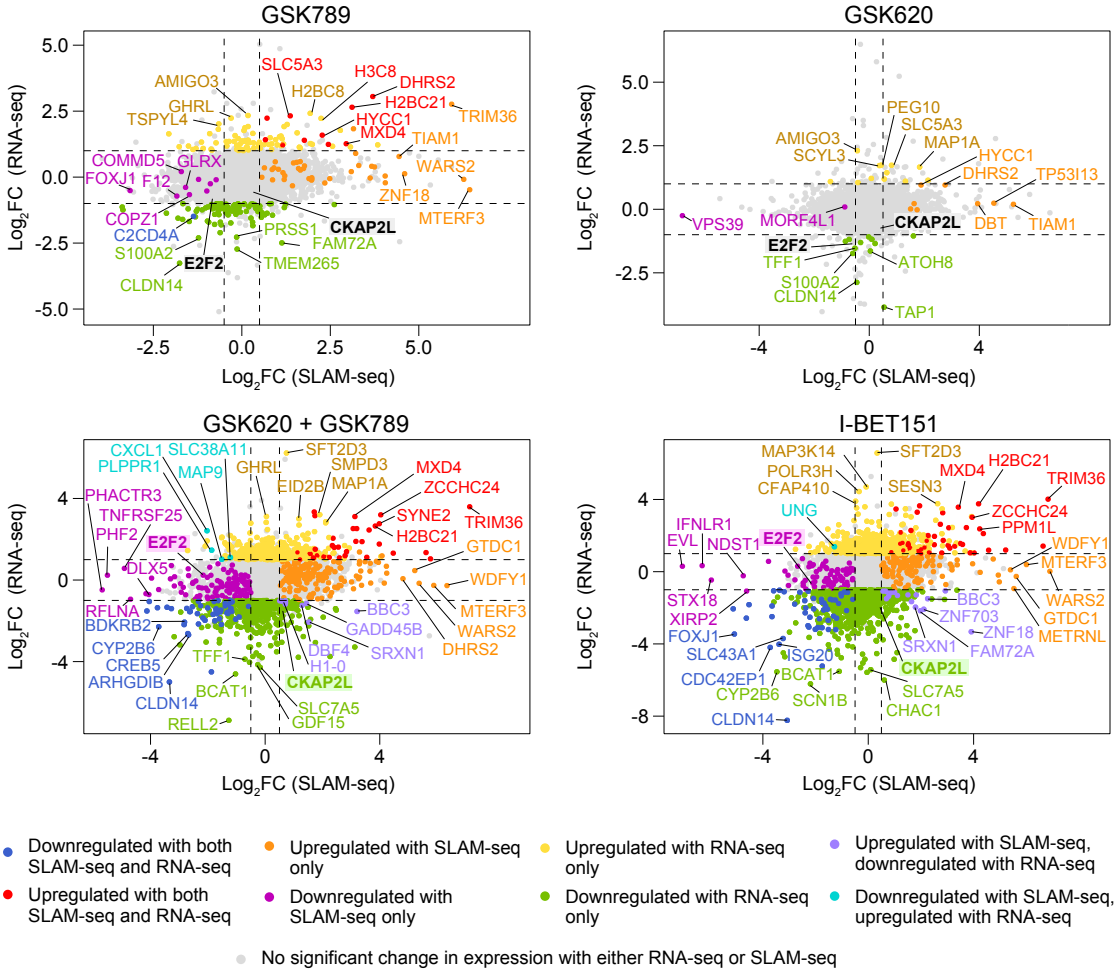

Figure 6.14. Integrated analysis of SLAM-seq and RNA-seq data reveals temporal changes in gene expression following BET inhibition. Scatter plots show $\log_2$FC values from SLAM-seq (x-axis) against $\log_2$FC values from RNA-seq (y-axis) in BON1 cells treated for 48 hours with 1 μM of GSK789, GSK620, I-BET151 or 0.5 μM each of GSK789 and GSK620. $\log_2$FC values are relative to DMSO control. Grey dots denote genes without significant expression changes in both assays. Coloured points indicate genes with significant expression changes (adjusted $p \leq 0.05$) with colours defined in key. Vertical and horizontal dashed lines mark thresholds for biological significance (absolute $\log_2$FC ≥ 0.5 for SLAM-seq and ≥ 1 for RNA-seq, respectively). In each scatter plot, up to 5 of the most significantly altered genes, based on $\log_2$FC values, are labelled. *E2F2* and *CKAP2L* are also highlighted.

GSK789 upregulated 10 genes across both SLAM-seq and RNA-seq analyses, whilst no genes were upregulated by GSK620 across both datasets. Comparatively, I-BET151 and the combination of GSK789/GSK620 led to the upregulation of 43 and 32 genes, respectively, at both early and late time points. Amongst these, 20 genes were commonly upregulated by both treatments, including several with known tumour suppressor roles, such as Tripartite Motif Containing 36 (*TRIM36*),[308] MAX Dimerisation Protein 4 (*MXD4*)[309] and Semaphorin 6C (*SEMA6C*).[310]

Significant upregulation of *BRD2* was observed using SLAM-seq by 2.1-fold (adjusted $p < 0.0001$) with I-BET151 and by 2.07-fold (adjusted $p < 0.0001$) with the combination GSK789/GSK620 treatment, while no significant changes were seen with GSK620 and GSK789 alone. *BRD3* and *BRD4* did not show any significant changes in expression in the SLAM-seq analyses across all treatments. Similarly, in RNA-seq analyses, there were no changes in BET gene expression that met the threshold for biological significance (absolute FC ≥ 2) across all treatments.

E2F2, which was observed to be significantly upregulated in metastatic human PNETs in the Mayo Clinic cohort (see section 4.2.4) was downregulated by both GSK789/GSK620 and I-BET151 in SLAM-seq analyses, but was not significantly altered in the RNA-seq data. Conversely, *CKAP2L*, which was identified as an upstream regulator in metastatic human PNETs, showed downregulation following treatment with both GSK789/GSK620 and I-BET151 according to RNA-seq, but not SLAM-seq. Neither the expression levels of *E2F2* nor *CKAP2L* were affected by GSK789 or GSK620 treatment alone **(Figure 6.14)**. These findings suggest that downregulation of *E2F2* represents an early consequence of dual BD inhibition, potentially initiating a cascade that may lead to the downstream suppression of *CKAP2L*.

6.2.9 ChIP-seq reveals alterations in genome-wide H3K27ac enrichment after BET inhibition

BET proteins function as scaffolds that bind to several histone modifications, including acetylated histone H3 at lysine 27 (H3K27ac).[130] In turn, they recruit chromatin modifying proteins, such as histone acetyltransferases (HATs), that further increase H3K27ac levels.[311,312]. Given that H32K27ac is a well-established chromatin marker of active transcription at both enhancers and promoters,[313] I utilised chromatin immunoprecipitation with next-generation sequencing (ChIP-seq) to examine genome-wide alterations in H3K27ac enrichment in BON1 cells following 6 hours of BET inhibitor treatment.

Overall, 14,710 consensus H3K27ac peaks were identified using the 'Diffbind R' package (see Section 2.4.4.7). These peaks were analysed for differential binding affinity. Treatment with GSK789 significantly increased the H3K27ac binding affinity of 2,435 peaks and decreased it in 4,230 peaks. Similarly, GSK620 increased binding affinity in 2,354 peaks and decreased it in 5,351 peaks.

The combination of GSK789/GSK620 and I-BET151 resulted in an increase in H3K27ac enrichment comparable to the single-compound treatments, affecting 2,181 and 1,955 peaks, respectively. However, both GSK789/GSK620 and I-BET151 led to a greater number of peaks with decreased H3K27ac enrichment, with 8,702 and 9,754 peaks showing reduced enrichment, respectively, nearly doubling the effect observed with single-compound treatments **(Figure 6.15)**.

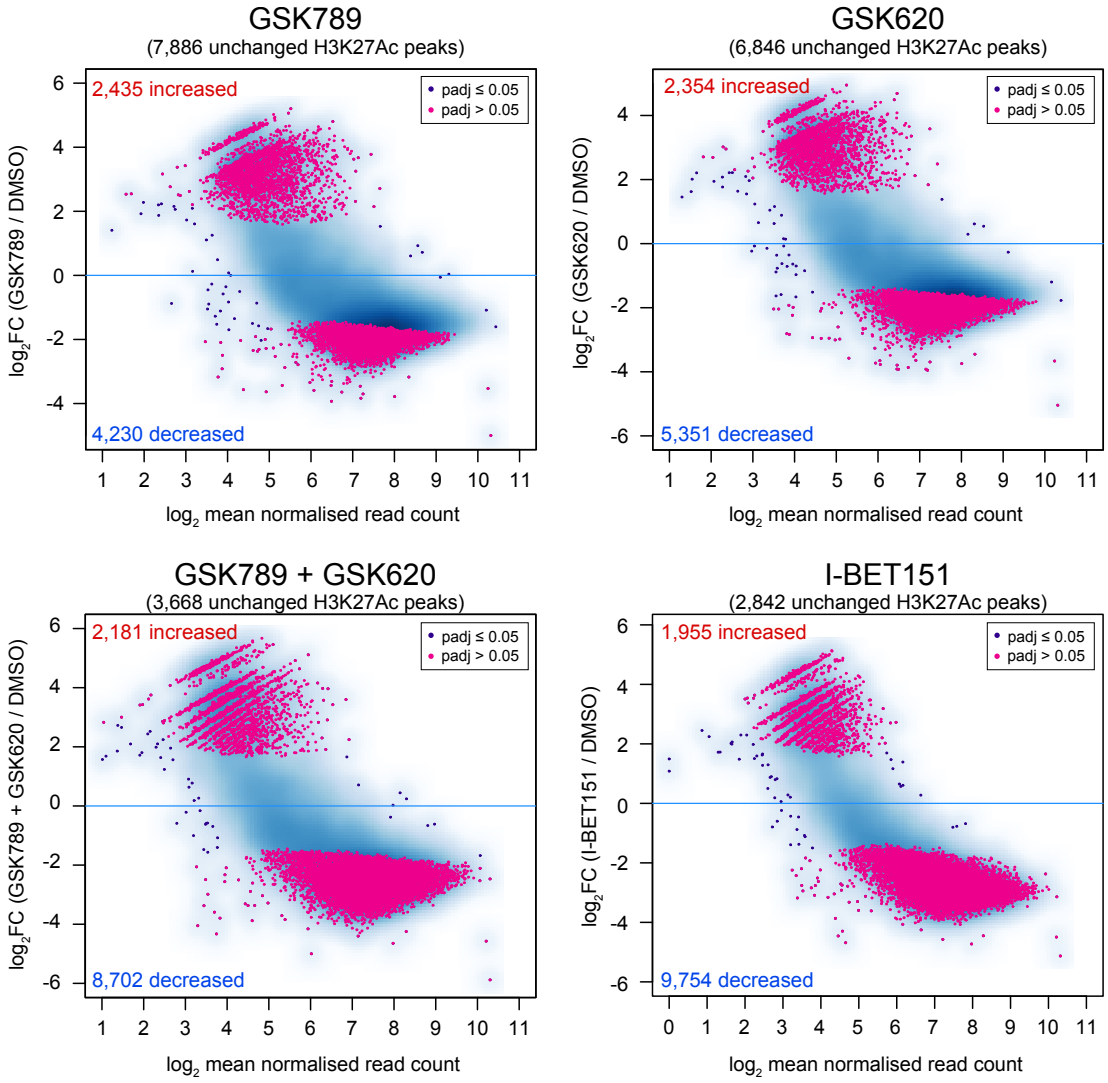

Figure 6.15. BET inhibition alters genome-wide H3K27ac enrichment in BON1 cells. MA plots showing differential H3K27ac enrichment in BON1 cells treated for 6 hours with 1 μM of GSK789, GSK620, I-BET151 or 0.5 μM each of GSK789 and GSK620. The x-axis represents the mean number of reads ($\log_2$ scaled) within the peaks across all samples. The y-axis represents the $\log_2$FC in H3K27ac enrichment compared to DMSO control. Points in magenta indicate peaks with a statistically significant increase or decrease in enrichment (adjusted $p \leq 0.05$) between treatment and control samples.

The 14,710 consensus H3K27ac peaks were categorised based on their location relative to transcription start sites (TSS), distinguishing between promoter (-3 kb upstream to +3 kb downstream of TSS) and non-promoter regions. Heatmap visualisation of H3K27ac signals at promoter regions revealed a decrease in enrichment across all treatment groups **(Figure 6.16A)**. This reduction was most pronounced following the combined GSK789/GSK620 treatment and I-BET151, indicating that targeting of both BD1 and BD2 may be required to fully displace H3K27ac from gene promoters. Interestingly, in non-promoter regions, the changes in H3K27ac enrichment were less marked, with some regions exhibiting an increase in signal after treatment with GSK789 and GSK620 alone **(Figure 6.16A)**.

Further examination of promoter and non-promoter regions revealed that the majority of H3K27ac peaks with decreased signal following BET inhibitor treatment were located in promoter regions within 1 kb of TSS. In contrast, H3K27ac peaks with increased signal were distributed across different genomic regions, with the majority located within intronic and distal intergenic regions **(Figure 6.16B)**. These findings suggest that, in BON1 cells, BET inhibitors exert a pronounced effect on regulatory elements essential for initiating gene expression, with a more nuanced impact on intronic and distal intergenic regions.

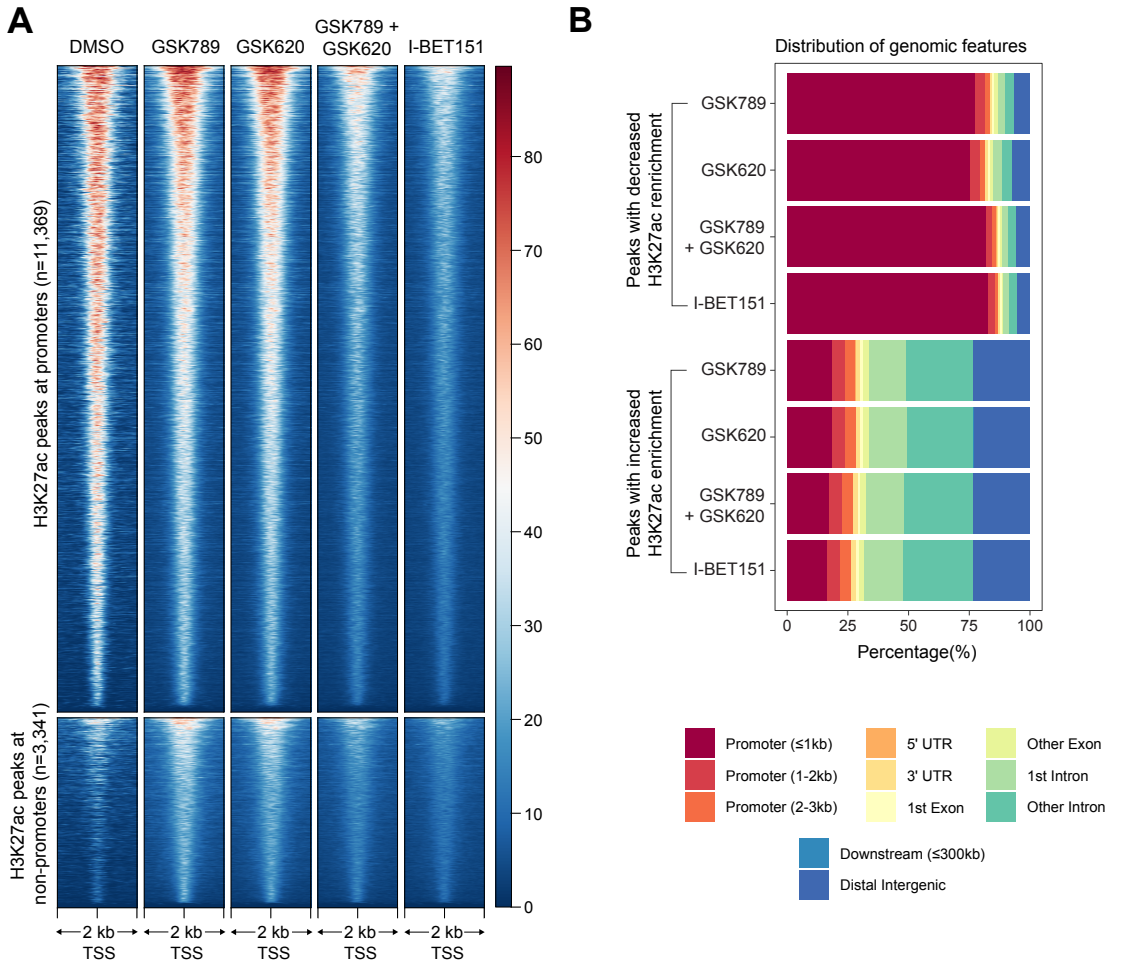

Figure 6.16. BET inhibition leads to decreased H3K27ac enrichment predominantly at promoter regions. (A) Heatmap visualisation of H3K27ac peaks at promoter regions (top panel) and non-promoter regions (bottom panel) across DMSO and BET inhibitor-treated BON1 cells. Each row represents a peak and is aligned at the TSS, extending 2kb upstream and downstream. Colour intensity reflects H3K27ac signal levels with red reflecting high enrichment signal and blue indicating lack of enrichment. **(B)** Distribution of genomic features for peaks with significantly altered H3K27ac enrichment, presented as a percentage for increased (top) and decreased (bottom) peaks across treatments. Colour key below indicates the type of genomic feature.

I next explored the biological pathways enriched in regions of differential H3K27ac binding using the Genomic Regions Enrichment of Annotations Tool (GREAT).[314] A Venn diagram of overlapping peaks *losing* H3K27ac enrichment after BET inhibitor treatments was constructed. This showed that H3K27ac binding was significantly decreased at 4,113 peaks across all treatment groups, indicating a core set of regulatory regions universally affected by BD-selective

and non-selective BET inhibitors **(Figure 6.17A)**. However, 3,214 peaks only showed loss of H3K27ac enrichment after treatment with either I-BET151 or the combination of GSK789/GSK620, suggesting that simultaneous BD1 and BD2 targeting is required to evict H3K27ac from chromatin at these specific sites **(Figure 6.17A)**. GREAT analysis showed that both sets of peaks losing H3K27ac were located close to the TSS in promoter-proximal regions **(Figure 6.17B & C)**. The 4,113 peaks with decreased H3K27ac enrichment across all groups were associated with genes involved in protein folding and stabilisation processes, indicating a potential disruption in cellular protein homeostasis regardless of whether BD1 or BD2 is inhibited **(Figure 6.17D)**. In contrast, the set of 3,214 peaks affected only by combined BD1 and BD2 inhibition were associated with genes involved in critical aspects of gene expression, such as mRNA processing and translation **(Figure 6.17E)**. These findings corroborate earlier RNA-seq and SLAM-seq findings that showed that targeting both BD1 and BD2 domains has a more substantial impact on gene expression.

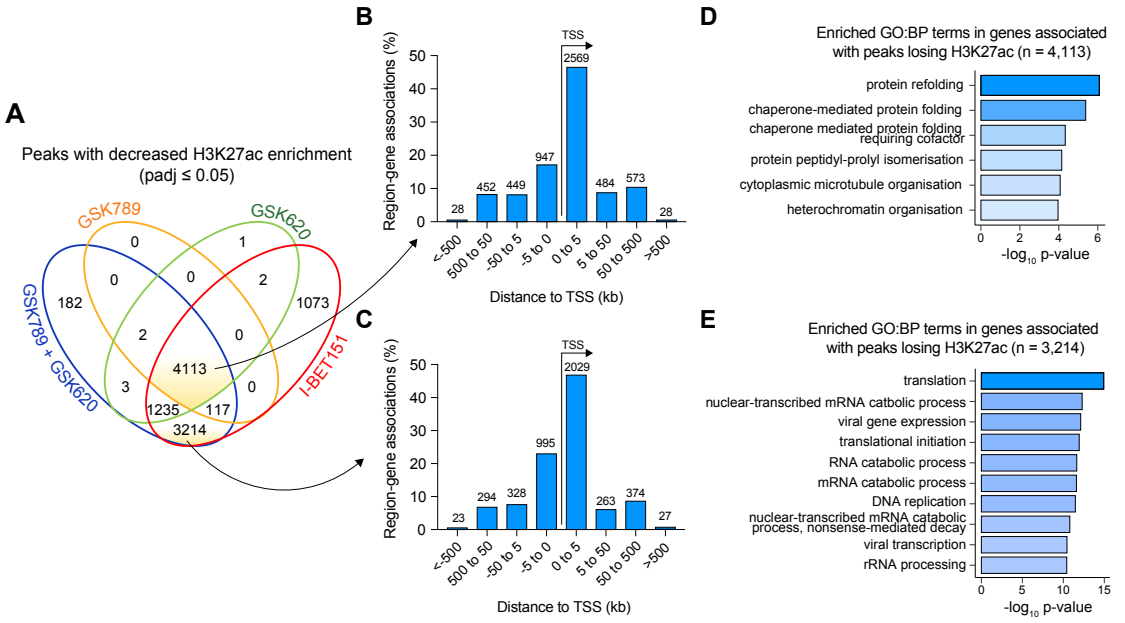

Figure 6.17. Simultaneous BD1 and BD2 inhibition decreases H3K27ac enrichment at promoters of genes involved in RNA processing and translation. **(A)** Venn diagram showing unique and shared H3K27ac ChIP-seq peaks with decreased enrichment after BET inhibitor treatments. [Caption continues on next page...]

Figure 6.17. Simultaneous BD1 and BD2 inhibition decreases H3K27ac enrichment at promoters of genes involved in RNA processing and translation **(B)** Distribution (relative to TSS) of 4,113 peaks with H3K27ac loss common to all treatments. **(C)** Distribution (relative to TSS) of 3,214 peaks with H3K27ac loss only after treatment with GSK789/GSK620 and I-BET151. Numbers above each bar indicate peak counts. **(D)** Enriched GO:BP terms in genes associated with the 4,113 universally affected peaks. **(E)** Enriched GO:BP terms in genes associated with the 3,214 peaks affected specifically by GSK789/GSK620 and I-BET151 treatment. Bar shading represents the statistical significance of the enrichment, represented as $-\log_{10}$ of the p-value.

A Venn diagram of overlapping peaks *gaining* H3K27ac enrichment after BET inhibition was also constructed. In contrast to the pattern of H3K27ac loss (where some peaks were uniquely affected by dual BD1 and BD2 inhibition) **(Figure 6.17A)**, almost all peaks with increased H3K27ac enrichment were shared across all treatment conditions **(Figure 6.18A)**. This points towards a general mechanism of transcriptional de-repression by BET inhibitors, irrespective of BD1 or BD2 selectivity. The majority of these 1,139 peaks were located 50 to 500 kb away from TSS **(Figure 6.18B)**, suggesting that BET inhibitors may activate distal regulatory elements, such as enhancers z. Enriched GO:BP terms for genes associated with these peaks highlighted processes related to endocrine pancreas development and differentiation **(Figure 6.18C)**. These findings are consistent with the GO:BP enrichment analysis of the RNA-seq data **(Figure 6.7C)** and suggest that BET inhibitors may reprogram BON1 cells towards a more differentiated phenotype.

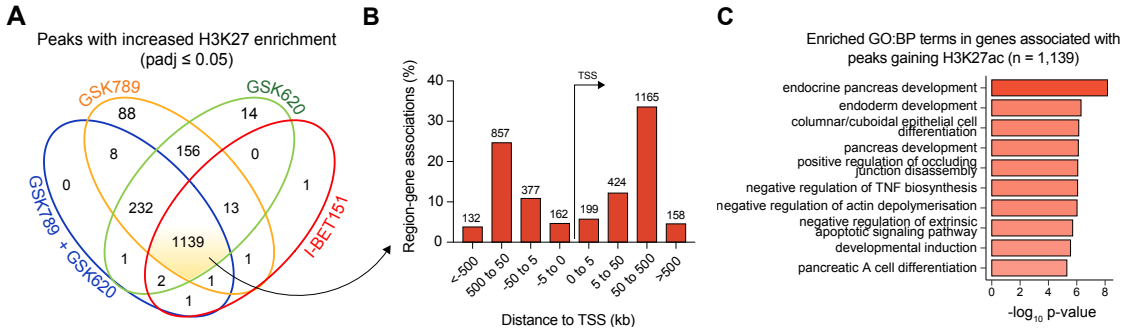

Figure 6.18. Simultaneous BD1 and BD2 inhibition increases H3K27ac enrichment at distal regulatory elements of genes involved in pancreas development and differentiation. **(A)** Venn diagram showing unique and shared H3K27ac ChIP-seq peaks with increased enrichment after indicated BET inhibitor treatments.

Figure 6.18. Simultaneous BD1 and BD2 inhibition increases H3K27ac enrichment at distal regulatory elements of genes involved in pancreas development and differentiation. (B) Distribution (relative to TSS) of 1,139 peaks gaining H3K27ac that were common to all treatments. Numbers above each bar indicate peak counts. **(C)** Enriched GO:BP terms in genes associated with the 1,139 universally affected peaks. Bar shading represents the statistical significance of the enrichment, represented as $-\log_{10}$ of the p-value.

6.2.10 Regions of H3K27ac loss following BET inhibition coincide with genome-wide BET protein binding sites

To examine whether regions of differential H3K27ac enrichment upon BET inhibition coincided with regions of BET protein occupancy, ChIP-seq data for BRD2, BRD3 and BRD4 from untreated BON1 cells were mapped to genomic regions with significantly altered H3K27ac marks. This analysis revealed that regions exhibiting a loss of H3K27ac enrichment post-treatment corresponded with sites bound by BET proteins, highlighting a targeted effect of BET inhibitors at functionally relevant genomic loci. In contrast, regions with gained H3K27ac after treatment were largely free of BET protein occupancy **(Figure 6.19A-D)**. These findings suggest that BET inhibition modulates H3K27ac enrichment not solely through direct displacement of BET proteins, but may also have indirect effects where increases in histone acetylation are not directly tied to BET protein binding.

6.2.11 BET inhibitors regulate the expression of PNET-relevant genes by reducing H3K27ac occupancy at super-enhancers

BET proteins are known to bind to super-enhancers (SE), which are cell type–specific regulatory regions that control the expression of genes crucial for cell lineage in normal tissues and oncogenes in cancer.[194,195] SEs are characterised by their high sensitivity to BET inhibition and their association with *MYC* expression in various cancers.[143,194] To explore the SE landscape of BON1 cells, I utilised the 'Ranking Ordering of SEs (ROSE)' algorithm,[129] which identified a total

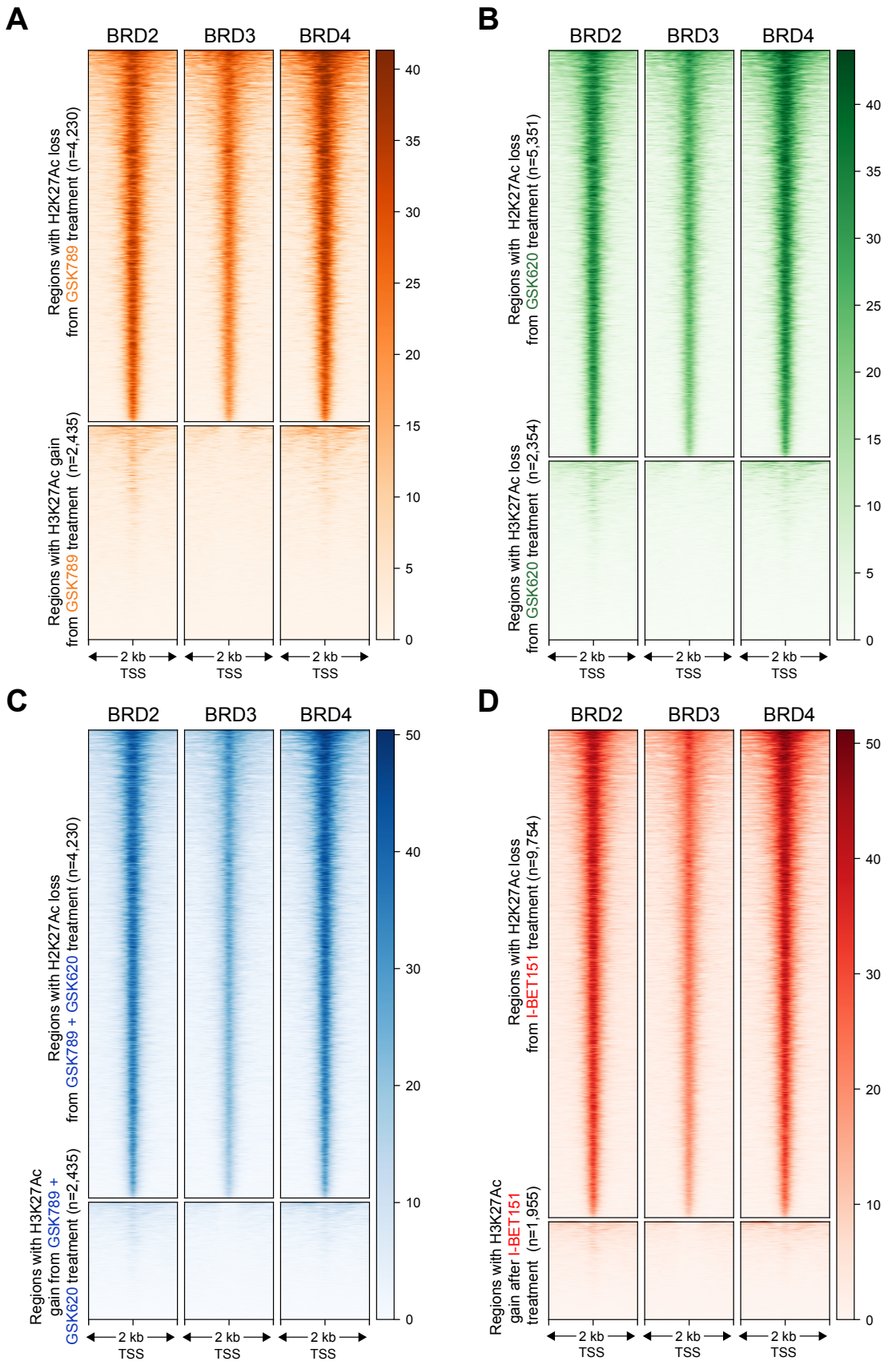

Figure 6.19. Regions of H3K27ac loss following BET inhibition coincide with genome-wide BET protein occupancy. [Caption continues on next page...]

Figure 6.19. Regions of H3K27ac loss following BET inhibition coincide with genome-wide BET protein occupancy. Heatmap visualisation of BRD2, BRD3 and BRD4 peak occupancy in untreated BON1 cells. BET protein ChIP-seq data were overlaid onto genomic regions with differential H3K27ac enrichment after treatment with **(A)** GSK789, **(B)** GSK620, **(C)** GSK789/GSK620 and **(D)** I-BET151, as seen in Figure 6.15. Each row represents a H3K27ac peak aligned to the TSS, extending 2kb upstream and downstream. Upper and lower sub-panels within each heatmap corresponding to regions of decreased and increased H3K27ac enrichment respectively. Colour intensity reflects occupancy signal of BRD2, BRD3 or BRD4, with darker shading reflecting higher enrichment.

of 476 SEs based on H3K27ac binding affinity **(Figure 6.20A)**. The median size of these SE regions was 16.3 kb, making them ~36-fold larger than typical enhancers, which had a median size of 454 bps. Genes associated with the identified SEs included those implicated in cancer, such as CREB-Binding Protein (*CREBBP*),[315] Lysine-Specific Demethyloase 4 (*KDM4B*)[316] and Zinc Finger Protein 217 (*ZNF217*),[317] as well as genes relevant to PNETs, including Somatostatin Receptor Type 5 (*SSTR5*),[318], Insulinoma-Associated 1 (*INSM1*),[319] Chromogranin A (*CHGA*) and NK2 Homeobox 2 (*NKX2-2*).[320] Notably, *MYC* was not found amongst the SE-associated genes.

ChIP-seq analysis showed a significant reduction in H3K27ac levels at SE sites after BET inhibitor treatment, regardless of whether the inhibition was BD-selective or non-selective. In contrast, typical enhancers showed increased sensitivity to dual BD1 and BD2 inhibition with I-BET151 or the combined GSK789/GSK620 treatment, as opposed to GSK789 or GSK620 alone **(Figure 6.20B)**. These findings suggest that the heightened sensitivity of SEs to BET inhibition in BON1 cells may occur independently of simultaneous BD1 and BD2 engagement.

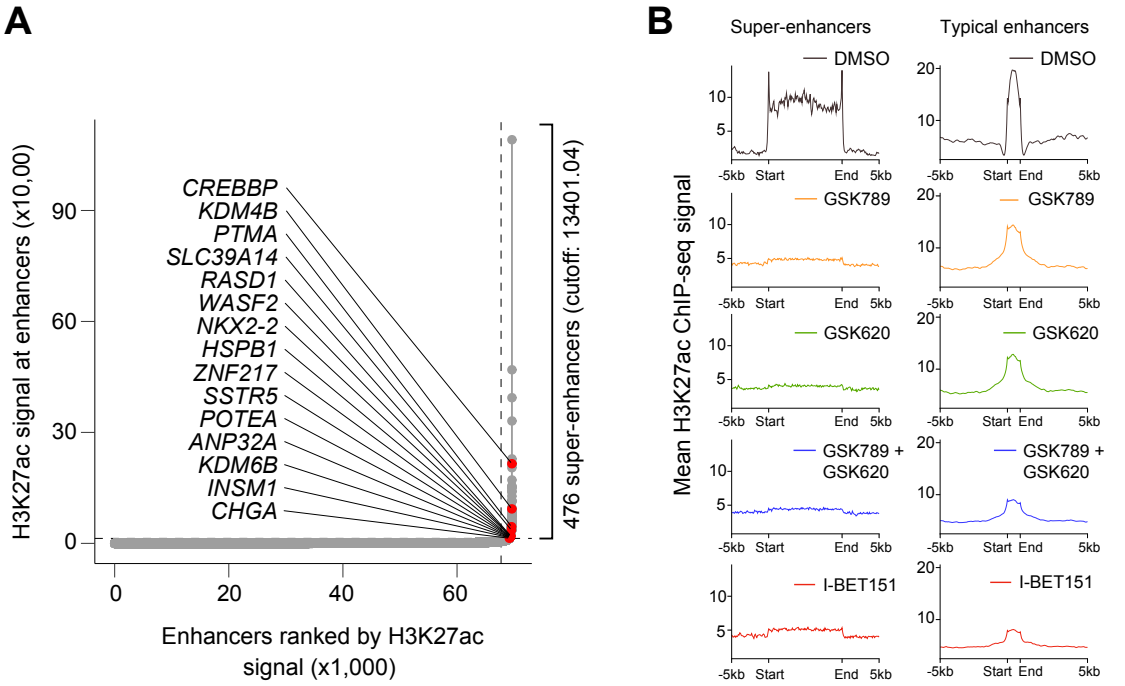

Figure 6.20. Characterisation of the SE landscape in BON1 cells. (A) Hockey stick plot showing the ranking of enhancer regions in BON1 cells based on normalised H3K27ac ChIP-seq signals from two biological replicates. The x-axis ranks enhancer regions by increasing H3K27ac signal intensity, shown on the y-axis. SEs are classified as those enhancers located to the right of the inflection point on the plot, with a H3K27ac signal cut-off of 13,401.04 as determined by the ROSE algorithm. Genes associated with SEs related to cancer or PNETs are labelled. **(B)** Metagene plots of global H3K27ac occupancy across all SEs and typical enhancers. The x-axis shows the start and end of the SE (left) or typical enhancer (right) regions, with ± 5 kb of adjacent sequence. The y-axis shows the mean H3K27ac signal density, normalised to reads per kilobase per million (RPKM).

GO:BP enrichment analysis of genes associated with the identified SEs highlighted the predominance of terms associated with nervous system development and neurogenesis **(Figure 6.21A)**. These findings align with the established role of SEs in sustaining cell identity[194] and underscores the evolutionary and functional link between neuroendocrine cells and neuronal pathways. Other terms enriched in SE genes included those related to RNA Polymerase II (RNA Pol II)-mediated transcription, consistent with the role of SEs in modulating genes critical for cell proliferation and survival.[194] To gain insights into possible transcription factors that may be involved in SE-associated transcriptional regulation in BON1 cells, *de novo* motif analysis was performed to identify sequence motifs enriched within SE

regions. This analysis identified DNA-binding motifs for a number of transcription factors that are regulated by, or are known to interact with, BET proteins, including snail family transcriptional repressor 2 (SNAI2),[321] mothers against decapentaplegic homolog 3 (SMAD3)[322] and paired box 5 (PAX5) **(Figure 6.21B)**.[323]

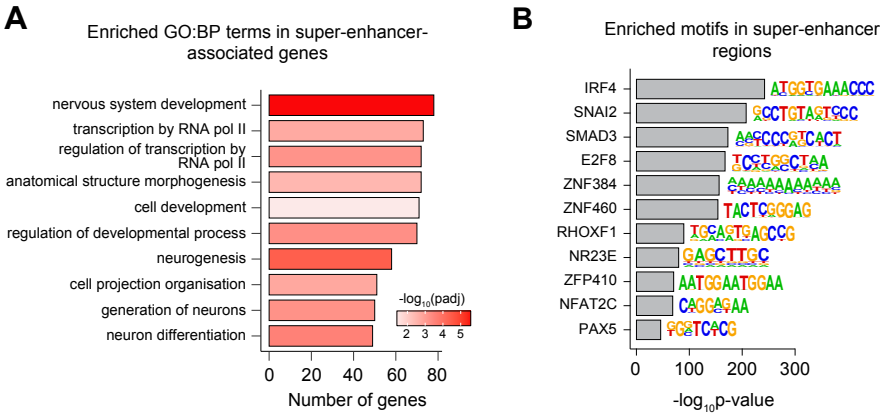

Figure 6.21. SE-driven genes in BON1 cells are implicated in endocrine lineage. (A) Bar plot showing the top 10 enriched GO:BP terms in 476 SE-associated genes identified in **Figure 6.20A**. The shading intensity of each bar represents the statistical significance of the enrichment, represented as $-\log_{10}$padj, with darker shading indicating higher statistical significance of the GO:BP terms. **(B)** Bar plot and sequence logos representing enriched motifs in SEs, ranked by $-\log_{10}$padj.

To identify high-confidence SEs in PNETs with relevance to BET inhibitor response, I leveraged publicly available ChIP-seq data (GSE140808) from a study that applied the ROSE algorithm to map the enhancer landscape in three human PNET samples.[324] These SEs were compared with those identified in BON1 cells. I further investigated their overlap with genes downregulated by both I-BET151 and GSK789/GSK620, as determined by SLAM-seq **(Figure 6.22A)**. This analysis led to the identification of two candidate genes: Refilin A (*RFLNA*) and NK2 Homeobox 2 (*NKX2-2*). Cross-referencing with the Super-Enhancer database (SEdb 2.0)[325] verified *NKX2-2*, but not *RFLNA*, as an SE in the pancreatic beta cell line EndoC-βH1 and in human pancreatic islets, with shared genomic coordinates in BON1 cells. Visualisation with the Integrated Genomics Viewer (IGV)[193] showed that BET protein occupancy paralleled H3K27ac distribution at the *NKX2-2* SE region in both BON1 cells and in human PNET samples **(Figure 6.22B)**. Despite these insights into the mechanistic roles of *NKX2-2* and *RFLNA*, RNA-seq analysis

of metastatic PNETs from the Mayo Clinic cohort revealed no upregulation of either gene compared to localised tumours and no association with survival outcomes.

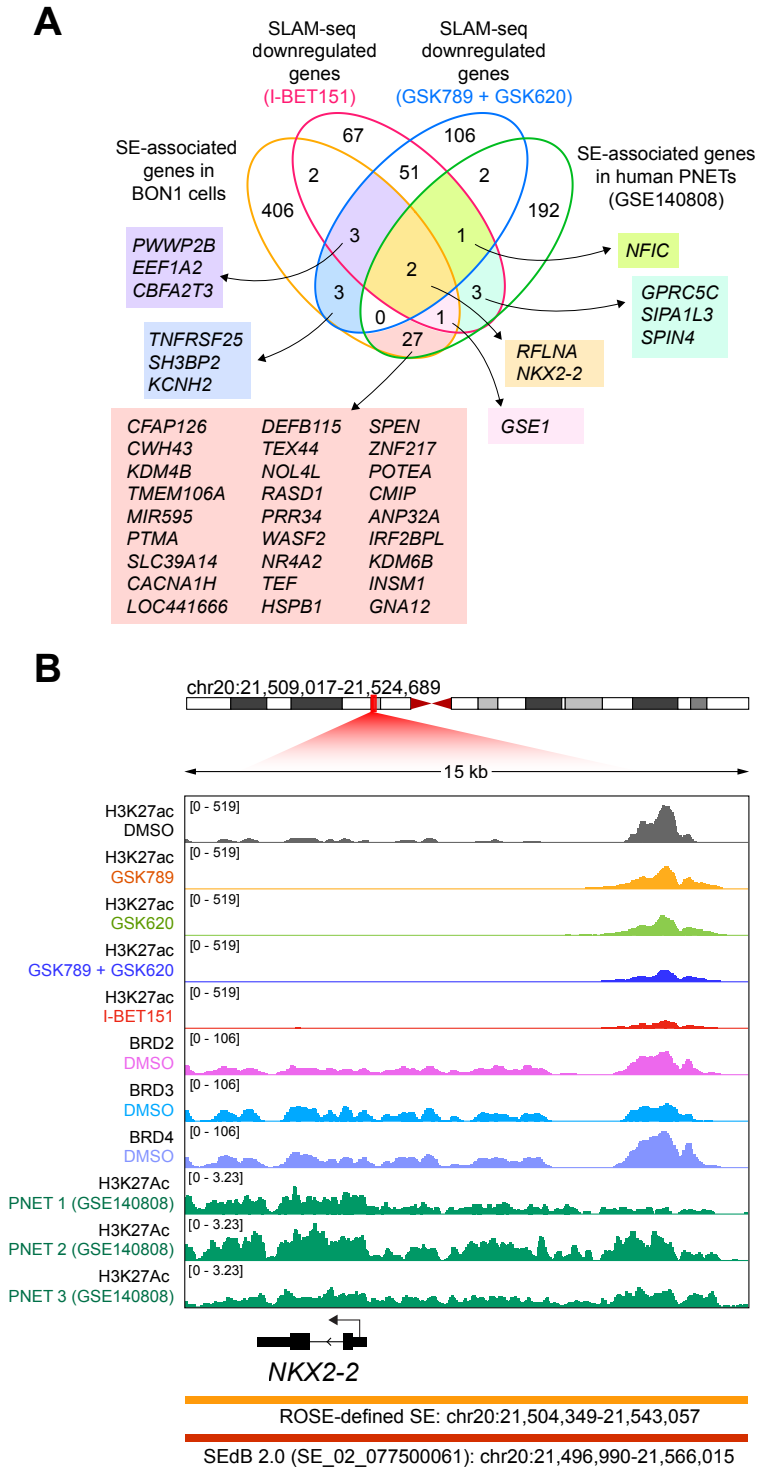

Figure 6.22. *NKX2-2* and *RFLNA* are BET inhibitor-responsive, SE-driven genes in BON1 cells and human PNETs. [Caption continues on next page...]

Figure 6.22. *NKX2-2* and *RFLNA* are BET inhibitor-responsive, SE-driven genes in BON1 cells and human PNETs. (A) Venn diagram showing the number of SE-associated genes in BON1 cells (orange ellipse) and in human PNET samples from the GSE140808 dataset (green ellipse). Magenta and blue ellipses contain genes with decreased nascent transcription per SLAM-seq following treatment with I-BET151 and the combination of GSK789/GSK620, respectively. Listed outside the Venn diagram are the names of genes associated with each overlap category.**(B)** IGV genome browser tracks showing H3K27ac and BET protein occupancy at the *NKX2-2* locus. Genomic coordinates on chromosome 20 are indicated, with a 15 kb region highlighted. H3K27ac profiles are shown for BON1 cells treated with DMSO control, 1 μM GSK789, GSK620, I-BET151, and 0.5 μM each of GSK789/GSK620. H3K27ac binding profiles from three human PNET samples in the GSE140808 dataset are also presented in addition to tracks showing binding peaks of BRD2, BRD3, and BRD4 in control-treated BON1 cells. The y-axis for each track denotes the range of read counts within square brackets. The *NKX2-2* gene is marked below the tracks, and the SE region is defined according to both ROSE algorithm coordinates (orange bar) and the SEdb 2.0 entry 'SE_02_077500061' (red bar).

Amongst the 30 SE-related genes shared by BON1 cells and human PNETs in the GSE140808 dataset, 27 showed no change in nascent transcription following 6 hours of treatment with I-BET151 or GSK789/GSK620, as per SLAM-seq analysis. To discern downstream changes that may not have been captured at an early time point, I extended the analysis to include RNA-seq data after 48 hours of treatment. This also revealed only two genes at the intersection of the RNA-seq and ChIP-seq datasets: Dexamethasone-Induced Ras-Related Protein 1 (*RASD1*) and Solute Carrier Family 39 Member 14 (*SLC39A14*) **(Figure 6.23A)**. Although *RFLNA* and *NKX2-2* exhibited downregulation in both SLAM-seq and RNA-seq analyses, a significant decrease in their expression on RNA-seq was observed only after treatment with I-BET151, rather than with the combination of GSK789/GSK620. Querying SEdb 2.0 confirmed the presence of *RASD1* and *SLC39A14* as SE-associated genes in EndoC-βH1 cells and in human pancreatic islets. Visualisation with IGV showed that BET proteins had a similar occupancy pattern as H3K27ac at the *RASD1* SE region in BON1 cells and in human PNET samples, suggesting a regulatory interaction **(Figure 6.23B)**, however, this pattern was not observed at the *SLC39A14* locus. Regardless, in the context of human PNETs in the Mayo Clinic cohort, neither *RASD1* nor *SLC39A14* demonstrated upregulation in metastatic

tumours or any association with patient survival, indicating a potential discrepancy between SE-driven gene expression and disease progression.

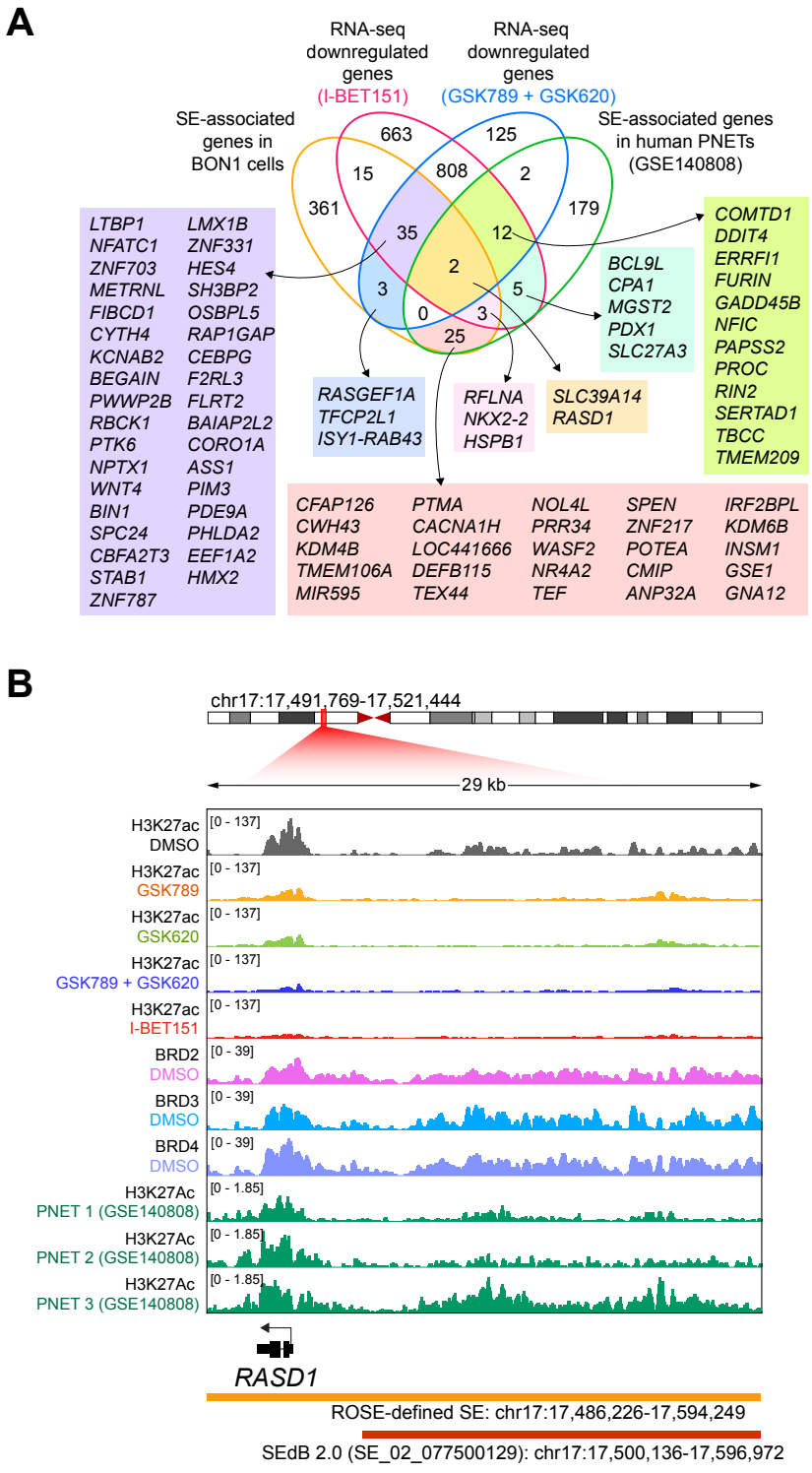

Figure 6.23. *RASD1* and *SLC39A14* are BET inhibitor-responsive, SE-driven genes in BON1 cells and human PNETs. [Caption continues on next page...]

Figure 6.23. *RASD1* and *SLC39A14* are BET inhibitor-responsive, SE-driven genes in BON1 cells and human PNETs. (A) Venn diagram showing the number of SE-associated genes in BON1 cells (orange ellipse) and in human PNET samples from the GSE140808 dataset (green ellipse). Magenta and blue ellipses represent genes with decreased transcription per RNA-seq following treatment with I-BET151 and the combination of GSK789/GSK620, respectively. Listed outside the Venn diagram are the names of genes associated with each overlap category. **(B)** IGV genome browser tracks showing H3K27ac and BET protein occupancy at the *RASD1* locus. Genomic coordinates on chromosome 17 are indicated, with a 29 kb region highlighted. H3K27ac profiles are shown for BON1 cells treated with DMSO control, 1 μM GSK789, GSK620, I-BET151, and 0.5 μM each of GSK789/GSK620. H3K27ac binding profiles from three human PNET samples in the GSE140808 dataset are also presented as well as tracks showing binding peaks of BRD2, BRD3, and BRD4 in DMSO-treated BON1 cells. The y-axis for each track denotes the range of read counts within square brackets. The *RASD1* gene is marked below the tracks, and the SE region is defined according to both ROSE algorithm coordinates (orange bar) and the SEdb 2.0 entry 'SE_02_077500129' (red bar).

6.2.12 Integrated ChIP-seq and transcriptomic analyses identify BET inhibitor candidates with clinical relevance in PNETs

Having established the genomic regions affected by BET inhibition, I subsequently integrated my ChIP-seq findings with transcriptomic data presented earlier in this chapter to more confidently identify potential therapeutic candidates in PNETs. I initially identified genes with H3K27ac loss at their promoter regions and concurrent SLAM-seq downregulation following simultaneous BD1 and BD2 inhibition. Focusing on genes consistently altered by both GSK789/GSK620 and I-BET151 yielded a high-confidence subset of 30 candidate targets **(Figure 6.24A)**. Pathway enrichment analysis indicated that these genes were significantly associated with cell cycle-related Reactome terms, such as 'mitotic G1 phase and G1/S transition' (adjusted $p = 0.001$) and 'G1/S transition' (adjusted $p = 0.02$). A network map generated by STRING (Search Tool for Retrieval of Interacting Genes/Proteins)[326] software highlighted *E2F2*, *CCND1*, Minichromosome Maintenance Complex Component 2 (*MCM2*) and *MCM5* as central nodes within a cell cycle-related interaction network **(Figure 6.24B)**. Amongst these genes, only *E2F2* showed elevated expression in metastatic compared to localised PNETs in the Mayo Clinic cohort.

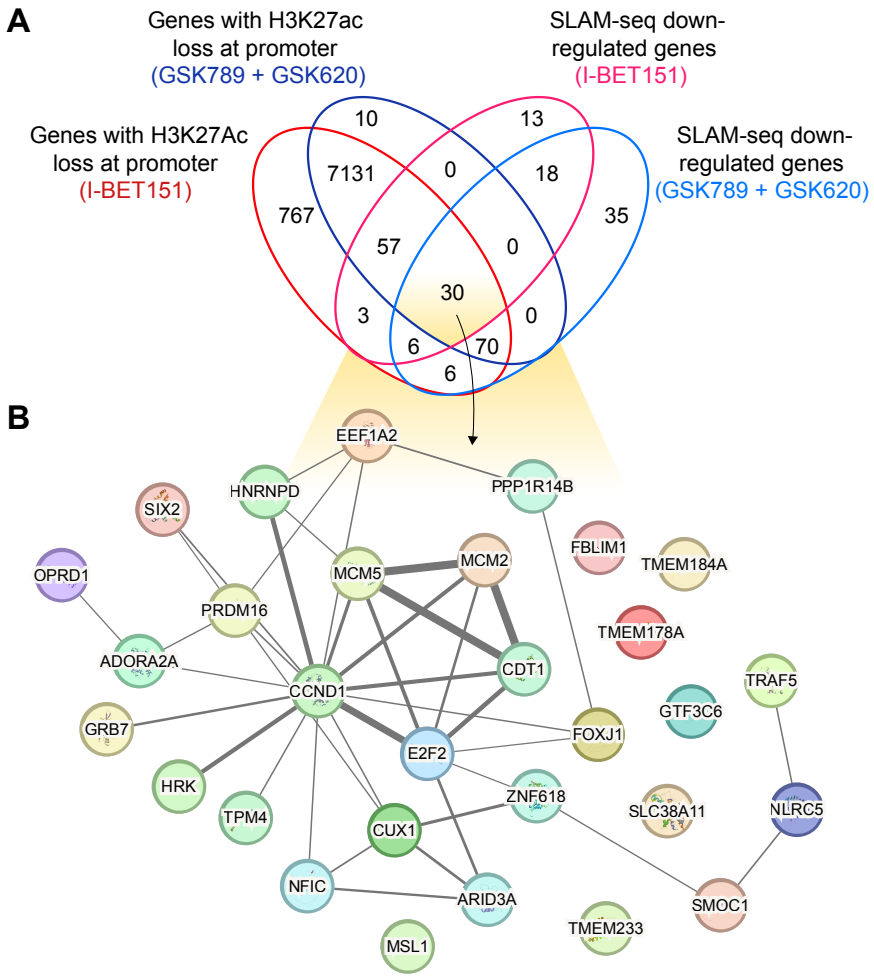

Figure 6.24. Integrated ChIP-seq and SLAM-seq analysis identifies direct targets of simultaneous BD1 and BD2 inhibition. (A) Venn diagram illustrating overlap between genes with H3K27ac loss at promoter regions and those with downregulated expression according to SLAM-seq data, following 6 hours of treatment with 0.5 μM each of GSK789/GSK620 or 1 μM of I-BET151. **(B)** STRING network map depicting interactions among the 30 candidate genes identified in (A). The thickness of the connecting lines indicates the strength of the relationship between two nodes, as calculated by STRING.

To correlate downstream transcriptional changes with the initial loss of H3K27ac at promoter regions following simultaneous BD1 and BD2 inhibition, I additionally examined the overlap between ChIP-seq and RNA-seq datasets, identifying 430 candidate genes **(Figure 6.25A)**. Pathway enrichment analysis of these genes revealed GO:BP terms associated with RNA processing and synthesis, such as 'ncRNA metabolic process' (adjusted $p < 0.0001$), 'ribosome biogenesis' (adjusted $p = 0.0007$) and cell cycle, such as 'mitotic cell cycle' (adjusted $p = 0.003$) **(Figure**

6.25B). Nine of the 30 genes exhibiting loss of H3K27ac at their promoters and showing downregulated expression according to SLAM-seq, also demonstrated downregulation in RNA-seq data: *CCND1*, Eukaryotic Translation Elongation Factor 1 Alpha 2 (*EEF1A2*), NLR Family CARD Domain Containing 5 (NLRC5), Forkhead Box J1 (*FOXJ1*), Tropomyosin 4 (*TPM4*), Transmembrane Protein 233 (*TMEM233*), Nuclear Factor I C (*NFIC*), PR/SET Domain 16 (*PRDM16*) and General Transcription Factor IIIC Subunit 6 (*GTF3C6*). Despite not being downregulated per SLAM-seq, *CKAP2L*, an upstream regulator that was identified in metastatic PNETs in Chapter 4, lost H3K27ac enrichment at its promoter and was downregulated according to RNA-seq.

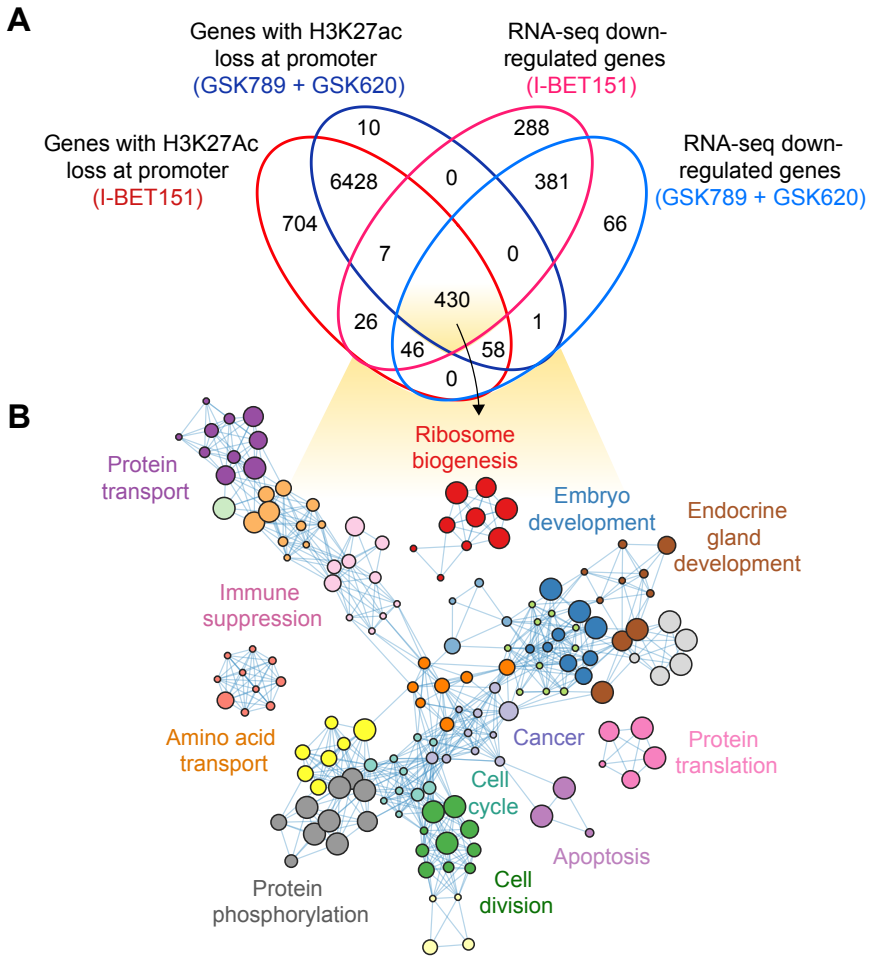

Figure 6.25. Integrated ChIP-seq and RNA-seq analysis identifies downstream transcriptional changes following loss of H3K27ac enrichment. [Caption continues on next page...]

Figure 6.25. ntegrated ChIP-seq and RNA-seq analysis identifies downstream transcriptional changes following loss of H3K27ac enrichment. **(A)** Venn diagram illustrating overlap between genes with H3K27ac loss at promoter regions and those with downregulated expression according to RNA-seq data, following 6 hours of treatment with 0.5 μM each of GSK789/GSK620 or 1 μM of I-BET151. **(B)** Metascape network diagram showing the relationship between enriched GO terms in 430 candidate genes identified in (A). Major pathway clusters are labelled.

Based on the comprehensive analyses described above, I selected three top candidate genes: *E2F2*, *CCND1*, and *CKAP2L*, for further investigation. These genes exhibited distinct patterns of response to BET inhibition: *E2F2* was uniquely affected in SLAM-seq, indicating immediate transcriptional impact, *CCND1* exhibited changes in both SLAM-seq and RNA-seq, pointing to sustained inhibition effects, and *CKAP2L* was highlighted for its downregulation in RNA-seq alone, suggesting its role as a late key player in the mechanistic response.

IGV was used to visualise H3K27ac peaks at the promoter regions of *E2F2* **(Figure 6.26A)**, *CCND1* **(Figure 6.26B)** and *CKAP2L* **(Figure 6.26C)**. This analysis revealed a treatment-associated reduction in H3K27ac occupancy within these regions, with the most significant reduction observed after treatment with I-BET151 or the combination of GSK789/GSK620.

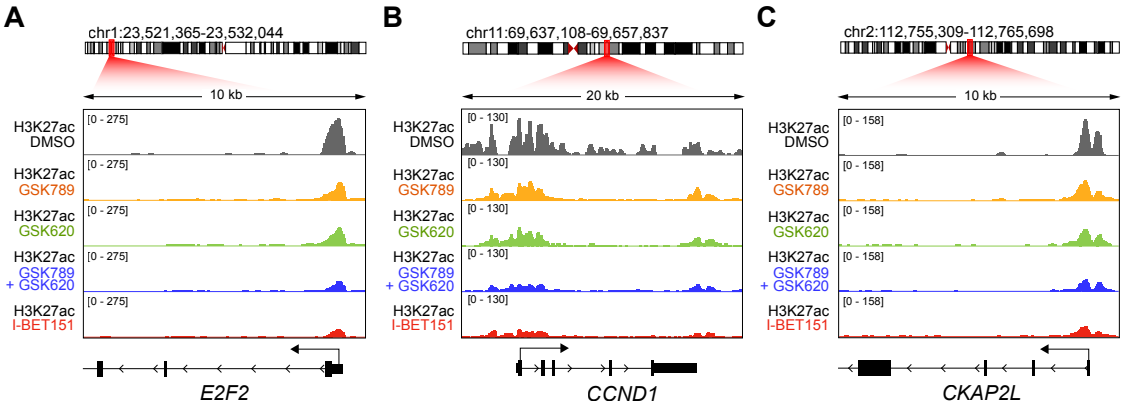

Figure 6.26. Simultaneous BD1 and BD2 inhibition leads to greater loss of H3K27ac occupancy at promoters of key BET inhibitor target genes. IGV browser tracks showing the binding profiles of two merged biological replicates of H3K27ac ChIP-seq reads at the promoter regions of **(A)** E2F2, **(B)** CCND1 and **(C)** CKAP2L in BON1 cells following 6 hours of treatment with DMSO control, 1 μM of GSK789, GSK620, I-BET151 or 0.5 μM each of GSK789/GSK620. Numbers in square brackets indicate the ranges of read counts.

Next, I examined the clinical relevance of the three selected BET inhibitor target genes by assessing the correlation between their mRNA expression levels in the Mayo Clinic cohort and the Ki-67 index, a well-established marker of proliferation and PNET aggressiveness. A moderate positive correlation was observed for *E2F2* ($r = 0.41$, p = 0.006) **(Figure 6.27A)**, while *CCND1* demonstrated a weak and statistically non-significant correlation ($r = 0.08$ p = 0.60) **(Figure 6.27B)**. Conversely, *CKAP2L* showed a strong positive correlation ($r = 0.53$, p = 0.0002) **(Figure 6.27C)** with the Ki-67 index, underscoring its potential role in tumour cell proliferation in aggressive PNETs.

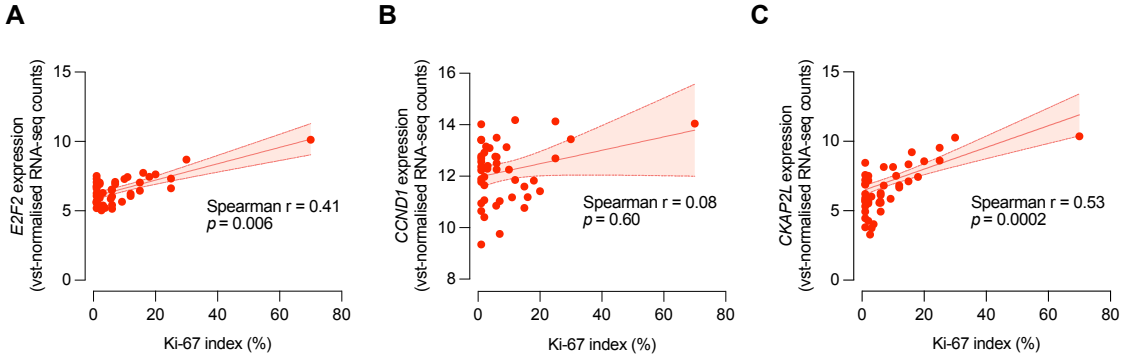

Figure 6.27. *E2F2* and *CKAP2L* mRNA expression levels correlate with Ki-67 index in human PNETs. Scatter plots illustrating the relationship between vst-normalised mRNA expression levels of **(A)** *E2F2*, **(B)** *CCND1* and **(C)** *CKAP2L* (from RNA-seq data from the Mayo Clinic PNET cohort) and the Ki-67 proliferation index (from surgical pathology reports). Spearman's rank correlation coefficient (r) and associated p-values are reported for each gene, indicating the strength and significance of the correlations. Red shaded areas suggest confidence intervals around the best-fit lines. vst = variance-stabilising transformation.

I subsequently explored the relationship between *E2F2*, *CCND1* and *CKAP2L* expression and clinical outcomes in patients with PNETs in the Mayo Clinic cohort. Utilising RNA-seq data, the expression levels for each gene were dichotomised into high- and low-expression groups based on median values. Differences in progression-free survival (PFS) were compared via Kaplan-Meier analysis. This analysis indicated a significantly reduced PFS in patients with high *E2F2* expression compared to those with low expression (median 22 months *vs* 120 months, p = 0.048) **(Figure 6.28A)**. In contrast, there was no significant difference in PFS

in patients with high *vs* low *CCND1* expression **(Figure 6.28B)**. Notably, high *CKAP2L* expression was associated with a marked reduction in PFS relative to low expression (median 23 months *vs* 105 months, p = 0.03) **(Figure 6.28C)**. These findings collectively reveal that *E2F2* and *CKAP2L* are key targets of BET inhibition, with their expression levels directly linked to differing survival outcomes in PNET patients. Moreover, the suppression of these targets requires both BD1 and BD2 to be concurrently inhibited.

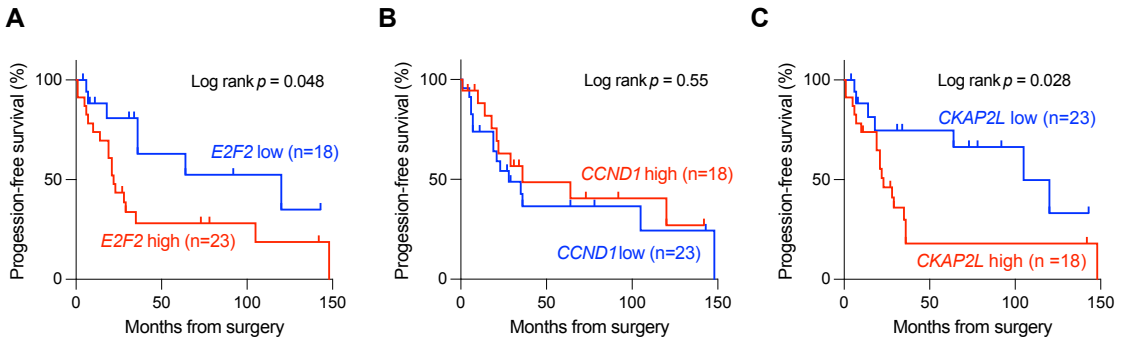

Figure 6.28. High *E2F2* and *CKAP2L* mRNA expression levels are associated with worse survival outcomes in human PNETs. Kaplan-Meier survival curves comparing PFS of patients with PNETs from the Mayo Clinic cohort, stratified into high (red line) and low (blue line) expression groups, based on median RNA-seq expression values for **(A)** *E2F2*, **(B)** *CCND1* and **(C)** *CKAP2L*. The log-rank test was applied to determine the statistical significance of differences in PFS between groups. The number of patients in each group is denoted in parentheses.

6.3 Discussion

In this chapter, I described the effects of BET inhibitors on modulating the transcriptomic and epigenomic landscape in BON1 PNET cells, with a focus on delineating the differential impact of targeting BD1 and BD2. Building upon the findings of the previous chapter, my bioinformatics analyses revealed that simultaneous inhibition of BD1 and BD2 induces more extensive changes in gene expression and histone acetylation patterns compared to targeting either domain individually. Furthermore, my studies have highlighted *E2F2* and *CKAP2L* as key BET inhibitor targets, which were downregulated only by combined BD1

and BD2 targeting, and whose expression levels correlated with PNET patient survival outcomes. Importantly, these findings challenge recent assertions that BD1-selective targeting is sufficient to phenocopy the effect of dual BD inhibition across all cancer contexts.[152,299,327]

6.3.1 The rationale for domain-selective BET inhibitors

A primary challenge encountered in the clinical translation of first-generation BD non-selective BET inhibitors has been the emergence of dose-limiting adverse effects, such as anaemia, thrombocytopaenia and gastrointestinal toxicity.[151,299] These toxicities occur independently of cancer type or the underlying chemical structure of the BET inhibitor compound being tested.[328] One attempted strategy for mitigating these effects has been to employ intermittent dosing schedules; however this is offset by a decrease in efficacy. Indeed, overall remission rates (complete or partial response) for first-generation BET inhibitors in oncology clinical trials, outside nuclear protein in testis (NUT) midline carcinoma (NMC), are generally $<$ 30%,[329–331] contrasting with the robust efficacy observed in pre-clinical studies.

Strategies such as combination therapies with other classes of anti-cancer medications, refined biomarker identification and improved patient stratification may provide an avenue for improved efficacy rates. However, overcoming challenges related to toxicity may be best achieved through the use of next-generation inhibitors that selectively target either BD1 or BD2 of the BET proteins. The impetus for their development comes from emerging *in vitro* evidence supporting distinct roles for BD1 and BD2 in various disease-related contexts. For example, it has been shown that BD1 is important for anchoring BET proteins to chromatin via binding to acetylated histones and thus in the maintenance of basal gene expression.[152,155,302] In contrast, BD2 has broader binding specificity for di-acetylated peptides on non-histone proteins, such as transcription factors, and facilitates gene expression in response to external stimuli.[152,303,332]

6.3.2 BD1-selective, BD2-selective and dual BD inhibition are each associated with distinct transcriptional changes in BON1 cells

My RNA-seq studies in BON1 cells revealed that 48 hours of treatment with 1 μM of GSK789 or GSK620 significantly altered the expression of ~5 and ~34 times fewer genes, respectively, than their combined administration at 0.5 μM each. This pattern was corroborated by SLAM-seq, which indicated that the number of differentially expressed nascent transcripts was 6 and 38 times fewer after treatment with 1 μM of GSK789 or GSK620, respectively, compared to their combination at 0.5 μM each. These findings diverge in part from those reported by Gilan et al.,[152] who also conducted SLAM-seq after 6 hours of treatment with 1 μM of the BD1-selective inhibitor GSK778, the BD2-selective inhibitor GSK046 and I-BET151 in two leukaemia cell lines. While their observations of minimal gene expression changes with BD2-selective inhibition align with my findings in BON1 cells, they reported that the gene expression alterations induced by BD1-selective inhibition were comparable to those by dual BD inhibition with I-BET151. These discrepant findings may be attributable to the distinct cellular context of PNETs *vs* leukaemia, or the pharmacological profiles of the specific BET inhibitor compounds used. For example, while GSK778 exhibits ~140-fold selectivity for BD1, it has been shown to partially inhibit BD2 at concentrations of 1 μM.[152] As illustrated in the synergy experiments in the previous chapter (see **Figure 5.9** on page 149), even a small amount of BD2 inhibition (e.g. with the addition of nanomolar concentrations of GSK620) when combined with BD1 inhibition, amplifies the suppressive impact on cell viability. Therefore, the apparent similarity between GSK778 and I-BET151 in the study by Gilan et al.[152] may reflect a shared mechanism of dual BD inhibition at the tested concentrations. In contrast to the first described BD-selective inhibitors, which exhibited either weak potency or limited ($\leq$ 100-fold) domain selectivity,[333] both GSK789 and GSK620 possess excellent selectivity for BD1 (>1000-fold)[156] and BD2 (>200-fold),[157] respectively. This high degree of selectivity strengthens

the likelihood that the results presented in this chapter are reflective of the true impact of domain-selective inhibition.

My finding that simultaneous inhibition of both BD1 and BD2 was necessary to achieve the full effect of BET inhibitors on gene expression in BON1 cells is consistent with a study that employed a novel 'bump-and-hole' chemical biology approach to mechanistically delineate the roles of both domains.[154] The authors engineered structurally non-disruptive mutations ('holes') into BD1 and BD2 across BET family members in a human osteosarcoma cell line, followed by synthesis of orthogonal 'bumped' BET inhibitors with high specificity for these modified domains. Fluorescence recovery after photobleaching (FRAP) assays revealed BD1 as the primary driver of chromatin binding, although BD2 also had a small impact. Interestingly, the influence of BD1 varied among BET proteins, with BRD3 most affected by BD2-selective inhibition. Nonetheless, targeting of both BDs was required for full displacement of all BET proteins from chromatin. Studies have also demonstrated BD2's crucial role in transcription initiation through its recruitment of non-histone proteins. Shi et al.[303] observed that while BD1 binds to acetylated histones, the transcription factor Twist simultaneously binds to BD2 of BRD4, facilitating the recruitment of the positive transcription elongation factor b (P-TEFb)/RNA Pol II transcription complex at target gene promoters and enhancers. Together, these findings underscore a cooperative role for BD1 and BD2 in the regulation of chromatin dynamics and gene expression by BET proteins. I hypothesise that the moderate perturbation in gene expression observed with BD1 inhibition in BON1 cells could result from a compensatory mechanism mediated by BD2, either through its recruitment of transcription factors or via residual chromatin binding activity.

6.3.3 Differences in transcriptomic response between I-BET151 and combination GSK789/GSK620 treatment

RNA-seq analyses in this chapter revealed that I-BET151 broadly altered downstream gene expression, more so than combined treatment with GSK789/GSK620, despite both strategies targeting BD1 and BD2 simultaneously. Whilst the extensive transcriptomic perturbations induced by I-BET151 could be seen as beneficial from an efficacy standpoint, they also raise concerns about increased toxicity. Interestingly, the combination of GSK789 and GSK620 induced a more selective transcriptomic response, while achieving comparable effects on cell viability (as shown in the previous chapter), at half the concentration of I-BET151. The ability to reduce dosage without compromising efficacy highlights a notable advantage of the combination BD1- and BD2-selective inhibitor approach, as this could potentially widen the therapeutic window and lower the risk of adverse events.

Amongst the GO:BP terms uniquely downregulated by I-BET151, 'regulation of cellular component organisation' was the most significantly impacted. This pathway encompasses processes fundamental to the precise organisation and function of cellular components, essential for maintaining cellular integrity and homeostasis. Downregulation of these processes by I-BET151 suggests a broad-reaching interference on cellular architecture and dynamics, undermining both the structural and functional stability of cells. While such effects may contribute towards the anti-proliferate impact of I-BET151, they could also lead to dose-limiting toxicities given the importance of these processes for the normal functioning of non-cancer cells. The combined targeting of BD1 and BD2 by GSK789 and GSK620, which downregulated ~1.5 times fewer genes than I-BET151, may offer a more nuanced approach to achieving a balance between disrupting cancer cell mechanisms while preserving essential cellular processes. Indeed, the pathways downregulated by both GSK789/GSK620 and I-BET151 were linked to the regulation of cell proliferation, response to external signals and signal transduction, indicating a more

focused disruption of cancer cell growth mechanisms without broadly impacting the fundamental processes essential for the viability of normal cells.

Upregulated GO:BP terms shared by both I-BET151 and the combination of GSK789/GSK620 were related to neuronal development and cilium assembly, suggesting that dual BD inhibition in PNET cells reprograms transcription towards a more differentiated state. Loss of cilia is frequently observed in cancers and contributes to tumourigenesis through disruption of growth-inhibitory signalling pathways;[334] thus, upregulation of cilia assembly and organisation may be a desired consequence of BET inhibition. The upregulated pathways unique to I-BET151 largely mirrored those jointly elevated by both I-BET151 and the GSK789/GSK620 combination, suggesting that the distinct toxicity profile of I-BET151 could stem more from its broad inhibition of essential cellular functions rather than from the activation of pathways linked to cell differentiation and development.

There are several possible reasons for why I-BET151 induced more extensive alterations in gene expression compared to the combination of GSK789 and GSK620, despite their shared mechanism of simultaneous BD1 and BD2 inhibition. At concentrations of ~1 μM, I-BET151 may also inhibit CREB-binding protein (CREBBP) and E1A binding protein p300 (EP300),[152] two transcriptional coactivators that regulate gene expression through histone acetyltransferase activity, and whose bromodomains share sequence homology with the BD1 and BD2 of the BET proteins.[152] In contrast, neither GSK789 nor GSK620 have been shown to engage non-BET bromodomain containing proteins at concentrations of 1 μM or less. It is also possible that I-BET151 might also interact with other proteins via bromodomain-independent mechanisms, as was recently shown with JQ1.[335] Lastly, the binding affinities of I-BET151, GSK789 and GSK620 for their respective bromodomains may differ; therefore, the chosen concentration of 0.5 μM each for GSK789 and GSK620 may not fully match the inhibitory effects of 1 μM of I-BET151, despite aiming for comparable target engagement of both BD1 and BD2.

6.3.4 *CKAP2L* and *E2F2* are clinically-relevant BET inhibitor targets in patients with PNETs

Building upon the findings of Chapter 4, in which *E2F2* mRNA expression and E2F targets were observed to be upregulated in metastatic compared to localised PNETs, this chapter identifies *E2F2* as a direct early target of simultaneous BD1 and BD2 inhibition. The E2F family of transcription factors are master regulators of the cell cycle, especially during the G1 to S phase transition, and are involved in DNA repair, differentiation and apoptosis.[336] The mammalian genome encodes eight known E2F proteins (E2F1-E2F8), and their transcriptional output is the cumulative effect of different family members that mediate both activator and repressor functions in a context-dependent manner.[337] Aberrant E2F2 activity has been implicated in various cancers, including glioblastoma[338] and ovarian cancer[339], and has been shown to mediate resistance to gemcitabine chemotherapy in pancreatic adenocarcinoma.[340] Although the role of E2F2 and interplay with BET proteins in PNETs has not previously been explored, existing literature demonstrates that BRD2 interacts directly with E2F2[224] and that BRD4 cooperates with E2F family members in transcriptional activation.[189] In hepatocellular carcinoma, *E2F2* was pinpointed as an early downstream target of JQ1, and high *E2F2* expression was correlated with poor prognosis.[147]

Notably, while E2F2 was downregulated following 6 hours of BET inhibition in my SLAM-seq experiments, RNA-seq did not indicate a significant difference in expression compared to control samples after 48 hours of treatment. Differences in measuring nascent transcription with SLAM-seq *vs* overall transcript abundance with RNA-seq may account for these observations.[185] Thus, whilst the production of new *E2F2* mRNA may be immediately decreased by BET inhibitors, steady-state levels of *E2F2* may not show a significant decrease at 48 hours, due to the persistence of pre-existing transcripts. Alternatively, compensatory mechanisms involving other transcriptional activators or chromatin remodellers may contribute to the restoration of *E2F2* expression levels over time.

CKAP2L was identified as a downregulated gene after 48 hours of BET inhibition, and its overexpression correlated with poorer PFS in patients with PNETs. IPA analysis further highlighted CKAP2L as a key inhibited upstream regulator in BET inhibitor-treated BON1 cells. These observations align with Chapter 4's finding of CKAP2L as the top activated regulator in metastatic PNETs. While the potential significance of CKAP2L in PNETs has not previously been explored, its recognised function in mitotic spindle formation in neural progenitor cells[228] hints at a plausible role in PNETs, given the shared developmental lineage between neural progenitors and neuroendocrine cells. Moreover, *Ckap2l* was identified as one of the top upregulated genes specific to actively replicating mouse pancreatic β-cells,[341] further hinting that its dysregulation may play a role in PNET progression. Whilst the absence of CKAP2L downregulation with SLAM-seq suggests that its expression is indirectly modulated by BET inhibition, intriguingly, a recent mass spectrometry study aimed at identifying CKAP2L binding partners in non-small cell lung carcinoma cell lines identified a direct interaction with BRD4.[262] Furthermore, CKAP2L was observed to interact with RNA Pol II and regulated the transcription elongation of genes involved in the spindle assembly checkpoint, cell cycle and E2F signalling pathways, mirroring the well-documented roles of BET proteins.[139] The interaction between CKAP2L, E2F transcription factors and BET proteins could provide a pivotal link in the network of regulatory mechanisms disrupted upon BET inhibition in PNETs and requires further elucidation.

The proto-oncogene *MYC* has been identified as a direct target that mediates the anti-proliferative effects of BET inhibition in many,[153,247,285,342–344] but not all,[303,345,346] cancer types. The underlying mechanism is thought to involve displacement of BET protein binding at *MYC*-associated super-enhancers, which are also marked by high levels of H3K27ac.[194] This model of BET inhibitor-mediated *MYC* inhibition diverges from my observations in BON1 cells for a number of reasons. Firstly, *MYC* was not identified as a SE in my ChIP-seq analysis of genome-wide H3K27ac binding. Furthermore, *MYC* expression was not significantly downregulated per SLAM-seq analyses, suggesting that it is not a direct target

of BET inhibition. Although *MYC* downregulation was observed after 48 hours of treatment with both I-BET151 and GSK789/GSK620 per RNA-seq, this may represent a secondary 'bystander' effect. Lastly, MYC was neither identified as a significantly activated upstream regulator in metastatic PNETs by IPA, nor did it emerge as a BET inhibitor-suppressed regulator in treated BON1 cells. These findings underscore the importance of context-dependent effects of BET inhibition.

In conclusion, through the comprehensive bioinformatics analyses described in this chapter, I have investigated the nuanced effects of BET inhibition in PNET BON1 cells, demonstrating that simultaneous inhibition of both BD1 and BD2 domains is essential for comprehensive modulation of the transcriptomic and epigenomic landscape, with *E2F2* and *CKAP2L* emerging as key targets. Notably, my findings indicate that a treatment strategy incorporating a combination of next-generation BD1- and BD2-selective inhibitors may lead to a more focused modulation of gene expression changes compared to I-BET151. This approach could potentially offer an advantage over first-generation BET inhibitors, whose clinical translation has been hampered by dose-limiting toxicities.

7 Conclusions

7.1 Study context

PNETs are heterogeneous tumours that are associated with varying levels of morbidity and mortality depending upon factors such as tumour functionality, grade and stage of disease. There is currently an unmet need to improve treatment outcomes for patients with unresectable metastatic PNETs, who have a median overall survival of < 60 months despite currently available systemic therapies.[13,14] Moreover, for patients with multiple endocrine neoplasia type 1 (MEN1), the most common hereditary syndrome associated with PNETs, these tumours may be challenging to treat due to the synchronous occurrence of multiple tumours in other glands and younger age of onset that may result in larger tumours that are resistant to treatment.[19] The aims of this thesis were to: characterise the presentation and treatment outcomes of MEN1-related tumours in children and adolescents; elucidate BET protein expression in human PNETs; and assess the efficacy and mechanisms of non-selective and BD-selective BET inhibitors in preclinical PNET models.

7.2 Summary of major findings

Chapter 3 explored the development of MEN1-related endocrine tumours by ≤18 years of age, their treatment outcomes and genotype-phenotype correlations were explored in an international cohort. This study was motivated by the scarcity of contemporary series focusing on children and adolescents with this syndrome and recent suggestions that clinically significant MEN1 manifestations are rare in this age group.[86] My analyses revealed that pancreatic and duodenal NETs developed in around 1 in 3 patients during childhood and adolescence, the majority of which were NF-PNETs, with 15% being metastatic. Genetic analysis also identified an association between pathogenic variants in the *MEN1* gene affecting the menin-JunD interaction domain and early tumour development, although this observation requires validation in other cohorts. Nonetheless, these findings are of importance because metastatic PNETs represent the leading cause of mortality in patients with MEN1[76,81] and there is an unmet need for effective systemic therapies that target the molecular pathways driving tumour growth. This led me to investigate the effectiveness of epigenetic modifiers, focusing on the BET family of epigenetic 'reader' proteins in subsequent chapters of this thesis.

My analysis of BET protein expression in surgically-resected PNETs in **Chapter 4** revealed consistent overexpression of BRD2, BRD3 and BRD4 across various tumour subtypes, stages and grades, relative to normal adjacent pancreatic islets. Whilst there were no differences in BET mRNA or protein expression levels between metastatic and localised tumours, RNA sequencing (RNA-seq) analysis highlighted upregulation of cell cycle-related pathways, notably E2F signalling, in metastatic PNETs. Recent molecular profiling studies in the literature have also demonstrated that a subset of aggressive PNETs are transcriptionally enriched for gene sets linked to cell cycle progression and E2F signalling.[260,261] These observations are relevant because BET proteins are known to physically interact with E2F transcription factors, thereby influencing their targeting to regulatory regions of genes involved in cell cycle control.[140,224,347] Moreover, BET inhibition has been shown to downregulate

the expression of E2F target genes.[189,225,226] Cytoskeleton-associated protein 2 like (CKAP2L), a microtubule-associated protein required for cell cycle progression in neural stem cells via transcriptional elongation of E2F genes,[228] was also predicted to be the most significantly activated upstream regulator in metastatic PNETs. My chromatin immunoprecipitation with next-generation sequencing (ChIP-seq) analyses in BON1 PNET cells revealed that E2F binding motifs were enriched within BRD2 and BRD4 binding sites, and that all three BET proteins bind to the promoter regions of E2F Transcription Factor 2 (*E2F2*) and *CKAP2L* themselves. Together, these results suggest the presence of a regulatory axis involving the BET proteins, CKAP2L and E2F2 that could influence cell cycle progression in aggressive PNETs, although these findings require experimental validation. Nonetheless, these findings highlight the clinical relevance of BET proteins in PNETs and set the stage for the investigations detailed in subsequent chapters, which explored BET inhibition as a therapeutic strategy for these tumours.

In **Chapter 5**, the effects of the first-generation (BD non-selective) BET inhibitor I-BET151 and the next-generation (BD-selective) BET inhibitors GSK789 and GSK620 were evaluated *in vitro*. These studies revealed that BD1-selective inhibition with GSK789 had a moderate effect on reducing cell viability and inducing cell cycle arrest, but did not significantly affect apoptosis. In contrast, BD2-selective inhibition with GSK620 had minimal impact on these cellular processes. However, combining these inhibitors synergistically reduced cell viability, markedly increased apoptosis, and induced more pronounced cell cycle arrest, compared to either domain being targeted individually. This synergy was consistent across multiple PNET cell lines and similar effects on viability were observed in *ex-vivo* cultured neoplastic islets from pancreatic β-cell specific *Men1* knockout mice. These results challenge the notion that targeting BD1 or BD2 individually matches the effectiveness of dual BD inhibition across various cancer contexts.[152,285] Instead, they suggest that simultaneous targeting of both domains is crucial for fully 'unlocking' the therapeutic potential of BET inhibition in PNETs. Moreover, using half the concentration—0.5 μM each—of GSK789 and GSK620 achieved an

efficacy comparable to 1 μM of I-BET151, suggesting that combinations of reduced dosages of BD1 and BD2-selective inhibitors could maintain similar therapeutic effectiveness. This strategy raises the interesting prospect of reducing drug-related toxicities, a common challenge in clinical trials of BET inhibitors, while maintaining effective tumour suppression.

In **Chapter 6**, a comprehensive examination of transcriptomic and epigenomic responses to BET inhibition was performed *in vitro*. Aligning with the findings of the previous chapter, simultaneous inhibition of both BD1 and BD2, via treatment with either I-BET151 or a combination of GSK789 and GSK620, resulted in more pronounced alterations in gene expression and H3K27ac occupancy compared to targeting either domain individually. Gene set enrichment analyses (GSEA) of genes altered by each inhibitor revealed downregulation of pathways associated with immune inflammatory response by BD2-selective inhibition alone, whilst pathways related to oncogenic processes such as mTOR signalling and cell cycle progression were downregulated by BD1-selective inhibition alone. These findings corroborate recent studies in the literature that have highlighted distinct roles for both domains, whereby BD2-selective inhibition affects the production of several key proinflammatory mediators while leaving cell viability and proliferation largely unaltered, whereas BD1-selective inhibition inhibits the expression of a subset of established oncogenic gene expression programs.[152,348] Additionally, my studies uncovered that the simultaneous targeting of both BD1 and BD2 was essential for the disruption of critical cellular pathways necessary for survival and growth, which may explain why the combination of GSK789 and GSK620 demonstrated superior efficacy compared to targeting BD1 individually. This suggests that while BD2-selective inhibition has minimal impact on cell viability and modulating gene expression, BD2 may cooperate with BD1 in the maintenance of oncogenic gene expression programs in PNETs. Further research is needed to elucidate the molecular mechanisms driving this interaction, including BD2's interactions with non-histone proteins.

Other novel findings described in **Chapter 6** include the distinct differences between the transcriptomic and epigenomic responses to I-BET151 and the GSK789/GSK620 combination. Despite both strategies targeting BD1 and BD2 concurrently, I-BET151 induced broader alterations in gene expression and acetylated histone H3 lysine 27 (H3K27ac) binding. The most significantly enriched Gene Ontology Biological Process (GO:BP) term in genes downregulated by I-BET151, but not GSK789/GSK620, was 'regulation of cellular component organisation', which encompasses processes crucial for maintaining cell structure and function, such as the arrangement of organelles and the cytoskeleton. Disruption of these fundamental processes could lead to cellular dysfunction of both tumour and normal cells, potentially contributing to dose-related toxicities. These results highlight the importance of further investigating the toxicity profiles and therapeutic windows of these treatment strategies *in vivo*, prior to clinical evaluation. The findings of this chapter also relate back to **Chapter 4**, as *E2F2* and *CKAP2L* were identified as key early and late targets, respectively, of BET inhibitors and were also noted to be upregulated in metastatic PNETs. Moreover, expression levels of both genes were positively correlated with tumour Ki-67 index and were associated with shorter progression-free survival in patients with PNETs, suggesting that their modulation by BET inhibitors may directly influence tumour aggressiveness and patient prognosis. Thus, it is plausible that these genes could be used as biomarkers to predict which patients are likely to have more aggressive disease course and could potentially benefit from BET inhibitor therapy. While further validation in clinical settings is required, this could represent a more personalised approach to systemic treatment in patients with advanced PNETs, moving beyond 'one-size-fits-all' strategies to tailored therapies based on specific molecular biomarkers.

7.3 Limitations

The findings presented in this thesis demonstrate the promising potential of BET inhibition for the treatment of PNETs. However, several limitations warrant

consideration, some of which have already been discussed in preceding chapters. Firstly, the efficacy studies of BET inhibitors were conducted using only three cell lines: two human (BON1, QGP1) and one murine (MIN6). In contrast to more common cancers, such as breast cancer, for which > 80 cell lines exist,[349] the field of PNET research has historically been limited by a paucity of available *in vitro* models.[350] This scarcity is partly due to the rarity of PNETs and their relatively slow proliferation rate compared to more aggressive cancers. Although molecular profiling studies have confirmed the neuroendocrine phenotype of the BON1, QGP1, and MIN6 cell lines,[165,351–353] concerns have been raised regarding the presence of genetic anomalies in these lines that are not typically observed in PNETs. For instance, MIN6 cells, derived from an insulinoma in a transgenic mouse model, express the Simian virus 40 (SV40) large tumour antigen (TAg), leading to the inactivation of tumor suppressors like p53 and Rb.[162] This mechanism does not occur in naturally arising well-differentiated human PNETs, complicating the extrapolation of data from this cell line into clinical settings. Although the BON1 and QGP1 cell lines are the most frequently-utilised cell lines, the presence of certain mutations (e.g., *TP53* and *KRAS*) and the absence of mutations commonly observed in human PNETs (e.g., *MEN1*, *ATRX* or *DAXX*) suggest that these cell lines may not accurately represent the genetic landscape of most PNETs encountered in clinical practice.[164,296] Instead, they may resemble more aggressive tumours, possibly even neuroendocrine carcinomas. Although *ex vivo* drug studies were performed in this thesis using pancreatic islets from *Men1* knockout mice, these studies also present limitations. Whilst tumours derived from this model are clinically relevant due to *MEN1* being the most commonly mutated somatic gene in sporadic PNETs,[100,101] the studies are limited by their *ex vivo* nature since conducting experiments in isolated pancreatic islets does not fully capture the complexity and interactions present in an *in vivo* environment. This limits our understanding of how BET inhibitors might interact with tumour microenvironments, immune responses, and other systemic factors present in live organisms. Therefore, while these studies

provide valuable insights, they do not replace the necessity for *in vivo* studies that can more comprehensively model the physiological context of PNETs.

In summary, my thesis provides insights into the onset and clinical behaviour of MEN1-related PNETs in paediatric and adolescent populations, highlights the potential significance of BET proteins in PNET biology, and explores the differential responses to BD-selective and non-selective BET inhibition in pre-clinical PNET models. Additionally, the identification of *E2F2* and *CKAP2L* upregulation as markers of disease aggressiveness and as critical targets impacted by concurrent BD1 and BD2 inhibition suggests that these genes underpin the therapeutic effectiveness of BET inhibitors in PNETs and also serve as potential biomarkers for stratifying patient response. Collectively, these studies lay the groundwork for future *in vivo* and mechanistic studies of BET inhibitors in PNETs, aiming to ultimately translate these findings into clinical trials that improve outcomes for patients with MEN1-related and sporadic PNETs. Potential avenues for future research that build upon the findings of this thesis are discussed in the next chapter.

8

Future studies

One of the major aims of this DPhil thesis was to investigate the efficacy of BET inhibition as a novel therapy for PNETs. Whilst the studies outlined in this thesis have generated evidence in support of this treatment strategy, further work is required before BET inhibitors can be translated into early phase clinical trials for patients with advanced PNETs. Furthermore, while the *in silico* data presented in this thesis are invaluable for hypothesis generation, they come with inherent limitations that necessitate experimental validation. Proposed experimental approaches to validate the relevance of my findings and suggested directions for future research are outlined below.

8.0.1 Validation of bioinformatics/*in silico* data

I utilised comprehensive transcriptomic and epigenomic analyses to identify potential molecular markers and pathways affected by BET inhibition in PNETs in a broad and unbiased manner. E2F2 and CKAP2L emerged as particularly significant targets due to their associations with PNET progression and responses to combined BD1 and BD2 inhibition. Although converging signals from RNA sequencing (RNA-seq), thiol (SH)-linked alkylation for the metabolic sequencing

of RNA (SLAM-seq), and chromatin immunoprecipitation with next-generation sequencing (ChIP-seq) analyses increase confidence in these targets, experimental validation is still needed to establish their biological relevance. This necessity arises because '-omics' technologies, whilst providing a wealth of data and insights into molecular mechanisms, can result in non-specific hits or false positives due to the potential for technical or biological noise in the data.[354] I therefore plan to validate the downregulation of *E2F2* and *CKAP2L* in response to dual BD inhibition by measuring mRNA levels using quantitative real-time PCR (qRT-PCR). Additionally, I will confirm the decrease in acetylated histone H3 lysine 27 (H3K27ac) enrichment, indicative of transcriptional activation changes, at the loci of both genes by employing chromatin immunoprecipitation followed by quantitative PCR (ChIP-qPCR). Changes in mRNA levels and H3K27ac enrichment do not necessarily correlate with alterations in protein expression. To address this, I will perform Western blot analysis to directly assess protein expression levels of E2F2 and CKAP2L in cell lines following BET inhibitor treatment. Immunohistochemistry staining of the Vienna PNET cohort will also be performed to validate whether CKAP2L and E2F2 are expressed at higher levels in metastatic versus localised tumours.

Another limitation of -omics analyses is that they provide a snapshot of cellular processes at a specific moment, without establishing functional relationships or revealing the dynamic interactions that govern these molecular events. To address this, functional assays will be conducted to directly assess the impact of perturbing E2F2 and CKAP2L on the behaviour of PNET cell lines *in vitro*. Specifically, I will use small interfering RNAs (siRNAs) or short hairpin RNAs (shRNAs) to knock down the expression of these genes, subsequently evaluating the resulting changes in cell proliferation, apoptosis, and cell cycle progression. These experiments will be complemented by overexpression studies, where *E2F2* and *CKAP2L* will be reintroduced into cells via plasmid vectors or lentiviral transduction, to determine if restoring their expression can counteract the phenotypic effects induced by BET inhibition. To further investigate the relationship between E2F2, CKAP2L and

BET family members, I will perform co-immunoprecipitation (co-IP) assays to examine the physical interactions between these proteins. This will help establish whether E2F2 and CKAP2L are direct regulatory targets of BET proteins or if their modulation occurs through indirect effects on transcriptional networks. These combined approaches will provide a comprehensive understanding of how BET inhibition influences these key regulators of cell cycle and proliferation, thereby substantiating their roles as potential therapeutic targets in PNETs.

8.0.2 Plans for *in vivo* studies including current and next-generation BET inhibitors

To validate the *in vitro* efficacy of I-BET151 and to assess the differential effects and pharmacology of GSK789 and GSK620, *in vivo* studies using established PNET mouse models are essential. While the *ex vivo* studies conducted on neoplastic cultured pancreatic islets from PNET-bearing *Men1*$^{L/L}$*/RIP2-Cre* mice corroborated the results from my *in vitro* viability experiments, these *ex vivo* models lack functional vasculature and an immune system and therefore, the complex interactions between drugs and the host organism are not recapitulated. This limitation underscores the need for *in vivo* models to fully evaluate the therapeutic potential of these compounds, including their pharmacokinetic properties and toxicity profiles. Due to restrictions imposed by the COVID-19 pandemic on animal work, performing an *in vivo* study was not feasible during the course of my DPhil. Consequently, I aim to perform a mouse study consisting of five treatment groups: 1) vehicle (DMSO); 2) I-BET151; 3) GSK789; 4) GSK620; and 5) a combination of GSK789 and GSK620. The *Men1*$^{L/L}$*/RIP2-Cre* model, previously utilised by Professor Thakker's group to assess the *in vivo* effects of JQ1,[60] will be utilised. A strength of this model is that it harbours PNETs with a similar genetic aetiology as those in humans, since somatic mutations of the *MEN1* gene are found in virtually all PNETs in MEN1 patients[202]and occur in $> 40\%$ of sporadic PNETs.[34,100] Moreover, in this model tumours develop within the tissue of origin

(i.e., the pancreas) ensuring that the tumour microenvironment and host interactions are preserved. This provides insights that are more relevant to the human condition than those obtained from xenograft models, where tumour cells are introduced into non-native locations in immunocompromised mice.

The typical dosing regimen for current-generation BET inhibitors in animal studies ranges from 30 to 50 mg/kg.[149,245,282,355–357] To translate animal doses into human equivalent doses (HED), the 'dose-by-factor' method is frequently used.[358,359] According to this method, the conversion factor between mice and humans is determined based on their respective body surface area ratios. The formula used for calculating the HED is given by:

$$\text{HED (mg/kg)} = \text{Animal Dose (mg/kg)} \times \left(\frac{K_m \text{ factor for mice}}{K_m \text{ factor for humans}} \right)$$

Here, K_m is the correction factor that normalises for differences in body surface area between species. For mice, this is typically around 3 and for humans, it is approximately 37.[358]

$$\text{HED for 30 mg/kg} = 30 \times \left(\frac{3}{37} \right) \approx 2.43 \text{ mg/kg},$$
$$\text{HED for 50 mg/kg} = 50 \times \left(\frac{3}{37} \right) \approx 4.05 \text{ mg/kg}.$$

Thus, the HED for BET inhibitors based on the doses used in previously published murine studies (30 to 50 mg/kg) would fall within the range of 2.43 to 4.05 mg/kg. Assuming an average human weight of 70 kg, this equates to a total dose of ~170 to 284 mg. It is worth noting that these doses exceed the maximum tolerated doses reported in clinical trials of first-generation BET inhibitors, which are usually around 80-100 mg once daily.[293,329,331,360] Therefore, for the proposed mouse study, doses lower than the traditional 30-50 mg/kg range will be considered to better align with safe clinical exposures. The synergistic efficacy observed with GSK789 and GSK620 *in vitro* suggests that lower doses might indeed be sufficient *in vivo*, particularly since the combination of both compounds

achieved reductions in cell viability on par with I-BET151 *in vitro*, but at reduced concentrations. Given that GSK789 and GSK620 have not yet been studied in murine cancer models, dose optimisation will be undertaken in collaboration with expert collaborators at GSK, employing pharmacokinetic and pharmacodynamic modelling to ensure effective target engagement while maintaining a safety profile conducive to potential clinical translation.

Similar to the protocol described in the previously published JQ1 study by Professor Thakker's group,[60] mice will be dosed twice-weekly with BET inhibitor compounds for four weeks, although alternative dosing regimens will also be explored. The mice would also be given 1 mg/mL of 5-bromo-2'-deoxyuridine (BrdU) continuously in drinking water for 30 days prior to sacrifice. BrDU is an analogue of the nucleoside thymidine and is incorporated into newly synthesised DNA of proliferating cells. Thus, the efficacy of BET inhibitor compounds would be assessed at the end of the treatment period by measuring BrDU incorporation into PNETs using immunohistochemistry. Another important aspect of this study will be the assessment of toxicity, which would be performed by regularly monitoring mice for weight loss and behavioural changes, as well as performing weekly blood draws to assess haematological parameters, liver and kidney function. Adherence to the principles of Replacement, Reduction, and Refinement (the 3 Rs)[361] will be a priority throughout these studies and humane endpoints will be established, ensuring that mice experiencing significant distress or health deterioration are humanely culled to minimise suffering.

8.0.3 Combining BET inhibitors with other targeted therapies

Incorporating combination therapies represents another potential strategy for enhancing the efficacy of BET inhibitors while potentially reducing the required dosage, thereby mitigating associated toxicities.[282] The rationale behind this approach lies in the ability of combination therapies to target multiple pathways

simultaneously, thereby exerting a more comprehensive anti-tumour effect. Examples of rational combination therapies have emerged from studies of BET inhibitor resistance that implicate upregulation of receptor tyrosine kinases (RTKs) and phosphoinositide 3-kinase (PI3K)/protein kinase B (AKT) signalling as a common resistance mechanism to BET inhibition.[362,363] Accordingly, the combination of BET inhibitors with RTK and PI3K inhibitors has been shown to be synergistic and overcomes therapy-induced resistance in preclinical cancer models.[363–366] Therefore, I plan to investigate the combination of I-BET151 or GSK789/GSK620 with sunitinib, an RTK inhibitor currently approved for the treatment of advanced PNETs,[65] to determine whether these combinations have synergistic effects *in vitro* and *in vivo*.

My RNA-seq and ChIP-seq studies suggest that dysregulated cell cycle pathways are a key feature of metastatic PNETs and that BET proteins are enriched at the promoters of key cell cycle-related genes. Therefore, it would seem logical to explore the combination of BET inhibitors with cyclin-dependent kinase (CDK) inhibitors. Indeed, in a study in which over 500 compounds were screened for potentially synergistic effects with BET inhibitors in treatment-resistant breast cancer cell lines, CDK inhibitors emerged as the top candidates.[367] Furthermore, synergistic effects were also demonstrated in non-small cell lung cancer cell lines, where depletion of *CKAP2L* using shRNA-mediated silencing enhanced the efficacy of the CDK9 inhibitor alvocidib.[262] Although CKAP2L inhibitors have yet to be developed, my findings indicate that dual BD BET inhibition reduces *CKAP2L* expression in BON1 cells, hinting at the potential for similar synergistic effects when combined with alvocidib treatment.

To assess these combinations, I will employ methodologies established in this DPhil thesis, which include evaluating changes in cell viability, apoptosis, and cell cycle alterations in PNET cell lines using CellTiter-Blue® viability assays, caspase 3/7 apoptosis assays, and flow cytometry, respectively. Initial studies will prioritise assessing cell viability and apoptosis with a single dose of each compound to quickly screen for efficacy. To evaluate potential synergistic effects, I will conduct

combination studies using an 8 x 8 matrix of serial dilutions for each drug, which will help in identifying not only the optimal dose combinations but also the interactions between the compounds, quantified by Bliss synergy scores. Subsequent assays will further investigate the impacts of these drug combinations on cell cycle distribution and morphological changes. Moreover, to probe the signalling pathways affected by these combination treatments in more detail, I will utilise phospho-kinase array analyses. This will enable the detection of changes in the phosphorylation status of key proteins within the RTK, PI3K/AKT and CDK-regulated pathways.

In summary, this thesis highlights the potential of BET inhibitors as a promising therapeutic approach for PNETs and paves the way for further research to validate and expand upon these initial findings. The proposed *in vivo* studies could provide critical insights into the pharmacodynamics and safety profiles of both current and next-generation BET inhibitors, potentially guiding their progression into clinical trials. Moreover, validation experiments intended to confirm the relevance of molecular markers identified through -omics analyses could help clarify the mechanistic underpinnings of BET inhibition in PNETs. Combining BET inhibitors with other targeted therapies offers a strategy to not only enhance therapeutic efficacy but also to mitigate the toxicities associated with higher doses, thereby addressing a significant challenge in current clinical trials of these compounds. The future studies outlined herein are essential for expanding upon the current data, validating the clinical relevance of these findings, and ultimately, improving the management and outcomes of patients with PNETs.

References

1. Hruban, R. H. & Iacobuzio-Donahue, C. A. in *Robbins and Cotran Pathological Basis of Disease* 10th Ed. (Elsevier, Philadelphia, PA, 2020).
2. Avolio, F., Pfeifer, A., Courtney, M., Gjernes, E., Ben-Othman, N., Vieira, A., Druelle, N., Faurite, B. & Collombat, P. From Pancreas Morphogenesis to β-Cell Regeneration. *Curr Top Dev Biol* **106,** 217–238 (2013).
3. Ellis, C., Ramzy, A. & Kieffer, T. J. Regenerative Medicine and Cell-Based Approaches to Restore Pancreatic Function. *Nat Rev Gastroenterol Hepatol* **14,** 612–628 (2017).
4. Slack, J. M. Developmental Biology of the Pancreas. *Development* **121,** 1569–1580 (1995).
5. Gittes, G. K. Developmental Biology of the Pancreas: A Comprehensive Review. *Dev Biol* **326,** 4–35 (2009).
6. Edlund, H. Developmental Biology of the Pancreas. *Diabetes* **50 Suppl 1,** S5–9 (2001).
7. Andrew, A., Kramer, B. & Rawdon, B. B. The Origin of Gut and Pancreatic Neuroendocrine (APUD) Cells–the Last Word? *J Pathol* **186,** 117–118 (1998).
8. Pictet, R. L., Rall, L. B., Phelps, P. & Rutter, W. J. The Neural Crest and the Origin of the Insulin-Producing and Other Gastrointestinal Hormone-Producing Cells. *Science* **191,** 191–192 (1976).
9. Fontaine, J., Le Lièvre, C. & Le Douarin, N. M. What Is the Developmental Fate of the Neural Crest Cells Which Migrate into the Pancreas in the Avian Embryo? *Gen Comp Endocrinol* **33,** 394–404 (1977).
10. Seaberg, R. M., Smukler, S. R., Kieffer, T. J., Enikolopov, G., Asghar, Z., Wheeler, M. B., Korbutt, G. & van der Kooy, D. Clonal Identification of Multipotent Precursors from Adult Mouse Pancreas That Generate Neural and Pancreatic Lineages. *Nat Biotechnol* **22,** 1115–1124 (2004).
11. Arntfield, M. & van der Kooy, D. The Adult Mammalian Pancreas Contains Separate Precursors of Pancreatic and Neural Crest Developmental Origins. *Stem Cells Dev* **22,** 2145–2157 (2013).
12. Hori, Y., Gu, X., Xie, X. & Kim, S. K. Differentiation of Insulin-Producing Cells from Human Neural Progenitor Cells. *PLoS Med* **2,** e103 (2005).
13. Dasari, A., Shen, C., Halperin, D., Zhao, B., Zhou, S., Xu, Y., Shih, T. & Yao, J. C. Trends in the Incidence, Prevalence, and Survival Outcomes in Patients With Neuroendocrine Tumors in the United States. *JAMA Oncol* **3,** 1335–1342 (2017).

14. Sonbol, M. B., Mazza, G. L., Mi, L., Oliver, T., Starr, J., Gudmundsdottir, H., Cleary, S. P., Hobday, T. & Halfdanarson, T. R. Survival and Incidence Patterns of Pancreatic Neuroendocrine Tumors Over the Last 2 Decades: A SEER Database Analysis. *Oncologist* **27,** 573–578 (2022).

15. Grimelius, L., Hultquist, G. T. & Stenkvist, B. Cytological Differentiation of Asymptomatic Pancreatic Islet Cell Tumours in Autopsy Material. *Virchows Arch A Pathol Anat Histol* **365,** 275–288 (1975).

16. Kimura, W., Kuroda, A. & Morioka, Y. Clinical Pathology of Endocrine Tumors of the Pancreas. Analysis of Autopsy Cases. *Dig Dis Sci* **36,** 933–942 (1991).

17. Schimmack, S., Svejda, B., Lawrence, B., Kidd, M. & Modlin, I. M. The Diversity and Commonalities of Gastroenteropancreatic Neuroendocrine Tumors. *Langenbecks Arch Surg* **396,** 273–298 (2011).

18. Yates, C. J., Newey, P. J. & Thakker, R. V. Challenges and Controversies in Management of Pancreatic Neuroendocrine Tumours in Patients with MEN1. *Lancet Diabetes Endocrinol* **3,** 895–905 (2015).

19. Frost, M., Lines, K. E. & Thakker, R. V. Current and Emerging Therapies for PNETs in Patients with or without MEN1. *Nat Rev Endocrinol* **14,** 216–227 (2018).

20. Zollinger, R. M. & Ellison, E. H. Primary Peptic Ulcerations of the Jejunum Associated with Islet Cell Tumors of the Pancreas. *Ann Surg* **142,** 709–723 (1955).

21. Gosain, R., Gupta, M., Roy, A. M., Strosberg, J., Glaser, K. M. & Iyer, R. Health-Related Quality of Life (HRQoL) in Neuroendocrine Tumors: A Systematic Review. *Cancers (Basel)* **14,** 1428 (2022).

22. Yao, J. C., Hassan, M., Phan, A., Dagohoy, C., Leary, C., Mares, J. E., Abdalla, E. K., Fleming, J. B., Vauthey, J.-N., Rashid, A. & Evans, D. B. One Hundred Years after "Carcinoid": Epidemiology of and Prognostic Factors for Neuroendocrine Tumors in 35,825 Cases in the United States. *J Clin Oncol* **26,** 3063–3072 (2008).

23. Williams, E. D., Siebenmann, R. E., Sobin, L. H. & Organization, W. H. *Histological Typing of Endocrine Tumours* (World Health Organization, 1980).

24. Rindi, G., Mete, O., Uccella, S., Basturk, O., La Rosa, S., Brosens, L. A. A., Ezzat, S., de Herder, W. W., Klimstra, D. S., Papotti, M. & Asa, S. L. Overview of the 2022 WHO Classification of Neuroendocrine Neoplasms. *Endocr Pathol* **33,** 115–154 (2022).

25. Bosman, F. T., Carneiro, F., Hruban, R. H. & Theise, N. D. *WHO Classification of Tumours of the Digestive System.* 4th ed. (International Agency for Research on Cancer, Lyon, France, 2010).

26. Basturk, O., Tang, L., Hruban, R. H., Adsay, V., Yang, Z., Krasinskas, A. M., Vakiani, E., La Rosa, S., Jang, K.-T., Frankel, W. L., Liu, X., Zhang, L., Giordano, T. J., Bellizzi, A. M., Chen, J.-H., Shi, C., Allen, P., Reidy, D. L., Wolfgang, C. L., Saka, B., Rezaee, N., Deshpande, V. & Klimstra, D. S. Poorly Differentiated Neuroendocrine Carcinomas of the Pancreas: A Clinicopathologic Analysis of 44 Cases. *Am J Surg Pathol* **38,** 437–447 (2014).

27. Basturk, O., Yang, Z., Tang, L. H., Hruban, R. H., Adsay, V., McCall, C. M., Krasinskas, A. M., Jang, K.-T., Frankel, W. L., Balci, S., Sigel, C. & Klimstra, D. S. The High-grade (WHO G3) Pancreatic Neuroendocrine Tumor Category Is Morphologically and Biologically Heterogenous and Includes Both Well Differentiated and Poorly Differentiated Neoplasms. *Am J Surg Pathol* **39,** 683 (2015).

28. Tang, L. H., Untch, B. R., Reidy, D. L., O'Reilly, E., Dhall, D., Jih, L., Basturk, O., Allen, P. J. & Klimstra, D. S. Well-Differentiated Neuroendocrine Tumors with a Morphologically Apparent High-Grade Component: A Pathway Distinct from Poorly Differentiated Neuroendocrine Carcinomas. *Clin Cancer Res* **22,** 1011–1017 (2016).

29. Lloyd, R. V., Osamura, R. Y., Klöppel, G. & Rosai, J. *WHO Classification of Tumours of Endocrine Organs* 4th ed. (International Agency for Research on Cancer, Lyon, France, 2017).

30. Yang, M., Zeng, L., Ke, N.-w., Tan, C.-l., Tian, B.-l., Liu, X.-b., Xiang, B. & Zhang, Y. World Health Organization Grading Classification for Pancreatic Neuroendocrine Neoplasms: A Comprehensive Analysis from a Large Chinese Institution. *BMC Cancer* **20,** 906 (2020).

31. Rindi, G., Klöppel, G., Alhman, H., Caplin, M., Couvelard, A., de Herder, W. W., Erikssson, B., Falchetti, A., Falconi, M., Komminoth, P., Körner, M., Lopes, J. M., McNicol, A.-M., Nilsson, O., Perren, A., Scarpa, A., Scoazec, J.-Y., Wiedenmann, B., all other Frascati Consensus Conference participants & European Neuroendocrine Tumor Society (ENETS). TNM Staging of Foregut (Neuro)Endocrine Tumors: A Consensus Proposal Including a Grading System. *Virchows Arch* **449,** 395–401 (2006).

32. Edge, S. B., Byrd, D. R. & Compton, C. C. *American Joint Committee on Cancer Staging Manual* 7th ed. (AJCC, New York, NY, 2010).

33. Bilimoria, K. Y., Bentrem, D. J., Merkow, R. P., Tomlinson, J. S., Stewart, A. K., Ko, C. Y. & Talamonti, M. S. Application of the Pancreatic Adenocarcinoma Staging System to Pancreatic Neuroendocrine Tumors. *J Am Coll Surg* **205,** 558–563 (2007).

34. Scarpa, A., Mantovani, W., Capelli, P., Beghelli, S., Boninsegna, L., Bettini, R., Panzuto, F., Pederzoli, P., delle Fave, G. & Falconi, M. Pancreatic Endocrine Tumors: Improved TNM Staging and Histopathological Grading Permit a Clinically Efficient Prognostic Stratification of Patients. *Mod Pathol* **23,** 824–833 (2010).

35. Luo, G., Javed, A., Strosberg, J. R., Jin, K., Zhang, Y., Liu, C., Xu, J., Soares, K., Weiss, M. J., Zheng, L., Wolfgang, C. L., Cives, M., Wong, J., Wang, W., Sun, J., Shao, C., Wang, W., Tan, H., Li, J., Ni, Q., Shen, L., Chen, M., He, J., Chen, J. & Yu, X. Modified Staging Classification for Pancreatic Neuroendocrine Tumors on the Basis of the American Joint Committee on Cancer and European Neuroendocrine Tumor Society Systems. *JCO* **35,** 274–280 (2017).

36. Bergsland, E. K., Woltering, E. A. & Rindo, G. in *AJCC Cancer Staging Manual* 8th ed. (AJCC, Chicago, USA, 2017).

37. Wang, H., Ding, D., Qin, T., Zhang, H., Liu, J., Zhao, J., Wu, C.-H., Javed, A., Wolfgang, C., Guo, S., Chen, Q., Zhao, W., Shi, W., Zhu, F., Guo, X., Li, X., Peng, F., He, R., Xu, S., Jin, J., Wu, Y., Nuer, A., Edil, B., Tien, Y.-W., Jin, G., Zheng, L., He, J., Liu, J., Liu, Y., Wang, M. & Qin, R. Prognostic Validity of the American Joint Committee on Cancer Eighth Edition Staging System for Well-Differentiated Pancreatic Neuroendocrine Tumors. *HPB (Oxford)* **24,** 681–690 (2022).

38. You, Y., Jang, J.-Y., Kim, S. C., Yoon, Y.-S., Park, J. S., Cho, C. K., Park, S.-J., Yang, J. D., Lee, W. J., Hong, T. H., Ahn, K. S., Jeong, C.-Y., Lee, H. K., Lee, S. E., Roh, Y. H., Kim, H. J., Kim, H. & Han, I. W. Validation of the 8th AJCC Cancer Staging System for Pancreas Neuroendocrine Tumors Using Korean Nationwide Surgery Database. *Cancer Res Treat* **51,** 1639–1652 (2019).

39. Amin, M. B., Edge, S. B., Greene, F. L., Byrd, D. R., Brookland, R. K., Washington, M. K., Gershenwald, J. E., Compton, C. C., Hess, K., Sullivan, D. C., Jessup, J. M., Brierley, J. D., Gaspar, L. E., Schilsky, R. L., Balch, C. M., Winchester, D. P., Asare, E. A., Madera, M., Gress, D. & Meyer, L. R. *American Joint Committee on Cancer Staging Manual* 8th ed. (Springer, New York, NY, 2017).

40. Partelli, S., Cirocchi, R., Crippa, S., Cardinali, L., Fendrich, V., Bartsch, D. K. & Falconi, M. Systematic Review of Active Surveillance versus Surgical Management of Asymptomatic Small Non-Functioning Pancreatic Neuroendocrine Neoplasms. *Br J Surg* **104,** 34–41 (2017).

41. Partelli, S., Massironi, S., Zerbi, A., Niccoli, P., Kwon, W., Landoni, L., Panzuto, F., Tomazic, A., Bongiovanni, A., Kaltsas, G., Sauvanet, A., Bertani, E., Mazzaferro, V., Caplin, M., Armstrong, T., Weickert, M. O., Ramage, J., Segelov, E., Butturini, G., Staettner, S., Cives, M., Frilling, A., Moulton, C. A., He, J., Boesch, F., Selberheer, A., Twito, O., Castaldi, A., De Angelis, C. G., Gaujoux, S., Holzer, K., Wilson, C. H., Almeamar, H., Vigia, E., Muffatti, F., Lucà, M., Lania, A., Ewald, J., Kim, H., Salvia, R., Rinzivillo, M., Smid, A., Gardini, A., Tsoli, M., Hentic, O., Colombo, S., Citterio, D., Toumpanakis, C., Ramsey, E., Randeva, H. S., Srirajaskanthan, R., Croagh, D., Regi, P., Gasteiger, S., Invernizzi, P., Ridolfi, C., Giovannini, M., Jang, J.-Y., Bassi, C. & Falconi, M. Management of Asymptomatic Sporadic Non-Functioning Pancreatic Neuroendocrine Neoplasms No Larger than 2 Cm: Interim Analysis of Prospective ASPEN Trial. *Br J Surg* **109,** 1186–1190 (2022).

42. Heidsma, C. M., Engelsman, A. F., van Dieren, S., Stommel, M. W. J., de Hingh, I., Vriens, M., Hol, L., Festen, S., Mekenkamp, L., Hoogwater, F. J. H., Daams, F., Klümpen, H. .-., Besselink, M. G., van Eijck, C. H. & Nieveen van Dijkum, E. J. Watchful Waiting for Small Non-Functional Pancreatic Neuroendocrine Tumours: Nationwide Prospective Cohort Study (PANDORA). *Br J Surg* **108,** 888–891 (2021).

43. Haynes, A. B., Deshpande, V., Ingkakul, T., Vagefi, P. A., Szymonifka, J., Thayer, S. P., Ferrone, C. R., Wargo, J. A. & Warshaw, A. L. Implications of Incidentally Discovered, Nonfunctioning Pancreatic Endocrine Tumors: Short-term and Long-term Patient Outcomes. *Archives of Surgery* **146,** 534–538 (2011).

44. Aziz, H., Howe, J. R. & Pawlik, T. M. Surgery vs Observation for Patients With Small Pancreatic Neuroendocrine Tumors. *JAMA Surg* **156,** 412–413 (2021).

45. Howe, J. R., Merchant, N. B., Conrad, C., Keutgen, X. M., Hallet, J., Drebin, J. A., Minter, R. M., Lairmore, T. C., Tseng, J. F., Zeh, H. J., Libutti, S. K., Singh, G., Lee, J. E., Hope, T. A., Kim, M. K., Menda, Y., Halfdanarson, T. R., Chan, J. A. & Pommier, R. F. The North American Neuroendocrine Tumor Society Consensus Paper on the Surgical Management of Pancreatic Neuroendocrine Tumors. *Pancreas* **49,** 1–33 (2020).

46. Kulke, M. H., Shah, M. H., Benson, A. B., Bergsland, E., Berlin, J. D., Blaszkowsky, L. S., Emerson, L., Engstrom, P. F., Fanta, P., Giordano, T., Goldner, W. S., Halfdanarson, T. R., Heslin, M. J., Kandeel, F., Kunz, P. L., Kuvshinoff, B. W., Lieu, C., Moley, J. F., Munene, G., Pillarisetty, V. G., Saltz, L., Sosa, J. A., Strosberg, J. R., Vauthey, J.-N., Wolfgang, C., Yao, J. C., Burns, J., Freedman-Cass, D. & National comprehensive cancer network. Neuroendocrine Tumors, Version 1.2015. *J Natl Compr Canc Netw* **13,** 78–108 (2015).

47. Kos-Kudła, B., Castaño, J. P., Denecke, T., Grande, E., Kjaer, A., Koumarianou, A., de Mestier, L., Partelli, S., Perren, A., Stättner, S., Valle, J. W. & Fazio, N. European Neuroendocrine Tumour Society (ENETS) 2023 Guidance Paper for Nonfunctioning Pancreatic Neuroendocrine Tumours. *J Neuroendocrinol* **35,** e13343 (2023).

48. Halfdanarson, T. R., Rabe, K. G., Rubin, J. & Petersen, G. M. Pancreatic Neuroendocrine Tumors (PNETs): Incidence, Prognosis and Recent Trend toward Improved Survival. *Ann Oncol* **19,** 1727–1733 (2008).

49. Tsoli, M., Spei, M.-E., Wallin, G., Kaltsas, G. & Daskalakis, K. Association of a Palliative Surgical Approach to Stage IV Pancreatic Neuroendocrine Neoplasms with Survival: A Systematic Review and Meta-Analysis. *Cancers* **12,** 2246 (8 2020).

50. Que, F. G., Nagorney, D. M., Batts, K. P., Linz, L. J. & Kvols, L. K. Hepatic Resection for Metastatic Neuroendocrine Carcinomas. *Am J Surg* **169,** 36–42, discussion 42–43 (1995).

51. Sarmiento, J. M., Heywood, G., Rubin, J., Ilstrup, D. M., Nagorney, D. M. & Que, F. G. Surgical Treatment of Neuroendocrine Metastases to the Liver: : A Plea for Resection to Increase Survival. *J Am Coll Surg* **197,** 29 (2003).

52. Scott, A. T., Breheny, P. J., Keck, K. J., Bellizzi, A. M., Dillon, J. S., O'Dorisio, T. M. & Howe, J. R. Effective Cytoreduction Can Be Achieved in Patients with Numerous Neuroendocrine Tumor Liver Metastases (NETLMs), *Surgery* **165,** 166–175 (2019).

53. Mayo, S. C., de Jong, M. C., Pulitano, C., Clary, B. M., Reddy, S. K., Gamblin, T. C., Celinksi, S. A., Kooby, D. A., Staley, C. A., Stokes, J. B., Chu, C. K., Ferrero, A., Schulick, R. D., Choti, M. A., Mentha, G., Strub, J., Bauer, T. W., Adams, R. B., Aldrighetti, L., Capussotti, L. & Pawlik, T. M. Surgical Management of Hepatic Neuroendocrine Tumor Metastasis: Results from an International Multi-Institutional Analysis. *Ann Surg Oncol* **17,** 3129–3136 (2010).

54. Chawla, A., Williams, R. T., Sich, N., Clancy, T., Wang, J., Ashley, S., Pezzi, C. & Swanson, R. Pancreaticoduodenectomy and Metastasectomy for Metastatic Pancreatic Neuroendocrine Tumors. *J Surg Oncol* **118,** 983–990 (2018).

55. Kjaer, J., Clancy, T. E., Thornell, A., Andersson, N., Hellman, P., Crona, J., Welin, S., Sulciner, M., Powell, B., Brais, L., Astone, K., Baddoo, W., Doherty, G., Chan, J. A., Norlén, O. & Stålberg, P. Benefit of Primary Tumor Resection in Stage IV, Grade 1 and 2, Pancreatic Neuroendocrine Tumors: A Propensity-Score Matched Cohort Study. *Ann Surg Open* **3,** e151 (2022).

56. Tierney, J. F., Chivukula, S. V., Wang, X., Pappas, S. G., Schadde, E., Hertl, M., Poirier, J. & Keutgen, X. M. Resection of Primary Tumor May Prolong Survival in Metastatic Gastroenteropancreatic Neuroendocrine Tumors. *Surgery* **165,** 644–651 (2019).

57. Gupta, S. Intra-Arterial Liver-Directed Therapies for Neuroendocrine Hepatic Metastases. *Semin Intervent Radiol* **30,** 28–38 (2013).

58. Yang, T. X., Chua, T. C. & Morris, D. L. Radioembolization and Chemoembolization for Unresectable Neuroendocrine Liver Metastases – A Systematic Review. *Surgical Oncology* **21,** 299–308 (2012).

59. Kennedy, A., Bester, L., Salem, R., Sharma, R. A., Parks, R. W. & Ruszniewski, P. Role of Hepatic Intra-Arterial Therapies in Metastatic Neuroendocrine Tumours (NET): Guidelines from the NET-Liver-Metastases Consensus Conference. *HPB (Oxford)* **17,** 29–37 (2015).

60. Lines, K. E., Stevenson, M., Filippakopoulos, P., Müller, S., Lockstone, H. E., Wright, B., Grozinsky-Glasberg, S., Grossman, A. B., Knapp, S., Buck, D., Bountra, C. & Thakker, R. V. Epigenetic Pathway Inhibitors Represent Potential Drugs for Treating Pancreatic and Bronchial Neuroendocrine Tumors. *Oncogenesis* **6,** e332–e332 (5 2017).

61. Das, S., Al-Toubah, T. & Strosberg, J. Chemotherapy in Neuroendocrine Tumors. *Cancers* **13,** 4872 (19 2021).

62. Rinke, A. & Gress, T. M. Neuroendocrine Cancer, Therapeutic Strategies in G3 Cancers. *Digestion* **95,** 109–114 (2017).

63. Rinke, A., Müller, H.-H., Schade-Brittinger, C., Klose, K.-J., Barth, P., Wied, M., Mayer, C., Aminossadati, B., Pape, U.-F., Bläker, M., Harder, J., Arnold, C., Gress, T., Arnold, R. & PROMID Study Group. Placebo-Controlled, Double-Blind, Prospective, Randomized Study on the Effect of Octreotide LAR in the Control of Tumor Growth in Patients with Metastatic Neuroendocrine Midgut Tumors: A Report from the PROMID Study Group. *J Clin Oncol* **27,** 4656–4663 (2009).

64. Yao, J. C., Shah, M. H., Ito, T., Bohas, C. L., Wolin, E. M., Van Cutsem, E., Hobday, T. J., Okusaka, T., Capdevila, J., de Vries, E. G. E., Tomassetti, P., Pavel, M. E., Hoosen, S., Haas, T., Lincy, J., Lebwohl, D., Öberg, K. & RAD001 in Advanced Neuroendocrine Tumors, Third Trial (RADIANT-3) Study Group. Everolimus for Advanced Pancreatic Neuroendocrine Tumors. *N Engl J Med* **364,** 514–523 (2011).

65. Raymond, E., Dahan, L., Raoul, J.-L., Bang, Y.-J., Borbath, I., Lombard-Bohas, C., Valle, J., Metrakos, P., Smith, D., Vinik, A., Chen, J.-S., Hörsch, D., Hammel, P., Wiedenmann, B., Van Cutsem, E., Patyna, S., Lu, D. R., Blanckmeister, C., Chao, R. & Ruszniewski, P. Sunitinib Malate for the Treatment of Pancreatic Neuroendocrine Tumors. *N Engl J Med* **364,** 501–513 (2011).

66. Caplin, M. E., Pavel, M., Ćwikła, J. B., Phan, A. T., Raderer, M., Sedláčková, E., Cadiot, G., Wolin, E. M., Capdevila, J., Wall, L., Rindi, G., Langley, A., Martinez, S., Blumberg, J., Ruszniewski, P. & CLARINET Investigators. Lanreotide in Metastatic Enteropancreatic Neuroendocrine Tumors. *N Engl J Med* **371,** 224–233 (2014).

67. Strosberg, J., El-Haddad, G., Wolin, E., Hendifar, A., Yao, J., Chasen, B., Mittra, E., Kunz, P. L., Kulke, M. H., Jacene, H., Bushnell, D., O'Dorisio, T. M., Baum, R. P., Kulkarni, H. R., Caplin, M., Lebtahi, R., Hobday, T., Delpassand, E., Van Cutsem, E., Benson, A., Srirajaskanthan, R., Pavel, M., Mora, J., Berlin, J., Grande, E., Reed, N., Seregni, E., Öberg, K., Lopera Sierra, M., Santoro, P., Thevenet, T., Erion, J. L., Ruszniewski, P., Kwekkeboom, D., Krenning, E. & NETTER-1 Trial Investigators. Phase 3 Trial of 177Lu-Dotatate for Midgut Neuroendocrine Tumors. *N Engl J Med* **376,** 125–135 (2017).

68. Chan, J., Geyer, S., Ou, F.-S., Knopp, M., Behr, S., Zemla, T., Acoba, J., Shergill, A., Wolin, E. M., Halfdanarson, T. R., Trikalinos, N., Konda, B., Vijayvergia, N., Dasari, N. A., Strosberg, J., Kohn, E. C., Kulke, M. H., O'Reilly, E. M. & Meyerhardt, J. A. LBA53 Alliance A021602: Phase III, Double-Blinded Study of Cabozantinib versus Placebo for Advanced Neuroendocrine Tumors (NET) after Progression on Prior Therapy (CABINET). *Ann Oncol* **34,** S1292 (2023).

69. Singh, S., Halperin, D. M., Myrehaug, S., Herrmann, K., Pavel, M., Kunz, P. L., Chasen, B., Capdevila, J., Tafuto, S., Oh, D.-Y., Yoo, C., Falk, S., Halfdanarson, T. R., Folitar, I., Zhang, Y., Santoro, P., Aimone, P., de Herder, W. W. & Ferone, D. [177Lu]Lu-DOTA-TATE in Newly Diagnosed Patients with Advanced Grade 2 and Grade 3, Well-Differentiated Gastroenteropancreatic Neuroendocrine Tumors: Primary Analysis of the Phase 3 Randomized NETTER-2 Study. *JCO* **42,** LBA588–LBA588 (3_suppl 2024).

70. Loharkar, S. & Basu, S. Peptide Receptor Radionuclide Therapy in Neuroendocrine Neoplasms and Related Tumors: From Fundamentals to Personalization and the Newer Experimental Approaches. *Expert Rev Precis Med Drug Dev* **8,** 1–32 (2023).

71. Bodei, L., Modlin, I. M., Luster, M., Forrer, F., Cremonesi, M., Hicks, R. J., Ezziddin, S., Kidd, M. & Chiti, A. Myeloid Neoplasms after Chemotherapy and PRRT: Myth and Reality. *Endocr Relat Cancer* **23,** C1–7 (2016).

72. Brandi, M. L., Agarwal, S. K., Perrier, N. D., Lines, K. E., Valk, G. D. & Thakker, R. V. Multiple Endocrine Neoplasia Type 1: Latest Insights. *Endocr Rev* **42,** 133–170 (2021).

73. Thakker, R. V., Newey, P. J., Walls, G. V., Bilezikian, J., Dralle, H., Ebeling, P. R., Melmed, S., Sakurai, A., Tonelli, F. & Brandi, M. L. Clinical Practice Guidelines for Multiple Endocrine Neoplasia Type 1 (MEN1). *J Clin Endocrinol Metab* **97,** 2990–3011 (2012).

74. Thakker, R. V. Multiple Endocrine Neoplasia Type 1 (MEN1) and Type 4 (MEN4). *Mol Cell Endocrinol* **386,** 2–15 (2014).

75. Waguespack, S. G. Beyond the "3 Ps": A Critical Appraisal of the Non-Endocrine Manifestations of Multiple Endocrine Neoplasia Type 1. *Front Endocrinol (Lausanne)* **13,** 1029041 (2022).

76. Gaujoux, S., Martin, G. L., Mirallié, E., Regenet, N., Le Bras, M., Pattou, F., Carnaille, B., Cardot-Bauters, C., Groussin, L., Faron, M., Chanson, P., Najah, H., Tabarin, A., Sauvanet, A., Ruszniewski, P., Lifante, J. C., Walter, T., Carrère, N., Caron, P., Deguelte, S., Delemer, B., Binquet, C., Jannot, A. S. & Goudet, P. Life Expectancy and Likelihood of Surgery in Multiple Endocrine Neoplasia Type 1: AFCE and GTE Cohort Study. *Br J Surg* **109,** 872–879 (2022).

77. Goudet, P., Murat, A., Binquet, C., Cardot-Bauters, C., Costa, A., Ruszniewski, P., Niccoli, P., Ménégaux, F., Chabrier, G., Borson-Chazot, F., Tabarin, A., Bouchard, P., Delemer, B., Beckers, A. & Bonithon-Kopp, C. Risk Factors and Causes of Death in MEN1 Disease. A GTE (Groupe d'Etude Des Tumeurs Endocrines) Cohort Study among 758 Patients. *World J Surg* **34,** 249–255 (2010).

78. Knudson, A. G., Meadows, A. T., Nichols, W. W. & Hill, R. Chromosomal Deletion and Retinoblastoma. *N Engl J Med* **295,** 1120–1123 (1976).

79. Pannett, A. A. & Thakker, R. V. Somatic Mutations in MEN Type 1 Tumors, Consistent with the Knudson "Two-Hit" Hypothesis. *J Clin Endocrinol Metab* **86,** 4371–4374 (2001).

80. Bassett, J. H., Forbes, S. A., Pannett, A. A., Lloyd, S. E., Christie, P. T., Wooding, C., Harding, B., Besser, G. M., Edwards, C. R., Monson, J. P., Sampson, J., Wass, J. A., Wheeler, M. H. & Thakker, R. V. Characterization of Mutations in Patients with Multiple Endocrine Neoplasia Type 1. *Am J Hum Genet* **62,** 232–244 (1998).

81. Dean, P. G., van Heerden, J. A., Farley, D. R., Thompson, G. B., Grant, C. S., Harmsen, W. S. & Ilstrup, D. M. Are Patients with Multiple Endocrine Neoplasia Type I Prone to Premature Death? *World J Surg* **24,** 1437–1441 (2000).

82. Thevenon, J., Bourredjem, A., Faivre, L., Cardot-Bauters, C., Calender, A., Murat, A., Giraud, S., Niccoli, P., Odou, M. F., Borson-Chazot, F., Barlier, A., Lombard-Bohas, C., Clauser, E., Tabarin, A., Parfait, B., Chabre, O., Castermans, E., Beckers, A., Ruszniewski, P., Le Bras, M., Delemer, B., Bouchard, P., Guilhem, I., Rohmer, V., Goichot, B., Caron, P., Baudin, E., Chanson, P., Groussin, L., Du Boullay, H., Weryha, G., Lecomte, P., Penfornis, A., Bihan, H., Archambeaud, F., Kerlan, V., Duron, F., Kuhn, J. M., Vergès, B., Rodier, M., Renard, M., Sadoul, J. L., Binquet, C. & Goudet, P. Higher Risk of Death among MEN1 Patients with Mutations in the JunD Interacting Domain: A Groupe d'etude Des Tumeurs Endocrines (GTE) Cohort Study. *Hum Mol Genet* **22,** 1940–8 (2013).

83. Van Leeuwaarde, R. S., Pieterman, C. R. C., Bleiker, E. M. A., Dekkers, O. M., van der Horst-Schrivers, A. N., Hermus, A. R., de Herder, W. W., Drent, M. L., Bisschop, P. H., Havekes, B., Vriens, M. R. & Valk, G. D. High Fear of Disease Occurrence Is Associated With Low Quality of Life in Patients With Multiple Endocrine Neoplasia Type 1: Results From the Dutch MEN1 Study Group. *J Clin Endocrinol Metab* **103,** 2354–2361 (2018).

84. Newey, P. J., Jeyabalan, J., Walls, G. V., Christie, P. T., Gleeson, F. V., Gould, S., Johnson, P. R., Phillips, R. R., Ryan, F. J., Shine, B., Bowl, M. R. & Thakker, R. V. Asymptomatic Children with Multiple Endocrine Neoplasia Type 1 Mutations May Harbor Nonfunctioning Pancreatic Neuroendocrine Tumors. *J Clin Endocrinol Metab* **94,** 3640–6 (2009).

85. Gonçalves, T. D., Toledo, R. A., Sekiya, T., Matuguma, S. E., Maluf Filho, F., Rocha, M. S., Siqueira, S. A., Glezer, A., Bronstein, M. D., Pereira, M. A., Jureidini, R., Bacchella, T., Machado, M. C., Toledo, S. P. & Lourenço Jr., D. M. Penetrance of Functioning and Nonfunctioning Pancreatic Neuroendocrine Tumors in Multiple Endocrine Neoplasia Type 1 in the Second Decade of Life. *J Clin Endocrinol Metab* **99,** E89–96 (2014).

86. Manoharan, J., Raue, F., Lopez, C. L., Albers, M. B., Bollmann, C., Fendrich, V., Slater, E. P. & Bartsch, D. K. Is Routine Screening of Young Asymptomatic MEN1 Patients Necessary? *World J Surg* **41,** 2026–2032 (2017).

87. Vannucci, L., Marini, F., Giusti, F., Ciuffi, S., Tonelli, F. & Brandi, M. L. MEN1 in Children and Adolescents: Data from Patients of a Regional Referral Center for Hereditary Endocrine Tumors. *Endocrine* **59,** 438–448 (2018).

88. Marini, F., Giusti, F., Tonelli, F. & Brandi, M. L. When Parathyroidectomy Should Be Indicated or Postponed in Adolescents with MEN1-related Primary Hyperparathyroidism. *Front Endocrinol* **9,** 597 (2018).

89. Herath, M., Parameswaran, V., Thompson, M., Williams, M. & Burgess, J. Paediatric and Young Adult Manifestations and Outcomes of Multiple Endocrine Neoplasia Type 1. *Clin Endocrinol (Oxf)* **91,** 633–638 (2019).

90. Goudet, P., Dalac, A., Le Bras, M., Cardot-Bauters, C., Niccoli, P., Lévy-Bohbot, N., du Boullay, H., Bertagna, X., Ruszniewski, P., Borson-Chazot, F., Vergès, B., Sadoul, J. L., Ménégaux, F., Tabarin, A., Kühn, J. M., d'Anella, P., Chabre, O., Christin-Maitre, S., Cadiot, G., Binquet, C. & Delemer, B. MEN1 Disease Occurring Before 21 Years Old: A 160-Patient Cohort Study From the Groupe d'étude Des Tumeurs Endocrines. *J Clin Endocrinol Metab* **100,** 1568–1577 (2015).

91. Frederiksen, A., Rossing, M., Hermann, P., Ejersted, C., Thakker, R. V. & Frost, M. Clinical Features of Multiple Endocrine Neoplasia Type 4: Novel Pathogenic Variant and Review of Published Cases. *J Clin Endocrinol Metab* **104,** 3637–3646 (2019).

92. Mosele, F., Remon, J., Mateo, J., Westphalen, C. B., Barlesi, F., Lolkema, M. P., Normanno, N., Scarpa, A., Robson, M., Meric-Bernstam, F., Wagle, N., Stenzinger, A., Bonastre, J., Bayle, A., Michiels, S., Bièche, I., Rouleau, E., Jezdic, S., Douillard, J.-Y., Reis-Filho, J. S., Dienstmann, R. & André, F. Recommendations for the Use of Next-Generation Sequencing (NGS) for Patients with Metastatic Cancers: A Report from the ESMO Precision Medicine Working Group. *Ann Oncol* **31,** 1491–1505 (2020).

93. Goldhirsch, A., Winer, E. P., Coates, A. S., Gelber, R. D., Piccart-Gebhart, M., Thürlimann, B., Senn, H.-J., Albain, K. S., André, F., Bergh, J., Bonnefoi, H., Bretel-Morales, D., Burstein, H., Cardoso, F., Castiglione-Gertsch, M., Coates, A. S., Colleoni, M., Costa, A., Curigliano, G., Davidson, N. E., Leo, A. D., Ejlertsen, B., Forbes, J. F., Gelber, R. D., Gnant, M., Goldhirsch, A., Goodwin, P., Goss, P. E., Harris, J. R., Hayes, D. F., Hudis, C. A., Ingle, J. N., Jassem, J., Jiang, Z., Karlsson, P., Loibl, S., Morrow, M., Namer, M., Osborne, C. K., Partridge, A. H., Penault-Llorca, F., Perou, C. M., Piccart-Gebhart, M. J., Pritchard, K. I., Rutgers, E. J. T., Sedlmayer, F., Semiglazov, V., Shao, Z.-M., Smith, I., Thürlimann, B., Toi, M., Tutt, A., Untch, M., Viale, G., Watanabe, T., Wilcken, N., Winer, E. P. & Wood, W. C. Personalizing the Treatment of Women with Early Breast Cancer:

Highlights of the St Gallen International Expert Consensus on the Primary Therapy of Early Breast Cancer 2013. *Ann Oncol* **24,** 2206–2223 (2013).

94. Rouzier, R., Perou, C. M., Symmans, W. F., Ibrahim, N., Cristofanilli, M., Anderson, K., Hess, K. R., Stec, J., Ayers, M., Wagner, P., Morandi, P., Fan, C., Rabiul, I., Ross, J. S., Hortobagyi, G. N. & Pusztai, L. Breast Cancer Molecular Subtypes Respond Differently to Preoperative Chemotherapy. *Clin Cancer Res* **11,** 5678–5685 (2005).

95. Oleinikov, K. & Grozinsky-Glasberg, S. Hereditary Syndromes Associated with Neuroendocrine Tumors. *Curr Opin Endocr Metab Res* **18,** 230–235 (2021).

96. Latif, F., Tory, K., Gnarra, J., Yao, M., Duh, F. M., Orcutt, M. L., Stackhouse, T., Kuzmin, I., Modi, W. & Geil, L. Identification of the von Hippel-Lindau Disease Tumor Suppressor Gene. *Science* **260,** 1317–1320 (1993).

97. Wallace, M. R., Marchuk, D. A., Andersen, L. B., Letcher, R., Odeh, H. M., Saulino, A. M., Fountain, J. W., Brereton, A., Nicholson, J., Mitchell, A. L., Brownstein, B. H. & Collins, F. S. Type 1 Neurofibromatosis Gene: Identification of a Large Transcript Disrupted in Three NF1 Patients. *Science* **249,** 181–186 (1990).

98. Consortium, E. C. 1. T. S. Identification and Characterization of the Tuberous Sclerosis Gene on Chromosome 16. *Cell* **75,** 1305–1315 (1993).

99. Van Slegtenhorst, M., de Hoogt, R., Hermans, C., Nellist, M., Janssen, B., Verhoef, S., Lindhout, D., van den Ouweland, A., Halley, D., Young, J., Burley, M., Jeremiah, S., Woodward, K., Nahmias, J., Fox, M., Ekong, R., Osborne, J., Wolfe, J., Povey, S., Snell, R. G., Cheadle, J. P., Jones, A. C., Tachataki, M., Ravine, D., Sampson, J. R., Reeve, M. P., Richardson, P., Wilmer, F., Munro, C., Hawkins, T. L., Sepp, T., Ali, J. B., Ward, S., Green, A. J., Yates, J. R., Kwiatkowska, J., Henske, E. P., Short, M. P., Haines, J. H., Jozwiak, S. & Kwiatkowski, D. J. Identification of the Tuberous Sclerosis Gene TSC1 on Chromosome 9q34. *Science* **277,** 805–808 (1997).

100. Jiao, Y., Shi, C., Edil, B. H., de Wilde, R. F., Klimstra, D. S., Maitra, A., Schulick, R. D., Tang, L. H., Wolfgang, C. L., Choti, M. A., Velculescu, V. E., Diaz, L. A., Vogelstein, B., Kinzler, K. W., Hruban, R. H. & Papadopoulos, N. DAXX/ATRX, MEN1, and mTOR Pathway Genes Are Frequently Altered in Pancreatic Neuroendocrine Tumors. *Science* **331,** 1199–1203 (2011).

101. Scarpa, A., Chang, D. K., Nones, K., Corbo, V., Patch, A.-M., Bailey, P., Lawlor, R. T., Johns, A. L., Miller, D. K., Mafficini, A., Rusev, B., Scardoni, M., Antonello, D., Barbi, S., Sikora, K. O., Cingarlini, S., Vicentini, C., McKay, S., Quinn, M. C. J., Bruxner, T. J. C., Christ, A. N., Harliwong, I., Idrisoglu, S., McLean, S., Nourse, C., Nourbakhsh, E., Wilson, P. J., Anderson, M. J., Fink, J. L., Newell, F., Waddell, N., Holmes, O., Kazakoff, S. H., Leonard, C., Wood, S., Xu, Q., Nagaraj, S. H., Amato, E., Dalai, I., Bersani, S., Cataldo, I., Dei Tos, A. P., Capelli, P., Davì, M. V., Landoni, L., Malpaga, A., Miotto, M., Whitehall, V. L. J., Leggett, B. A., Harris, J. L., Harris, J., Jones, M. D., Humphris, J., Chantrill, L. A., Chin, V., Nagrial, A. M., Pajic, M., Scarlett, C. J., Pinho, A., Rooman, I., Toon, C., Wu, J., Pinese, M., Cowley, M., Barbour, A., Mawson, A., Humphrey, E. S., Colvin, E. K., Chou, A., Lovell, J. A., Jamieson, N. B., Duthie, F., Gingras, M.-C., Fisher, W. E., Dagg, R. A., Lau, L. M. S., Lee, M., Pickett, H. A., Reddel, R. R., Samra, J. S., Kench, J. G., Merrett, N. D., Epari, K., Nguyen, N. Q., Zeps, N., Falconi, M., Simbolo, M., Butturini, G., Van Buren, G., Partelli, S., Fassan, M., Khanna, K. K.,

Gill, A. J., Wheeler, D. A., Gibbs, R. A., Musgrove, E. A., Bassi, C., Tortora, G., Pederzoli, P., Pearson, J. V., Waddell, N., Biankin, A. V. & Grimmond, S. M. Whole-Genome Landscape of Pancreatic Neuroendocrine Tumours. *Nature* **543,** 65–71 (2017).

102. Corbo, V., Dalai, I., Scardoni, M., Barbi, S., Beghelli, S., Bersani, S., Albarello, L., Doglioni, C., Schott, C., Capelli, P., Chilosi, M., Boninsegna, L., Becker, K.-F., Falconi, M. & Scarpa, A. MEN1 in Pancreatic Endocrine Tumors: Analysis of Gene and Protein Status in 169 Sporadic Neoplasms Reveals Alterations in the Vast Majority of Cases. *Endocr Relat Cancer* **17,** 771–783 (2010).

103. Mafficini, A. & Scarpa, A. Genomic Landscape of Pancreatic Neuroendocrine Tumours: The International Cancer Genome Consortium. *J Endocrinol* **236,** R161–R167 (2018).

104. Cao, Y., Gao, Z., Li, L., Jiang, X., Shan, A., Cai, J., Peng, Y., Li, Y., Jiang, X., Huang, X., Wang, J., Wei, Q., Qin, G., Zhao, J., Jin, X., Liu, L., Li, Y., Wang, W., Wang, J. & Ning, G. Whole Exome Sequencing of Insulinoma Reveals Recurrent T372R Mutations in YY1. *Nat Commun* **4,** 2810 (2013).

105. Parekh, V. I., Modali, S. D., Welch, J., Simonds, W. F., Weinstein, L. S., Kebebew, E. & Agarwal, S. K. Frequency and Consequence of the Recurrent YY1 p.T372R Mutation in Sporadic Insulinomas. *Endocr Relat Cancer* **25,** L31–L35 (2018).

106. Hong, X., Qiao, S., Li, F., Wang, W., Jiang, R., Wu, H., Chen, H., Liu, L., Peng, J., Wang, J., Jia, C., Liang, X., Dai, H., Jiang, J., Zhang, T., Liao, Q., Dai, M., Cong, L., Han, X., Guo, D., Liang, Z., Li, D., Zheng, Z., Ye, C., Li, S., Zhao, Y., Wu, K. & Wu, W. Whole-Genome Sequencing Reveals Distinct Genetic Bases for Insulinomas and Non-Functional Pancreatic Neuroendocrine Tumours: Leading to a New Classification System. *Gut* **69,** 877–887 (2020).

107. Waddell, N., Pajic, M., Patch, A.-M., Chang, D. K., Kassahn, K. S., Bailey, P., Johns, A. L., Miller, D., Nones, K., Quek, K., Quinn, M. C. J., Robertson, A. J., Fadlullah, M. Z. H., Bruxner, T. J. C., Christ, A. N., Harliwong, I., Idrisoglu, S., Manning, S., Nourse, C., Nourbakhsh, E., Wani, S., Wilson, P. J., Markham, E., Cloonan, N., Anderson, M. J., Fink, J. L., Holmes, O., Kazakoff, S. H., Leonard, C., Newell, F., Poudel, B., Song, S., Taylor, D., Waddell, N., Wood, S., Xu, Q., Wu, J., Pinese, M., Cowley, M. J., Lee, H. C., Jones, M. D., Nagrial, A. M., Humphris, J., Chantrill, L. A., Chin, V., Steinmann, A. M., Mawson, A., Humphrey, E. S., Colvin, E. K., Chou, A., Scarlett, C. J., Pinho, A. V., Giry-Laterriere, M., Rooman, I., Samra, J. S., Kench, J. G., Pettitt, J. A., Merrett, N. D., Toon, C., Epari, K., Nguyen, N. Q., Barbour, A., Zeps, N., Jamieson, N. B., Graham, J. S., Niclou, S. P., Bjerkvig, R., Grützmann, R., Aust, D., Hruban, R. H., Maitra, A., Iacobuzio-Donahue, C. A., Wolfgang, C. L., Morgan, R. A., Lawlor, R. T., Corbo, V., Bassi, C., Falconi, M., Zamboni, G., Tortora, G., Tempero, M. A., Australian Pancreatic Cancer Genome Initiative, Gill, A. J., Eshleman, J. R., Pilarsky, C., Scarpa, A., Musgrove, E. A., Pearson, J. V., Biankin, A. V. & Grimmond, S. M. Whole Genomes Redefine the Mutational Landscape of Pancreatic Cancer. *Nature* **518,** 495–501 (2015).

108. Allis, C. D. & Jenuwein, T. The Molecular Hallmarks of Epigenetic Control. *Nat Rev Genet* **17,** 487–500 (2016).

109. Hyun, K., Jeon, J., Park, K. & Kim, J. Writing, Erasing and Reading Histone Lysine Methylations. *Exp Mol Med* **49,** e324–e324 (2017).

110. Jenuwein, T. & Allis, C. D. Translating the Histone Code. *Science* **293,** 1074–1080 (2001).

111. Jones, P. A., Issa, J.-P. J. & Baylin, S. Targeting the Cancer Epigenome for Therapy. *Nat Rev Genet* **17,** 630–641 (2016).

112. Du, R., Huang, C., Liu, K., Li, X. & Dong, Z. Targeting AURKA in Cancer: Molecular Mechanisms and Opportunities for Cancer Therapy. *Mol Cancer* **20,** 15 (2021).

113. Bird, A. DNA Methylation Patterns and Epigenetic Memory. *Genes Dev* **16,** 6–21 (2002).

114. Okano, M., Bell, D. W., Haber, D. A. & Li, E. DNA Methyltransferases Dnmt3a and Dnmt3b Are Essential for de Novo Methylation and Mammalian Development. *Cell* **99,** 247–257 (1999).

115. Leonhardt, H., Page, A. W., Weier, H. U. & Bestor, T. H. A Targeting Sequence Directs DNA Methyltransferase to Sites of DNA Replication in Mammalian Nuclei. *Cell* **71,** 865–873 (1992).

116. Kohli, R. M. & Zhang, Y. TET Enzymes, TDG and the Dynamics of DNA Demethylation. *Nature* **502,** 472–479 (2013).

117. Bird, A. P. CpG-rich Islands and the Function of DNA Methylation. *Nature* **321,** 209–213 (1986–0021).

118. Ren, R., Horton, J. R., Zhang, X., Blumenthal, R. M. & Cheng, X. Detecting and Interpreting DNA Methylation Marks. *Curr Opin Struct Biol* **53,** 88–99 (2018).

119. Iyer, S. & Agarwal, S. K. Epigenetic Regulation in the Tumorigenesis of MEN1-associated Endocrine Cell Types. *J Mol Endocrinol* **61,** R13–R24 (2018).

120. Huang, J., Gurung, B., Wan, B., Matkar, S., Veniaminova, N. A., Wan, K., Merchant, J. L., Hua, X. & Lei, M. The Same Pocket in Menin Binds Both MLL and JUND but Has Opposite Effects on Transcription. *Nature* **482,** 542–546 (2012).

121. Agarwal, S. K., Guru, S. C., Heppner, C., Erdos, M. R., Collins, R. M., Park, S. Y., Saggar, S., Chandrasekharappa, S. C., Collins, F. S., Spiegel, A. M., Marx, S. J. & Burns, A. L. Menin Interacts with the AP1 Transcription Factor JunD and Represses JunD-activated Transcription. *Cell* **96,** 143–152 (1999).

122. Clapier, C. R., Iwasa, J., Cairns, B. R. & Peterson, C. L. Mechanisms of Action and Regulation of ATP-dependent Chromatin-Remodelling Complexes. *Nat Rev Mol Cell Biol* **18,** 407–422 (2017).

123. Karakose, E., Wang, H., Inabnet, W., Thakker, R. V., Libutti, S., Fernandez-Ranvier, G., Suh, H., Stevenson, M., Kinoshita, Y., Donovan, M., Antipin, Y., Li, Y., Liu, X., Jin, F., Wang, P., Uzilov, A., Argmann, C., Schadt, E. E., Stewart, A. F., Scott, D. K. & Lambertini, L. Aberrant Methylation Underlies Insulin Gene Expression in Human Insulinoma. *Nat Commun* **11,** 5210 (2020).

124. Demars, J. & Gicquel, C. Epigenetic and Genetic Disturbance of the Imprinted 11p15 Region in Beckwith-Wiedemann and Silver-Russell Syndromes. *Clin Genet* **81,** 350–361 (2012).

125. Cejas, P., Drier, Y., Dreijerink, K. M. A., Brosens, L. A. A., Deshpande, V., Epstein, C. B., Conemans, E. B., Morsink, F. H. M., Graham, M. K., Valk, G. D., Vriens, M. R., Fernandez-del Castillo, C., Ferrone, C., Adar, T., Bowden, M., Whitton, H. J., Da Silva, A., Font-Tello, A., Long, H. W., Gaskell, E., Shoresh, N., Heaphy, C. M., Sicinska, E., Kulke, M. H., Chung, D. C., Bernstein, B. E. & Shivdasani, R. A. Enhancer Signatures Stratify and Predict Outcomes of Non-Functional Pancreatic Neuroendocrine Tumors. *Nat Med* **25,** 1260–1265 (2019).

126. Kouzarides, T. Chromatin Modifications and Their Function. *Cell* **128,** 693–705 (2007).

127. Creyghton, M. P., Cheng, A. W., Welstead, G. G., Kooistra, T., Carey, B. W., Steine, E. J., Hanna, J., Lodato, M. A., Frampton, G. M., Sharp, P. A., Boyer, L. A., Young, R. A. & Jaenisch, R. Histone H3K27ac Separates Active from Poised Enhancers and Predicts Developmental State. *Proc Natl Acad Sci U S A* **107,** 21931–21936 (2010).

128. Duttke, S. H., Lacadie, S. A., Ibrahim, M. M., Glass, C. K., Corcoran, D. L., Benner, C., Heinz, S., Kadonaga, J. T. & Ohler, U. Human Promoters Are Intrinsically Directional. *Mol Cell* **57,** 674–684 (2015).

129. Whyte, W. A., Orlando, D. A., Hnisz, D., Abraham, B. J., Lin, C. Y., Kagey, M. H., Rahl, P. B., Lee, T. I. & Young, R. A. Master Transcription Factors and Mediator Establish Super-Enhancers at Key Cell Identity Genes. *Cell* **153,** 307–319 (2013).

130. Fujisawa, T. & Filippakopoulos, P. Functions of Bromodomain-Containing Proteins and Their Roles in Homeostasis and Cancer. *Nat Rev Mol Cell Biol* **18,** 246–262 (2017).

131. Filippakopoulos, P., Picaud, S., Mangos, M., Keates, T., Lambert, J.-P., Barsyte-Lovejoy, D., Felletar, I., Volkmer, R., Müller, S., Pawson, T., Gingras, A.-C., Arrowsmith, C. H. & Knapp, S. Histone Recognition and Large-Scale Structural Analysis of the Human Bromodomain Family. *Cell* **149,** 214–231 (2012).

132. Lovén, J., Hoke, H. A., Lin, C. Y., Lau, A., Orlando, D. A., Vakoc, C. R., Bradner, J. E., Lee, T. I. & Young, R. A. Selective Inhibition of Tumor Oncogenes by Disruption of Super-Enhancers. *Cell* **153,** 320–334 (2013).

133. Bechter, O. & Schöffski, P. Make Your Best BET: The Emerging Role of BET Inhibitor Treatment in Malignant Tumors. *Pharmacol Ther* **208,** 107479 (2020).

134. Shang, E., Nickerson, H. D., Wen, D., Wang, X. & Wolgemuth, D. J. The First Bromodomain of Brdt, a Testis-Specific Member of the BET Sub-Family of Double-Bromodomain-Containing Proteins, Is Essential for Male Germ Cell Differentiation. *Development* **134,** 3507–3515 (2007).

135. Belkina, A. C. & Denis, G. V. BET Domain Co-Regulators in Obesity, Inflammation and Cancer. *Nat Rev Cancer* **12,** 465–477 (2012).

136. Liu, W., Ma, Q., Wong, K., Li, W., Ohgi, K., Zhang, J., Aggarwal, A. & Rosenfeld, M. G. Brd4 and JMJD6-associated Anti-Pause Enhancers in Regulation of Transcriptional Pause Release. *Cell* **155,** 1581–1595 (2013).

137. Rahman, S., Sowa, M. E., Ottinger, M., Smith, J. A., Shi, Y., Harper, J. W. & Howley, P. M. The Brd4 Extraterminal Domain Confers Transcription Activation Independent of pTEFb by Recruiting Multiple Proteins, Including NSD3. *Mol Cell Biol* **31,** 2641–2652 (2011).

138. Conrad, R. J., Fozouni, P., Thomas, S., Sy, H., Zhang, Q., Zhou, M.-M. & Ott, M. The Short Isoform of BRD4 Promotes HIV-1 Latency by Engaging Repressive SWI/SNF Chromatin-Remodeling Complexes. *Mol Cell* **67,** 1001–1012.e6 (2017).

139. Eischer, N., Arnold, M. & Mayer, A. Emerging Roles of BET Proteins in Transcription and Co-Transcriptional RNA Processing. *Wiley Interdiscip Rev RNA* **14,** e1734 (2023).

140. Sinha, A., Faller, D. V. & Denis, G. V. Bromodomain Analysis of Brd2-dependent Transcriptional Activation of Cyclin A. *Biochem J* **387,** 257–269 (Pt 1 2005).

141. Lamonica, J. M., Deng, W., Kadauke, S., Campbell, A. E., Gamsjaeger, R., Wang, H., Cheng, Y., Billin, A. N., Hardison, R. C., Mackay, J. P. & Blobel, G. A. Bromodomain Protein Brd3 Associates with Acetylated GATA1 to Promote Its Chromatin Occupancy at Erythroid Target Genes. *Proc Natl Acad Sci U S A* **108,** E159–168 (2011).

142. Jang, M. K., Mochizuki, K., Zhou, M., Jeong, H.-S., Brady, J. N. & Ozato, K. The Bromodomain Protein Brd4 Is a Positive Regulatory Component of P-TEFb and Stimulates RNA Polymerase II-dependent Transcription. *Mol Cell* **19,** 523–534 (2005).

143. Kotekar, A., Singh, A. K. & Devaiah, B. N. BRD4 and MYC: Power Couple in Transcription and Disease. *FEBS J.* **290,** 4820–4842 (2023).

144. Qin, Z.-Y., Wang, T., Su, S., Shen, L.-T., Zhu, G.-X., Liu, Q., Zhang, L., Liu, K.-W., Zhang, Y., Zhou, Z.-H., Zhang, X.-N., Wen, L.-Z., Yao, Y.-L., Sun, W.-J., Guo, Y., Liu, K.-J., Liu, L., Wang, X.-W., Wei, Y.-L., Wang, J., Xiao, H.-L., Liu, P., Bian, X.-W., Chen, D.-F. & Wang, B. BRD4 Promotes Gastric Cancer Progression and Metastasis through Acetylation-Dependent Stabilization of Snail. *Cancer Res* **79,** 4869–4881 (2019).

145. Jiao, F., Han, T., Yuan, C., Liang, Y., Cui, J., Zhuo, M. & Wang, L. Caveolin-2 Is Regulated by BRD4 and Contributes to Cell Growth in Pancreatic Cancer. *Cancer Cell Int* **20,** 55 (2020).

146. Li, G.-Q., Guo, W.-Z., Zhang, Y., Seng, J.-J., Zhang, H.-P., Ma, X.-X., Zhang, G., Li, J., Yan, B., Tang, H.-W., Li, S.-S., Wang, L.-D. & Zhang, S.-J. Suppression of BRD4 Inhibits Human Hepatocellular Carcinoma by Repressing MYC and Enhancing BIM Expression. *Oncotarget* **7,** 2462–2474 (2016).

147. Hong, S. H., Eun, J. W., Choi, S. K., Shen, Q., Choi, W. S., Han, J.-W., Nam, S. W. & You, J. S. Epigenetic Reader BRD4 Inhibition as a Therapeutic Strategy to Suppress E2F2-cell Cycle Regulation Circuit in Liver Cancer. *Oncotarget* **7,** 32628–32640 (2016).

148. Wong, C., Laddha, S. V., Tang, L., Vosburgh, E., Levine, A. J., Normant, E., Sandy, P., Harris, C. R., Chan, C. S. & Xu, E. Y. The Bromodomain and Extra-Terminal Inhibitor CPI203 Enhances the Antiproliferative Effects of Rapamycin on Human Neuroendocrine Tumors. *Cell Death Dis* **5,** e1450 (2014).

149. Filippakopoulos, P., Qi, J., Picaud, S., Shen, Y., Smith, W. B., Fedorov, O., Morse, E. M., Keates, T., Hickman, T. T., Felletar, I., Philpott, M., Munro, S., McKeown, M. R., Wang, Y., Christie, A. L., West, N., Cameron, M. J., Schwartz, B., Heightman, T. D., La Thangue, N., French, C. A., Wiest, O., Kung, A. L., Knapp, S. & Bradner, J. E. Selective Inhibition of BET Bromodomains. *Nature* **468,** 1067–1073 (2010).

150. Seal, J., Lamotte, Y., Donche, F., Bouillot, A., Mirguet, O., Gellibert, F., Nicodeme, E., Krysa, G., Kirilovsky, J., Beinke, S., McCleary, S., Rioja, I., Bamborough, P., Chung, C.-W., Gordon, L., Lewis, T., Walker, A. L., Cutler, L., Lugo, D., Wilson, D. M., Witherington, J., Lee, K. & Prinjha, R. K. Identification of a Novel Series of BET Family Bromodomain Inhibitors: Binding Mode and Profile of I-BET151 (GSK1210151A). *Bioorg Med Chem Lett* **22,** 2968–2972 (2012).

151. Andrieu, G., Belkina, A. C. & Denis, G. V. Clinical Trials for BET Inhibitors Run Ahead of the Science. *Drug Discov Today Technol* **19,** 45–50 (2016).

152. Gilan, O., Rioja, I., Knezevic, K., Bell, M. J., Yeung, M. M., Harker, N. R., Lam, E. Y. N., Chung, C.-W., Bamborough, P., Petretich, M., Urh, M., Atkinson, S. J., Bassil, A. K., Roberts, E. J., Vassiliadis, D., Burr, M. L., Preston, A. G. S., Wellaway, C., Werner, T., Gray, J. R., Michon, A.-M., Gobbetti, T., Kumar, V., Soden, P. E., Haynes, A., Vappiani, J., Tough, D. F., Taylor, S., Dawson, S.-J., Bantscheff, M., Lindon, M., Drewes, G., Demont, E. H., Daniels, D. L., Grandi, P., Prinjha, R. K. & Dawson, M. A. Selective Targeting of BD1 and BD2 of the BET Proteins in Cancer and Immunoinflammation. *Science* **368,** 387–394 (2020).

153. Faivre, E. J., McDaniel, K. F., Albert, D. H., Mantena, S. R., Plotnik, J. P., Wilcox, D., Zhang, L., Bui, M. H., Sheppard, G. S., Wang, L., Sehgal, V., Lin, X., Huang, X., Lu, X., Uziel, T., Hessler, P., Lam, L. T., Bellin, R. J., Mehta, G., Fidanze, S., Pratt, J. K., Liu, D., Hasvold, L. A., Sun, C., Panchal, S. C., Nicolette, J. J., Fossey, S. L., Park, C. H., Longenecker, K., Bigelow, L., Torrent, M., Rosenberg, S. H., Kati, W. M. & Shen, Y. Selective Inhibition of the BD2 Bromodomain of BET Proteins in Prostate Cancer. *Nature* **578,** 306–310 (7794 2020).

154. Runcie, A. C., Zengerle, M., Chan, K.-H., Testa, A., Beurden, L. van, Baud, M. G. J., Epemolu, O., Ellis, L. C. J., Read, K. D., Coulthard, V., Brien, A. & Ciulli, A. Optimization of a "Bump-and-Hole" Approach to Allele-Selective BET Bromodomain Inhibition. *Chem Sci* **9,** 2452–2468 (2018).

155. Tyler, D. S., Vappiani, J., Cañeque, T., Lam, E. Y. N., Ward, A., Gilan, O., Chan, Y.-C., Hienzsch, A., Rutkowska, A., Werner, T., Wagner, A. J., Lugo, D., Gregory, R., Molina, C. R., Garton, N., Wellaway, C. R., Jackson, S., MacPherson, L., Figueiredo, M., Stolzenburg, S., Bell, C. C., House, C., Dawson, S.-J., Hawkins, E. D., Drewes, G., Prinjha, R. K., Rodriguez, R., Grandi, P. & Dawson, M. A. Click Chemistry Enables Preclinical Evaluation of Targeted Epigenetic Therapies. *Science* **356,** 1397–1401 (2017).

156. Watson, R. J., Bamborough, P., Barnett, H., Chung, C.-W., Davis, R., Gordon, L., Grandi, P., Petretich, M., Phillipou, A., Prinjha, R. K., Rioja, I., Soden, P., Werner, T. & Demont, E. H. GSK789: A Selective Inhibitor of the First Bromodomains (BD1) of the Bromo and Extra Terminal Domain (BET) Proteins. *J Med Chem* **63,** 9045–9069 (2020).

157. Seal, J. T., Atkinson, S. J., Aylott, H., Bamborough, P., Chung, C.-w., Copley, R. C. B., Gordon, L., Grandi, P., Gray, J. R. J., Harrison, L. A., Hayhow, T. G., Lindon, M., Messenger, C., Michon, A.-M., Mitchell, D., Preston, A., Prinjha, R. K., Rioja, I., Taylor, S., Wall, I. D., Watson, R. J., Woolven, J. M. & Demont, E. H. The Optimization of a Novel, Weak Bromo and Extra Terminal Domain (BET) Bromodomain Fragment Ligand to a Potent and Selective Second Bromodomain (BD2) Inhibitor. *J Med Chem* **63,** 9093–9126 (2020).

158. Sheppard, G. S., Wang, L., Fidanze, S. D., Hasvold, L. A., Liu, D., Pratt, J. K., Park, C. H., Longenecker, K., Qiu, W., Torrent, M., Kovar, P. J., Bui, M., Faivre, E., Huang, X., Lin, X., Wilcox, D., Zhang, L., Shen, Y., Albert, D. H., Magoc, T. J., Rajaraman, G., Kati, W. M. & McDaniel, K. F. Discovery of N-Ethyl-4-[2-(4-Fluoro-2,6-Dimethyl-Phenoxy)-5-(1-Hydroxy-1-Methyl-Ethyl)Phenyl] 6-Methyl-7-Oxo-1H-pyrrolo[2,3-c]Pyridine-2-Carboxamide (ABBV-744), a BET Bromodomain Inhibitor with Selectivity for the Second Bromodomain. *J Med Chem* **63,** 5585–5623 (2020).

159. Shi, S. R., Cote, R. J. & Taylor, C. R. Antigen Retrieval Techniques: Current Perspectives. *J Histochem Cytochem* **49,** 931–937 (2001).

160. Evers, B. M., Townsend, C. M., Upp, J. R., Allen, E., Hurlbut, S. C., Kim, S. W., Rajaraman, S., Singh, P., Reubi, J. C. & Thompson, J. C. Establishment and Characterization of a Human Carcinoid in Nude Mice and Effect of Various Agents on Tumor Growth. *Gastroenterology* **101,** 303–311 (1991).

161. Kaku, M., Nishiyama, T., Yagawa, K. & Abe, M. Establishment of a Carcinoembryonic Antigen-Producing Cell Line from Human Pancreatic Carcinoma. *Gan* **71,** 596–601 (1980).

162. Miyazaki, J., Araki, K., Yamato, E., Ikegami, H., Asano, T., Shibasaki, Y., Oka, Y. & Yamamura, K. Establishment of a Pancreatic Beta Cell Line That Retains Glucose-Inducible Insulin Secretion: Special Reference to Expression of Glucose Transporter Isoforms. *Endocrinology* **127,** 126–132 (1990).

163. Horoszewicz, J. S., Leong, S. S., Kawinski, E., Karr, J. P., Rosenthal, H., Chu, T. M., Mirand, E. A. & Murphy, G. P. LNCaP Model of Human Prostatic Carcinoma. *Cancer Res* **43,** 1809–1818 (1983).

164. Vandamme, T., Beyens, M., Peeters, M., Camp, G. V. & Beeck, K. O. de. Next Generation Exome Sequencing of Pancreatic Neuroendocrine Tumor Cell Lines BON-1 and QGP-1 Reveals Different Lineages. *Cancer Genet* **208,** 523 (2015).

165. Hofving, T., Arvidsson, Y., Almobarak, B., Inge, L., Pfragner, R., Persson, M., Stenman, G., Kristiansson, E., Johanson, V. & Nilsson, O. The Neuroendocrine Phenotype, Genomic Profile and Therapeutic Sensitivity of GEPNET Cell Lines. *Endocr Relat Cancer* **25,** 367–380 (2018).

166. O'Brien, J., Wilson, I., Orton, T. & Pognan, F. Investigation of the Alamar Blue (Resazurin) Fluorescent Dye for the Assessment of Mammalian Cell Cytotoxicity. *Eur J Biochem* **267,** 5421–5426 (2000).

167. Ianevski, A., Giri, A. K. & Aittokallio, T. SynergyFinder 3.0: An Interactive Analysis and Consensus Interpretation of Multi-Drug Synergies across Multiple Samples. *Nucleic Acids Res* **50,** W739–W743 (2022).

168. Greco, W. R., Bravo, G. & Parsons, J. C. The Search for Synergy: A Critical Review from a Response Surface Perspective. *Pharmacol Rev* **47,** 331–385 (1995).

169. Lam, L. T., Lin, X., Faivre, E. J., Yang, Z., Huang, X., Wilcox, D. M., Bellin, R. J., Jin, S., Tahir, S. K., Mitten, M., Magoc, T., Bhathena, A., Kati, W. M., Albert, D. H., Shen, Y. & Uziel, T. Vulnerability of Small-Cell Lung Cancer to Apoptosis Induced by the Combination of BET Bromodomain Proteins and BCL2 Inhibitors. *Mol Cancer Ther* **16,** 1511–1520 (2017).

170. Hogg, S. J., Newbold, A., Vervoort, S. J., Cluse, L. A., Martin, B. P., Gregory, G. P., Lefebure, M., Vidacs, E., Tothill, R. W., Bradner, J. E., Shortt, J. & Johnstone, R. W. BET Inhibition Induces Apoptosis in Aggressive B-Cell Lymphoma via Epigenetic Regulation of BCL-2 Family Members. *Mol Cancer Ther* **15,** 2030–2041 (2016).

171. McIlwain, D. R., Berger, T. & Mak, T. W. Caspase Functions in Cell Death and Disease. *Cold Spring Harb Perspect Biol* **5,** a008656 (2013).

172. O'Brien, M., Moravec, R. & Riss, T. Caspase-Glo 3/7 Assay: Use Fewer Cells and Spend Less Time with This Homogeneous Assay. *Cell Notes* **6,** 13–15 (2003).

173. Feoktistova, M., Geserick, P. & Leverkus, M. Crystal Violet Assay for Determining Viability of Cultured Cells. *Cold Spring Harb Protoc* **2016,** pdb.prot087379 (2016).

174. Cecchini, M. J., Amiri, M. & Dick, F. A. Analysis of Cell Cycle Position in Mammalian Cells. *J Vis Exp,* 3491 (2012).

175. Livak, K. J. & Schmittgen, T. D. Analysis of Relative Gene Expression Data Using Real-Time Quantitative PCR and the 2(-Delta Delta C(T)) Method. *Methods* **25,** 402–408 (2001).

176. Moll, P., Ante, M., Seitz, A. & Reda, T. QuantSeq 3 mRNA Sequencing for RNA Quantification. *Nat Methods* **11,** i–iii (2014).

177. Gene Ontology Consortium, Aleksander, S. A., Balhoff, J., Carbon, S., Cherry, J. M., Drabkin, H. J., Ebert, D., Feuermann, M., Gaudet, P., Harris, N. L., Hill, D. P., Lee, R., Mi, H., Moxon, S., Mungall, C. J., Muruganugan, A., Mushayahama, T., Sternberg, P. W., Thomas, P. D., Van Auken, K., Ramsey, J., Siegele, D. A., Chisholm, R. L., Fey, P., Aspromonte, M. C., Nugnes, M. V., Quaglia, F., Tosatto, S., Giglio, M., Nadendla, S., Antonazzo, G., Attrill, H., Dos Santos, G., Marygold, S., Strelets, V., Tabone, C. J., Thurmond, J., Zhou, P., Ahmed, S. H., Asanitthong, P., Luna Buitrago, D., Erdol, M. N., Gage, M. C., Ali Kadhum, M., Li, K. Y. C., Long, M., Michalak, A., Pesala, A., Pritazahra, A., Saverimuttu, S. C. C., Su, R., Thurlow, K. E., Lovering, R. C., Logie, C., Oliferenko, S., Blake, J., Christie, K., Corbani, L., Dolan, M. E., Drabkin, H. J., Hill, D. P., Ni, L., Sitnikov, D., Smith, C., Cuzick, A., Seager, J., Cooper, L., Elser, J., Jaiswal, P., Gupta, P., Jaiswal, P., Naithani, S., Lera-Ramirez, M., Rutherford, K., Wood, V., De Pons, J. L., Dwinell, M. R., Hayman, G. T., Kaldunski, M. L., Kwitek, A. E., Lauledерkind, S. J. F., Tutaj, M. A., Vedi, M., Wang, S.-J., D'Eustachio, P., Aimo, L., Axelsen, K., Bridge, A., Hyka-Nouspikel, N., Morgat, A., Aleksander, S. A., Cherry, J. M., Engel, S. R., Karra, K., Miyasato, S. R., Nash, R. S., Skrzypek, M. S., Weng, S., Wong, E. D., Bakker, E., Berardini, T. Z., Reiser, L., Auchincloss, A., Axelsen, K., Argoud-Puy, G., Blatter, M.-C., Boutet, E., Breuza, L., Bridge, A., Casals-Casas, C., Coudert, E., Estreicher, A., Livia Famiglietti, M., Feuermann, M., Gos, A.,

Gruaz-Gumowski, N., Hulo, C., Hyka-Nouspikel, N., Jungo, F., Le Mercier, P., Lieberherr, D., Masson, P., Morgat, A., Pedruzzi, I., Pourcel, L., Poux, S., Rivoire, C., Sundaram, S., Bateman, A., Bowler-Barnett, E., Bye-A-Jee, H., Denny, P., Ignatchenko, A., Ishtiaq, R., Lock, A., Lussi, Y., Magrane, M., Martin, M. J., Orchard, S., Raposo, P., Speretta, E., Tyagi, N., Warner, K., Zaru, R., Diehl, A. D., Lee, R., Chan, J., Diamantakis, S., Raciti, D., Zarowiecki, M., Fisher, M., James-Zorn, C., Ponferrada, V., Zorn, A., Ramachandran, S., Ruzicka, L. & Westerfield, M. The Gene Ontology Knowledgebase in 2023. *Genetics* **224,** iyad031 (2023).

178. Schaefer, C. F., Anthony, K., Krupa, S., Buchoff, J., Day, M., Hannay, T. & Buetow, K. H. PID: The Pathway Interaction Database. *Nucleic Acids Res* **37,** D674–D679 (Database issue 2009).

179. Kanehisa, M., Furumichi, M., Sato, Y., Kawashima, M. & Ishiguro-Watanabe, M. KEGG for Taxonomy-Based Analysis of Pathways and Genomes. *Nucleic Acids Res* **51,** D587–D592 (2023).

180. Milacic, M., Beavers, D., Conley, P., Gong, C., Gillespie, M., Griss, J., Haw, R., Jassal, B., Matthews, L., May, B., Petryszak, R., Ragueneau, E., Rothfels, K., Sevilla, C., Shamovsky, V., Stephan, R., Tiwari, K., Varusai, T., Weiser, J., Wright, A., Wu, G., Stein, L., Hermjakob, H. & D'Eustachio, P. The Reactome Pathway Knowledgebase 2024. *Nucleic Acids Res* **52,** D672–D678 (2024).

181. Krämer, A., Green, J., Pollard Jr, J. & Tugendreich, S. Causal Analysis Approaches in Ingenuity Pathway Analysis. *Bioinformatics* **30,** 523–530 (2014).

182. Liberzon, A., Birger, C., Thorvaldsdóttir, H., Ghandi, M., Mesirov, J. P. & Tamayo, P. The Molecular Signatures Database (MSigDB) Hallmark Gene Set Collection. *Cell Syst* **1,** 417–425 (2015).

183. Wissink, E. M., Vihervaara, A., Tippens, N. D. & Lis, J. T. Nascent RNA Analyses: Tracking Transcription and Its Regulation. *Nat Rev Genet* **20,** 705–723 (2019).

184. Core, L. J., Waterfall, J. J. & Lis, J. T. Nascent RNA Sequencing Reveals Widespread Pausing and Divergent Initiation at Human Promoters. *Science* **322,** 1845–1848 (2008).

185. Muhar, M., Ebert, A., Neumann, T., Umkehrer, C., Jude, J., Wieshofer, C., Rescheneder, P., Lipp, J. J., Herzog, V. A., Reichholf, B., Cisneros, D. A., Hoffmann, T., Schlapansky, M. F., Bhat, P., von Haeseler, A., Köcher, T., Obenauf, A. C., Popow, J., Ameres, S. L. & Zuber, J. SLAM-seq Defines Direct Gene-Regulatory Functions of the BRD4-MYC Axis. *Science* **360,** 800–805 (2018).

186. Neumann, T., Herzog, V. A., Muhar, M., von Haeseler, A., Zuber, J., Ameres, S. L. & Rescheneder, P. Quantification of Experimentally Induced Nucleotide Conversions in High-Throughput Sequencing Datasets. *BMC Bioinformatics* **20,** 258 (2019).

187. Russo, J., Heck, A. M., Wilusz, J. & Wilusz, C. J. Metabolic Labeling and Recovery of Nascent RNA to Accurately Quantify mRNA Stability. *Methods* **120,** 39–48 (2017).

188. Furey, T. S. ChIP–Seq and beyond: New and Improved Methodologies to Detect and Characterize Protein–DNA Interactions. *Nat Rev Genet* **13,** 840–852 (2012).

189. Chapuy, B., McKeown, M. R., Lin, C. Y., Monti, S., Roemer, M. G., Qi, J., Rahl, P. B., Sun, H. H., Yeda, K. T., Doench, J. G., Reichert, E., Kung, A. L., Rodig, S. J., Young, R. A., Shipp, M. A. & Bradner, J. E. Discovery and Characterization of Super-Enhancer Associated Dependencies in Diffuse Large B-Cell Lymphoma. *Cancer Cell* **24,** 777–790 (2013).

190. Brown, J. D., Feldman, Z. B., Doherty, S. P., Reyes, J. M., Rahl, P. B., Lin, C. Y., Sheng, Q., Duan, Q., Federation, A. J., Kung, A. L., Haldar, S. M., Young, R. A., Plutzky, J. & Bradner, J. E. BET Bromodomain Proteins Regulate Enhancer Function during Adipogenesis. *Proc Natl Acad Sci U S A* **115,** 2144–2149 (2018).

191. Landt, S. G., Marinov, G. K., Kundaje, A., Kheradpour, P., Pauli, F., Batzoglou, S., Bernstein, B. E., Bickel, P., Brown, J. B., Cayting, P., Chen, Y., DeSalvo, G., Epstein, C., Fisher-Aylor, K. I., Euskirchen, G., Gerstein, M., Gertz, J., Hartemink, A. J., Hoffman, M. M., Iyer, V. R., Jung, Y. L., Karmakar, S., Kellis, M., Kharchenko, P. V., Li, Q., Liu, T., Liu, X. S., Ma, L., Milosavljevic, A., Myers, R. M., Park, P. J., Pazin, M. J., Perry, M. D., Raha, D., Reddy, T. E., Rozowsky, J., Shoresh, N., Sidow, A., Slattery, M., Stamatoyannopoulos, J. A., Tolstorukov, M. Y., White, K. P., Xi, S., Farnham, P. J., Lieb, J. D., Wold, B. J. & Snyder, M. ChIP-seq Guidelines and Practices of the ENCODE and modENCODE Consortia. *Genome Res.* **22,** 1813–1831 (2012).

192. Browne, J. A., Harris, A. & Leir, S.-H. An Optimized Protocol for Isolating Primary Epithelial Cell Chromatin for ChIP. *PLoS One* **9,** e100099 (2014).

193. Robinson, J. T., Thorvaldsdóttir, H., Winckler, W., Guttman, M., Lander, E. S., Getz, G. & Mesirov, J. P. Integrative Genomics Viewer. *Nat Biotechnol* **29,** 24–26 (1 2011).

194. Hnisz, D., Abraham, B. J., Lee, T. I., Lau, A., Saint-André, V., Sigova, A. A., Hoke, H. A. & Young, R. A. Super-Enhancers in the Control of Cell Identity and Disease. *Cell* **155,** 934–947 (2013).

195. Qian, H., Zhu, M., Tan, X., Zhang, Y., Liu, X. & Yang, L. Super-Enhancers and the Super-Enhancer Reader BRD4: Tumorigenic Factors and Therapeutic Targets. *Cell Death Discov.* **9,** 1–11 (2023).

196. Hamdan, F. H. & Johnsen, S. A. Super Enhancers – New Analyses and Perspectives on the Low Hanging Fruit. *Transcription* **9,** 123–130 (2017).

197. Crabtree, J. S., Scacheri, P. C., Ward, J. M., McNally, S. R., Swain, G. P., Montagna, C., Hager, J. H., Hanahan, D., Edlund, H., Magnuson, M. A., Garrett-Beal, L., Burns, A. L., Ried, T., Chandrasekharappa, S. C., Marx, S. J., Spiegel, A. M. & Collins, F. S. Of Mice and MEN1: Insulinomas in a Conditional Mouse Knockout. *Mol Cell Biol* **23,** 6075–6085 (2003).

198. Casey, R. T., Saunders, D., Challis, B. G., Pitfield, D., Cheow, H., Shaw, A. & Simpson, H. L. Radiological Surveillance in Multiple Endocrine Neoplasia Type 1: A Double-Edged Sword? *Endocr Connect* **6,** 151–158 (2017).

199. Shariq, O. A., Lines, K. E., English, K. A., Jafar-Mohammadi, B., Prentice, P., Casey, R., Challis, B. G., Selberherr, A., Boon, H., Cranston, T., Ryan, F. J., Mihai, R., Healy, U., Kurzawinski, T., Dattani, M. T., Bancos, I., Dy, B. M., Lyden, M. L., Young, W. F., McKenzie, T. J., Richards, D. & Thakker, R. V. Multiple Endocrine Neoplasia Type 1 in Children and Adolescents: Clinical Features and Treatment Outcomes. *Surgery* **171,** 77–87 (2022).

200. Mitre, N., Mack, K., Babovic-Vuksanovic, D., Thompson, G. & Kumar, S. Ischemic Stroke as the Presenting Symptom of Primary Hyperparathyroidism Due to Multiple Endocrine Neoplasia Type 1. *J Pediatr* **153,** 582–5 (2008).

201. Gan, H.-W., Bulwer, C., Jeelani, O., Levine, M. A., Korbonits, M. & Spoudeas, H. A. Treatment-Resistant Pediatric Giant Prolactinoma and Multiple Endocrine Neoplasia Type 1. *Int J Pediatr Endocrinol* **2015,** 15 (2015).

202. Lemos, M. C. & Thakker, R. V. Multiple Endocrine Neoplasia Type 1 (MEN1): Analysis of 1336 Mutations Reported in the First Decade Following Identification of the Gene. *Hum Mutat* **29,** 22–32 (2008).

203. Turner, J. J., Leotlela, P. D., Pannett, A. A., Forbes, S. A., Bassett, J. H., Harding, B., Christie, P. T., Bowen-Jones, D., Ellard, S., Hattersley, A., Jackson, C. E., Pope, R., Quarrell, O. W., Trembath, R. & Thakker, R. V. Frequent Occurrence of an Intron 4 Mutation in Multiple Endocrine Neoplasia Type 1. *J Clin Endocrinol Metab* **87,** 2688–93 (2002).

204. Mutch, M. G., Dilley, W. G., Sanjurjo, F., DeBenedetti, M. K., Doherty, G. M., Wells Jr., S. A., Goodfellow, P. J. & Lairmore, T. C. Germline Mutations in the Multiple Endocrine Neoplasia Type 1 Gene: Evidence for Frequent Splicing Defects. *Hum Mutat* **13,** 175–85 (1999).

205. Bartsch, D. K., Slater, E. P., Albers, M., Knoop, R., Chaloupka, B., Lopez, C. L., Fendrich, V., Kann, P. H. & Waldmann, J. Higher Risk of Aggressive Pancreatic Neuroendocrine Tumors in MEN1 Patients with MEN1 Mutations Affecting the CHES1 Interacting MENIN Domain. *J Clin Endocrinol Metab* **99,** E2387–91 (2014).

206. Ito, T., Igarashi, H., Uehara, H., Berna, M. J. & Jensen, R. T. Causes of Death and Prognostic Factors in Multiple Endocrine Neoplasia Type 1: A Prospective Study: Comparison of 106 MEN1/Zollinger-Ellison Syndrome Patients with 1613 Literature MEN1 Patients with or without Pancreatic Endocrine Tumors. *Med Baltim* **92,** 135–81 (2013).

207. Peipert, B. J., Goswami, S., Yount, S. E. & Sturgeon, C. Health-Related Quality of Life in MEN1 Patients Compared with Other Chronic Conditions and the United States General Population. *Surgery* **163,** 205–211 (2018).

208. Goggins, M., Overbeek, K. A., Brand, R., Syngal, S., Del Chiaro, M., Bartsch, D. K., Bassi, C., Carrato, A., Farrell, J., Fishman, E. K., Fockens, P., Gress, T. M., van Hooft, J. E., Hruban, R. H., Kastrinos, F., Klein, A., Lennon, A. M., Lucas, A., Park, W., Rustgi, A., Simeone, D., Stoffel, E., Vasen, H. F. A., Cahen, D. L., Canto, M. I. & Bruno, M. Management of Patients with Increased Risk for Familial Pancreatic Cancer: Updated Recommendations from the International Cancer of the Pancreas Screening (CAPS) Consortium. *Gut* **69,** 7–17 (2020).

209. Cohen-Cohen, S., Brown, D. A., Himes, B. T., Wheeler, L. P., Ruff, M. W., Major, B. T., Singh Ospina, N. M., Atkinson, J. L. D., Meyer, F. B., Bancos, I., Young, W. F. & Van Gompel, J. J. Pituitary Adenomas in the Setting of Multiple Endocrine Neoplasia Type 1: A Single-Institution Experience. *J Neurosurg,* 1–7 (2020).

210. De Laat, J. M., Dekkers, O. M., Pieterman, C. R. C., Kluijfhout, W. P., Hermus, A. R., Pereira, A. M., van der Horst-Schrivers, A. N., Drent, M. L., Bisschop, P. H., Havekes, B., de Herder, W. W. & Valk, G. D. Long-Term Natural Course of Pituitary Tumors in Patients With MEN1: Results From the DutchMEN1 Study Group (DMSG). *J Clin Endocrinol Metab* **100,** 3288–3296 (2015).

211. Arya, V. B., Aylwin, S. J. B., Hulse, T., Ajzensztejn, M., Kalitsi, J., Kalogirou, N., Bodi, I., Thomas, N., Hampton, T., Kapoor, R. R. & Buchanan, C. R. Prolactinoma in Childhood and Adolescence-Tumour Size at Presentation Predicts Management Strategy: Single Centre Series and a Systematic Review and Meta-Analysis. *Clin Endocrinol Oxf* (2020).

212. Vergès, B., Boureille, F., Goudet, P., Murat, A., Beckers, A., Sassolas, G., Cougard, P., Chambe, B., Montvernay, C. & Calender, A. Pituitary Disease in MEN Type 1 (MEN1): Data from the France-Belgium MEN1 Multicenter Study. *J Clin Endocrinol Metab* **87,** 457–65 (2002).

213. Nastos, C., Papaconstantinou, D., Kofopoulos-Lymperis, E., Peppa, M., Pikoulis, A., Lykoudis, P., Palazzo, F., Patapis, P. & Pikoulis, E. Optimal Extent of Initial Parathyroid Resection in Patients with Multiple Endocrine Neoplasia Syndrome Type 1: A Meta-Analysis. *Surgery* **169,** 302–310.

214. Wang, N., Wu, R., Tang, D. & Kang, R. The BET Family in Immunity and Disease. *Sig Transduct Target Ther* **6,** 1–22 (1 2021).

215. Cochran, A. G., Conery, A. R. & Sims, R. J. Bromodomains: A New Target Class for Drug Development. *Nat Rev Drug Discov* **18,** 609–628 (2019).

216. Lu, T., Lu, W. & Luo, C. A Patent Review of BRD4 Inhibitors (2013-2019). *Expert Opin Ther Pat* **30,** 57–81 (2020).

217. Chen, H., Liu, Z., Zheng, L., Wang, R. & Shi, L. BET Inhibitors: An Updated Patent Review (2018-2021). *Expert Opin Ther Pat* **32,** 953–968 (2022).

218. Zhou, S., Zhang, S., Wang, L., Huang, S., Yuan, Y., Yang, J., Wang, H., Li, X., Wang, P., Zhou, L., Yang, J., Xu, Y., Gao, H., Zhang, Y., Lv, Y. & Zou, X. BET Protein Inhibitor JQ1 Downregulates Chromatin Accessibility and Suppresses Metastasis of Gastric Cancer via Inactivating RUNX2/NID1 Signaling. *Oncogenesis* **9,** 33 (2020).

219. Zhang, Z., Ma, P., Jing, Y., Yan, Y., Cai, M.-C., Zhang, M., Zhang, S., Peng, H., Ji, Z.-L., Di, W., Gu, Z., Gao, W.-Q. & Zhuang, G. BET Bromodomain Inhibition as a Therapeutic Strategy in Ovarian Cancer by Downregulating FoxM1. *Theranostics* **6,** 219–230 (2016).

220. Huang, Y., Nahar, S., Nakagawa, A., Fernandez de Barrena, M. G., Mertz, J. A., Bryant, B. M., Adams, C. E., Mino-Kenudson, M., Von Alt, K. N., Chang, K., Conery, A. R., Hatton, C., Sims, R. J., Fernandez-Zapico, M. E., Wang, X., Lillemoe, K. D., Castillo, C. F.-d., Warshaw, A. L., Thayer, S. P. & Liss, A. S. Regulation of GLI Underlies a Role for BET Bromodomains in Pancreatic Cancer Growth and the Tumor Microenvironment. *Clin Cancer Res* **22,** 4259–4270 (2016).

221. Mazur, P. K., Herner, A., Mello, S. S., Wirth, M., Hausmann, S., Sánchez-Rivera, F. J., Lofgren, S. M., Kuschma, T., Hahn, S. A., Vangala, D., Trajkovic-Arsic, M., Gupta, A., Heid, I., Noël, P. B., Braren, R., Erkan, M., Kleeff, J., Sipos, B., Sayles, L. C., Heikenwalder, M., Heßmann, E., Ellenrieder, V., Esposito, I., Jacks, T., Bradner, J. E., Khatri, P., Sweet-Cordero, E. A., Attardi, L. D., Schmid, R. M., Schneider, G., Sage, J. & Siveke, J. T. Combined Inhibition of BET Family Proteins and Histone Deacetylases as a Potential Epigenetics-Based Therapy for Pancreatic Ductal Adenocarcinoma. *Nat Med* **21,** 1163–1171 (2015).

222. Sadanandam, A., Wullschleger, S., Lyssiotis, C. A., Grötzinger, C., Barbi, S., Bersani, S., Körner, J., Wafy, I., Mafficini, A., Lawlor, R. T., Simbolo, M., Asara, J. M., Bläker, H., Cantley, L. C., Wiedenmann, B., Scarpa, A. & Hanahan, D. A Cross-Species Analysis in Pancreatic Neuroendocrine Tumors Reveals Molecular Subtypes with Distinctive Clinical, Metastatic, Developmental, and Metabolic Characteristics. *Cancer Discov* **5,** 1296–1313 (2015).

223. Young, K., Lawlor, R. T., Ragulan, C., Patil, Y., Mafficini, A., Bersani, S., Antonello, D., Mansfield, D., Cingarlini, S., Landoni, L., Pea, A., Luchini, C., Piredda, L., Kannan, N., Nyamundanda, G., Morganstein, D., Chau, I., Wiedenmann, B., Milella, M., Melcher, A., Cunningham, D., Starling, N., Scarpa, A. & Sadanandam, A. Immune Landscape, Evolution, Hypoxia-Mediated Viral Mimicry Pathways and Therapeutic Potential in Molecular Subtypes of Pancreatic Neuroendocrine Tumours. *Gut* **70,** 1904–1913 (2021).

224. Denis, G. V., Vaziri, C., Guo, N. & Faller, D. V. RING3 Kinase Transactivates Promoters of Cell Cycle Regulatory Genes through E2F. *Cell Growth Differ* **11,** 417–424 (2000).

225. Xu, L., Chen, Y., Mayakonda, A., Koh, L., Chong, Y. K., Buckley, D. L., Sandanaraj, E., Lim, S. W., Lin, R. Y.-T., Ke, X.-Y., Huang, M.-L., Chen, J., Sun, W., Wang, L.-Z., Goh, B. C., Dinh, H. Q., Kappei, D., Winter, G. E., Ding, L.-W., Ang, B. T., Berman, B. P., Bradner, J. E., Tang, C. & Koeffler, H. P. Targetable BET Proteins- and E2F1-dependent Transcriptional Program Maintains the Malignancy of Glioblastoma. *Proc Natl Acad Sci U S A* **115,** E5086–E5095 (2018).

226. Kim, D.-H., Sun, D., Storck, W. K., Welker Leng, K., Jenkins, C., Coleman, D. J., Sampson, D., Guan, X., Kumaraswamy, A., Rodansky, E. S., Urrutia, J. A., Schwartzman, J. A., Zhang, C., Beltran, H., Labrecque, M. P., Morrissey, C., Lucas, J. M., Coleman, I. M., Nelson, P. S., Corey, E., Handelman, S. K., Sexton, J. Z., Aggarwal, R., Abida, W., Feng, F. Y., Small, E. J., Spratt, D. E., Bankhead III, A., Rao, A., Gesner, E. M., Attwell, S., Lakhotia, S., Campeau, E., Yates, J. A., Xia, Z. & Alumkal, J. J. BET Bromodomain Inhibition Blocks an AR-Repressed, E2F1-Activated Treatment-Emergent Neuroendocrine Prostate Cancer Lineage Plasticity Program. *Clin Cancer Res* **27,** 4923–4936 (2021).

227. Qian, Z. R., Ter-Minassian, M., Chan, J. A., Imamura, Y., Hooshmand, S. M., Kuchiba, A., Morikawa, T., Brais, L. K., Daskalova, A., Heafield, R., Lin, X., Christiani, D. C., Fuchs, C. S., Ogino, S. & Kulke, M. H. Prognostic Significance of MTOR Pathway Component Expression in Neuroendocrine Tumors. *JCO* **31,** 3418–3425 (2013).

228. Yumoto, T., Nakadate, K., Nakamura, Y., Sugitani, Y., Sugitani-Yoshida, R., Ueda, S. & Sakakibara, S.-i. Radmis, a Novel Mitotic Spindle Protein That Functions in Cell Division of Neural Progenitors. *PLoS One* **8,** e79895 (2013).

229. Myatt, S. S. & Lam, E. W.-F. The Emerging Roles of Forkhead Box (Fox) Proteins in Cancer. *Nat Rev Cancer* **7,** 847–859 (11 2007).

230. Bunz, F., Dutriaux, A., Lengauer, C., Waldman, T., Zhou, S., Brown, J. P., Sedivy, J. M., Kinzler, K. W. & Vogelstein, B. Requirement for P53 and P21 to Sustain G2 Arrest After DNA Damage. *Science* **282,** 1497–1501 (1998).

231. El-Deiry, W. S., Tokino, T., Velculescu, V. E., Levy, D. B., Parsons, R., Trent, J. M., Lin, D., Mercer, W. E., Kinzler, K. W. & Vogelstein, B. WAF1, a Potential Mediator of P53 Tumor Suppression. *Cell* **75,** 817–825 (1993).

232. Puissant, A., Frumm, S. M., Alexe, G., Bassil, C. F., Qi, J., Chanthery, Y. H., Nekritz, E. A., Zeid, R., Gustafson, W. C., Greninger, P., Garnett, M. J., McDermott, U., Benes, C. H., Kung, A. L., Weiss, W. A., Bradner, J. E. & Stegmaier, K. Targeting MYCN in Neuroblastoma by BET Bromodomain Inhibition. *Cancer Discov* **3,** 308–323 (2013).

233. Subramanian, A., Narayan, R., Corsello, S. M., Peck, D. D., Natoli, T. E., Lu, X., Gould, J., Davis, J. F., Tubelli, A. A., Asiedu, J. K., Lahr, D. L., Hirschman, J. E., Liu, Z., Donahue, M., Julian, B., Khan, M., Wadden, D., Smith, I. C., Lam, D., Liberzon, A., Toder, C., Bagul, M., Orzechowski, M., Enache, O. M., Piccioni, F., Johnson, S. A., Lyons, N. J., Berger, A. H., Shamji, A. F., Brooks, A. N., Vrcic, A., Flynn, C., Rosains, J., Takeda, D. Y., Hu, R., Davison, D., Lamb, J., Ardlie, K., Hogstrom, L., Greenside, P., Gray, N. S., Clemons, P. A., Silver, S., Wu, X., Zhao, W.-N., Read-Button, W., Wu, X., Haggarty, S. J., Ronco, L. V., Boehm, J. S., Schreiber, S. L., Doench, J. G., Bittker, J. A., Root, D. E., Wong, B. & Golub, T. R. A Next Generation Connectivity Map: L1000 Platform and the First 1,000,000 Profiles. *Cell* **171,** 1437–1452.e17 (2017).

234. Keenan, A. B., Jenkins, S. L., Jagodnik, K. M., Koplev, S., He, E., Torre, D., Wang, Z., Dohlman, A. B., Silverstein, M. C., Lachmann, A., Kuleshov, M. V., Ma'ayan, A., Stathias, V., Terryn, R., Cooper, D., Forlin, M., Koleti, A., Vidovic, D., Chung, C., Schürer, S. C., Vasiliauskas, J., Pilarczyk, M., Shamsaei, B., Fazel, M., Ren, Y., Niu, W., Clark, N. A., White, S., Mahi, N., Zhang, L., Kouril, M., Reichard, J. F., Sivaganesan, S., Medvedovic, M., Meller, J., Koch, R. J., Birtwistle, M. R., Iyengar, R., Sobie, E. A., Azeloglu, E. U., Kaye, J., Osterloh, J., Haston, K., Kalra, J., Finkbiener, S., Li, J., Milani, P., Adam, M., Escalante-Chong, R., Sachs, K., Lenail, A., Ramamoorthy, D., Fraenkel, E., Daigle, G., Hussain, U., Coye, A., Rothstein, J., Sareen, D., Ornelas, L., Banuelos, M., Mandefro, B., Ho, R., Svendsen, C. N., Lim, R. G., Stocksdale, J., Casale, M. S., Thompson, T. G., Wu, J., Thompson, L. M., Dardov, V., Venkatraman, V., Matlock, A., Van Eyk, J. E., Jaffe, J. D., Papanastasiou, M., Subramanian, A., Golub, T. R., Erickson, S. D., Fallahi-Sichani, M., Hafner, M., Gray, N. S., Lin, J.-R., Mills, C. E.,

Muhlich, J. L., Niepel, M., Shamu, C. E., Williams, E. H., Wrobel, D., Sorger, P. K., Heiser, L. M., Gray, J. W., Korkola, J. E., Mills, G. B., LaBarge, M., Feiler, H. S., Dane, M. A., Bucher, E., Nederlof, M., Sudar, D., Gross, S., Kilburn, D. F., Smith, R., Devlin, K., Margolis, R., Derr, L., Lee, A. & Pillai, A. The Library of Integrated Network-Based Cellular Signatures NIH Program: System-Level Cataloging of Human Cells Response to Perturbations. *Cell Syst* **6,** 13–24 (2018).

235. Evers, B. M., Ishizuka, J., Townsend, C. M. & Thompson, J. C. The Human Carcinoid Cell Line, BON. A Model System for the Study of Carcinoid Tumors. *Ann N Y Acad Sci* **733,** 393–406 (1994).

236. Ney, A., Canciani, G., Hsuan, J. J. & Pereira, S. P. Modelling Pancreatic Neuroendocrine Cancer: From Bench Side to Clinic. *Cancers* **12,** 3170 (11 2020).

237. Liu, T., Ortiz, J. A., Taing, L., Meyer, C. A., Lee, B., Zhang, Y., Shin, H., Wong, S. S., Ma, J., Lei, Y., Pape, U. J., Poidinger, M., Chen, Y., Yeung, K., Brown, M., Turpaz, Y. & Liu, X. S. Cistrome: An Integrative Platform for Transcriptional Regulation Studies. *Genome Biol* **12,** R83 (2011).

238. Yu, G., Wang, L.-G. & He, Q.-Y. ChIPseeker: An R/Bioconductor Package for ChIP Peak Annotation, Comparison and Visualization. *Bioinformatics* **31,** 2382–2383 (2015).

239. Taing, L., Dandawate, A., L'Yi, S., Gehlenborg, N., Brown, M. & Meyer, C. A. Cistrome Data Browser: Integrated Search, Analysis and Visualization of Chromatin Data. *Nucleic Acids Res* **52,** D61–D66 (2024).

240. Donner, A. J., Ebmeier, C. C., Taatjes, D. J. & Espinosa, J. M. CDK8 Is a Positive Regulator of Transcriptional Elongation within the Serum Response Network. *Nat Struct Mol Biol* **17,** 194–201 (2010).

241. Heinz, S., Benner, C., Spann, N., Bertolino, E., Lin, Y. C., Laslo, P., Cheng, J. X., Murre, C., Singh, H. & Glass, C. K. Simple Combinations of Lineage-Determining Transcription Factors Prime Cis-Regulatory Elements Required for Macrophage and B Cell Identities. *Mol Cell* **38,** 576–589 (2010).

242. French, C. A., Miyoshi, I., Kubonishi, I., Grier, H. E., Perez-Atayde, A. R. & Fletcher, J. A. BRD4-NUT Fusion Oncogene: A Novel Mechanism in Aggressive Carcinoma. *Cancer Res* **63,** 304–307 (2003).

243. Yang, L., Zhang, Y., Shan, W., Hu, Z., Yuan, J., Pi, J., Wang, Y., Fan, L., Tang, Z., Li, C., Hu, X., Tanyi, J. L., Fan, Y., Huang, Q., Montone, K., Dang, C. V. & Zhang, L. Repression of BET Activity Sensitizes Homologous Recombination–Proficient Cancers to PARP Inhibition. *Sci Transl Med* **9,** eaal1645 (2017).

244. Trojer, P. Targeting BET Bromodomains in Cancer. *Annu Rev Cancer Biol* **6,** 313–336 (2022).

245. Dawson, M. A., Prinjha, R. K., Dittmann, A., Giotopoulos, G., Bantscheff, M., Chan, W.-I., Robson, S. C., Chung, C.-w., Hopf, C., Savitski, M. M., Huthmacher, C., Gudgin, E., Lugo, D., Beinke, S., Chapman, T. D., Roberts, E. J., Soden, P. E., Auger, K. R., Mirguet, O., Doehner, K., Delwel, R., Burnett, A. K., Jeffrey, P., Drewes, G., Lee, K., Huntly, B. J. P. & Kouzarides, T. Inhibition of BET Recruitment to Chromatin as an Effective Treatment for MLL-fusion Leukaemia. *Nature* **478,** 529–533 (7370 2011).

246. Baratta, M. G., Schinzel, A. C., Zwang, Y., Bandopadhayay, P., Bowman-Colin, C., Kutt, J., Curtis, J., Piao, H., Wong, L. C., Kung, A. L., Beroukhim, R., Bradner, J. E., Drapkin, R., Hahn, W. C., Liu, J. F. & Livingston, D. M. An In-Tumor Genetic Screen Reveals That the BET Bromodomain Protein, BRD4, Is a Potential Therapeutic Target in Ovarian Carcinoma. *Proc Natl Acad Sci U S A* **112,** 232–237 (2015).

247. Zuber, J., Shi, J., Wang, E., Rappaport, A. R., Herrmann, H., Sison, E. A., Magoon, D., Qi, J., Blatt, K., Wunderlich, M., Taylor, M. J., Johns, C., Chicas, A., Mulloy, J. C., Kogan, S. C., Brown, P., Valent, P., Bradner, J. E., Lowe, S. W. & Vakoc, C. R. RNAi Screen Identifies Brd4 as a Therapeutic Target in Acute Myeloid Leukaemia. *Nature* **478,** 524–528 (2011).

248. Rhyasen, G. W., Yao, Y., Zhang, J., Dulak, A., Castriotta, L., Jacques, K., Zhao, W., Gharahdaghi, F., Hattersley, M. M., Lyne, P. D., Clark, E., Zinda, M., Fawell, S. E., Mills, G. B. & Chen, H. BRD4 Amplification Facilitates an Oncogenic Gene Expression Program in High-Grade Serous Ovarian Cancer and Confers Sensitivity to BET Inhibitors. *PLoS One* **13,** e0200826 (2018).

249. Segura, M. F., Fontanals-Cirera, B., Gaziel-Sovran, A., Guijarro, M. V., Hanniford, D., Zhang, G., González-Gomez, P., Morante, M., Jubierre, L., Zhang, W., Darvishian, F., Ohlmeyer, M., Osman, I., Zhou, M.-M. & Hernando, E. BRD4 Sustains Melanoma Proliferation and Represents a New Target for Epigenetic Therapy. *Cancer Res* **73,** 6264–6276 (2013).

250. Lawrence, B., Blenkiron, C., Parker, K., Tsai, P., Fitzgerald, S., Shields, P., Robb, T., Yeong, M. L., Kramer, N., James, S., Black, M., Fan, V., Poonawala, N., Yap, P., Coats, E., Woodhouse, B., Ramsaroop, R., Yozu, M., Robinson, B., Henare, K., Koea, J., Johnston, P., Carroll, R., Connor, S., Morrin, H., Elston, M., Jackson, C., Reid, P., Windsor, J., MacCormick, A., Babor, R., Bartlett, A., Damianovich, D., Knowlton, N., Grimmond, S., Findlay, M. & Print, C. Recurrent Loss of Heterozygosity Correlates with Clinical Outcome in Pancreatic Neuroendocrine Cancer. *NPJ Genom Med* **3,** 1–12 (1 2018).

251. Pea, A., Yu, J., Marchionni, L., Noe, M., Luchini, C., Pulvirenti, A., de Wilde, R. F., Brosens, L. A., Rezaee, N., Javed, A., Chianchiano, P., Gobbo, S., Regi, P., Salvia, R., Bassi, C., He, J., Weiss, M. J., Cameron, J. L., Offerhaus, G. J. A., Hruban, R. H., Lawlor, R. T., Scarpa, A., Heaphy, C. M., Wood, L. D. & Wolfgang, C. L. Genetic Analysis of Small Well-differentiated Pancreatic Neuroendocrine Tumors Identifies Subgroups With Differing Risks of Liver Metastases. *Ann Surg* **271,** 566–573 (2020).

252. Shehata, B. M., Steelman, C. K., Abramowsky, C. R., Olson, T. A., French, C. A., Saxe, D. F., Ricketts, R. R. & Katzenstein, H. M. NUT Midline Carcinoma in a Newborn with Multiorgan Disseminated Tumor and a 2-Year-Old with a Pancreatic/Hepatic Primary. *Pediatr Dev Pathol* **13,** 481–485 (2010).

253. Huijbregts, L., Petersen, M. B. K., Berthault, C., Hansson, M., Aiello, V., Rachdi, L., Grapin-Botton, A., Honore, C. & Scharfmann, R. Bromodomain and Extra Terminal Protein Inhibitors Promote Pancreatic Endocrine Cell Fate. *Diabetes* **68,** 761–773 (2019).

254. Sun, R., Wu, Y., Hou, W., Sun, Z., Wang, Y., Wei, H., Mo, W. & Yu, M. Bromodomain-Containing Protein 2 Induces Insulin Resistance via the mTOR/Akt Signaling Pathway and an Inflammatory Response in Adipose Tissue. *Cell Signal* **30,** 92–103 (2017).

255. Liu, N., Ling, R., Tang, X., Yu, Y., Zhou, Y. & Chen, D. Post-Translational Modifications of BRD4: Therapeutic Targets for Tumor. *Front Oncol* **12,** 847701 (2022).

256. Wu, S.-Y., Lee, A.-Y., Lai, H.-T., Zhang, H. & Chiang, C.-M. Phospho Switch Triggers Brd4 Chromatin Binding and Activator Recruitment for Gene-Specific Targeting. *Mol Cell* **49,** 843–857 (2013).

257. Borgo, C., D'Amore, C., Sarno, S., Salvi, M. & Ruzzene, M. Protein Kinase CK2: A Potential Therapeutic Target for Diverse Human Diseases. *Sig Transduct Target Ther* **6,** 1–20 (1 2021).

258. Welker, S., Götz, C., Servas, C., Laschke, M. W., Menger, M. D. & Montenarh, M. Glucose Regulates Protein Kinase CK2 in Pancreatic β-Cells and Its Interaction with PDX-1. *Int J Biochem Cell Biol* **45,** 2786–2795 (2013).

259. Weinstein, J. N., Collisson, E. A., Mills, G. B., Shaw, K. R. M., Ozenberger, B. A., Ellrott, K., Shmulevich, I., Sander, C. & Stuart, J. M. The Cancer Genome Atlas Pan-Cancer Analysis Project. *Nat Genet* **45,** 1113–1120 (10 2013).

260. Yang, K. C., Kalloger, S. E., Aird, J. J., Lee, M. K. C., Rushton, C., Mungall, K. L., Mungall, A. J., Gao, D., Chow, C., Xu, J., Karasinska, J. M., Colborne, S., Jones, S. J. M., Schrader, J., Morin, R. D., Loree, J. M., Marra, M. A., Renouf, D. J., Morin, G. B., Schaeffer, D. F. & Gorski, S. M. Proteotranscriptomic Classification and Characterization of Pancreatic Neuroendocrine Neoplasms. *Cell Rep* **37** (2021).

261. Zhou, Y., Liu, S., Liu, C., Yang, J., Lin, Q., Zheng, S., Chen, C., Zhou, Q. & Chen, R. Single-Cell RNA Sequencing Reveals Spatiotemporal Heterogeneity and Malignant Progression in Pancreatic Neuroendocrine Tumor. *Int J Biol Sci* **17,** 3760–3775 (2021).

262. Monteverde, T., Sahoo, S., La Montagna, M., Magee, P., Shi, L., Lee, D., Sellers, R., Baker, A. R., Leong, H. S., Fassan, M. & Garofalo, M. CKAP2L Promotes Non–Small Cell Lung Cancer Progression through Regulation of Transcription Elongation. *Cancer Res* **81,** 1719–1731 (2021).

263. Wang, P. & He, X. Oncogenic and Prognostic Role of CKAP2L in Hepatocellular Carcinoma. *Int J Clin Exp Pathol* **13,** 923–933 (2020).

264. Li, Q., Yan, M., Wang, C., Wang, K. & Bao, G. CKAP2L, a Crucial Target of miR-326, Promotes Prostate Cancer Progression. *BMC Cancer* **22,** 666 (2022).

265. Yi, B., Fu, Q., Zheng, Z., Zhang, M., Liu, D., Liang, Z., Xu, S. & Zhang, Z. Pan-Cancer Analysis Reveals the Prognostic and Immunotherapeutic Value of Cytoskeleton-Associated Protein 2-Like. *Sci Rep* **13,** 8368 (1 2023).

266. Millour, J., de Olano, N., Horimoto, Y., Monteiro, L. J., Langer, J. K., Aligue, R., Hajji, N. & Lam, E. W. F. ATM and P53 Regulate FOXM1 Expression via E2F in Breast Cancer Epirubicin Treatment and Resistance. *Mol Cancer Ther* **10,** 1046–1058 (2011).

267. Zhang, P., Li, R., Xiao, H., Liu, W., Zeng, X., Xie, G., Yang, W., Shi, L., Yin, Y. & Tao, K. BRD4 Inhibitor AZD5153 Suppresses the Proliferation of Colorectal Cancer Cells and Sensitizes the Anticancer Effect of PARP Inhibitor. *Int J Biol Sci* **15,** 1942–1954 (2019).

268. Hay, N. Reprogramming Glucose Metabolism in Cancer: Can It Be Exploited for Cancer Therapy? *Nat Rev Cancer* **16,** 635–649 (2016).

269. Koppenol, W. H., Bounds, P. L. & Dang, C. V. Otto Warburg's Contributions to Current Concepts of Cancer Metabolism. *Nat Rev Cancer* **11,** 325–337 (2011).

270. Ashton, T. M., McKenna, W. G., Kunz-Schughart, L. A. & Higgins, G. S. Oxidative Phosphorylation as an Emerging Target in Cancer Therapy. *Clin Cancer Res* **24,** 2482–2490 (2018).

271. Viale, A., Pettazzoni, P., Lyssiotis, C. A., Ying, H., Sánchez, N., Marchesini, M., Carugo, A., Green, T., Seth, S., Giuliani, V., Kost-Alimova, M., Muller, F., Colla, S., Nezi, L., Genovese, G., Deem, A. K., Kapoor, A., Yao, W., Brunetto, E., Kang, Y., Yuan, M., Asara, J. M., Wang, Y. A., Heffernan, T. P., Kimmelman, A. C., Wang, H., Fleming, J. B., Cantley, L. C., DePinho, R. A. & Draetta, G. F. Oncogene Ablation-Resistant Pancreatic Cancer Cells Depend on Mitochondrial Function. *Nature* **514,** 628–632 (2014).

272. Mi, W., You, J., Li, L., Zhu, L., Xia, X., Yang, L., Li, F., Xu, Y., Bi, J., Liu, P., Chen, L. & Li, F. BET Inhibition Induces GDH1-dependent Glutamine Metabolic Remodeling and Vulnerability in Liver Cancer. *Life Metab* **3,** loae016 (2024).

273. Walker, L. S. K. & Sansom, D. M. The Emerging Role of CTLA4 as a Cell-Extrinsic Regulator of T Cell Responses. *Nat Rev Immunol* **11,** 852–863 (2011).

274. Leach, D. R., Krummel, M. F. & Allison, J. P. Enhancement of Antitumor Immunity by CTLA-4 Blockade. *Science* **271,** 1734–1736 (1996).

275. García-Torralba, E., Garcia-Lorenzo, E., Doger, B., Spada, F. & Lamarca, A. Immunotherapy in Neuroendocrine Neoplasms: A Diamond to Cut. *Cancers* **16,** 2530 (14 2024).

276. Goltz, D., Gevensleben, H., Vogt, T. J., Dietrich, J., Golletz, C., Bootz, F., Kristiansen, G., Landsberg, J. & Dietrich, D. CTLA4 Methylation Predicts Response to Anti–PD-1 and Anti–CTLA-4 Immunotherapy in Melanoma Patients. *JCI Insight* **3,** e96793.

277. Vaddi, P. K., Osborne, D. G., Nicklawsky, A., Williams, N. K., Menon, D. R., Smith, D., Mayer, J., Reid, A., Domenico, J., Nguyen, G. H., Robinson, W. A., Ziman, M., Gao, D., Zhai, Z. & Fujita, M. CTLA4 mRNA Is Downregulated by miR-155 in Regulatory T Cells, and Reduced Blood CTLA4 Levels Are Associated with Poor Prognosis in Metastatic Melanoma Patients. *Front Immunol* **14,** 1173035 (2023).

278. Zhu, Y. & Wu, M. Noninvasive Radiomic Analysis of Enhanced CT Predicts CTLA4 Expression and Prognosis in Head and Neck Squamous Cell Carcinoma. *Sci Rep* **13,** 16782 (2023).

279. Kulkarni, A., Anderson, A. G., Merullo, D. P. & Konopka, G. Beyond Bulk: A Review of Single Cell Transcriptomics Methodologies and Applications. *Curr Opin Biotechnol* **58,** 129–136 (2019).

280. Stegle, O., Teichmann, S. A. & Marioni, J. C. Computational and Analytical Challenges in Single-Cell Transcriptomics. *Nat Rev Genet* **16,** 133–145 (2015).

281. Filippakopoulos, P. & Knapp, S. Next-Generation Epigenetic Inhibitors. *Science* **368,** 367–368 (2020).

282. Shorstova, T., Foulkes, W. D. & Witcher, M. Achieving Clinical Success with BET Inhibitors as Anti-Cancer Agents. *Br J Cancer* **124,** 1478–1490 (9 2021).

283. Tanaka, M., Roberts, J. M., Seo, H.-S., Souza, A., Paulk, J., Scott, T. G., DeAngelo, S. L., Dhe-Paganon, S. & Bradner, J. E. Design and Characterization of Bivalent BET Inhibitors. *Nat Chem Biol* **12,** 1089–1096 (2016).

284. Wellaway, C. R., Bamborough, P., Bernard, S. G., Chung, C.-w., Craggs, P. D., Cutler, L., Demont, E. H., Evans, J. P., Gordon, L., Karamshi, B., Lewis, A. J., Lindon, M. J., Mitchell, D. J., Rioja, I., Soden, P. E., Taylor, S., Watson, R. J., Willis, R., Woolven, J. M., Wyspiańska, B. S., Kerr, W. J. & Prinjha, R. K. Structure-Based Design of a Bromodomain and Extraterminal Domain (BET) Inhibitor Selective for the N-Terminal Bromodomains That Retains an Anti-inflammatory and Antiproliferative Phenotype. *J Med Chem* **63,** 9020–9044 (2020).

285. Slavish, P. J., Chi, L., Yun, M.-K., Tsurkan, L., Martinez, N. E., Jonchere, B., Chai, S. C., Connelly, M., Waddell, M. B., Das, S., Neale, G., Li, Z., Shadrick, W. R., Olsen, R. R., Freeman, K. W., Low, J. A., Price, J. E., Young, B. M., Bharatham, N., Boyd, V. A., Yang, J., Lee, R. E., Morfouace, M., Roussel, M. F., Chen, T., Savic, D., Guy, R. K., White, S. W., Shelat, A. A. & Potter, P. M. Bromodomain-Selective BET Inhibitors Are Potent Antitumor Agents against MYC-driven Pediatric Cancer. *Cancer Res* **80,** 3507–3518 (2020).

286. Tredup, C., Ndreshkjana, B., Schneider, N. S., Tjaden, A., Kemas, A. M., Youhanna, S., Lauschke, V. M., Berger, B.-T., Krämer, A., Berger, L. M., Röhm, S., Knapp, S., Farin, H. F. & Müller, S. Deep Annotation of Donated Chemical Probes (DCP) in Organotypic Human Liver Cultures and Patient-Derived Organoids from Tumor and Normal Colorectum. *ACS Chem Biol* **18,** 822–836 (2023).

287. Preston, A., Atkinson, S., Bamborough, P., Chung, C.-w., Craggs, P. D., Gordon, L., Grandi, P., Gray, J. R. J., Jones, E. J., Lindon, M., Michon, A.-M., Mitchell, D. J., Prinjha, R. K., Rianjongdee, F., Rioja, I., Seal, J., Taylor, S., Wall, I., Watson, R. J., Woolven, J. & Demont, E. H. Design and Synthesis of a Highly Selective and In Vivo-Capable Inhibitor of the Second Bromodomain of the Bromodomain and Extra Terminal Domain Family of Proteins. *J Med Chem* **63,** 9070–9092 (2020).

288. Greco, W. R., Faessel, H. & Levasseur, L. The Search for Cytotoxic Synergy Between Anticancer Agents: A Case of Dorothy and the Ruby Slippers? *J Natl Cancer Inst* **88,** 699–700 (1996).

289. González-Gualda, E., Baker, A. G., Fruk, L. & Muñoz-Espín, D. A Guide to Assessing Cellular Senescence in Vitro and in Vivo. *FEBS J.* **288,** 56–80 (2021).

290. Wang, L., Matkar, S., Xie, G., An, C., He, X., Kong, X., Liu, X. & Hua, X. BRD4 Inhibitor IBET Upregulates P27kip/Cip Protein Stability in Neuroendocrine Tumor Cells. *Cancer Biol Ther* **18,** 229–236 (2017).

291. Devaiah, B. N., Lewis, B. A., Cherman, N., Hewitt, M. C., Albrecht, B. K., Robey, P. G., Ozato, K., Sims, R. J. & Singer, D. S. BRD4 Is an Atypical Kinase That Phosphorylates Serine2 of the RNA Polymerase II Carboxy-Terminal Domain. *Proc Natl Acad Sci U S A* **109,** 6927–6932 (2012).

292. Roboz, G. J., Desai, P., Lee, S., Ritchie, E. K., Winer, E. S., DeMario, M., Brennan, B., Nüesch, E., Chesne, E., Brennan, L., Lechner, K., Kornacker, M. & DeAngelo, D. J. A Dose Escalation Study of RO6870810/TEN-10 in Patients with Acute Myeloid Leukemia and Myelodysplastic Syndrome. *Leuk Lymphoma* **62,** 1740–1748 (2021).

293. Shapiro, G. I., LoRusso, P., Dowlati, A., T Do, K., Jacobson, C. A., Vaishampayan, U., Weise, A., Caimi, P. F., Eder, J. P., French, C. A., Labriola-Tompkins, E., Boisserie, F., Pierceall, W. E., Zhi, J., Passe, S., DeMario, M., Kornacker, M. & Armand, P. A Phase 1 Study of RO6870810, a Novel Bromodomain and Extra-Terminal Protein Inhibitor, in Patients with NUT Carcinoma, Other Solid Tumours, or Diffuse Large B-cell Lymphoma. *Br J Cancer* **124,** 744–753 (2021).

294. Hudson, A. L. & Colvin, E. K. Transgenic Mouse Models of SV40-Induced Cancer. *ILAR Journal* **57,** 44–54 (2016).

295. Ding, D., Zheng, R., Tian, Y., Jimenez, R., Hou, X., Weroha, S. J., Wang, L., Shi, L. & Huang, H. Retinoblastoma Protein as an Intrinsic BRD4 Inhibitor Modulates Small Molecule BET Inhibitor Sensitivity in Cancer. *Nat Commun* **13,** 6311 (2022).

296. Boora, G. K., Kanwar, R., Kulkarni, A. A., Pleticha, J., Ames, M., Schroth, G., Beutler, A. S. & Banck, M. S. Exome-Level Comparison of Primary Well-Differentiated Neuroendocrine Tumors and Their Cell Lines. *Cancer Genet* **208,** 374–381 (2015).

297. Zhang, L., Cai, T., Lin, X., Huang, X., Bui, M. H., Plotnik, J. P., Bellin, R. J., Faivre, E. J., Kuruvilla, V. M., Lam, L. T., Lu, X., Zha, Z., Feng, W., Hessler, P., Uziel, T., Zhang, Q., Cavazos, A., Han, L., Ferguson, D. C., Mehta, G., Shanmugavelandy, S. S., Magoc, T. J., Rowe, J., Goodwin, N. C., Dorritie, K. A., Boyiadzis, M., Albert, D. H., McDaniel, K. F., Kati, W. M., Konopleva, M. & Shen, Y. Selective Inhibition of the Second Bromodomain of BET Family Proteins Results in Robust Antitumor Activity in Preclinical Models of Acute Myeloid Leukemia. *Mol Cancer Ther* **20,** 1809–1819 (2021).

298. Wang, K., Tang, J., Fan, S., Su, H., Yu, R., Zhang, Y., Wu, H., Lv, Y., Zhang, S. & Zou, X. ABBV-744 Induces Autophagy in Gastric Cancer Cells by Regulating PI3K/AKT/mTOR/p70S6k and MAPK Signaling Pathways. *Neoplasia* **45,** 100936 (2023).

299. Viviano, M., Cipriano, A., Fabbrizi, E., Feoli, A., Castellano, S., Sbardella, G., Mai, A., Milite, C. & Rotili, D. Successes and Challenges in the Development of BD1-selective BET Inhibitors: A Patent Review. *Expert Opin Ther Pat* **0,** 1–17 (2024).

300. Qi, J. & Shi, Y. Selective Targeting of Different Bromodomains by Small Molecules. *Cancer Cell* **37,** 764–766 (2020).

301. Divakaran, A., Harki, D. A. & Pomerantz, W. C. K. Recent Progress and Structural Analyses of Domain-Selective BET Inhibitors. *Med Res Rev* **43,** 972–1018 (2023).

302. Baud, M. G. J., Lin-Shiao, E., Cardote, T., Tallant, C., Pschibul, A., Chan, K.-H., Zengerle, M., Garcia, J. R., Kwan, T. T.-L., Ferguson, F. M. & Ciulli, A. A Bump-and-Hole Approach to Engineer Controlled Selectivity of BET Bromodomain Chemical Probes. *Science* **346,** 638–641 (2014).

303. Shi, Y., Qian, Z. R., Zhang, S., Li, W., Masugi, Y., Li, T., Chan, J. A., Yang, J., Da Silva, A., Gu, M., Liu, L., Hamada, T., Kosumi, K., Dutton, T., Brais, L. K., Nishihara, R., Fuchs, C. S., Ogino, S. & Kulke, M. H. Cell Cycle Protein Expression in Neuroendocrine Tumors: Association of CDK4/CDK6, CCND1, and Phospho-RB1 With Proliferative Index. *Pancreas* **46,** 1347–1353 (2017).

304. Huang, B., Yang, X.-D., Zhou, M.-M., Ozato, K. & Chen, L.-F. Brd4 Coactivates Transcriptional Activation of NF-kappaB via Specific Binding to Acetylated RelA. *Mol Cell Biol* **29,** 1375–1387 (2009).

305. Gamsjaeger, R., Webb, S. R., Lamonica, J. M., Billin, A., Blobel, G. A. & Mackay, J. P. Structural Basis and Specificity of Acetylated Transcription Factor GATA1 Recognition by BET Family Bromodomain Protein Brd3. *Mol Cell Biol* **31,** 2632–2640 (2011).

306. Schröder, S., Cho, S., Zeng, L., Zhang, Q., Kaehlcke, K., Mak, L., Lau, J., Bisgrove, D., Schnölzer, M., Verdin, E., Zhou, M.-M. & Ott, M. Two-Pronged Binding with Bromodomain-containing Protein 4 Liberates Positive Transcription Elongation Factor b from Inactive Ribonucleoprotein Complexes. *J Biol Chem* **287,** 1090–1099 (2012).

307. Pepper, M. A., Dulken, B. W., Wang, Y., Zemek, A. J., Martin, B. A., Charu, V. & Longacre, T. A. S100 Protein Expression in Primary and Metastatic Neuroendocrine Neoplasms: A Specific Marker of Pancreatic Origin. *Am J Surg Pathol* **48,** 157–162 (2024).

308. Tong, Q., Yi, M., Kong, P., Xu, L., Huang, W., Niu, Y., Gan, X., Zhan, H., Tian, R. & Yan, D. TRIM36 Inhibits Tumorigenesis through the Wnt/β-Catenin Pathway and Promotes Caspase-Dependent Apoptosis in Hepatocellular Carcinoma. *Cancer Cell Int* **22,** 278 (2022).

309. Madden, S. K., de Araujo, A. D., Gerhardt, M., Fairlie, D. P. & Mason, J. M. Taking the Myc out of Cancer: Toward Therapeutic Strategies to Directly Inhibit c-Myc. *Mol Cancer* **20,** 3 (2021).

310. Hung, Y.-H., Hsu, S.-H., Hou, Y.-C., Chu, P.-Y., Su, Y.-Y., Shan, Y.-S., Hung, W.-C. & Chen, L.-T. Semaphorin 6C Suppresses Proliferation of Pancreatic Cancer Cells via Inhibition of the AKT/GSK3/β-Catenin/Cyclin D1 Pathway. *Int J Mol Sci* **23,** 2608 (2022).

311. Wu, T., Kamikawa, Y. F. & Donohoe, M. E. Brd4's Bromodomains Mediate Histone H3 Acetylation and Chromatin Remodeling in Pluripotent Cells through P300 and Brg1. *Cell Rep* **25,** 1756–1771 (2018).

312. Islam, R., Jenkins, C. E., Cao, Q., Wong, J., Bilenky, M., Carles, A., Moksa, M., Weng, A. P. & Hirst, M. RUNX1 Colludes with NOTCH1 to Reprogram Chromatin in T Cell Acute Lymphoblastic Leukemia. *iScience* **26,** 106795 (2023).

313. Heintzman, N. D., Stuart, R. K., Hon, G., Fu, Y., Ching, C. W., Hawkins, R. D., Barrera, L. O., Van Calcar, S., Qu, C., Ching, K. A., Wang, W., Weng, Z., Green, R. D., Crawford, G. E. & Ren, B. Distinct and Predictive Chromatin Signatures of Transcriptional Promoters and Enhancers in the Human Genome. *Nat Genet* **39,** 311–318 (2007).

314. McLean, C. Y., Bristor, D., Hiller, M., Clarke, S. L., Schaar, B. T., Lowe, C. B., Wenger, A. M. & Bejerano, G. GREAT Improves Functional Interpretation of Cis-Regulatory Regions. *Nat Biotechnol* **28,** 495–501 (2010).

315. Kumar, M., Molkentine, D., Molkentine, J., Bridges, K., Xie, T., Yang, L., Hefner, A., Gao, M., Bahri, R., Dhawan, A., Frederick, M. J., Seth, S., Abdelhakiem, M., Beadle, B. M., Johnson, F., Wang, J., Shen, L., Heffernan, T., Sheth, A., Ferris, R. L., Myers, J. N., Pickering, C. R. & Skinner, H. D. Inhibition of Histone Acetyltransferase Function Radiosensitizes CREBBP/EP300 Mutants via Repression of Homologous Recombination, Potentially Targeting a Gain of Function. *Nat Commun* **12,** 6340 (2021).

316. Xiang, Y., Yan, K., Zheng, Q., Ke, H., Cheng, J., Xiong, W., Shi, X., Wei, L., Zhao, M., Yang, F., Wang, P., Lu, X., Fu, L., Lu, X. & Li, F. Histone Demethylase KDM4B Promotes DNA Damage by Activating Long Interspersed Nuclear Element-1. *Cancer Res* **79,** 86–98 (2019).

317. Cohen, P. A., Donini, C. F., Nguyen, N. T., Lincet, H. & Vendrell, J. A. The Dark Side of ZNF217, a Key Regulator of Tumorigenesis with Powerful Biomarker Value. *Oncotarget* **6,** 41566–41581 (2015).

318. Qian, Z. R., Li, T., Ter-Minassian, M., Yang, J., Chan, J. A., Brais, L. K., Masugi, Y., Thiaglingam, A., Brooks, N., Nishihara, R., Bonnemarie, M., Masuda, A., Inamura, K., Kim, S. A., Mima, K., Sukawa, Y., Dou, R., Lin, X., Christiani, D. C., Schmidlin, F., Fuchs, C. S., Mahmood, U., Ogino, S. & Kulke, M. H. Association Between Somatostatin Receptor Expression and Clinical Outcomes in Neuroendocrine Tumors. *Pancreas* **45,** 1386–1393 (2016).

319. Tanigawa, M., Nakayama, M., Taira, T., Hattori, S., Mihara, Y., Kondo, R., Kusano, H., Nakamura, K., Abe, Y., Ishida, Y., Okabe, Y., Hisaka, T., Okuda, K., Fujino, K., Ito, T., Kawahara, A., Naito, Y., Yamaguchi, R., Akiba, J., Akagi, Y. & Yano, H. Insulinoma-Associated Protein 1 (INSM1) Is a Useful Marker for Pancreatic Neuroendocrine Tumor. *Med Mol Morphol* **51,** 32–40 (2018).

320. Yang, M. X., Coates, R. F., Ambaye, A., Cortright, V., Mitchell, J. M., Buskey, A. M., Zubarik, R., Liu, J. G., Ades, S. & Barry, M. M. NKX2.2, PDX-1 and CDX-2 as Potential Biomarkers to Differentiate Well-Differentiated Neuroendocrine Tumors. *Biomark Res* **6,** 15 (2018).

321. Shafran, J. S., Jafari, N., Casey, A. N., Győrffy, B. & Denis, G. V. BRD4 Regulates Key Transcription Factors That Drive Epithelial-Mesenchymal Transition in Castration-Resistant Prostate Cancer. *Prostate Cancer Prostatic Dis* **24,** 268–277 (2021).

322. Reggiani, F., Talarico, G., Gobbi, G., Sauta, E., Torricelli, F., Manicardi, V., Zanetti, E., Orecchioni, S., Falvo, P., Piana, S., Lococo, F., Paci, M., Bertolini, F., Ciarrocchi, A. & Sancisi, V. BET Inhibitors Drive Natural Killer Activation in Non-Small Cell Lung Cancer via BRD4 and SMAD3. *Nat Commun* **15,** 2567 (2024).

323. Oien, D. B., Sharma, S., Hattersley, M. M., DuPont, M., Criscione, S. W., Prickett, L., Goeppert, A. U., Drew, L., Yao, Y., Zhang, J. & Chan, H. M. BET Inhibition Targets ABC-DLBCL Constitutive B-cell Receptor Signaling through PAX5. *Blood Adv* **7,** 5108–5121 (2023).

324. Font-Tello, A., Kesten, N., Xie, Y., Taing, L., Varešlija, D., Young, L. S., Hamid, A. A., Van Allen, E. M., Sweeney, C. J., Gjini, E., Lako, A., Hodi, F. S., Bellmunt, J., Brown, M., Cejas, P. & Long, H. W. FiTAc-seq: Fixed-Tissue ChIP-seq for H3K27ac Profiling and Super-Enhancer Analysis of FFPE Tissues. *Nat Protoc* **15,** 2503–2518 (2020).

325. Wang, Y., Song, C., Zhao, J., Zhang, Y., Zhao, X., Feng, C., Zhang, G., Zhu, J., Wang, F., Qian, F., Zhou, L., Zhang, J., Bai, X., Ai, B., Liu, X., Wang, Q. & Li, C. SEdb 2.0: A Comprehensive Super-Enhancer Database of Human and Mouse. *Nucleic Acids Res* **51,** D280–D290 (2023).

326. Szklarczyk, D., Gable, A. L., Nastou, K. C., Lyon, D., Kirsch, R., Pyysalo, S., Doncheva, N. T., Legeay, M., Fang, T., Bork, P., Jensen, L. J. & von Mering, C. The STRING Database in 2021: Customizable Protein-Protein Networks, and Functional Characterization of User-Uploaded Gene/Measurement Sets. *Nucleic Acids Res* **49,** D605–D612 (2021).

327. Modukuri, R. K., Yu, Z., Tan, Z., Ta, H. M., Ucisik, M. N., Jin, Z., Anglin, J. L., Sharma, K. L., Nyshadham, P., Li, F., Riehle, K., Faver, J. C., Duong, K., Nagarajan, S., Simmons, N., Palmer, S. S., Teng, M., Young, D. W., Yi, J. S., Kim, C. & Matzuk, M. M. Discovery of Potent BET Bromodomain 1 Stereoselective Inhibitors Using DNA-encoded Chemical Library Selections. *Proc Natl Acad Sci U S A* **119,** e2122506119 (2022).

328. Sun, Y., Han, J., Wang, Z., Li, X., Sun, Y. & Hu, Z. Safety and Efficacy of Bromodomain and Extra-Terminal Inhibitors for the Treatment of Hematological Malignancies and Solid Tumors: A Systematic Study of Clinical Trials. *Front Pharmacol* **11,** 621093 (2020).

329. Amorim, S., Stathis, A., Gleeson, M., Iyengar, S., Magarotto, V., Leleu, X., Morschhauser, F., Karlin, L., Broussais, F., Rezai, K., Herait, P., Kahatt, C., Lokiec, F., Salles, G., Facon, T., Palumbo, A., Cunningham, D., Zucca, E. & Thieblemont, C. Bromodomain Inhibitor OTX015 in Patients with Lymphoma or Multiple Myeloma: A Dose-Escalation, Open-Label, Pharmacokinetic, Phase 1 Study. *Lancet Haematol* **3,** e196–204 (2016).

330. Borthakur, G., Odenike, O., Aldoss, I., Rizzieri, D. A., Prebet, T., Chen, C., Popovic, R., Modi, D. A., Joshi, R. H., Wolff, J. E. & Jonas, B. A. A Phase 1 Study of the Pan-Bromodomain and Extraterminal Inhibitor Mivebresib (ABBV-075) Alone or in Combination with Venetoclax in Patients with Relapsed/Refractory Acute Myeloid Leukemia. *Cancer* **127,** 2943–2953 (2021).

331. Ameratunga, M., Braña, I., Bono, P., Postel-Vinay, S., Plummer, R., Aspegren, J., Korjamo, T., Snapir, A. & de Bono, J. S. First-in-Human Phase 1 Open Label Study of the BET Inhibitor ODM-207 in Patients with Selected Solid Tumours. *Br J Cancer* **123,** 1730–1736 (2020).

332. Bisgrove, D. A., Mahmoudi, T., Henklein, P. & Verdin, E. Conserved P-TEFb-interacting Domain of BRD4 Inhibits HIV Transcription. *Proc Natl Acad Sci U S A* **104,** 13690–13695 (2007).

333. Petretich, M., Demont, E. H. & Grandi, P. Domain-Selective Targeting of BET Proteins in Cancer and Immunological Diseases. *Curr Opin Chem Biol* **57,** 184–193 (2020).

334. Higgins, M., Obaidi, I. & McMorrow, T. Primary Cilia and Their Role in Cancer. *Oncol Lett* **17,** 3041–3047 (2019).

335. Huber, A. D., Poudel, S., Wu, J., Miller, D. J., Lin, W., Yang, L., Bwayi, M. N., Rimmer, M. A., Gee, R. R. F., Seetharaman, J., Chai, S. C. & Chen, T. A Bromodomain-Independent Mechanism of Gene Regulation by the BET Inhibitor JQ1: Direct Activation of Nuclear Receptor PXR. *Nucleic Acids Research* **52,** 1661–1676 (2024).

336. Attwooll, C., Denchi, E. L. & Helin, K. The E2F Family: Specific Functions and Overlapping Interests. *EMBO J* **23,** 4709–4716 (2004).

337. Kent, L. N. & Leone, G. The Broken Cycle: E2F Dysfunction in Cancer. *Nat Rev Cancer* **19,** 326–338 (2019).

338. Nakahata, A. M., Suzuki, D. E., Rodini, C. O., Fiuza, M. L. & Okamoto, O. K. RNAi-mediated Knockdown of E2F2 Inhibits Tumorigenicity of Human Glioblastoma Cells. *Oncol Lett* **8,** 1487–1491 (2014).

339. Reimer, D., Sadr, S., Wiedemair, A., Stadlmann, S., Concin, N., Hofstetter, G., Müller-Holzner, E., Marth, C. & Zeimet, A. G. Clinical Relevance of E2F Family Members in Ovarian Cancer–an Evaluation in a Training Set of 77 Patients. *Clin Cancer Res* **13,** 144–151 (2007).

340. Liu, Q., Song, C., Li, J., Liu, M., FU, L., Jiang, J., Zeng, Z. & Zhu, H. E2F2 Enhances the Chemoresistance of Pancreatic Cancer to Gemcitabine by Regulating the Cell Cycle and Upregulating the Expression of RRM2. *Med Oncol* **39,** 124 (2022).

341. Klochendler, A., Caspi, I., Corem, N., Moran, M., Friedlich, O., Elgavish, S., Nevo, Y., Helman, A., Glaser, B., Eden, A., Itzkovitz, S. & Dor, Y. The Genetic Program of Pancreatic β-Cell Replication In Vivo. *Diabetes* **65,** 2081–2093 (2016).

342. Delmore, J. E., Issa, G. C., Lemieux, M. E., Rahl, P. B., Shi, J., Jacobs, H. M., Kastritis, E., Gilpatrick, T., Paranal, R. M., Qi, J., Chesi, M., Schinzel, A. C., McKeown, M. R., Heffernan, T. P., Vakoc, C. R., Bergsagel, P. L., Ghobrial, I. M., Richardson, P. G., Young, R. A., Hahn, W. C., Anderson, K. C., Kung, A. L., Bradner, J. E. & Mitsiades, C. S. BET Bromodomain Inhibition as a Therapeutic Strategy to Target C-Myc. *Cell* **146,** 904–917 (2011).

343. Mertz, J. A., Conery, A. R., Bryant, B. M., Sandy, P., Balasubramanian, S., Mele, D. A., Bergeron, L. & Sims, R. J. Targeting MYC Dependence in Cancer by Inhibiting BET Bromodomains. *Proc Natl Acad Sci U S A* **108,** 16669–16674 (2011).

344. Trabucco, S. E., Gerstein, R. M., Evens, A. M., Bradner, J. E., Shultz, L. D., Greiner, D. L. & Zhang, H. Inhibition of Bromodomain Proteins for the Treatment of Human Diffuse Large B-cell Lymphoma. *Clin Cancer Res* **21,** 113–122 (2015).

345. Lockwood, W. W., Zejnullahu, K., Bradner, J. E. & Varmus, H. Sensitivity of Human Lung Adenocarcinoma Cell Lines to Targeted Inhibition of BET Epigenetic Signaling Proteins. *Proc Natl Acad Sci U S A* **109,** 19408–19413 (2012).

346. Lenhart, R., Kirov, S., Desilva, H., Cao, J., Lei, M., Johnston, K., Peterson, R., Schweizer, L., Purandare, A., Ross-Macdonald, P., Fairchild, C., Wong, T. & Wee, S. Sensitivity of Small Cell Lung Cancer to BET Inhibition Is Mediated by Regulation of ASCL1 Gene Expression. *Mol Cancer Ther* **14,** 2167–2174 (2015).

347. Ghari, F., Quirke, A.-M., Munro, S., Kawalkowska, J., Picaud, S., McGouran, J., Subramanian, V., Muth, A., Williams, R., Kessler, B., Thompson, P. R., Fillipakopoulos, P., Knapp, S., Venables, P. J. & La Thangue, N. B. Citrullination-Acetylation Interplay Guides E2F-1 Activity during the Inflammatory Response. *Sci Adv* **2,** e1501257 (2016).

348. Liu, C.-S., Rioja, I., Bakr, A., Veldwijk, M. R., Sperk, E., Herskind, C., Weichenhan, D., Prinjha, R. K., Plass, C., Schmezer, P. & Popanda, O. Selective Inhibitors of Bromodomain BD1 and BD2 of BET Proteins Modulate Radiation-Induced Profibrotic Fibroblast Responses. *Int J Cancer* **151,** 275–286 (2022).

349. Dai, X., Cheng, H., Bai, Z. & Li, J. Breast Cancer Cell Line Classification and Its Relevance with Breast Tumor Subtyping. *J Cancer* **8,** 3131–3141 (2017).

350. Grozinsky-Glasberg, S., Shimon, I. & Rubinfeld, H. The Role of Cell Lines in the Study of Neuroendocrine Tumors. *Neuroendocrinology* **96,** 173–187 (2012).

351. Zhao, R., Lu, J., Li, Q., Xiong, F., Zhang, Y., Zhu, J., Peng, G. & Yang, J. Single-Cell Heterogeneity Analysis and CRISPR Screens in MIN6 Cell Line Reveal Transcriptional Regulators of Insulin. *Cell Cycle* **20,** 2053–2065 (2021).

352. Vandamme, T., Peeters, M., Dogan, F., Pauwels, P., Van Assche, E., Beyens, M., Mortier, G., Vandeweyer, G., de Herder, W., Van Camp, G., Hofland, L. J. & Op de Beeck, K. Whole-Exome Characterization of Pancreatic Neuroendocrine Tumor Cell Lines BON-1 and QGP-1. *J Mol Endocrinol* **54,** 137–147 (2015).

353. Luley, K. B., Biedermann, S. B., Künstner, A., Busch, H., Franzenburg, S., Schrader, J., Grabowski, P., Wellner, U. F., Keck, T., Brabant, G., Schmid, S. M., Lehnert, H. & Ungefroren, H. A Comprehensive Molecular Characterization of the Pancreatic Neuroendocrine Tumor Cell Lines BON-1 and QGP-1. *Cancers (Basel)* **12,** 691 (2020).

354. Rajkumar, A. P., Qvist, P., Lazarus, R., Lescai, F., Ju, J., Nyegaard, M., Mors, O., Børglum, A. D., Li, Q. & Christensen, J. H. Experimental Validation of Methods for Differential Gene Expression Analysis and Sample Pooling in RNA-seq. *BMC Genomics* **16,** 548 (2015).

355. Chaidos, A., Caputo, V., Gouvedenou, K., Liu, B., Marigo, I., Chaudhry, M. S., Rotolo, A., Tough, D. F., Smithers, N. N., Bassil, A. K., Chapman, T. D., Harker, N. R., Barbash, O., Tummino, P., Al-Mahdi, N., Haynes, A. C., Cutler, L., Le, B., Rahemtulla, A., Roberts, I., Kleijnen, M., Witherington, J. J., Parr, N. J., Prinjha, R. K. & Karadimitris, A. Potent Antimyeloma Activity of the Novel Bromodomain Inhibitors I-BET151 and I-BET762. *Blood* **123,** 697–705 (2014).

356. Tarantelli, C., Bernasconi, E., Gaudio, E., Cascione, L., Restelli, V., Arribas, A. J., Spriano, F., Rinaldi, A., Mensah, A. A., Kwee, I., Ponzoni, M., Zucca, E., Carrassa, L., Riveiro, M. E., Rezai, K., Stathis, A., Cvitkovic, E. & Bertoni, F. BET Bromodomain Inhibitor Birabresib in Mantle Cell Lymphoma: In Vivo Activity and Identification of Novel Combinations to Overcome Adaptive Resistance. *ESMO Open* **3,** e000387 (2018).

357. Berenguer-Daizé, C., Astorgues-Xerri, L., Odore, E., Cayol, M., Cvitkovic, E., Noel, K., Bekradda, M., MacKenzie, S., Rezai, K., Lokiec, F., Riveiro, M. E. & Ouafik, L. OTX015 (MK-8628), a Novel BET Inhibitor, Displays in Vitro and in Vivo Antitumor Effects Alone and in Combination with Conventional Therapies in Glioblastoma Models. *Int J Cancer* **139,** 2047–2055 (2016).

358. US Food and Drug Administration. *Guidance for Industry: Estimating the Maximum Safe Starting Dose in Adult Healthy Volunteer* (US Food and Drug Administration, Rockville, MD, 2005).

359. Nair, A. B. & Jacob, S. A Simple Practice Guide for Dose Conversion between Animals and Human. *J Basic Clin Pharm* **7,** 27–31 (2016).

360. Postel-Vinay, S., Herbschleb, K., Massard, C., Woodcock, V., Soria, J.-C., Walter, A. O., Ewerton, F., Poelman, M., Benson, N., Ocker, M., Wilkinson, G. & Middleton, M. First-in-Human Phase I Study of the Bromodomain and Extraterminal Motif Inhibitor BAY 1238097: Emerging Pharmacokinetic/Pharmacodynamic Relationship and Early Termination Due to Unexpected Toxicity. *Eur J Cancer* **109,** 103–110 (2019).

361. Burden, N., Chapman, K., Sewell, F. & Robinson, V. Pioneering Better Science through the 3Rs: An Introduction to the National Centre for the Replacement, Refinement, and Reduction of Animals in Research (NC3Rs). *J Am Assoc Lab Anim Sci* **54,** 198–208 (2015).

362. Iniguez, A. B., Alexe, G., Wang, E. J., Roti, G., Patel, S., Chen, L., Kitara, S., Conway, A., Robichaud, A. L., Stolte, B., Bandopadhayay, P., Goodale, A., Pantel, S., Lee, Y., Cheff, D. M., Hall, M. D., Guha, R., Davis, M. I., Menard, M., Nasholm, N., Weiss, W. A., Qi, J., Beroukhim, R., Piccioni, F., Johannessen, C. & Stegmaier, K. Resistance to Epigenetic-Targeted Therapy Engenders Tumor Cell Vulnerabilities Associated with Enhancer Remodeling. *Cancer Cell* **34,** 922–938.e7 (2018).

363. Kurimchak, A. M., Shelton, C., Duncan, K. E., Johnson, K. J., Brown, J., O'Brien, S., Gabbasov, R., Fink, L. S., Li, Y., Lounsbury, N., Abou-Gharbia, M., Childers, W. E., Connolly, D. C., Chernoff, J., Peterson, J. R. & Duncan, J. S. Resistance to BET Bromodomain Inhibitors Is Mediated by Kinome Reprogramming in Ovarian Cancer. *Cell Rep* **16,** 1273–1286 (2016).

364. Stratikopoulos, E. E., Dendy, M., Szabolcs, M., Khaykin, A. J., Lefebvre, C., Zhou, M.-M. & Parsons, R. Kinase and BET Inhibitors Together Clamp Inhibition of PI3K Signaling and Overcome Resistance to Therapy. *Cancer Cell* **27,** 837–851 (2015).

365. Oh, D. H., Ma, X., Hogg, S. J., He, J., Kearney, C., Brasacchio, D., Susanto, O., Maher, B., Jennings, I. G., Newbold, A., Fraser, P., Gruber, E., Kats, L. M., Gregory, G. P., Johnstone, R. W., Thompson, P. E. & Shortt, J. Rationally Designed Chimeric PI3K-BET Bromodomain Inhibitors Elicit Curative Responses in MYC-driven Lymphoma. *Proc Natl Acad Sci U S A* **120,** e2306414120 (2023).

366. Zeng, F., Li, Y., Meng, Y., Sun, H., He, Y., Yin, M., Chen, X. & Deng, G. BET Inhibitors Synergize with Sunitinib in Melanoma through GDF15 Suppression. *Exp Mol Med* **55,** 364–376 (2023).

367. Shu, S., Wu, H.-J., Ge, J. Y., Zeid, R., Harris, I. S., Jovanović, B., Murphy, K., Wang, B., Qiu, X., Endress, J. E., Reyes, J., Lim, K., Font-Tello, A., Syamala, S., Xiao, T., Reddy Chilamakuri, C. S., Papachristou, E. K., D'Santos, C., Anand, J., Hinohara, K., Li, W., McDonald, T. O., Luoma, A., Modiste, R. J., Nguyen, Q.-D., Michel, B., Cejas, P., Kadoch, C., Jaffe, J. D., Wucherpfennig, K. W., Qi, J., Liu, X. S., Long, H., Brown, M., Carroll, J. S., Brugge, J. S., Bradner, J., Michor, F. & Polyak, K. Synthetic Lethal and Resistance Interactions with BET Bromodomain Inhibitors in Triple-Negative Breast Cancer. *Mol Cell* **78,** 1096–1113.e8 (2020).